Structural insights into the soluble form of CLIC1 and its mechanism of membrane insertion

Joseph Cassar

Thesis submitted for the degree of Doctor of Philosophy

University of Kent

Department of Natural Sciences

2022

Foreword

Declaration

The work carried out on this thesis is the product of my own research and was undertaken through the supervision of Dr Jose Luis Ortega Roldan. No part of the research has been used for any other qualification.

Joseph Cassar

2022

Acknowledgments

I have spent the last many months writing in exclusively scientific format, so please excuse my colloquial tone. Jose, I feel a massive sense of gratitude for everything you have done for me. For allowing me to join your lab as an undergraduate to picking me as your PhD candidate to providing support everyday with experiments in the lab. It is something that I will never forget and a debt I will never be able to truly repay. I regard you not just as a supervisor but as a great friend. I will miss our chats and I'm sure that we will cross paths again many times.

Next to my family who have had to put up with a rollercoaster of exams, success, failures. But have been with me and believed in me every step of the way. Finally, we have a good results day. I mean it's taken long enough but it all worked out in the end. My mother and father have often placed my siblings and I of greater importance than their own well-being. This has enabled myself to discover and pursue what I truly enjoy with endless support.

Next, I will like to thank my one true uni friend, Oliver Powell and my secondary school friends, Matt, Lucas, James and Bailey for their unwavering support and fun warzone games to keep myself going through the project.

For those in Bioscience, I would like to mention a few words. Lorena for providing my initial training when I joined the facility. Gary for providing a fountain of knowledge of NMR and his general guidance. Also to Richard, who was my academic advisor and helped to kickstart my career into research.

Finally I would like to thank myself. I have learnt a lot over the past 3 years. I have pushed myself to a place that I didn't think I was capable of being in. I am currently

sat here with food poisoning and I could probably throw up at any minute. However we are still here writing and there’s no chance that I am going to give up now.

Publications

Lorena Varela, Alex C.Hendry, Joseph Cassar, Ruben Martin-Escolano, Diego Cantoni, Felipe Ossa, John C.Edwards, Vahitha Abdul-Salem and Jose L.Ortega-Roldan. (2022). A Zn^{2+} triggered two-step mechanism of CLIC1 membrane insertion and activation into chloride channels. Journal of cell science. https://doi.org/10.1242/jcs.259704

Angela Serrano-Sanchez, Joseph Cassar, Lisa J. White, Precious I.A.Popoola, Jennifer R. Hiscock and Jose L.Ortega-Roldan. (2022). Elucidation of small molecule passive permeation across lipid membranes using conventional solution state NMR methods. BioRxiv, 510446.

https://doi.org/10.1101/2022.10.01.510446

Abstract

The chloride intracellular channel (CLIC) family has a unique characteristic which enables this human protein to be expressed as a soluble protein, however with an increase in the levels of intracellular zinc ions it can insert into the membrane. In the membrane, CLIC proteins have chloride ion channel activity. To date, the exact mechanism of CLIC1 insertion into the membrane is unknown.

Utilising biophysical techniques such as SAXS and NMR, we have identified that CLIC can exist in an ensemble of structures within solution that likely aid its insertion into the membrane. Further studies demonstrate that zinc can bind to CLIC1 and alters the relaxation properties of regions in the N-terminal domain that surround the predicted transmembrane region. We demonstrate that zinc is able to further promote higher order oligomeric states which would aid membrane insertion as previous literature suggests chloride ion channel conductance occurs in a tetrameric arrangement.

Mutations to residues impacted by zinc binding are able to disrupt the equilibrium of oligomeric states in solution, further pointing to the importance of these regions and residues for the metamorphic activity of CLIC1. A more detailed understanding of the mechanism of insertion of CLIC1, will aid pharmacological development of inhibitors for CLIC1. CLIC1 is upregulated in the membrane bound form in cancers such as glioblastoma. Inhibition of this mechanistic switch will provide a novel drug target for many cancers with poor prognosis.

Table of contents

CHAPTER 1: INTRODUCTION 19

1.1-Chloride intracellular channel 1 20

1.1.1 The discovery of NCC27 20

1.1.2 The metamorphic ability of the CLIC family 21

1.2- Metamorphic proteins 23

1.2.1- Proteins that exhibit metamorphic activity 23

1.2.2- The molecular mechanism of the metamorphic MLKL 25

1.3- CLIC1 structure in solution 26

1.3.1-The first crystal structure 26

1.3.2- Homology of the CLIC1 structure 27

1.3.3- Computational analysis of the CLIC1 structure 30

1.4- Flexibility and stability of CLIC1 in solution 32

1.4.1- Flexibility of CLIC1 predicted from the crystal structure 32

1.4.2- Flexibility of CLIC1 is enhanced by the lowering of pH from 7.4 to 5.5 32

1.4.3- Flexibility of the transmembrane domain in CLIC1 33

1.4.4- The stability of CLIC1 is affected by Histidine mutations and Cysteine mutations 34

1.5 - Divalent cations act as the trigger for membrane insertion of CLIC1 35

1.5.1 Zinc and calcium can promote a switch from soluble CLIC1 to a membrane bound channel 35

1.5.2- CLIC homologues EXC-4 and DmCLIC bind to the Ca+ ions 37

1.5.3- Association of CLIC function and calcium 39

1.6- The Chloride Ion Channel 40

1.6.1- Structure of the chloride ion channel....40

1.6.2- The composition of the lipid bilayer affects membrane insertion and chloride channel activity....41

1.6.3- Mutagenesis studies identify important residues for Chloride channel conductance....42

1.7 Implications of CLIC proteins in disease progression....43

1.7.1 The role of CLIC in tumourigenesis....43

1.7.2 The role of CLIC in neurodegenerative diseases....44

1.7.3 The role of CLIC in cardiovascular disease....45

1.7.4- The role of the CLIC family in hearing loss....46

1.7.5- CLIC1 as a cancer therapeutic target....46

1.8- Protein NMR....50

1.8.1- Introduction to NMR....50

1.8.2- The HSQC is the gold standard for protein NMR....50

1.8.3- Ligand interactions and chemical shift perturbations....54

1.9- The use of small angle x ray scattering in determining protein structure and dynamics....57

1.9.1- Theory of SAXS and sample preparation....57

1.9.2- Use of SAXS data to understand protein structure and dynamics....58

1.10- Aims of the CLIC1 research....61

CHAPTER 2: MATERIALS AND METHODS....62

2.1 - Materials....63

2.1.1- General materials....63

2.1.2- Buffers....65

2.1.3- Plasmids....66

2.1.4- Bacterial cells....68

2.1.5- Equipment....68

2.1.6- Software....68

2.2- Methods..... 70

2.2.1- Transformation 70

2.2.2- CLIC1 expression and purification..... 70

2.2.3- CLIC1 M9 media expression..... 71

2.2.4- Protein concentration determination..... 72

2.2.5- MST assay 72

2.2.6- NMR 72

2.2.7- Backbone assignments 73

2.2.8- Zinc titration NMR experiments 74

2.2.9- Relaxation NMR experiments..... 74

2.2.10-Residual dipolar coupling NMR experiments 75

2.2.11- SAXS 76

2.2.12- Tryptophan fluorescence..... 79

CHAPTER 3: PROBING THE SOLUTION STRUCTURE OF CLIC1 80

3.1- Abstract 81

3.2- Introduction 82

3.3-Results 83

3.3.1- Intermolecular forces within CLIC1 are strikingly less than the structural homologue GST01..... 83

3.3.2- B-factor analysis can identify flexible regions predicted from the crystal structure..... 86

3.3.3-Backbone assignment of CLIC1 facilitates structure and dynamics NMR experiments on CLIC1 90

3.3.4- NMR relaxation identifies flexible regions in CLIC1..... 93

3.3.5- SAXS can elucidate new minor states of CLIC1 which are not seen in structural homologues..... 94

3.3.6- NMR can provide restraints to develop a refined CLIC1 structure..... 105

3.4- Discussion 111

3.5- Conclusion..... 118

3.6- Future work..... 119

CHAPTER 4: ELUCIDATING THE ROLE OF ZN2+ IN AIDING THE MEMBRANE INSERTION OF CLIC1.....120

4.1- Abstract 121

4.2- Introduction 122

4.3- Results 124

4.3.1- MST identifies divalent cation binding to CLIC1 and the affinity of the interaction 124

4.3.2- NMR identifies residue specific changes to CLIC1 upon Zinc binding 125

4.3.3- The CLIC1 structure is not impacted by Zinc in the same mechanism as pH.....132

4.3.4- An N terminal his tag prevents oligomerisation effects upon Zn binding.....136

4.3.5- Zinc promotes the oligomerisation of CLIC1 and higher order states.....144

4.3.6- Alphafold predicts the structure of the dimer 146

4.3.7- Zinc binding enhances relaxation of N terminal loops in CLIC1 151

4.4- Discussion 154

4.5- Conclusion..... 162

4.6- Future work..... 163

CHAPTER 5: MUTATIONS CAN DISRUPT THE EQUILIBRIUM OF CLIC1 IN SOLUTION 164

5.1- Introduction 165

5.2- Results 166

5.3- Discussion and future work 173

CHAPTER 6: FINAL DISCUSSION 174

6.1- Updated model of CLIC1 membrane insertion 175

6.2- Limitations of the research..... 182

6.3- The CLIC1 insertion mechanism draws similarities with the annexin family..... 184

6.4- Future development of research into CLIC1..... 185

6.5- Impact of this research in the field..... 189

6.6- Final conclusion 190

BIBLIOGRAPHY 191

APPENDIX..... 208

List of figures

FIGURE 1.1: SEQUENCE HOMOLOGY MAP FOR CLIC1-4 21

FIGURE 1.2: THE CLIC1 1K0M CRYSTAL STRUCTURE VIEWED IN PYMOL..... 27

FIGURE 1.3: SEQUENCE ALIGNMENT OF CLIC1 COMPARED TO OTHER MEMBERS OF THE CLIC FAMILY AND ITS HOMOLOGUES PRESENTED AS A PERCENT IDENTITY MATRIX 29

FIGURE 1.4: COMPUTATIONAL ANALYSIS PREDICTION OF FLEXIBLE REGIONS OF CLIC1..... 30

FIGURE 1.5: CURRENT MECHANISM OF CLIC1 MEMBRANE INSERTION AND ACTIVATION..... 36

FIGURE 1.6: FLUORESCENCE MICROSCOPY OF GFP-LABELLED CLIC1 IN GIANT UNILAMELLAR ASOLECTIN VESICLES (GUVS). 37

FIGURE 1.7: THE CALCIUM BINDING SITE FOR DMCLIC1 FROM THE CRYSTAL STRUCTURE 2YV7 38

FIGURE 1.8: THE PROPOSED PATHWAY THROUGH WHICH METFORMIN INHIBITION OF CLIC1 LEADS TO REDUCED CANCER CELL PROLIFERATION 48

FIGURE 1.9: PULSE SEQUENCE FOR TYPICAL HSQC EXPERIMENT 52

FIGURE 1.10: - THE ROLE OF THE TROSY PEAK IN ENHANCING S/N IN LARGE PROTEINS..... 53

FIGURE 1.11: SMALL ANGLE X RAY SCATTERING EXPERIMENT 58

FIGURE 2.1: CLIC1_PET-28 DNA VECTOR MAP..... 66

FIGURE 2.2: GST O-1_PET-28 DNA VECTOR MAP 67

FIGURE 2.3: EOM PARAMETERS..... 78

FIGURE 3.1: INTERMOLECULAR FORCES CHARACTERISED USING THE PROTEINS INTERACTION CALCULATION(PIC) IN PROTEINS 86

FIGURE 3.2: B FACTOR ANALYSIS SCORE FOR CLIC1 AND ITS STRUCTURAL HOMOLOGUE GST OMEGA-1 PER RESIDUE..... 90

FIGURE 3.3: ASSIGNMENTS ON A 15N TROSY HSQC OF CLIC1 91

FIGURE 3.4: TALOS PREDICTION OF SECONDARY STRUCTURE FROM THE BACKBONE CHEMICAL SHIFTS OF CLIC1..... 92

FIGURE 3.5: CLIC1 DEMONSTRATES THREE HIGHLY FLEXIBLE AND DYNAMIC REGIONS WITHIN ITS STRUCTURE..... 94

FIGURE 3.6: BEAMLINE 21 USAGE PARAMETERS REPORT 96

FIGURE 3.7: ANALYSIS OF CLIC1 BY SMALL ANGLE X-RAY SCATTERING..... 97

FIGURE 3.8: FOXS SERVER COMPARISON OF CLIC1 CRYSTAL STRUCTURE PREDICTED SCATTERING DATA AGAINST EXPERIMENTAL CLIC1 SCATTERING DATA..... 98

FIGURE 3.9: PDB BEAD MODEL OF THE CLIC1 AVERAGE MONOMER STRUCTURE FROM THE EXPERIMENTAL SAXS DATA..... 99

FIGURE 3.10: COMPARISON OF THE EOM ENSEMBLE OF CLIC1 STRUCTURES AGAINST THE EXPERIMENTAL SCATTERING DATA 101

FIGURE 3.11: ANALYSIS OF GST 0-1 BY SMALL ANGLE X-RAY SCATTERING 103

FIGURE 3.12: FOXS SERVER COMPARISON OF GST O-1 CRYSTAL STRUCTURE PREDICTED SCATTERING DATA AGAINST EXPERIMENTAL GST O-1 SCATTERING DATA..... 104

FIGURE 3.13: COMPLETE SET OF RESIDUAL DIPOLAR COUPLING SPECTRA 108

FIGURE 3.14: RDC VALUES FROM THE CRYSTAL STRUCTURE DO NOT MATCH EXPERIMENTAL CLIC1 RDC VALUES..... 109

FIGURE 3.15: PDB STRUCTURE OF CLIC1 IN SOLUTION FITTED USING EXPERIMENTAL RDC VALUES 110

FIGURE 4.1: CLIC1 BINDS TO ZINC AND CALCIUM DEMONSTRATED BY MST 125

FIGURE 4.2: TROSY-HSQC OF CLIC1 BINDING TO 1MR ZN2+ 128

FIGURE 4.3. CLIC1 PEAK INTENSITY CHANGES AFTER ZINC BINDING 131

FIGURE 4.4: NMR PH TITRATION OF CLIC1 FROM PH 7.4 TO PH 5.5 134

FIGURE 4.5: INTENSITY LOSS OF PEAKS IN CLIC1 136

FIGURE 4.6: A HIS-TAG DISRUPTS THE FORMATION OF CLIC1 DIMER CAUSING CLIC1 TO EXIST EXCLUSIVELY AS A MONOMER 138

FIGURE 4.7: TROSY-HSQC OF CLIC1 HIS-TAG WITH ZN2+ TITRATION 140

FIGURE 4.8: CLIC1 EXPERIENCES GREATER INTENSITY LOSSES FROM ZINC IN THE N TERMINAL DOMAIN THAN THE C TERMINAL DOMAINS 142

FIGURE 4.9: PYMOL MODE OF GREATEST CLIC1 HIS-TAG PEAK INTENSITY CHANGES AFTER ZINC BINDING 143

FIGURE 4.10: ZINC BINDING PROMOTES OLIGOMERISATION OF CLIC1 145

FIGURE 4.11: FOXS SERVER COMPARISON OF CLIC1 OXIDISED DIMER CRYSTAL STRUCTURE PREDICTED SCATTERING DATA AGAINST EXPERIMENTAL CLIC1 DIMER SCATTERING DATA 147

FIGURE 4.12: FOXS SERVER COMPARISON OF ALPHAFOLD CLIC1 DIMER PREDICTED SCATTERING DATA AGAINST EXPERIMENTAL CLIC1 DIMER SCATTERING DATA 149

FIGURE 4.13: FOXS SERVER COMPARISON OF THE ALPHAFOLD CLIC1 DIMER STRUCTURE PREDICTED SCATTERING DATA AGAINST EXPERIMENTAL CLIC1 ZINC BOUND DIMER SCATTERING DATA 150

FIGURE 4.14: CLIC1 EXHIBITS AN INCREASE IN FLEXIBILITY OF SO SPECIFIC N TERMINAL RESIDUES IN THE PRESENCE OF 1MR ZINC 152

FIGURE 4.15: PYMOL MODEL OF THE CLIC1 N TERMINAL DOMAIN RESIDUES WITH THE LOWEST R2/R1 VALUES WHEN BOUND TO ZINC 153

FIGURE 5.1: P65A, F66A AND R29A CLIC1 MUTANTS DISRUPT THE EQUILIBRIUM OF CLIC1 OLIGOMERIC STATES..... 169

FIGURE 5.2: POSITION AND CONSERVATION OF MUTATIONS IN THE CLIC1 STRUCTURE..... 172

FIGURE 6.1: A MULTI-STEP CLIC1 MECHANISM OF INSERTION MODEL 181

Acronyms

CD- Circular dichroism

CLIC- Chloride intracellular channel

CSP- Chemical shift perturbation

CV- Column volumns

DNA- Deoxyribonucleic acid

DTT- Dithiothreitol

EDTA- Ethylenediaminetetraacetic acid

EOM- Ensemble optimisation method

FoXS- Fast x-ray scattering

FRET- Forster resonance energy transfer

GSH- Glutathione

GST- Glutathione S-transferase

GST0-1- Glutathione S-transferase omega 1

GUV- Giant unilamellar vesicles

HEPES- 4-(2-hydroxyethyl)-1-piperazineethansulfonic acid

HSQC- Heteronuclear single quantum coherence spectroscopy

IscU- Iron-sulfur cluster protein U

kDa- Kilodalton

LB- Luria borth

MAD2- Mitotic arrest deficient 2

MLKL- Mixed lineage kinase domain-like protein

MR- Molar ratio

MST- Microscale thermophoresis

NCC27- Nuclear chloride channel-27

NMR- Nuclear magnetic resonance

NUS- Non-uniform sampling

PEG- Polyethylene glycol

pH- Potential of hydrogen

pHLIP- pH-low insertion peptide

RDC- Residual dipolar couplings

ROS- Reactive oxygen species

RPM- Revolutions per minute

SapA- Saposin A

SAXS- Small angle x-ray scattering

SEC- Size exclusion chromatography

TEV-Tobacco etch virus

TM- Transmembrane

TRIS- Trisaminomethane

TROSY- Transverse Relaxation Optimised Spectroscopy

Chapter 1: Introduction

1.1-Chloride intracellular channel 1

1.1.1 The discovery of NCC27

CLIC1 was initially discovered as the first ion channel to be present in the nuclear membrane. Previously it was believed that ion channels only exist at the plasma membrane of cells. It was discovered as a homologue to p64 in rat tissues and began the discovery of the entire class of the chloride intracellular family of proteins. Initially named Nuclear chloride channel-27(NCC27) (Howell, Duncan and Ashley, 1996).But after CLIC1 was discovered in the cytoplasm and in the plasma membrane in addition to the nuclear membrane it was renamed to Chloride Intracellular channel (Tonini *et al.*, 2000a). CLIC1 was identified to exist as a small 27kDa protein in the cytoplasm after being expressed in addition to the chloride ion channel in the membrane. (Valenzuela et al., 1997). The electrophysiological characteristics of the chloride ion channel were identified to be the same whether embedded into the plasma membrane or the nuclear membrane. Using antibody tagging it was identified in the membrane, the N terminal side exists on the outside of the membrane and C-terminus projecting inwards of the membrane (Tonini *et al.*, 2000b)

This 241 amino acid protein was discovered to be highly conserved among many species and is widely expressed among cells and tissues in mammalian cultures (Duran et al., 2009).However when cultured in non polarized cells, the large majority of CLIC1 was present in the cytoplasm and a small minority was present in the plasma membrane. Although in polarized cells the large majority of CLIC1 was present in subapical membrane vesicles and a much smaller amount in the cytoplasm (Ulmasov *et al.*, 2007). This was the first discovery that an equilibrium between membrane bound and cytosolic CLIC1 was cell type specific.

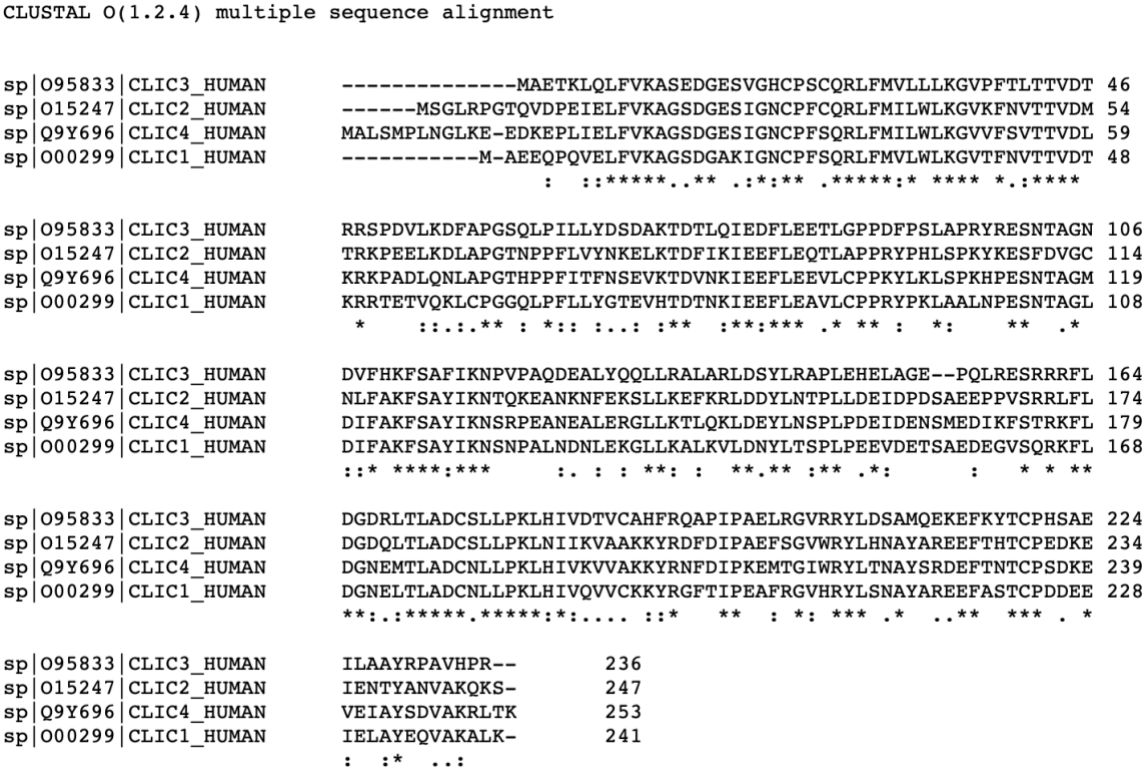


Figure 1.1: Sequence homology map for CLIC1-4. The homology map was generated using the Clustal Omega Multiple Sequence Alignment tool. The notation used in this alignment is “*” when referring to complete identity of a residue across all CLIC members. “:” denotes when 3 of the four CLIC members have sequence identity and “.” is used to denote when 2 of the four CLIC members have an identical residue.

1.1.2 The metamorphic ability of the CLIC family

The discovery of CLIC1 to exist in two different forms as an active chloride ion channel and as a soluble protein led to the question of how this equilibrium is controlled. Cytosolic CLIC1 can under certain stimuli can exhibit structural plasticity that allows significant structural changes to facilitate likely as a higher order oligomer its insertion into the membrane. The first stimuli that was identified that could trigger membrane insertion was oxidation. Oxidation caused a covalent bond to form between residues Cys-24 and Cys-59 that stabilised a dimeric form. The use of hydrogen peroxide was able to cause significant structural changes in the dimeric form that exposed a hydrophobic surface that was believed could dock to the membrane. This led to the first hypothesis of understanding the metamorphic ability of CLIC1, that it is redox controlled (Littler *et al.*, 2004). In this model published they demonstrate that CLIC1 interacts with lipids prior to oxidation. So it remains unclear how such an event occurs when the hydrophobic region of CLIC1 is still occluded by the structure.

Another hypothesis that was proposed is that the insertion of soluble CLIC1 into the membrane is controlled through a reduction in pH. A decrease in pH has been documented to promote the interaction of CLIC1 with lipids and hence the amount of active chloride channels present significantly increased upon the lowering of pH (Warton *et al.*, 2002a). Although pH had no effect on the structure of CLIC1 through CD and fluorescence spectra. In addition the lowering of pH did not promote the oligomerisation of the protein in the multimer that is predicted to act as the chloride ion channel.

Although further analysis also identifies CLIC1 chloride ion channel conductance to increase in the presence in basic conditions, with the lowest chloride conductance at a neutral pH of 7. Such a non-specific stimuli suggests the overall mechanism of

insertion is significantly more complex than a purely pH driven process (Tulk *et al.*, 2002a).

1.2- Metamorphic proteins

1.2.1- Proteins that exhibit metamorphic activity

For a small selection of proteins that have a defined 3D structure they are able to interconvert between multiple stable states over various timescales. Proteins naturally can exist as an ensemble and heterogeneity is a hallmark of a dynamic protein but metamorphic proteins differ in that the different states undergo large conformational changes largely in the absence of a ligand or cofactor (Dishman and Volkman, 2018).This again is distinguishable from Intrinsically disordered proteins as they lack a stable 3D structure and interconvert rapidly as an ensemble (Lella and Mahalakshmi, 2017).

The reasoning behind the metamorphic activity of some proteins has long been debated however it is largely agreed that if multiple states are present and can interconvert that each of those states of a metamorphic protein are responsible for a separate function (Madhurima, Nandi and Sekhar, 2021). In the case of the CLIC family, the membrane bound state acts a chloride ion channel and the other state which is a cytoplasmic protein is believed to provide an alternative function for the cell. Recent evidence suggests that the CLIC family in the soluble form has oxidoreductase activity. Fluorescece assays detected the ability of CLIC1,2 and 4 to reduce 2-hydroxyethyl disulphide which means CLIC could play an important role in protecting the cell from oxidative stress (Khamici H, 2015). Studies studying the oxidoreductase activity of CLIC1 demonstrated no activity was present in a C24A mutant (Turkewitz, 2021). This is surprising that the N terminal cysteine plays such an important role in the enzymatic activity of CLIC1 as this cysteine is not conserved across the CLIC family or CLIC homologues (the GST family) which one would expect to exhibit similar activity. Further studies are needed to confirm the role of the soluble form of CLIC1 in the cell.

However there are many other metamorphic proteins that exist. One is the iron sulfur cluster protein U (IscU). This protein exists as two distinctly different states. It can exists as a folded globular protein and a dynamically disordered structure (Jin *et al.*, 2009). Both these states interact with greater affinity to different proteins that play a role in iron-sulfur cluster biosynthesis and the interconversion between these states can be altered by pH and temperature. However both forms of IscU are required for biosynthesis and aberration of one form will affect biological function. Both states are required for the pathway but equally the equilibrium can be altered to favour one state if required for homeostasis (Markley *et al.*, 2013).

Selecase is a metamorphic protein that exists in 3 different structures. It is a metallopeptidase and exists as a monomer, dimer and tetramer. So in this case, the metamorphic protein interconverts between different oligomeric states as opposed to various conformations of the monomer. Interestingly, selecase use the oligomers in order to control activity of the monomer. The monomer is the only active version of the protein and the higher order oligomers are inactive. As the concentration of selecase increases, the activity of the enzyme decreases as the presence of higher order oligomers increases which is the inverse of normal enzymatic function. The metamorphosis acts as a mechanism to prevent uncontrolled function of selecase by promoting the inactive form as the concentration increases. This controls the equilibrium of selecase activity (Lõpez-Pelegrín *et al.*, 2014).

A further class of metamorphic proteins can exhibit metamorphosis between a soluble protein and a membrane bound protein. α and β pore forming toxins are examples of this (Iacovache, Bischofberger and van der Goot, 2010). They undergo large structural rearrangements from the soluble monomeric form to an oligomeric membrane spanning region. The β pore forming toxins undergo a transition that converts an alpha

helical domain into a long beta sheet that forms a large component of the pore in the membrane bound form (Tilley and Saibil, 2006).

1.2.2- The molecular mechanism of the metamorphic MLKL

Mixed lineage kinase domain-like protein shares many similarities with CLIC1 beyond its metamorphosis. MLKL can exist as a soluble peptide with 2 domains separated by a two-helical linker. The soluble form is perceived as the inactive form and phosphorylation can trigger conformational changes and oligomerisation that leads to insertion into the membrane (Dondelinger *et al.*, 2014).

The conformational change causes rearrangement of the N terminal domain to allow lipid interaction and insertion into the membrane. Once in the membrane, MLKL acts as a oligomer where it disrupts the structure of the membrane that facilitates cell death. So the membrane bound form is currently the only known active form of MLKL and it acts by disrupting the integrity of the membrane through forming a cation channel that causes a large influx or Mg^{2+}, Na^{+} and K^{+}. The large influx of ions disrupts homeostasis of osmotic potential and hence leads to necroptosis (Hildebrand *et al.*, 2014; Davies *et al.*, 2020).

1.3- CLIC1 structure in solution

1.3.1-The first crystal structure

The first crystal structure of CLIC1 was discovered in 2001 and was crystallised with glutathione bound to the redox active site. It was determined to exist as an N and C domain linked by a proline rich linker that spans from Cys89 to Asn100. In the N terminal domain there are 3 alpha helices and 3 beta sheets whilst in the C terminal domain there are no beta sheets. There are 3 large alpha helices, 3 small alpha helices and one of these smaller helices makes up the foot loop region which is determined to be largely flexible and extends from Leu148 to Arg165 through large B factor scores in the crystal structure 1K0M. In both structures there is no electron density for residues 1-5. However these residues are disordered and based on homology modelling likely just extend out from the structure with a large degree of flexibility (Harrop et al., 2001). The foot loop region is also completely disordered in some the crystal forms discovered by this same group.

The structure also demonstrates the predicted transmembrane domain that spans from residues 24 to 46 consists of one alpha helix, beta sheet and loop. Mutations of R29A and K37A altered the kinetics between the open and closed state in addition to altering the electrophysiological properties of the chloride ion channel (Averaimo et al., 2013).

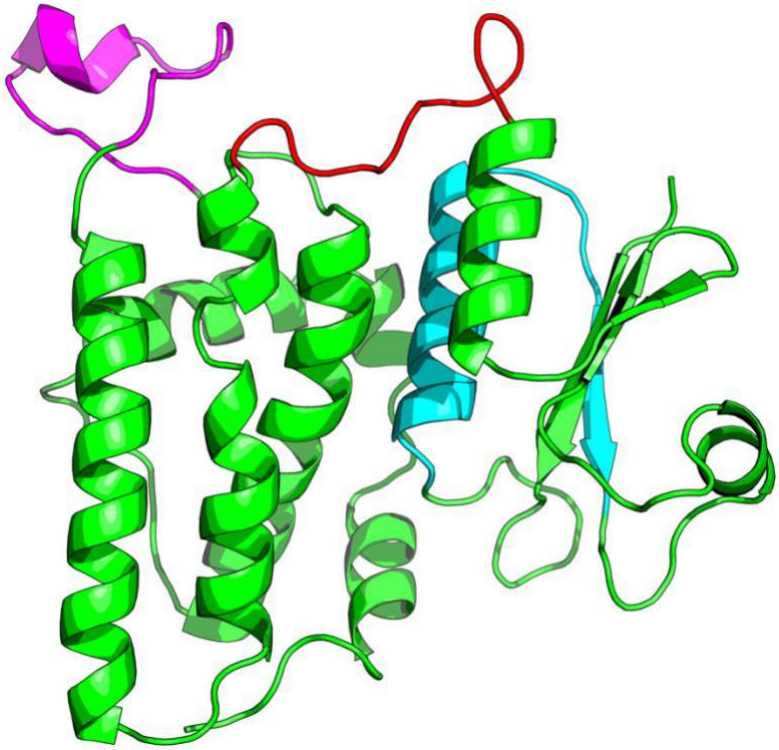


Figure 1.2: The CLIC1 1K0M crystal structure viewed in Pymol. 3 key parts of CLIC1 are depicted. Predicted transmembrane region (cyan) is residues 26-46, Footloop (magenta) is residues 147-165, Interdomain loop (red) is residues 88 to 101.

1.3.2- Homology of the CLIC1 structure

The CLIC1 family exist a classical Glutathione S transferase fold which makes these proteins part of the GST superfamily. The GST superfamily is largely responsible for the function of detoxification which is carried out by converting glutathione in the reduced form to electrophilic compounds (Townsend and Tew, 2003). One of the large difference between the GST family and the CLIC family is that the GST proteins largely exist as stable dimers whereas in the CLIC family they largely exist in a monomer-

dimer equilibrium. With the dimer being held together by non-covalent interactions that facilitates the conversion between the two states (Littler *et al.*, 2004).

Of the GST superfamily, the CLIC proteins are most similar to the Omega Class (Dulhunty *et al.*, 2001). GST omega 1 exhibits 24% sequence identity to CLIC1 and adopts a very similar conformation with large parts of the C-terminus adopting the secondary structre of alpha helices and a linker also exists that bridges the N terminal domain and the C terminal domain.

The CLIC family is highly conserved in vertebrates with 6 CLIC paralogues present (CLIC1-6). With sequence identity across all six being in excess of 50% demonstrated in figure 1.3 (Rao *et al.*, 2017). There also exists CLIC1 homologues in invertebrates. Some recently studied homologues include EXC-4 in C.elegans, DmCLIC in Drosophila and SspA in bacteria. Although these invertebrate CLIC homologues demonstrate >35% sequence identity to its vertebrate counterparts. Conserved regions include large parts of the predicted transmembrane region. Interestingly the active site residues in CLIC for enzymatic reaction are often not conserved in the invertebrate CLIC proteins yet they are still able to insert into the membrane and act as a chloride ion channel (Gururaja Rao *et al.*, 2018).

A

%	CLIC1_HUMAN	DMCLIC_DROME	EXC4_CAELL
CLIC1_HUMAN	100	26.03	25.32
DMCLIC_DROME	26.03	100	41.34
EXC4_CAELL	25.32	41.34	100

B

%	CLIC1_HUMAN	CLIC2_HUMAN	CLIC3_HUMAN	CLIC4_HUMAN	CLIC5_HUMAN	CLIC6_HUMAN
CLIC1_HUMAN	100	60.17	50.85	66.39	62.66	61.83
CLIC2_HUMAN	60.17	100	49.15	63.82	63.97	62.70
CLIC3_HUMAN	50.85	49.15	100	49.15	50.42	47.46
CLIC4_HUMAN	66.39	63.82	49.15	100	73.12	72.95
CLIC5_HUMAN	62.66	63.97	50.42	73.12	100	54.11
CLIC6_HUMAN	62.70	62.70	47.46	72.95	54.1	100

Figure 1.3: Sequence alignment of CLIC1 compared to other members of the CLIC family and its homologues presented as a percent identity matrix. A) Human CLIC1 sequence alignment against 2 structural homologues that have been crystalised with a bound calcium atom. The two homologues are DmCLIC from the invertebrate Drosophila melanogaster and EXC-4 from the invertebrate Caenorhabditis elegans. B) Human CLIC1 sequence alignment against the other members of the human CLIC1 family, CLIC2-CLIC6.

1.3.3- Computational analysis of the CLIC1 structure

Molecular dynamic simulations and gaussian network models of the CLIC1 crystal structure were carried out to determine which regions of the structure exhibit structural plasticity. The results suggest there was high levels of plasticity in the N terminus, C terminus, the transmembrane region and the foot loop. With the Gaussian network models predicting greater levels of plasticity in N terminal loops than NAMD molecular dynamics predicts. In the crystal structure, the foot loop region is highly disordered and molecular dynamic simulations suggest this region of residues 147-164 undergoes the highest fluctuations within the protein. This results in a high number of different conformations the loop could exist as (Jones *et al.*, 2013).

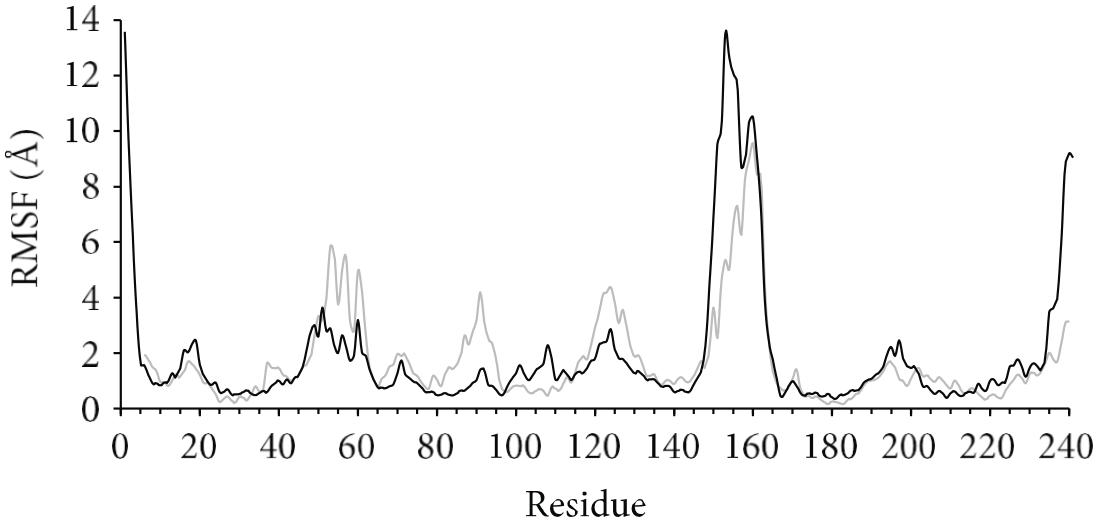


Figure 1.4: Computational analysis prediction of flexible regions of CLIC1. Residues are plotted against the root mean square fluctuations of Ca atoms from the 1K0M structure. The black trace describes root mean square fluctuations produced from molecular dynamics simulations from NAMD whilst the white trace is produced

from gaussian network models. High fluctuations seen in regions 48-63, 89-94 and the foot loop region at 146-165. Adapted from (Jones *et al.*, 2013).

1.4- Flexibility and stability of CLIC1 in solution

1.4.1- Flexibility of CLIC1 predicted from the crystal structure

When the original structure of CLIC1 was solved through crystallography and identified 1K0N there was some potential plasticity in the structure seen (Harrop et al., 2001). The N terminal and C- terminal domain are linked by a loop that extends from Cys89 to Asn100. The electron density of the structures showed some disagreement in the orientation of different structures. Two different conformations of the loop were identified and this displaced the position of the N terminal helices. The identification of two different conformations suggests there is plasticity in the loop linking the two domains. By allowing flexibility in this linker, it could potentially allow the possibility of a reorientation of the two domains in respect to each other (Ferofontov et al., 2018). The authors originally proposed this flexibility could be important to the function of the CLIC family to act as a soluble protein but also convert into a chloride ion channel (Harrop *et al.*, 2001).

1.4.2- Flexibility of CLIC1 is enhanced by the lowering of pH from 7.4 to 5.5

Chloride ion channel activity has demonstrated to be enhanced at pH 5.5 compared to a neutral pH of 7.4. Tryptophan fluorescence and light scattering data demonstrates CLIC1 does not change size or change the major state when the pH is lowered to 5.5. When urea is used to unfold CLIC1 at pH 7.4, the protein undergoes a 2 state model of folded to unfolded where all the secondary structure unfolds in one transition. However when Urea is used to unfold Clic1 at pH 5.5 the transition switches to a 3 state model. The presence of an intermediate appears to increase the α helical content of the protein and exposes a hydrophobic patch. The formation of this intermediate can also be stabilised at pH 7 if the temperature is increased to 37°C. This unfolded intermediate could potentially prime CLIC1 for membrane insertion by exposing the transmembrane region. Beta strand 2 also demonstrates a propensity to form an alpha

helix and it is believed this region could also play an important role in membrane insertion as part of the transmembrane region (Fanucchi, Adamson and Dirr, 2008a).

Hydrogen deuterium exchange using mass spectrometry also indicated an increase in flexibility at lower pH, 5.5. The greatest increase in hydrogen deuterium exchange rates occurred in the N terminal domain and in large parts of the transmembrane region. The rate increase of hydrogen deuterium exchanged provides evidence that these regions of CLIC1 are increasing their exposure to solvent as the pH decreases. The increased of flexibility of CLIC1 at lower pH is likely to aid its switch to a membrane protein as near to the membrane surface is significantly more acidic than the cytosolic region which exists at neutral pH. There are pore forming toxins in bacteria that have been demonstrated to form intermediates similar to this proposed mechanism for CLIC1 that would prime the structure for insertion (Stoychev *et al.*, 2009).

1.4.3- Flexibility of the transmembrane domain in CLIC1

The transmembrane domain of the CLIC family is predicted to be the helix a1 and the strand B2 both on the N terminal domain. This transmembrane domain spans residues Cys24 to Val46 in CLIC1 and is highly conserved among all the CLIC family. A peptide containing these residues was synthesised devoid of the remaining residues of CLIC1 and was incubated with either SDS micelles or palmitoyl-2-oleoyl-sn-glycero-3-phosphate (POPC) liposomes. In the presence of these membrane mimetic systems the entire transmembrane domain forms a helix which is in agreement with the predicted conformation of the transmembrane domain. There was also an increase in helical content of CLIC1 as the concentration of CLIC was increased. Given that oligomerisation is also concentration dependent, this suggests that the formation of the transmembrane helix may be a concentration dependent process and promoted through interaction with other TM domains. It also suggests that the dimerization and oligomerisation events seen by the CLIC family may involve interactions of the TM

domain given its ability to oligomerise without the remaining parts of the protein (Peter *et al.*, 2013).

Biophysical methods such as fluorescence resonance energy transfer (FRET) have identified separation of the N and C terminal domains to prime CLIC1 for insertion into the membrane. There was also increased FRET distances between Trp35 and Cys89 likely as a result of the transmembrane domain being buried in lipids which only occurred upon CLIC1 incubation with lipids. The shorter distances occurred with soluble CLIC1 and those FRET distances matched the predicted values from the crystal structure. Although the increased distances could also come as a result of intermediate states or oligomers not just the membrane bound form and so is difficult to truly identify the dynamics in this system (Goodchild *et al.*, 2010a).

1.4.4- The stability of CLIC1 is affected by Histidine mutations and Cysteine mutations

Clic1 at pH 7 undergoes a two state unfolding transition in chemical unfolding with Urea. At pH 5.5, this transition becomes a three state model with a stable intermediate state. With the H207F mutant the transition is identical to the wild type with two states at pH 7 and 3 at pH 5.5. Whilst with the H74A and H185F mutant, the dynamics of CLIC are altered such as that the stable intermediate can form even at neutral pH. This could be due to either due to the Histidines ability for pH sensing or alternatively the removal of key interactions within the N terminus that shift the thermodynamics to more favourably promote unfolding (Achilonu I, 2012).

1.5 - Divalent cations act as the trigger for membrane insertion of CLIC1

1.5.1 Zinc and calcium can promote a switch from soluble CLIC1 to a membrane bound channel

For many years the mechanism of the conversion of the CLIC proteins from a soluble monomer into a chloride ion channel has remained elusive. There are many reports suggesting oxidation acts as a trigger, pH plays a role in insertion and along with lipid composition. To an extent all these factors may still play an intricate role in this multi step process. But it was recently discovered that the use of Ca^{2+} ions and to a greater extent Zn^{2+} ions can promote insertion of CLIC into the membrane. When the binding of Zn^{2+} ions to CLIC1 is saturated, this results in the entirety of all soluble CLIC inserting as the membrane bound form. This clear mechanism was elucidated using microscopy and tryptophan fluorescence (Varela et al., 2019).

The mechanism describes a process by where Varela et al hypothesise that the levels of intracellular zinc which are linked upstream and downstream of ROS signalling is causing the molecular switch of CLIC1 into the membrane bound form. The use of ionomycin is known to increase intracellular levels of Ca and Zn. With treatment of ionomycin, the levels of CLIC1 inserted into the membrane increased drastically.

The binding of Zinc and Calcium was also identified using MST. MST is a biophysical technique used to determine protein-ligand interactions through the movement of fluorescent molecules. In the microscopy experiments, zinc promoted greater insertion into the membrane which was determined through tryptophan fluorescence of the membrane fraction containing protein and lipids. When the binding affinity was calculated, zinc and calcium had similar affinities. The affinities calculated were 0.3±0.1 mM for Ca^{2+} and 0.7±0.2 mM for Zn2. This suggests that the binding of Zinc must promote greater structural changes compared to the structural changes trigged by calcium. The authors propose the lowering of pH that promotes chloride efflux is

involved in the gating mechanism of the chloride ion channel as opposed to promoting the switch between soluble and membrane bound CLIC1 (Varela et al., 2019).

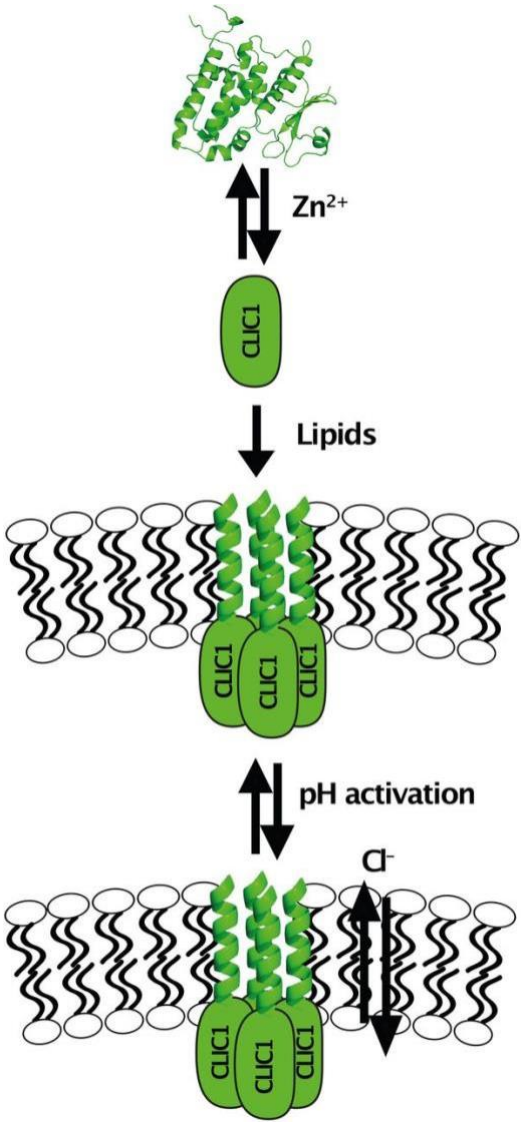


Figure 1.5: Current mechanism of CLIC1 membrane insertion and activation. The current data demonstrates that divalent cations can trigger membrane insertion of CLIC1, in particular Zinc. Prediction suggests Zinc binds to CLIC1 and triggers a conformational changes that causes CLIC1 to interact with the membrane and oligomerise. Once in the membrane, a pH gating mechanism controls the activity of the channel adapted from (Varela et al., 2019).

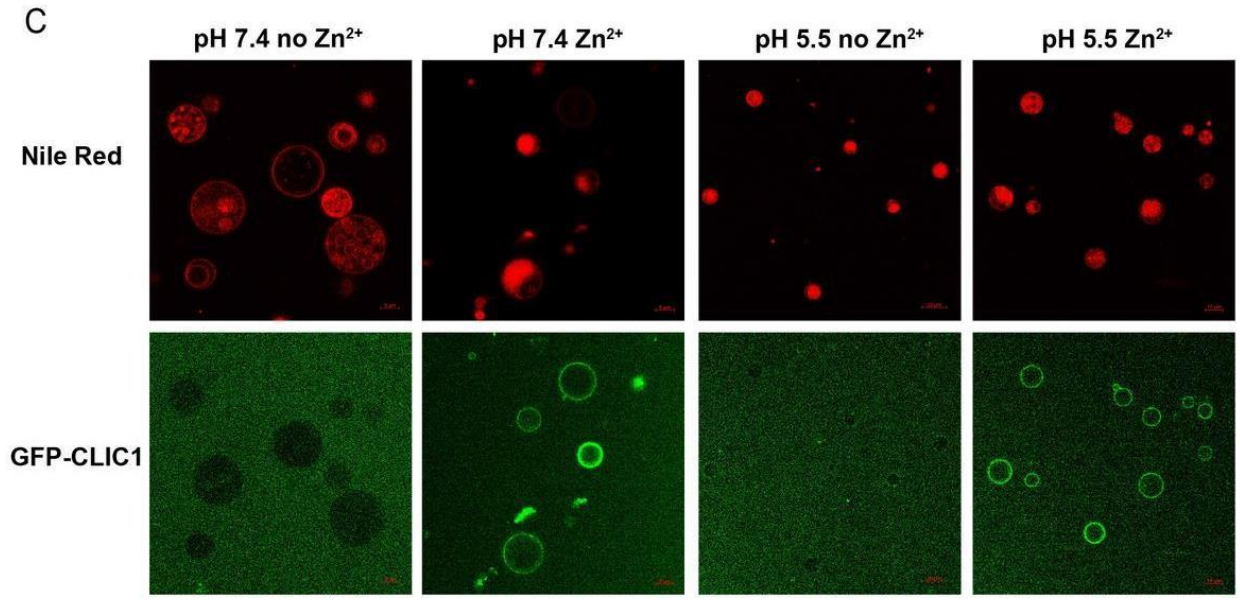


Figure 1.6: Fluorescence microscopy of GFP-labelled CLIC1 in Giant unilamellar asolectin vesicles (GUVS). The top row represents GFP-labelled CLIC1 in the presence of Nile red and the bottom row is without Nile red. At both pH 7.4 and pH 5.5, the addition of Zn^{2+} causes membrane insertion of CLIC1 into the asolectin vesicles. The insertion mechanism of CLIC1 is not pH dependent.

1.5.2- CLIC homologues EXC-4 and DmCLIC bind to Ca^{2+} ions

Exc-4 and DmCLIC are CLIC homologues from the organisms Caenorhabditis and Drosophila melanogaster. They are structural homologues of CLIC1 and share 20-25% sequence similarity with human CLICs. They both contain a putative transmembrane domain and are able to insert into lipid membranes where they can act as chloride ion channels. During the purification of these constructs, they were placed in a thrombin cleavage site containing 2.5mM CaCl2.

Upon analysis of the X-ray structure, a calcium ion was found bound to both homologues (2yv7 and 2yv9). The affinity of this divalent cation is likely to be high as calcium was not added to the crystallography samples nor the buffer in which the protein was purified.

The calcium ion was bound during the cleavage of the thrombin tag. In both structures the ion is bound in the same binding site.

The binding site exists between β-strand 3 and α-helix 3 and is ligated by residues Pro-84, Pro-85, Asn-97 and Leu-95 in EXC-4. The same residues are involved in coordinating the bound Calcium ion in DmClic. The affinity of the bound calcium ion is also likely to be high given the fact that many crystals were grown in the presence of 100mM EDTA (Harrop, S.J. *et al.* 2007*)*. This suggests that at lower concentrations of EDTA, the binding is not reversible. Although at high concentrations it may be able to coordinate the ligand. The calcium binding site also overlaps the GSH binding site, which indicates if the protein is bound to calcium it is unlikely to be able to bind GSH in solution. It also demonstrates a higher affinity for binding to calcium than GSH. It was initially believed the CLIC family might bind to GSH as part of its function as a soluble protein but the overlapping of these two sites suggests this function is unlikely (Littler, D.R. et al. 2004).

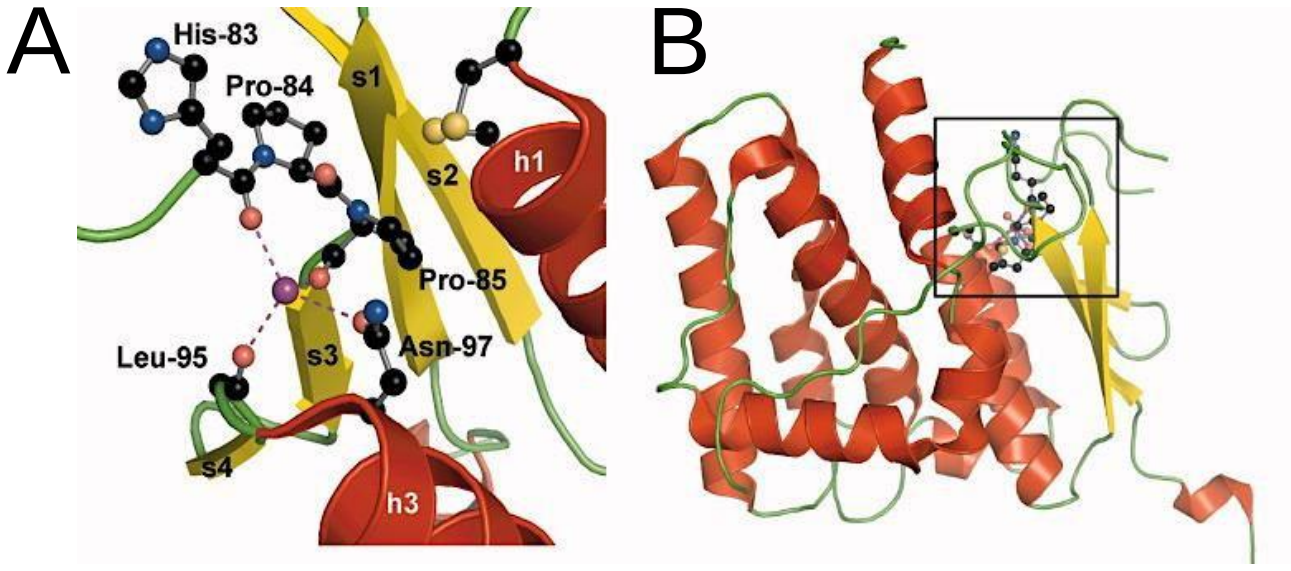


Figure 1.7: The calcium binding site for DmCLIC1 from the crystal structure 2yv7. A) The bound calcium is located in between a beta strand and an alpha helix in the N terminal side of CLIC1. With residues Leu-95, Asn-97, Proline-85 and Proline

84 making contact to the calcium ion through side chains. A purple dashed line represents interactions of side chains from residues to the calcium atom. The calcium atom is represented as a purple sphere. B) A zoomed out view of the calcium binding site within the context of the 2yv7 crystal structure. Adapted from (Harrop, S.J. *et al.* 2007*).*

1.5.3- Association of CLIC function and calcium

In the development of the tumours, reactive oxygen species act to induce oxidative damage to cells that can cause tumorigenic mutations. Changes to CLIC1 expression has been demonstrated to play a role in the homeostasis of reactive oxygen species levels but the mechanism is unclear. In Clic1 knockdown cells, the levels of intracellular calcium increased and this was also confirmed with the use of channel blocker IAA94 which also led to an increase in levels of calcium like the CLIC1 knockdown cells. In the CLIC1 knockdown cells, the levels of ROS were significantly elevated suggesting there is interplay between the two effects. So BAPTA-AM was used to act as an intracellular calcium chelator. The use of the chelator decreased the levels of intracellular calcium and the levels of ROS (Board *et al.*, 2004).

To confirm that levels of reactive oxygen species were not affecting calcium levels a antioxidant Trolox was added to CLIC1 knockdown cells. In the presence and absence of Trolox, there was no change to basal calcium levels. Demonstrating it is levels of calcium that alter the levels of ROS and not the inverse. CLIC1 as a membrane bound channel is able to affect the levels of calcium entering the cell. Through this calcium signalling mechanism, CLIC1 as a chloride ion channel is directly involved in tumorigenesis through the elevation of ROS (Lee *et al.*, 2019).

1.6- The Chloride Ion Channel

1.6.1- Structure of the chloride ion channel

In order to function as a chloride ion channel it has been proposed that the entire N terminal domain must reorganise in order to expose the transmembrane and hydrophobic stretch to lipids to allow the TM region to pass through the membrane. (Goodchild *et al.*, 2011). At a pH of 5.5, a more unstable and partially unfolded conformation of CLIC was identified (Fanucchi, Adamson and Dirr, 2008b).

Once in the membrane, each monomer or subunit of the channel only bridges the membrane once, although the entire number of TM regions and monomers that make up the entire channel is currently unknown. CLIC can insert into the membrane in a variety of oligomeric states although the chloride ion conductance changes between these states. A minimum of four monomers are required to form a fully functioning channel although it has been seen in CLIC5 that a large number of monomers can assemble to form a functioning mega-channel (Singh, Cousin and Ashley, 2007a).

When CLIC is oxidised although it does not promote oligomerisation it can promote insertion into the membrane. FRET studies have demonstrated oxidised CLIC exists as a varying amount of 6 to 8 subunits when inserted into the membrane as a functioning ion channel (Singh and Ashley, 2006). Although this may not be relevant in vivo and oxidised CLIC is not required for a functional ion channel. But it does again demonstrate the need for multiple monomers to combine to create an ion channel.

Although there has been differences in chloride conductance between native chloride ion channels and recombinant proteins reconstituted in lipid bilayers. Which suggests there are intermediate modifications to CLIC1 that occurs in vivo.

1.6.2- The composition of the lipid bilayer affects membrane insertion and chloride channel activity

It is known that the interaction of proteins with a lipid membrane can be aided or altered by the composition of lipids that exist within the membrane and by the amount of cholesterol in the bilayer. It has been demonstrated that an increase in cholesterol levels not only increases the rate of insertion of CLIC1 into lipid bilayers but also increases the level of chloride conductance of the channel. The maximal percentage of cholesterol used was 16% which up to that value showed an increase in chloride ion channel activity (Valenzuela *et al.*, 2013). Although in vesicles where cholesterol levels were as high as 30%, this demonstrated a significant decrease in chloride channel conductance (Tulk *et al.*, 2002b).

The use of X-ray and neutron scattering data indicated a cholesterol binding site in Clic1 with a GXXXG motif that is conserved in the CLIC family and its homologues that also insert into the membrane. Specular reflection determined the thickness of the insertion of CLIC1 into the membrane and with cholesterol CLIC1 inserted deeper into the membrane than without. When the two glycine residues of the GXXXG motif are mutated, it significantly impairs the ability of CLIC1 to bind to the membrane. When cholesterol is present in membranes, CLIC1 demonstrated significantly higher membrane interaction. Although the development of a model of a CLIC1- cholesterol complex is still not provided with experimental data. Only a prediction of several potential cholesterol binding sites is given. It is also important to point out within this experiment calcium was used in addition to cholesterol and the experiments without cholesterol lacked calcium. The addition of calcium in the cholesterol samples are likely to have an impact on the ability of CLIC1 to insert into the membrane (Valenzuela et all, 2019).

1.6.3- Mutagenesis studies identify important residues for Chloride channel conductance

Charged residues in ion channels are often involved in the mechanism of ion transport often through selectivity filters or gating of the channel. As such in CLIC1 there are two charged residues that exist within the transmembrane region. These two residues are R29 and K37. Both residues were mutated to alanine in separate studies and distinctly changed the properties of the channel.

The K37A mutant caused an increased in chloride ion channel conductance. A faster flow of ions is surprising given that positive residues was thought to attract negative ions such as the chloride ion in the mechanism of the channel. Although this increase in chloride conductance occurred at a variety of membrane potentials, the mutation has no effect on the kinetics of the open and closed conformation times. Whilst the R29A mutant causes a change in the biophysical properties by increasing the likelihood the channel exists in the closed state. The channel conductance for R29A was almost identical to the wild type channel however at a negative membrane potential the existence of the closed state was elevated by the mutation.

1.7 Implications of CLIC proteins in disease progression

1.7.1 The role of CLIC in tumourigenesis

CLIC1 has been demonstrated to play a role in tumourigenesis. CLIC1 is overexpressed in cancers such as breast cancer (Wulfkuhle et al., 2002), gastric cancer, colorectal cancer etc. Due to overexpression of CLIC1, it can act as a tumour marker where it can be detected in the plasma of patients. Although conversely downregulation of CLIC1 has also been demonstrated to enhance proliferative activity and reduced the number of cells entering apoptosis.

The upregulation of CLIC1 as a chloride ion channel is demonstrated to play an important role in the development of Glioblastoma which is the most aggressive form of brain tumour seen in vertebrates (Wilson *et al.*, 2004).

The overexpression of CLIC1 as a chloride ion channel is seen to be directly correlated to the increase in tumour grade with the highest level of expression in Glioblastoma. The chloride ion channel provides an advantage for cancer stem cells as it aids migration and invasion and promotes tumorigenesis (Setti *et al.*, 2013).

Cancer cells are able to invade the space around by using invadopodia which protrude into the surrounding area. Upon exposure to extracellular vesicles cancer cells showed invadopodia formation. This demonstrates through this mechanism extracellular vesicles can transfer CLIC1 proteins and contribute to the formation of invadopodia. This provides a direct mechanism through which CLIC1 promotes malignant transformation and tumour proliferation (Thuringer *et al.*, 2018).

CLIC1 has been heavily implicated in its role in pancreatic cancer to the point that its role within the development of the cancer has been classed an oncogene. The study

demonstrated that there was an upregulation in the expression of CLIC1 in tissues extracted from pancreatic cancer compared to healthy control tissues.

In addition, an increasing amount of CLIC1 in tissues directly correlated with the increasingly severity of grade of tumour and was inversely linked with patient survival. This suggests a role in CLIC1 in the development of the tumour. Since the study determined, the overexpression of CLIC1 as an independent factor in predicting the patients prognosis, it presents a novel avenue for drug design specifically for pancreatic cancer (Peretti *et al.*, 2014).

CLIC1 knockout pancreatic cells presented with reduced levels of cell proliferation, migration and ability to invade. This would explain the link between poor prognosis and high levels of CLIC expression as these traits clearly aided by CLIC1 provide advantageous traits for the development of the tumour (Lu *et al.*, 2015).

1.7.2 The role of CLIC in neurodegenerative diseases

A large number of neurodegenerative diseases including Alzheimers are believed to be aided by inflammatory reactions that involve microglial activation. The proliferation of the microglial cells in these inflammatory reactions require chloride currents to stimulate this process. CLIC1 is demonstrated to play an active role in promoting microglial activation. β amyloid protein infiltrates microglia and exerts a toxicity on the microglia which is a characteristic of Alzheimers. When B amyloid is incubated with microglia, CLIC1 expression increases along with chloride conductance (Novarino *et al.*, 2004).

In addition, the activation of the microglia produces reactive oxygen species (ROS) in the cell. The reactive oxygen species is known to cause neurodegeneration which contributes to Alzheimers disease. When CLIC1 was inhibited in its channel form, this

results in a loss of chloride conductance from the channel and also inhibits the production of reactive oxygen species. This demonstrates the important of CLIC1 channel activity in the production of ROS by microglia. It is also shown that B amyloid protein promotes the translocation of soluble CLIC1 to the membrane where it acts as a chloride channel. Therefore the B amyloid protein directly causes a mechanism to promote chloride conductance and the promotion of ROS that leads to neurotoxicity and Alzheimers disease (Milton *et al.*, 2008).

1.7.3 The role of CLIC in cardiovascular disease

In the development of atherosclerosis, a key step is oxidative damage to endothelial cells which leads to inflammation. Oxidative damage is caused by the production of reactive oxygen species (ROS). In patients with atherosclerosis, CLIC1 is overexpressed which suggests the channel plays an important role in the progression of the disease. The CLIC1 knockout cells used were human umbilical vein endothelial cells. These cells and cells which had the CLIC1 inhibitor indanyloxyacetic acid-94 saw reduced ROS production. This demonstrates a clear mechanism about which overexpression of CLIC1 can contribute to the development of atherosclerosis in humans and cause cellular oxidative stress (Xu *et al.*, 2016).

The intracellular chloride channels have also been proven to play a role in the development of atrial fibrillation which refers to a arrhythmia or a irregular heartbeat. In patients with AF CLIC 1, 4 and 5 were upregulated in cells when analysed using electron microscopy (Jiang *et al.*, 2017).

The CLIC family has also been demonstrated to play a clear role in the development of pulmonary hypertension(PH). In patients with pulmonary arterial hypertension, endothelial cells were extracted and elevated expression of CLIC4 was identified.

CLIC4 overexpression affects the integrity of the endothelial lining of the heart and this allows the influx of inflammatory mediators and cytokines that lead to inflammation. CLIC4 knockout mice had a reduced ability to develop pulmonary hypertension (Wilkins et al., 2014).

1.7.4- The role of the CLIC family in hearing loss

CLIC5 was implicated in hearing loss in a Turkish family that experience an impairment of hearing as an autosomal recessive disorder. It was a result of the introduction of a mutation to residue 96 in CLIC1 that introduced a stop codon. The result is a severely shortened CLIC5 that lacks the entirety of the C terminus. This mutation results initially in minor hearing loss but ultimately progresses into severe or complete hearing loss (Seco *et al.*, 2015).

In the mice model, mice with a jitterbug mutation also have a complete absence of CLIC5. In these jitterbug mice without CLIC5 they presented with complete deafness around the age of 7 months. In mice with the absence of CLIC5 there was a reduced number of vestibular hair cells which are sensory receptors found in the inner ear (Gagnon *et al.*, 2006). It is predicted the absence of CLIC5 results in the disruption of cytoskeletal filaments or by impacting the transport of chloride ions in these vestibular hair cells which ultimately affects the structure of the hair cells in the inner ear causing hearing impairment (Singh et al., 2007b).

1.7.5- CLIC1 as a cancer therapeutic target

Early evidence has indicated the potential viability of CLIC1 as a cancer therapeutic target (Peretti *et al.*, 2014). The reason is due to the differentiation between CLIC1 in cancer stem cells and normal stem cells. Clic1 exists largely in the cytoplasm in stem cells and largely exists as a chloride ion channel in the membrane in cancer stem cells.

Thus it allows drugs to target at the membrane bound form of CLIC1 to not bind to and inhibit the function of CLIC1 in the cytoplasm.

One of the most promising drugs to target CLIC1 to date is metformin. The activation of CLIC1 during mitosis allows metformin to be a selective inhibitor of CLIC1 during mitosis so its acts to slow down cell cycle progression and reduce proliferation of cancer cells. Metformin is traditionally used to treat type II diabetes however recent evidence demonstrates that Metformin acts as a strong inhibitor of the Akt-dependent cell survival pathway.

The current pathway through which metformin inhibition of CLIC1 prevents proliferation is currently unknown. However this is the proposed pathway as CLIC1 promotes progression of cervical cancer through the pathway. Interestingly Metformin did not inhibit the pathway in differentiated cells which demonstrates its potential specificity for cancer cells. The drug has an antiproliferative effect that has a significantly higher efficacy for glioblastoma cells and tumour initiating cells than it does for healthy stem cells. Although this data has only been demonstrated in vitro and further studies must be completed in vivo to demonstrate the potential uses of Metformin as a potential therapeutic (Würth *et al.*, 2013).

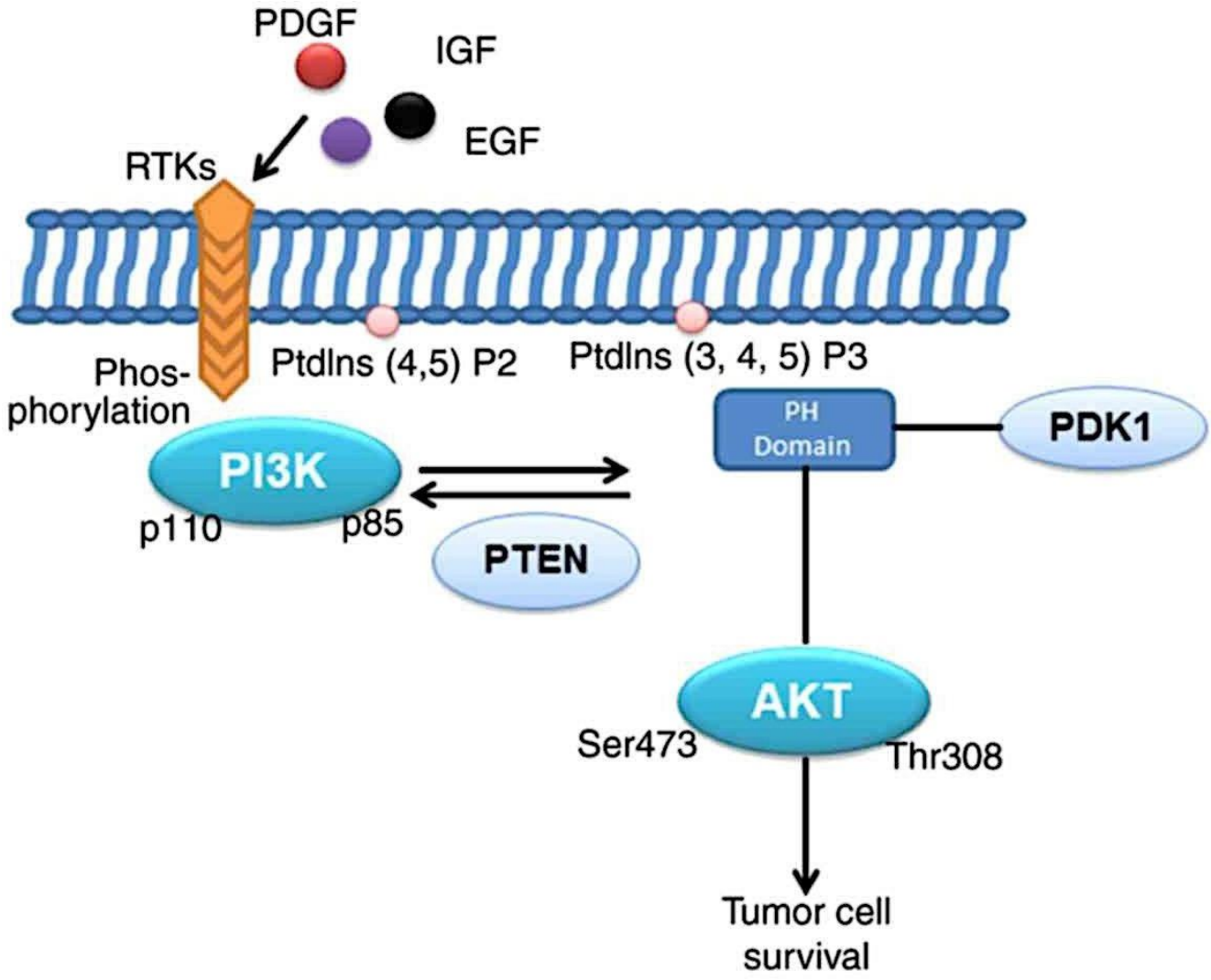


Figure 1.8: The proposed pathway through which metformin inhibition of CLIC1 leads to reduced cancer cell proliferation. Metformin inhibits CLIC1 which in turn inhibits the PI3K/AKT pathway. PI3K/AKT pathway is dysregulated in cancer cells and promotes cell growth, proliferation, survival and metabolism that aids cancer cell progression. Adapted from (Qu *et al.*, 2022).

A further study attempted to elucidate the mechanism of antiproliferative activity of Metformin. Evidence proved in agreement with a previous study that Metformin only exhibits its activity when CLIC1 undergoes metamorphosis and inserts into the membrane as a chloride ion channel. Similarly Metformin provides no antiproliferative

effects. In cancer stem cells, CLIC1 is activated during mitosis and hence the role of Metformin in preventing proliferation of cancer stem cells is by slowly down cell cycle progression. Further studies indicated that a mutation of Arg29 to Alanine prevented the effects of Metformin on reducing proliferation (Gritti et al., 2013).

Another drug that has potential therapeutic benefit by inhibiting CLIC1 is IAA-94. The use of IAA-94 was demonstrated to significantly reduce the chloride conductance of the channel which in turn reduced the proliferation of microglia. In addition when artificial bilayers were used, it completely inhibited chloride conductance if the use of IAA94 saturated CLIC1. Although studies have yet to determine whether IAA94 binds to the soluble form of CLIC1 or the membrane bound form (Warton *et al.*, 2002b).

1.8- Protein NMR

1.8.1- Introduction to NMR

In an NMR experiment, the sample acts like a magnet when placed in an external magnetic field, B_0. Nuclei which have an even number of protons and neutrons do not have a spin and a magnetic moment in a magnetic field.. Nuclei such as ^{1}H, ^{15}N and ^{13}C have a spin of ½ due to sum of neutrons and protons being an odd number. In a magnetic field, these nuclei either align with the magnetic field referred to as a parallel orientation or against the magnetic field referred to as an antiparallel orientation. Nuclei that align with B_0 are seen as low energy and nuclei that align in an antiparallel orientation are depicted as high energy. In an NMR experiment, the frequency that causes the nuclei to flip from the lower energy level to the higher energy level is measured (Mlynárik, 2017).

1.8.2- The HSQC is the gold standard for protein NMR

Nuclear magnetic resonance is a powerful tool that can provide information to both structure and dynamics of proteins in addition to interactions between ligands and proteins. This information is derived from the fact that each atom in a different environment inside a molecule such as a protein can give rise to a unique spectroscopic signal whose frequency depends upon a phenomemon called the chemical shift. Given the large number of atoms seen in macro molecules such as proteins and a limited possible range of chemical shifts for each nucleus this can often lead to overlap of signals for atoms and overcrowding of the spectrum. To reduce this effect, isotope labelling is commonplace to provide higher resolution between peaks of a protein spectrum. ^{1}H is naturally more abundant in proteins than ^{15}N. By uniformly labelling all nitrogen atoms as ^{15}N this increases the abundance of nitrogen isotopes for NMR increasing the signal to noise. The most common types of labelling for

proteins is ^{15}N labelling for a 2-dimensional NMR spectrum and in addition to this ^{13}C labelling for a 3- dimension NMR spectrum (Tugarinov, Kanelis and Kay, 2006).

Most of the 2D and 3D-NMR experiments currently used are built upon from the Heteronuclear Single Quantum Coherence (HSQC) experiment. This experiment is heteronuclear because the resulting spectra show correlations or peaks between two different nuclei, typically ^{1}H and ^{15}N or ^{1}H and ^{13}C. In typical heteronuclear correlation spectra each axis of the spectra reports on a single nucleus. In the case of proteins this results in a single peak per residue from the backbone as there is only one amide bond per residue with the exception of proline which cannot be seen on an HSQC. The HSQC depends on a network of strong J-couplings in the backbone of the protein. J couplings are defined as an interaction between nuclei with spin mediated through bonds. In the HSQC the J couplings result in fast transfers of magnetic excitation leading to sensitive spectra (protein NMR signals decay quickly due to molecular tumbling).

The 2D ^{1}H-^{15}N HSQC pulse sequence (fig 1.9) which forms the building blocks of many other NMR pulse sequences used today is relatively simple to describe and can be dissected into a set of consecutive blocks. In order it first involves a relaxation delay D1 which brings the magnetisation to equilibrium. This is followed a ^{1}H-^{15}N INEPT sequence which acts as the preparation time and selectively transfers excitation between nuclei $^{1}H \Rightarrow ^{15}N$ in this case or ^{1}H-$^{13}C \Rightarrow ^{15}N$-$^{13}C$ etc in other sequences. This is followed by an evolution time to allow for detection of the second or 'indirect' dimensions chemical shifts (in this case ^{15}N). This is followed by another mixing time which is a reverse ^{1}H-^{15}N INEPT sequence (transferring magnetisation between $^{15}N \Rightarrow ^{1}H$ before finally an evolution time to allow for detection of signals from the directly detected nucleus which in this case and typically is ^{1}H; as this gives maximum

sensitivity . The signal is measured as a set of decaying sinusoidal signals at the frequencies of the observed nuclei and is described as a Free Induction Decay or FID. During the acquisition a series of decoupling pulses are applied on the indirect channel (^{15}N) to remove ^{1}H-^{15}N couplings which would otherwise spit the spectrum of each peak into a pair of signals separated by the ^{1}H-^{15}N J coupling $^{1}J_{HN}$ (Marion, 2013).

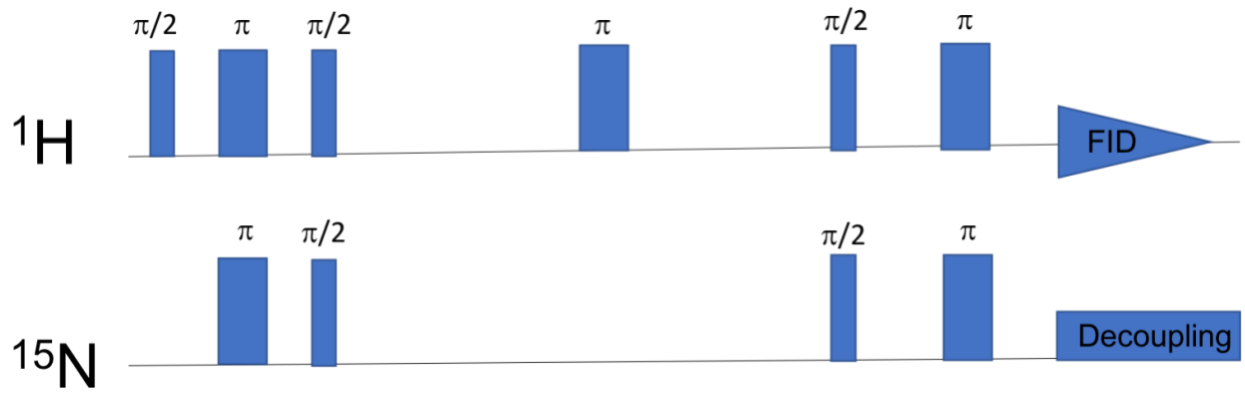


Figure 1.9: Pulse sequence for typical HSQC experiment. The sequence measures correlations between two (hetero) nuclei through J-couplings. The two lines labelled ^{1}H and ^{15}N represent two channels in the spectrometer which may be independently pulsed and are selective for the relevant nuclei. Time flows from left to right. Broadband non-selective high power pulses are represented by square boxes of different lengths single width = π/2 and double width = π. The acquisition of the data in the direct (^{1}H) dimension is represented by a triangular filled symbol labelled FID which represents the acquisition of the raw signal. The low box on the indirect channel (^{15}N) represents the ^{1}H-^{15}N decoupling sequence.

For larger proteins, in the case of ^{1}H-^{15}N correlation the experiment is modified into an optimised method called the Transverse Relaxation Opimised SpectroscopY or the TROSY experiment which measures one of the 4 sub components of the coupled

correlation spectrum peak which are separated by $^{1}J_{HN}$ in each dimension. For an HSQC, one peak is present for each residue so for larger proteins then the number of residues increases and hence the number of peaks. This results in a greater chance of signal overlap and overcrowding leading to poor spectral quality. This problem is aggravated in the case of larger molecules (typically RMM > 25 kDa that tumble more slowly because of their molecular mass). In an HSQC, for proteins with a lower molecular weight it makes sense to measure the combined peaks in the HSQC multiplet of 4 peaks to create a peak that maximises signal to noise. However, the four peaks of the multiplet return to equilibrium (or relax) at different rates with one peak relaxing slowly to give a very sharp line (the TROSY peak), two relaxing at a mixture of slow and fast rates called (semi TROSY peaks) giving and one relaxing very quickly (anti-TROSY) which is very broad.

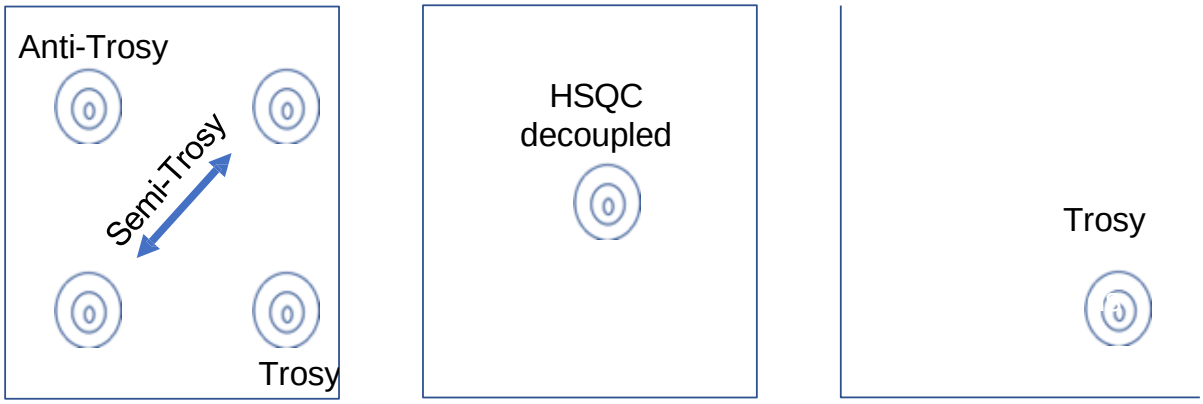


Figure 1.10: - The role of the TROSY peak in enhancing S/N in large proteins. Spectra run left to right. Far left spectrum represents a HSQC without a decoupling sequence. The four components are shown of the Anti-Trosy, 2 Semi-Trosy peaks, and the Trosy peak. The middle spectrum details a decoupled HSQC spectrum with only one peak that exists as an average of all 4 TROSY peaks. The far right spectrum is a TROSY spectrum where only the TROSY peak is selected to enhance signal to noise ratio in larger proteins >25kDa.

The TROSY peak is always sharper than the combined decoupled peak measured in an HSQC. However, for proteins less than 30kDa the height of the TROSY peak while having ¼ of the peak volume (peak area/volume is proportional number of nuclei measured) is less intense. However, above 30kDa the TROSY peak is so sharp that its intensity is greater than the decoupled HSQC which has 4 times the volume. Therefore a TROSY experiment that selects for the TROSY peak and filters out the other TROSY peaks that relax more quickly gives a sharper and more intense spectrum (Fernández and Wider, 2003).

1.8.3- Ligand interactions and chemical shift perturbations

To identify changes in proteins 3D structure and dynamics upon changes in environment or the addition of a ligand, a 2D ^{1}H-^{15}N HSQC spectrum is often used. For ligand binding, often a reference spectrum is created with no ligand present before a subsequent set of HSQC experiments are measured under the same conditions but with an increasing concentration of ligand, typically, if possible, until the binding site is saturated.

The binding events typically disturb NMR active nuclei in the ligand and residues within the protein through three mechanisms. One is through the ligand making direct contact with side chains or main chains of residues in the protein, this can cause conformational changes in the protein. Secondly the ligand has its own magnetic field and susceptibility which will affect that of the protein (this is especially important for aromatic and multiply bonded moieties which have ring currents which create local magnetic fields). Finally, the ligand can cause changes in the dynamics of the protein favouring one or more interchanging states which are accessible to the protein and have different chemical shifts which are observed as an average (Maity, Gundampati and Kumar, 2019).

Overall these chemical shift perturbation (CSPs) are seen as the peak assigned to a specific residue shifts position from that of the unbound state to that of the bound state as the titration goes on if the rate of exchange between the two states is less than the observed chemical shift difference between the two states (fast exchange). The observed shift is the average of that for the two states weighted by their populations. However, for systems where the rate of exchange is slower than the chemical shift due to tighter binding there will be two separate peaks seen for each affected residue, one for the bound state and one for an unbound state and these will be at the chemical shift expected for each of these states (slow exchange), and during the titration all that will happen is the intensity of the two peaks will alter reciprocally.

These chemical shift perturbations which occur for both ^{1}H and ^{15}N (typically calculated in the ratio of approximately 1:5 in magnitude) can be mapped onto the structure of the protein and identify regions of interest that alter their environment due to ligand binding. Typically these changes are localised to close proximity of the binding site ligand allowing the location to be localised onto the proteins structure if the peaks can be assigned to specific residues.

However, one of the difficulties with chemical shift perturbation data is distinguishing between residues that directly bind to the ligand or alter their environment as a result of conformational changes or allosteric changes in dynamics. Additional structural data is then required in order to make this distinction so in some (more rare) cases CSP values alone can sometimes lack specificity for determining their origin. It has also been found that for residues with lengthy side chains, interactions with ligands may sometimes result in little to no changes to the backbone resonances, therefore resulting in minor CSP changes. A consequence of this is that an important residue for ligand contact would be masked and not picked up by CSP changes.

Finally in some cases as the populations of the bound and free state change across a titration this can cause the signals to enter the so called intermediate exchange regime where the signal broadens sometimes to the point of disappearing (often at the midpoint of the titration). While this broadening contains information on exchange rates, it can also be problematic is the chemical shifts of the bound or free state are broadened so much they can't be observed. This is especially important if values of K_d are being determined from the titration as an incomplete titration curve, especially one missing the saturation point may not be suitable for fitting (Williamson, 2013).

1.9- The use of small angle x ray scattering in determining protein structure and dynamics

1.9.1- Theory of SAXS and sample preparation

SAXS is a useful technique for determining the conformations of flexible proteins in solution. It can identify both the shape and size of a protein in solution and even complexes of proteins. SAXS is a low resolution technique that provides fast data collection with sample preparation being minimal. This technique can provide information about the ensembles or lack thereof that exist in solution for proteins. The scattering data represents the sampling of space that exists as a result of the tumbling of the protein. The space sampled by the protein is a result of the averaging of all conformations in solution (Bernadó, Mylonas, M. v. Petoukhov, *et al.*, 2007).

Practically SAXS works by a solution of protein in buffer illuminated by an X-ray beam. The intensity of the X-rays scattered by the solution is recorded by the X-ray detector and averaged. When the X-rays pass through the sample, the intensity of the X-rays from the buffer is also collected and averaged. Hence in data processing, the intensity of the buffer X-rays is subtracted from the total intensity of the X-rays that provides only the intensity of the protein in question.

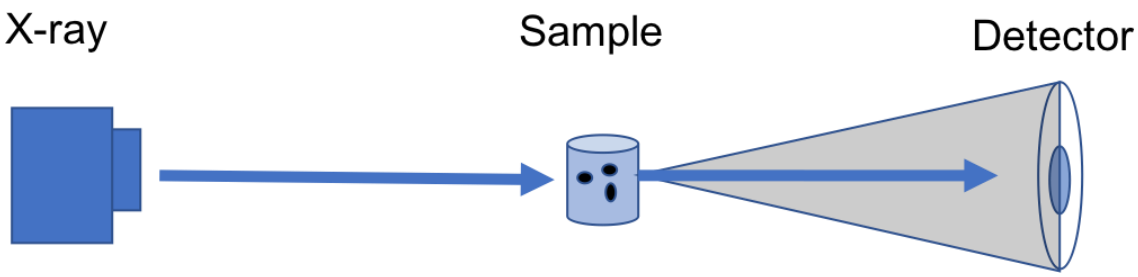


Figure 1.11: Small angle x ray scattering experiment- X-ray beam is used to illuminate the sample presented containing protein and buffer. The X-rays are scattered by the sample and hit the detector where they are recorded and averaged.

Many proteins exists in different oligomeric states in solution and to that extent SAXS is usually coupled to a size exclusion column. Common size exclusion columns used include the Superdex 200 which has a mass range of 10 to 600 kDa and the KW-Shodex 403 which provides a mass range of 10 to kDa. The use of a size exclusion column allows the user to separate SAXS raw data from different oligomeric states. The use of a column also identifies the presence of aggregation that could interfere with the quality of the SAXS data.

In order to receive high quality SAXS data that provides accurate data to the size and shape of the particles of the protein certain sample preparation considerations must be made. One consideration that must be made is radiation damage. 2% glycerol is typically added to the buffer used in SAXS and glycerol protects the sample against radiation damage. Radiation damage to a protein will result in potential unfolding or aggregation which can alter SAXS data leading to incorrect analysis. Another consideration is the quality of the sample itself. Poor sample preparation can lead to aggregation and denaturing of the protein that will result in incorrect size and shape analysis of the protein (Jeffries *et al.*, 2015).

1.9.2- Use of SAXS data to understand protein structure and dynamics

If the experimental scattering data matches the predicted scattering data of the crystal structure then the system exists as a monodisperse system. However in many cases where proteins are flexible and sample multiple conformations in space, the system exists as a polydisperse system. As such the flexible protein can not be represented

accurately by a single model and must require an ensemble modelling approach. The mixture of all ensembles in solution will then match the experimental scattering data (Bernadó, Mylonas, M. v Petoukhov, *et al.*, 2007).

In order to compare PDB's and experimental scattering data, the web server FoXS can be utilised (Fast X-ray Scattering). This web server is a rapid method for comparing a single or ensemble of structures against raw experimental data(Schneidman-Duhovny, Hammel and Sali, 2010). If the experimental data does match the model then this demonstrates a good fit however with poor fitting, the model/models presented then do not fully account for all conformations that the protein is sampling in solution. For monodisperse systems the model used will likely be a crystal structure. For a polydisperse system seen in SAXS, a collection of models will be averaged usually created by the use of the ensemble optimisation method (EOM).

Ensemble optimisation method is a multi-step process that results in an ensemble of structures that best describes and fits the X-ray scattering data. Using EOM, the initial input data requires the denotion of which parts of the structure are flexible and can be reorientated and which parts of the structure should act as rigid bodies and can not be flexible in model generation. The initial step is the generation of a large number of random models of different conformations of the protein based on the flexible regions defined by user input.

After the generation of typically thousands of heterogenous models all sampling different conformational spaces, the scattering scores of all the models are calculated. Then finally EOM attempts to find a minimum number of models that together combined best fit the experimental scattering data. Each ensemble of models generated by EOM will have a chi squared score based on its fit to the experimental

data. EOM will select the ensemble with the lowest chi squared score that denotes the best fit (Tria *et al.*, 2015).

1.10- Aims of the CLIC1 research

The aims and reasoning behind the title of this work was to identify structural insights into the soluble form of CLIC1 and into the mechanism of membrane insertion. The methodology behind understanding these two truths consisted of:

- Purify and understand the structure of CLIC1 in solution
- To identify flexible regions of CLIC1 and timescale upon which they move
- To understand regions of CLIC1 that are involved in its insertion into the membrane
- To utilise SAXS and NMR to provide information about structure and dynamics
- To predict regions of CLIC1 that are impacted upon Zinc binding
- To mutate residues in CLIC1 that are identified to be important from NMR studies

Chapter 2: Materials and methods

2.1 - Materials

2.1.1- General materials	Company	Product code
Asolectin		
Acrylamide(30%)	Fischer Scientific	A3699
Agar	Melford	A20020
Agarose	Melford	A20085
Ammonium persulfate	Fischer Scientific	A3678
Ampicillin	Melford	A40040
Calcium Chloride	Fischer Scientific	10161800
cOmplete mini Protease Inhibitor	Roche	4693124001
DTT	Melford	D11000
dH20		
D-glucose	Fischer Scientific	AAA1682836
EDTA	Fischer Scientific	S25687
Glycerol	Fischer Scientific	G33-500
Hepes	Melford	H75030
Imidazole	Fischer Scientific	
IPTG	Melford	I56000
Kanamycin	Sigma-Aldrich	K1377

Liquid Nitrogen		
Manganese chloride	Sigma-Aldrich	1375127
Potassium Phosphate	Sigma- Aldrich	P5655
Sodium Acetate	Fischer Scientific	S2889
Sodium Chloride	Fischer Scientific	S316060
Sodium Dodecyl Sulfate	Fischer Scientific	15525017
TEMED	Sigma Aldrich	GE17-1312-01
Tris	Melford	T60050
Tris-Base	Melford	T60040
Tryptone	Melford	T60060
Urea	Sigma-Aldrich	U5128
Yeast Extract	Melford	Y20025
Zinc Chloride	Sigma- Aldrich	208086

2.1.2- Buffers	Composition
Miller LB Broth	1% NaCl 1% Tryptone 0.5% Yeast Extract
Lysis buffer	1mM DTT 1mM EDTA 150mM NaCl 50mM Tris pH 8.0
Hepes buffer	10mM NaCl 50mM Hepes pH 7.4
Phosphate buffer	50mM NaCl 50mM Sodium Phosphate pH 7.4
Hepes NMR buffer	50mM NaCl 50mM Hepes pH 7.4
Sodium acetate buffer	20mM NaCl 20mM Sodium Acetate pH 5.5
Bis-Tris buffer	20mM NaCl 20mM Bis-Tris pH 6.5
M9 media(1L)	100ml M9 Salts 1ml of 1M MgSO4 1ml of 0.1M CaCl2 1ml of Ampicillin 1ml Thiamine HCL of 1M 4g of C13 Glucose 1g of NH4CL pH 7.4
Strep-column elution buffer	50mM Biotin+ Lysis buffer pH 7.4
TEV cleavage buffer	50mM Tris 1mM DTT 1mM EDTA pH 8
Nickel-column elution buffer	50mM Imidazole + Lysis buffer pH 7.4
Strep-column recharging buffer	100mM NaOH
M9 Salt solution10X	66g of NA_2HPO_4 33g of KH_2PO_4 5.5g of NaCl pH 7.4

2.1.3- Plasmids

CLIC1 and GST 0-1 were cloned into pET-28 vectors for expression and purification. Depending on the application, CLIC1 was cloned with a N-terminal His or a C-terminal GFP followed by a C-terminal His tag. In all cases, a TEV cleavage site was included. GST 0-1 has an N terminal his tag with a thrombin cleavage site.

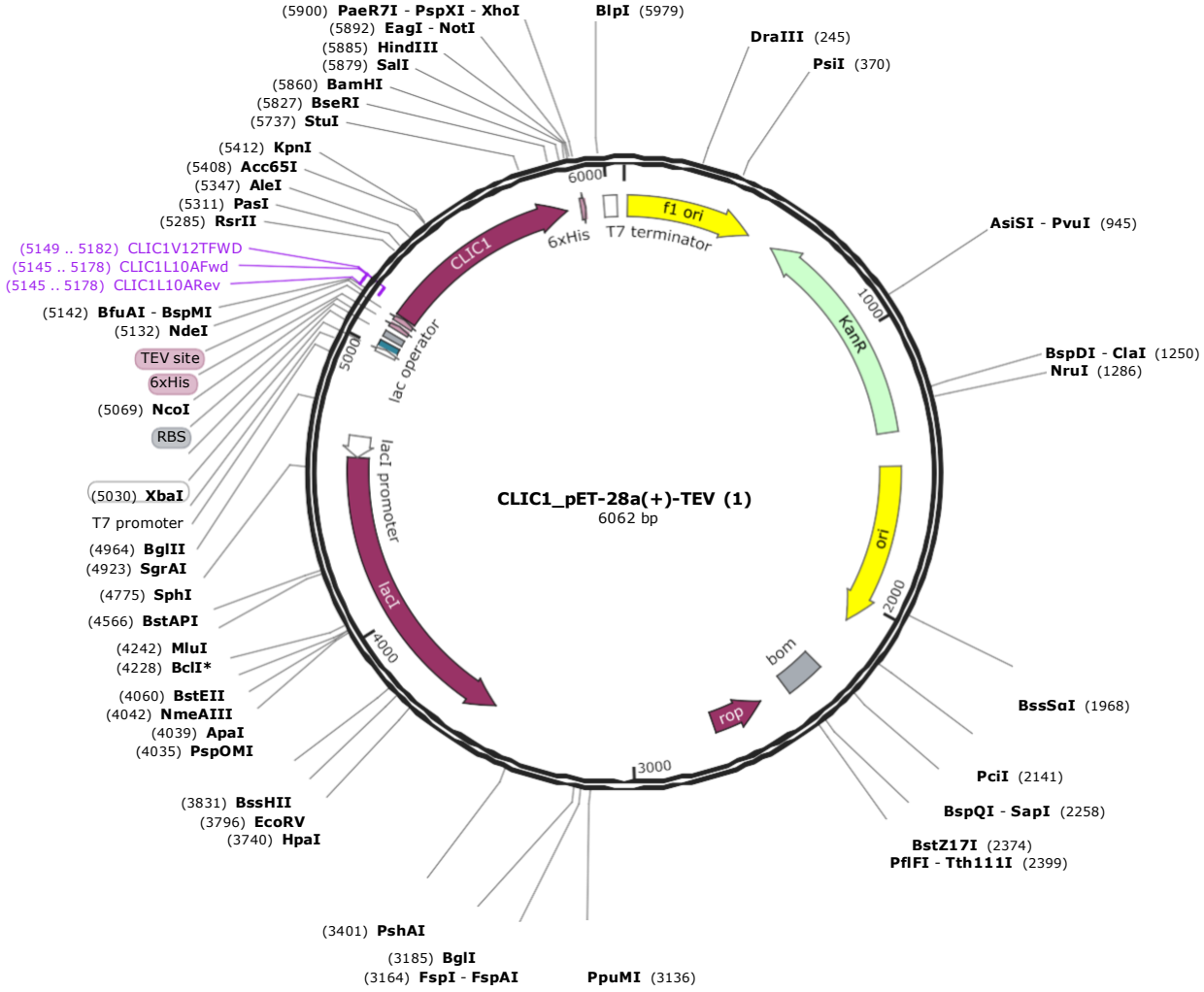


Figure 2.1: CLIC1_pET-28 DNA vector map- CLIC1 DNA map is complete with N terminal His-tag, TEV cleavage site and Kanamycin resistance.

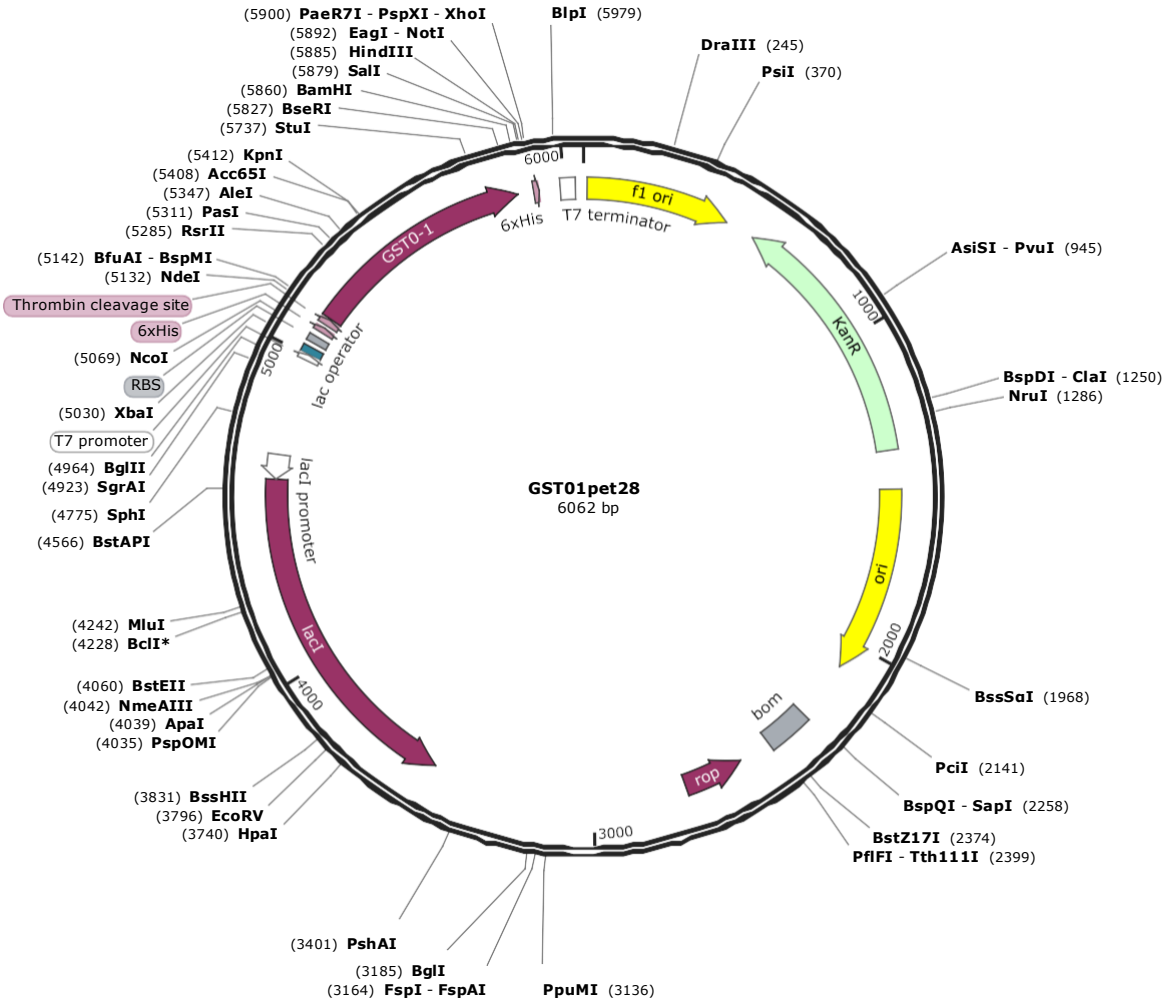


Figure 2.2: GST O-1_pET-28 DNA vector map- GST O-1 DNA map is complete with N terminal His-tag, thrombin cleavage site and Kanamycin resistance.

2.1.4- Bacterial cells

MAX Efficiency™ DH5α Competent Cells

OverExpress™ C43(DE3) Chemically Competent Cells

BL21(DE3) Competent Cells

2.1.5- Equipment

Centrifuge

MST plate reader

Nanodrop

600 and 800MHz NMR

Size Exclusion Chromatagram

Shaking Incubator

Stationary Incubator

Ultracentrifuge

2.1.6- Software	Application	Company
NMRview	NMR peak picking and generating peak lists	OneMoon Scientific
NMRpipe	Processing NMR data	NIH and NIST
QTIPlot	NMR analysis	IONDEV Srl

Pymol	View CLIC1 structure and NMR analysis	DeLano Scientific LLC
M0 Affinity Analysis	MST analysis	Nanotemper
Atsas software suite	SAXS analysis	EMBL
Scatter	SAXS analysis	European synchrotron radiation faciility

2.2- Methods

2.2.1- Transformation

1 µl of DNA (construct may vary) was added to 10 µl of C43 cells. This mixture was incubated on ice for 15 minutes. The mixture was then heat shocked for 45 seconds in a heat block before being transferred immediately to ice for a further 5 minutes. After this time elapsed 500 µl of LB broth was added to this mixture. The LB mixture is incubated at 37C for 1 hour shaking at 200RPM. After the 1 hour, 250 µl of the LB is streaked onto agar plates. The agar plates are left to dry before being inverted and placed in a stationary incubator at 37°C overnight. These plates are removed from the incubator after 12 hours and placed at 4°C.

2.2.2- CLIC1 expression and purification

A starter culture is prepared containing 400ml LB, 1mg/ml kanamycin. This starter culture is inoculated using a colony of CLIC1 from transformed C43 cells. This is grown overnight at 37°C at 200RPM which acts as the starter culture.

8L of LB media is prepared and each 1L has 50ml of LB added along with 1mg/ml of kanamycin. These LB growths are incubated at 37°C at 200RPM until they reach an OD of 0.7. Once they reach OD0.7, 1mM of IPTG is added. Upon addition of IPTG the culture is placed at 30°C at 200RPM for 16 hours. Upon which the cells are ready to harvest.

The cells are spun at 6000rpm for 15 minutes at 4°C. The supernatant is discarded and the cells are resuspended in 100ml lysis buffer with a c0mplete protease inhibitor tablet. Once resuspended, the cells are sonicated. 15 seconds of sonication and 15 seconds of rest for the cells for 15 minutes total. The sonicated cells are ultracentrifuged at 45000 rpm for 45 minutes at 4°C.

The nickel column is equilibrated using 5 CV of lysis buffer before the sample is added and passes through the column. 5 CV of lysis buffer is added to wash the column. 5 CV of elution buffer is added. Each of these samples are collected in 15ml falcon tubes and regeneration buffer is run through the nickel column. The elution sample is added to Tobacco Etch Virus protease at a concentration of 20mg/ml. This mixture is pipetted into a 7kDa dialysis membrane and placed into a TEV cleavage buffer at room temperature overnight.

After cleavage the nickel column is again equilibrated using 5CV of lysis buffer and the sample is added. The flowthrough is collected before the wash and elution buffers and regeneration buffers are added with 5 CV each. All samples are collected in 15ml falcon tubes. The flowthrough sample is placed in a 10kDa concentrator and spun at 4000rpm. The sample is concentrated down to 5ml total volume.

All fractions collected from the 2 nickel runs have 5ul of sample extracted and added to 15ul of loading dye. These samples are run on an SDS gel by gel electrophoresis and the resulting gel is stained by Instant Comassie Blue. The concentrated sample is added to the HPLC and fluorescence is measured at a wavelength of 280nm. The sample is gel filtrated into either 100mM NaCl 50mM Hepes pH 7.4 for general use or 50mM NaCl 50mM Hepes pH 7.4 for NMR samples. The fractions containing the monomer and dimer of CLIC1 are collected. These fractions are concentrated using the 10kDa concentrators to a desired concentration and frozen using liquid nitrogen.

2.2.3- CLIC1 M9 media expression

Cell cultures are grown to OD0.7 in LB media. After reaching 0.7, the LB is centrifuged at 6000rpm for 15 minutes at 4C. The supernatant is discarded and the pellets are resuspended by gently shaking in M9 media. The ratio of LB to M9 resuspension is

4:1. So in a typical growth 8L of LB is grown and the pellet is resuspended in 2L of M9 media. This media is then placed in a shaking incubator for 45 minutes at 30°C at 2000rpm. After this time has elapsed, 1mM of IPTG is added to induce expression of CLIC1 and cell cultures are left overnight for a minimum of 8 hours. For a single labelled growth N^{15} label is used and glucose. For a double labelled growth N^{15} and C^{13} is used in replace of the glucose. For a triple labelled growth, N^{15} and C^{13} are used with D_2O replacing the miliQ water used in the M9 media to remove the protons from CLIC1. In a triple labelled growth the sample after being produced is placed back into a miliQ water based buffer to back exchange the amides.

2.2.4- Protein concentration determination

Protein concentration is determined using the Nanodrop One at a UV absorbance of 280nm. A theoretical extinction coefficient of 17800 m^{-1} cm^{-1} was calculated using ProtParam for CLIC1 and 41160 m^{-1} cm^{-1} for GST o-1 (Gasteiger et al, 2005).

2.2.5- MST assay

All microscale thermophoresis experiments were performed on the Monolith NT.115 and used Monolith NT.115 capillaries. Samples contained a total volume of 50μl of CLIC1 at 500nM concentration in 50mM Hepes buffer pH 7.4. For each ligand a maximum of 10mM/20MR Zn^{2+}/ Ca^{2+} was added and a serial dilution was performed for all 12 capillaries. With the final 12^{th} capillary containing 4.88nM of ligand. All ligand binding assays were analysed using M0 affinity analysis V2.3 using a dose response curve and a line of best fit was calculated using the K_d model.

2.2.6- NMR

Clic1 NMR samples were collected at 30°C on the Bruker Avance III spectrophotometer which acts at a ^1H frequency of 600MHz using a QCIP cryoprobe. Samples were 300μl

with 15ul/5% D20 added and placed in a 5mm Shigemi tube. All spectra were processed in NMRPipe and viewed and analysed using NMRviewJ (Johnsona and Blevinsb, 1994; Delaglio ~' *et al.*, 1995)

	Experiment name	Number of scans	Number of increments	D1(S)	TD	NUS (%)
1	HSQC	128	256	1	1020	100
2	TROSY-HSQC	64	512	1	1024	100
3	BEST-TROSY HSQC	32	256	0.2	1024	100
4	HNCACB	220	110(N)X128(C)	0.2	1000	10
5	HNCO	128	128(N)X200(C)	0.2	1000	10
6	CBCA(CO)NH	220	100(N)X110(C)	0.2	1000	10
7	HNCA	220	128(N)X110(C)	0.2	1000	8

2.2.7- Backbone assignments

Backbone resonance assignments were obtained for 186 of the 227 non-proline CLIC1 residues using a traditional set of TROSY-based 3D experiments. A HNCA,

HNCACB, HNCO and CBCA(CO)NH were collected with non-uniform sampling (NUS). For NUS, 8-10% of the points were collected using random sampling schedules. The spectra were reconstructed using the graphical user interface created by MddNMR and compressed sensing was used. The data was processed and analysed as normal using NMRpipe and NMRview respectively.

2.2.8- Zinc titration NMR experiments

300uM of His-tagged CLIC1 at pH 6.5 was measured using a TROSY-HSQC experiment. A 22.5mM zinc stock at pH 5.5 was used and 1μl additions of the stock to the sample increases the zinc concentration of the sample by 0.25MR. Final Zinc concentrations of 0.25MR, 0.5MR and 1MR were used and to the final 1MR zinc sample, 1mM EDTA was added.

This titration was repeated for the same CLIC1 concentration without the presence of a His-tag using zinc concentrations 0.4MR, 0.75MR, 1MR, 2MR, 3MR, 5MR, 7MR.

2.2.9- Relaxation NMR experiments

^{15}N heteronuclear NOE, T_1 and T_2 experiments were carried out on CLIC1. Sets were completed on 500μM CLIC1 in a buffer of 50mM NaCl 50mM Hepes pH 7.4 in the absence and presence of 1MR Zn^{2+}. Intensity was calculated for each assigned residue over the course of a series of different time delays for T1 and T2 calculations. The intensity was fitted against the time delay using the equation y=a*exp(-b*x). The rate of intensity loss is calculated for each residue for T1 and T2. For each value, 1/T1 and 1/T2 is calculated to give R1 and R2 respectively.

Experiment number	T1 delay(s)	T2 delay(s)

1	0.01	0.0036
2	1.4	0.0072
3	0.2	0.0252
4	1.2	0.0108
5	0.4	0.018
6	1	0.036
7	0.6	0.0144
8	0.8	0.0036
9	0.01	0.0072
10	0.6	0.0252

2.2.10-Residual dipolar coupling NMR experiments

CLIC1 sample was at a concentration of 800μm. A PEG/Hexanol stock was made as a 16% w/v solution of PEG/Hexanol using a standard methodology(Prestegard et al., 2005). 50% of the PEG/Hexanol stock is mixed with 50% of the sample to give a final sample of 400μM CLIC1 consisting of 8% PEG/Hexanol.

The D20 splitting of the sample is measured and determined to be 23HZ. A TROSY-HSQC and a standard HSQC was run. An additional TROSY and HSQC are run of the sample at the same 400μM concentration of CLIC1 and in Hepes buffer pH 7.4 without

alignment media to act as a reference spectrum. Coupling constants were obtained using line splittings in the Nitrogen dimension.

The N^{15} chemical shift of every assigned residue is calculated between the aligned and unaligned spectrum. This chemical shift difference is calculated between the aligned and unaligned TROSY but also between the aligned and unaligned HSQC. The N^{15} HSQC shift is subtracted from the N^{15} TROSY shift for every assigned residue that is sufficiently resolved to give an accurate J coupling. The final shift value for each residue is multiplied by the base frequency which is 60.802538 in the 600MHz spectrometer. This value is then multiplied by 2 to give residual dipolar couplings.

((Aligned Trosy- Unaligned Trosy) – (Aligned HSQC-Unaligned HSQC) x BF)) x 2

(Trosy J couplings- HSQC J couplings) x BF x 2 = Residual dipolar couplings

2.2.11- SAXS

Samples were collected on Beamline 21 in the synchrotron at Diamond light source. Samples existed between 10-20mg/ml and were in a 50mM Hepes buffer pH 7.4 with 5% glycerol. SEC-SAXS was implemented and the SEC column coupled was the KW-403 Shodex. The KW-403 Shodex allows a sample volume of 4.6ml with a mass range of 10-700 kDa and a flow rate of 0.16ml/min. Scattering data has a default scattering vector range from 0.0026 to 0.34 A. Results were analysed using SCATTER and ATSAS software suite.

Atsas Software	Function
Primus	Graphical user interface to for analysis of SAXS data.
DAMMIN	Ab initio shape determination using dummy atom modelling.
DAMMIF	Rapid shape determination of SAXS data
SREFLEX	Prediction of flexible regions and refinement of potential structures of high resolution protein saxs data
EOM	Optimising an ensemble of protein structures that together fit a saxs scattering curve
CRYSOL	The comparison and fitting of experimental scattering data to protein crystal structures and a chi squared score for the fit
DAMAVER	The alignment of the ab initio bead models in order to select the most suitable one
GNOM	Fourier transformation that determines the Pair distance distribution function.

Specific parameters used for SAXS analysis are discussed in further detail within the results section.

Core symmetry	P1
Chain type	Random coil
Number of domains	4
Total number of models	10,000
Calculate intensity	Yes
Number of harmonics	15
Maximum value	0.5
Number of points	51
Run Genetic Algorithm	1 time

Figure 2.3: EOM parameters. Ensemble optimisation method is split into three sub sections. Where Ranch generates a pool of models based upon sequence and structural information. Subdomains are placed into the program with missing residues identified to be potentially flexible. Form Factor maker then takes these models and and generates an intensity file and size distribution for EOM. GAJOE then selects an ensemble of models that together best describe the experimental scattering data.

2.2.12- Tryptophan fluorescence

The intrinsic tryptophan fluorescence spectrum of CLIC1 (that contains a single Tryptophan residue in position 35) was collected using a Varian Cary Eclipse fluorimeter at a temperature of 30C. The sample was excited at a wavelength of 280nm and the emission was recorded between 300 and 400nm. CLIC1 samples were in HEPES buffer pH 7.4 and at a concentration of 1mM.

Chapter 3: Probing the solution structure of CLIC1

3.1- Abstract

CLIC1 undergoes major morphological changes in order to insert into the membrane and act as a chloride ion channel. Many homologues of CLIC proteins including GST O-1 only exist as a soluble protein and do not have ion channel activity. In order to probe the reasoning behind CLIC1s unique ability to insert into the membrane we used SAXS and NMR to identify its structure in solution and identify any regions of the structure that are involved in these conformational changes. Analysis using NMR and SAXS identified a novel minor state of CLIC1 that exists in solution as a direct result of elevated flexibility of the loop linking the N- and C-terminal domains. This elevated flexibility is likely a consequence of reduced intermolecular interactions between these domains compared to structural homologues. In summary, we have identified structural features that allows CLIC1 to be unique in existing as both a soluble and membrane protein.

3.2- Introduction

The crystal structure of CLIC1 has long been known and has several structural homologues that also consist of the conserved GST fold(Harrop *et al.*, 2001). However few attempts so far have been able to identify structural characteristics of CLIC1 that make it distinct from its homologues in its ability to exist as both a soluble and membrane protein. These distinct features if present would be identifiable in solution via SAXS, NMR and bioinformatics. Literature that led to this study. Previous attempts such as Molecular dynamic simulations completed on CLIC1 highlighted the foot-loop of the C terminal domain as a largely dynamic region which is in agreement with the crystal structure(Jones *et al.*, 2013) . Other attempts using Hydrogen Deuterium Exchange and Mass spectrometry highlighted the N terminal domain as being significantly more unstable than the C terminal domain (Stoychev *et al.*, 2009). NMR data will identify the residues that experience multiple environments and will allow identification of dynamic regions.(Chao and Byrd, 2018) These dynamic regions may account for the reasoning behind the unique ability for CLIC1 to exist as a soluble and membrane bound protein. Any regions that are involved in metamorphosis are likely to well conserved and present in all members of the CLIC family so identification of the causes of metamorphosis should be consistent among all CLIC proteins.

3.3-Results

3.3.1- Intermolecular forces within CLIC1 are strikingly less than the structural homologue GST01

In order to identify why Clic1 exhibits metamorphic activity, bioinformatics was used to identify the number of intermolecular interactions between the two CLIC domains. Then these types and number of intermolecular forces can be compared with structural homologues. CLIC1 was compared to its structural homologues GST O-1 and EXC-4. Glutathione S-transferase Omega-1 is a homologue of CLIC1 but exists only as a soluble protein with dehydroascorbate reductase activity. Although it contains a GST fold like CLIC1 it is unable to insert into the membrane and does not exhibit metamorphic activity(Board *et al.*, 2000). Whereas EXC-4 is a CLIC1 homologue in *C.elegans* that is metamorphic and can act as a chloride ion channel in the membrane(Littler *et al.*, 2008). To that extent it would expected that CLIC1 is greater in similarity for the number and position of intermolecular interactions for EXC-4 than it is GST 0-1.

Protein interactions calculator is a useful tool and allowed the breakdown of intermolecular forces between 3 categories (Srinivasan et al, 2007). Interactions were characterised between the N terminal and C-terminal domains, between the N-terminal domain and the loop, between the C-terminal domain and the loop. The data(figure 3.1) suggests a striking difference between CLIC1 and GST0-1. The overall number of intermolecular forces has decreased by 35.8% for Clic1 compared to GST0-1. With the greatest difference in intermolecular forces occurring in cross terminal interactions with a 50% difference between GSTO-1 and CLIC1. EXC-4 also exhibits a similar reduction in cross-terminal interactions. It has a 48.3% difference in cross-terminal interactions between EXC-4 and GSTO-1. This suggests a low number of cross terminal interactions is key across

CLIC1 homologues that can insert into the membrane and may be a key cause for the difference in ability to insert into the membrane.

In CLIC1, the predicted transmembrane region is residue 26-46 (Berry and Hobert, 2006)(Hare *et al.*, 2016).This region is N-terminal and hence the region that is more likely to have a greater level of flexibility in order for the structure to reorientate itself to expose this hydrophobic transmembrane region. On the N terminal side, GST Omega-1 has 9 hydrogen bonds and this is significantly reduced to 2 in EXC-4, although CLIC1 only has one less hydrogen bond at 8. Therefore, we didn't find a significant reduction in N terminal interactions between CLIC1 and GST O-1 that could explain the properties of the putative TM region.

CLIC1	Hydrophobic	Hydrogen bonds	Aromatic-aromatic	Aromatic-sulphur	Cation Pi	Ionic	Total
Cross-terminal	9	18	0	0	1	2	30
N-terminal to loop	8	8	0	0	0	1	17
C-terminal to loop	3	11	0	0	0	0	14
Total	20	37	0	0	1	3	61

GST-O1	Hydrophobic	Hydrogen bonds	Aromatic-aromatic	Aromatic-sulphur	Cation Pi	Ionic	Total
Cross-terminal	20	31	2	1	2	4	60
N-terminal to loop	7	9	1	0	0	1	18
C-terminal to loop	4	12	0	0	0	1	17
Total	31	52	3	1	2	6	95

EXC-4	Hydrophobic	Hydrogen bonds	Aromatic-aromatic	Aromatic-sulphur	Cation Pi	Ionic	Total
Cross-terminal	13	14	0	0	1	3	31
N-terminal to loop	12	2	1	0	0	0	15
C-terminal to loop	0	12	0	0	0	0	12
Total	25	28	1	0	1	3	58

Figure 3.1: Intermolecular forces characterised using the Proteins Interaction Calculation(PIC) in proteins. a) Clic1 with loop defined residues 88-100 b) GST O-1 with loop defined residues 96-107 and c) EXC-4 with loop defined residues 108-119

3.3.2- B-factor analysis can identify flexible regions predicted from the crystal structure

For proteins, the term B-factor is coined to describe the reduction of signal of X-ray or neutron scattering. In the case of protein crystallography, the reduction of signal from the X-ray for atoms can be used to predict flexible regions of the protein. With higher B factors indicating greater levels of flexibility and potential disorder and lower B factors indicating more ordered and rigid regions. Where a protein exhibits high B factors in regions of the structure it indicates that multiple conformations of this region of the protein are more likely to exist and the single frozen structure calculated from the crystal is not truly accurate of the dynamics of the system in solution.

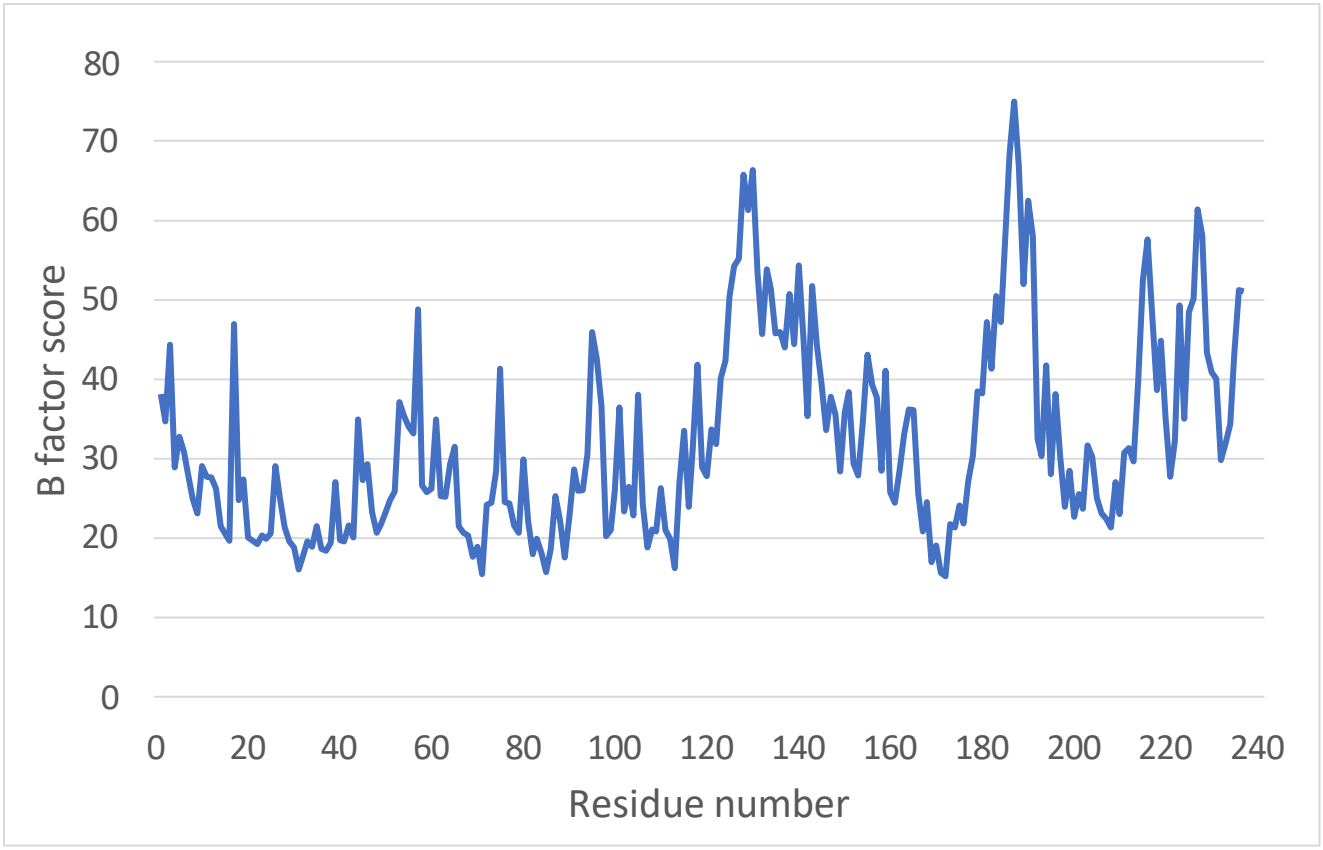
To identify differences in GSTO-1 and CLIC1 the B factors of the respective crystal structures x and 1k0m were analysed over the complete sequence. For CLIC1 using

the crystal structure 1k0m, 3 regions were identified to have an elevated B factor. The three regions were residues 42-62, 88-100 and 147-164. The segment 147-164 has the lowest B factor score of these regions but still peaking above the average score. This region is a foot loop in the C terminal side of CLIC1. The 2nd region with a high B factor score is the region of residues 42-64. This region peaks high above the average and is largely a disordered loop with a small alpha helix at the centre of this region. The final region of residues is 88-100 which is a flexible linker than links the n terminal and C terminal domains of CLIC1 and this has a peak B factor greater than all other regions of CLIC1.

Alternatively in GST Omega-1 one of the most striking differences is that the C terminal foot loop does not exist. And hence this region of flexibility in CLIC1 is replaced with a low B factor score in GST O-1 suggesting a significantly more rigid section. There are 2 loops also that demonstrate elevated B-factor scores in GST and these correspond to residues 125-152 and residues 182- 198. These loops do exist in CLIC1 but their B factor scores suggest they are more rigid within the CLIC structure than its homologue.

Although the exact B factors values are not comparable between different structures due to the differing scales, comparison can be made for regions that deviate largely from the average B factor score which is what we analyse. Intra structure analysis demonstrates that within the CLIC structure the linker bridging domain 1 and 2 is one of the 2 regions with the highest B factor score suggesting elevated flexibility. Whilst in GST Omega 1- this linker bridging the domains is only the 3rd highest B factor peak score and is just over half the score of the most flexible regions within the GST structure. This suggests the linker in GST is not one of the most flexible regions in the structure. The final loop that shows an elevated B factor score is comprised of residues

55 to 70 in GST O-1 and this aligns with residues 42-62 in CLIC1 which equally shows an elevated B factor score.


B factor score
80
70
60
50
40
30
20
10
0
0
20
40
60
80
100
120
140
160
180
200
220
240
Residue number

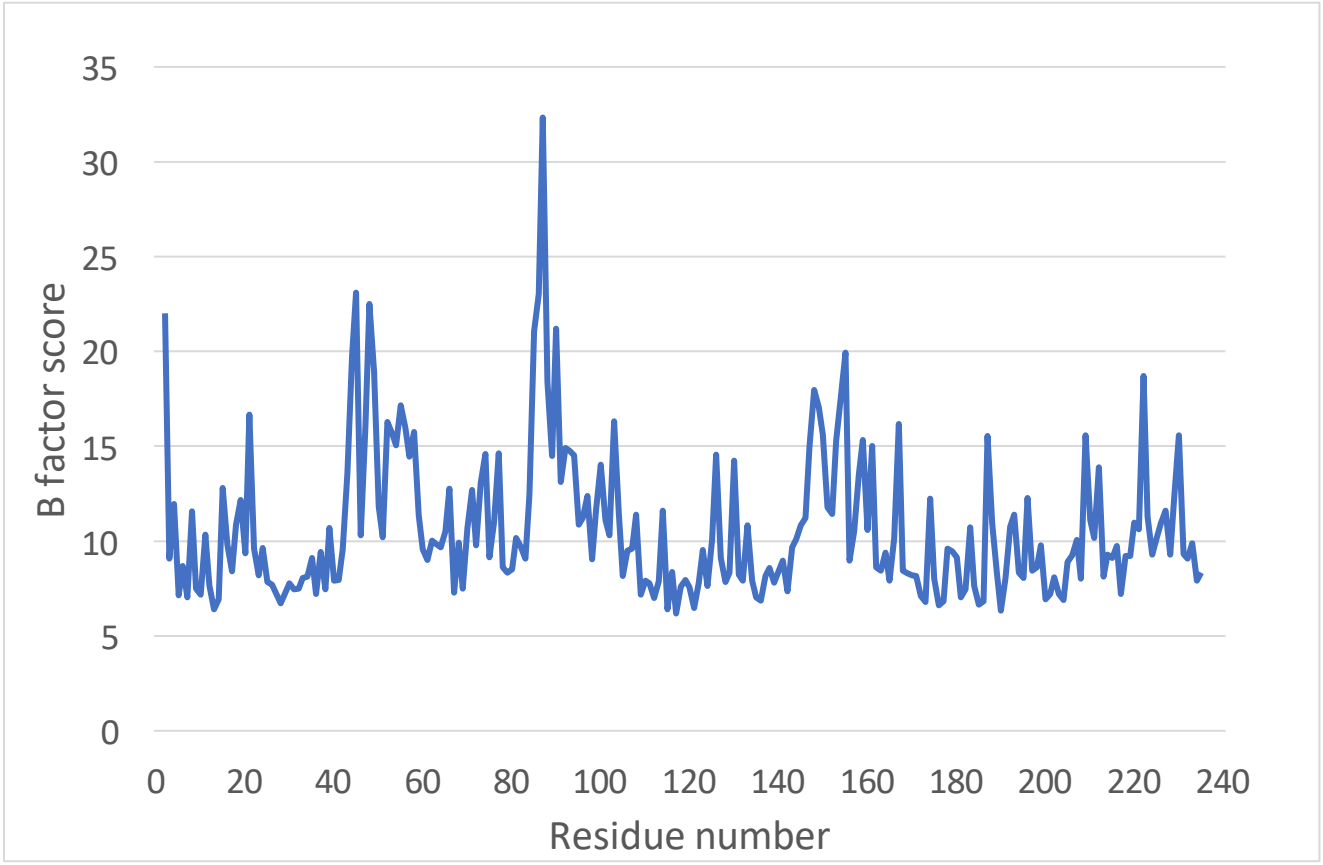

B factor score
35
30
25
20
15
10
5
0
0
20
40
60
80
100
120
140
160
180
200
220
240
Residue number

Figure 3.2: B factor analysis score for CLIC1 and its structural homologue GST omega-1 per residue. a) GST-O1-B factor score using the crystal structure 1EEM b) Clic1 B-factor score for chain A for the 1K0M crystal structure

3.3.3-Backbone assignment of CLIC1 facilitates structure and dynamics NMR experiments on CLIC1

In order to derive region and residue specific information on CLIC1 in regards to its interaction, dynamics and structure, backbone resonances assignment must be completed for the protein. Backbone resonances assignment will enable each peak on an ^{15}N-^{1}H NMR spectrum to be assigned to a specific residue of CLIC1. A triple labelled sample of CLIC1 was prepared to a concentration of 500uM. The sample was then transferred to a 50mM Phosphate and 50mM NaCl buffer, pH 7.4.

A standard set of 3D TROSY based experiments were collected for CLIC1 given its large size of 27kDa for the monomer and small amounts of dimer present in equilibrium which would exist as a 54kDa size protein. The list of experiments collected included a 2D N-H TROSY, a HNCO, HNCA, HN(CO)CA and a HNCACB and HN(CO)CACB.. Assignments were completed and are shown on a 2D Trosy in figure 3.3. The residues in the 15N-1H NMR spectrum which are assigned are well-dispersed at a 400μM concentration of CLIC1. CLIC1 is a protein with a length of 241 amino acids and 90% of the backbone resonances were assigned with missing residues having significant overlap or unable to match to a i-1 or i+1 residue with confidence. The residues missing signals may be a result of flexibility within this region or a result of conformational variability.

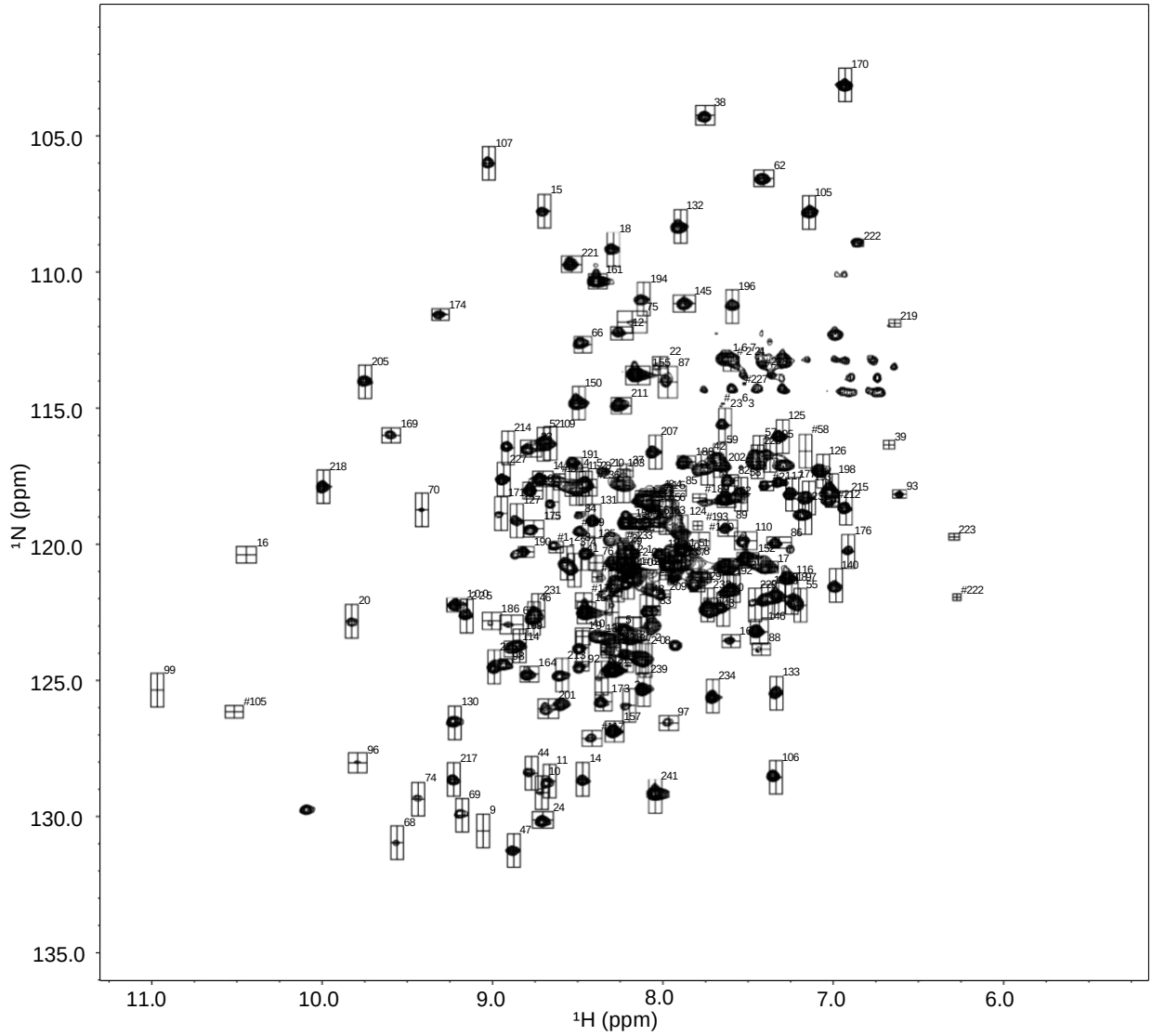


Figure 3.3: Assignments on a 15N TROSY HSQC of CLIC1. Assignments were collected using a 400uM triple labelled sample on a 800MHz spectrometer at the Crick Institute in pH 7.4 50mM Hepes 50mM NaCl buffer.

TALOS is an artificial neural network that provides phi and psi backbone angles based on chemical shift assignments of a given sequence. TALOS then used the chemical shifts and bond angles to make predictions as to the secondary structure components of the protein. (Berjanskii and Wishart, 2005).The latest version of TALOS is predicted to be 89% accurate. The secondary structure predictions of CLIC1 by TALOS in figure 3.4 are largely consistent with the secondary structure elements seen in the crystal

structure 1K0N. Seeing the consistency of the secondary structure elements matched to the crystal structure also provides confidence in the backbone assignments of the NMR data to CLIC1.

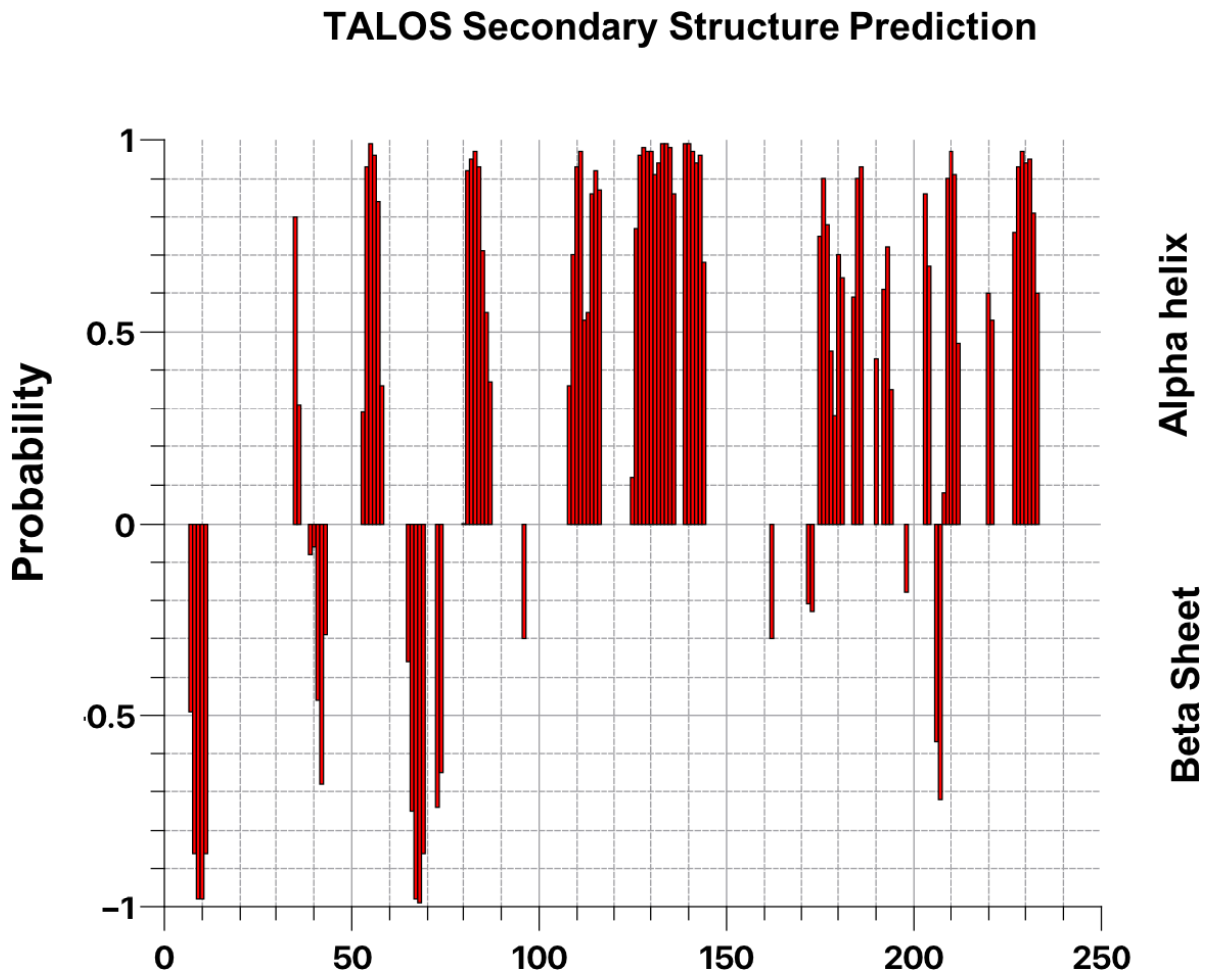


Figure 3.4: Talos prediction of secondary structure from the backbone chemical shifts of CLIC1. Secondary structure predictions for ^{13}C, ^{1}H, ^{15}N chemical shifts. Red bars are present for each residue that is assigned in CLIC1. Values indicate probability of the residue to reside as part of a secondary structure element. Values >0 indicate probability of residue being part of alpha helical content and values <0 indicate probability of residue forming part of a beta sheet.

3.3.4- NMR relaxation identifies flexible regions in CLIC1

Given the reduced number of intermolecular interactions bridging the two domains for CLIC1 compared to its structural homologue GSTO-1, we expect the structure of CLIC1 in solution to be more flexible.

We attempted to use NMR to elucidate the regions of elevated flexibility and the timescales through which they exchange environments. By identifying regions of higher flexibility we can attempt to elucidate minor states of CLIC1 that are likely involved in promoting oligomerisation and insertion into the membrane. In order to determine the flexibility of certain regions of CLIC1 we calculated R2/R1 and plotted this data. Initially during data collection, we perform a series of TROSY-based experiments with variable T1 and T2 delays. This allowed us to measure the transverse magnetisation decay and the longitudinal magnetisation recovery for T2 and T1 respectively. In both cases, pulse sequences were optimized so that a loss of S/N could be measured as a decay graph and rates measured for each residue corresponding to T1 and T2. R2 and R1 were then calculated as 1/T1 and 1/T2. Elevated R2/R1 residues suggest that they experience chemical exchange and experience a correlation time that is slower than other residues within CLIC1. Additionally residues with a very low R2/R1 values indicate these residues have high levels of internal mobility and tumble more quickly than the average residue. Suggesting their correlation time is much quicker than other residues within the protein.

A region of CLIC that exhibits a quick T1 and high R1 would act like a small molecule and wobble on a very quick timescale (ps-ns) which is typical for many loops. For regions of CLIC that undergo slow dynamic motions (μs-ms) then T2 is low and R2 is high. On this plot, CLIC1 demonstrates two types of dynamic motions in figure 3.5. It

observes a fast ns-ps time scale dynamic motion that exists between residues 145-170 which acts as a result of increased R1. In addition a much slower timescale motion is identified for the region 45-50 and 85 to 100 which is shown through an increased R2.

For most residues that undergo exchange, the range of the error bars will increase. This is due to the intrinsic properties of exchange where sampling of multiple conformational states can often lead to broadening. This broadening reduces the signal to noise especially if exchange occurs on an intermediate exchange regime. With a broader peak, this reduce the height of the peak and as S/N is calculated at the linewidth at half peak heigh this subsequently reduces the S/N value and increase the error within the measurement.

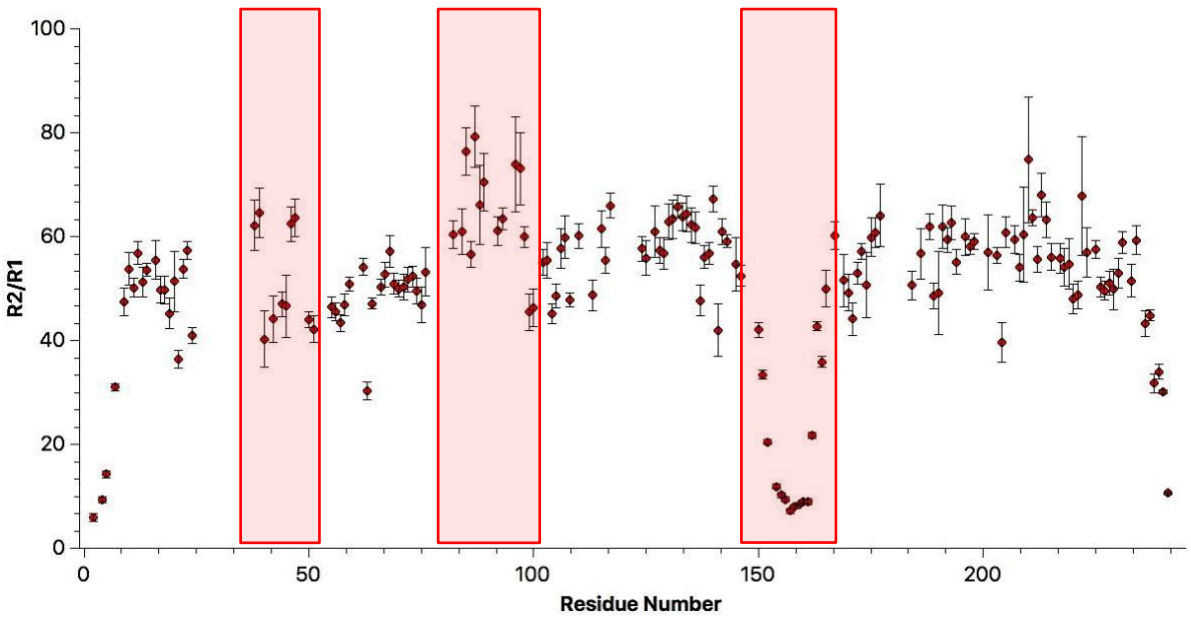


Figure 3.5: CLIC1 demonstrates three highly flexible and dynamic regions within its structure- ^{15}N R1/R2 relaxation rates of CLIC1 at 303K in 800MHz. The regions highlighted in red define residues 45-50, 85-100 and 145-170 which deviate significantly from the average R2/R1 value. Error bars are derived from S/N of peaks during the fitting process on NMRview which using the monte carlo approach estimates the standard deviations of the residue intensities.

3.3.5- SAXS can elucidate new minor states of CLIC1 which are not seen in structural homologues

Small angle X ray scattering is a useful low resolution tool to identify flexibility and the structure of proteins in solution. Many proteins often do not adopt a single structure in solution and exist as an ensemble of different conformations that will play a key role in the protein function. To that extent, SAXS could be used to identify whether CLIC1 exists in multiple conformations in solution and whether any additional states play a role in its ability to be a metamorphic protein that can insert into the membrane. To identify the structure of CLIC1 in solution using SAXS, standard beamline parameters were used demonstrated in figure 3.6.

Initially it was important to identify whether the structure of CLIC1 in solution matched the structure of the crystal(1K0M). FOXS is an online web server that compares experimental scattering data against predicted scattering data of PDB structures and provides a fitting along with a chi squared score to provide a numerical figure to assess the fit. (Schneidman-Duhovny et al., 2016). 1K0M predicted scattering data was generated by FOXS and compared with the raw experimental data shown in figure 3.8. In this comparison we found the predicted scattering data of 1K0M to be a poor fit with our experimental scattering data. The chi squared score which determines the fitting between the two data sets was 3.86. The high chi-squared score >1.5 indicates that the 1K0M structure alone does not demonstrate the only conformation that CLIC1 exhibits in solution. There must be multiple conformations of CLIC1 that would together account for the scattering pattern seen.The chi squared score is calculated through attempting to minimize the value with respect to c_1 and c_2. The parameters c_1 and c_2 refer to the excluded volume of atoms and the density of the water in the hydration layer.

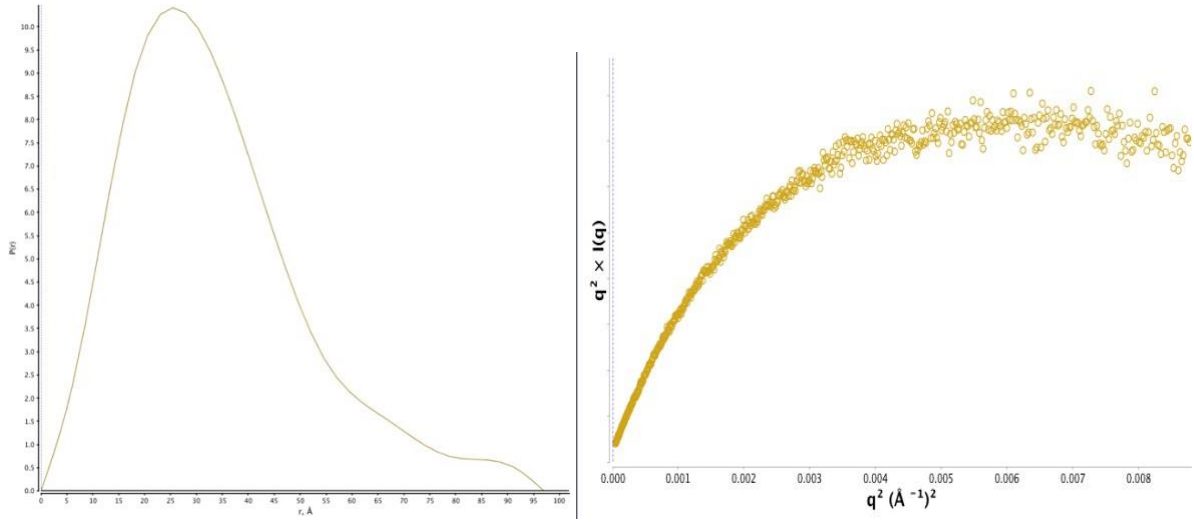
To provide a visual aid of the average structure seen in solution of CLIC1, we used DAMMIF(Petoukhov *et al.*, 2012). DAMMIF uses the experimental SAXS data to create a dummy model which gives an insight into the shape of the protein in solution. The dummy model generated by DAMMIF for CLIC1 is seen in figure 3.9 and is a distinctly different shape to that of the CLIC1 crystal structure.

Wavelength	0.9537 Å
Energy	13.0 keV
Beam centre X	129.29 mm

Beam centre y	19.8 mm
Sample to detector distance	3688.7 mm
Detector	EigerX 4M (Dectris)
Source	Bending magnet
Flux	$4x10^{12}$ photons.s^{-1}
Q range	0.0045-0.34 $Å^{-1}$
Q definition	$4\pi*\sin(\theta)/\lambda$
Intensity units	cm^{-1}(absolute intensity scaled to water scatter at 0.0163)
Capillary diameter	1.5mm
Default exposure temperature	15 °C
Beam size at sample	1.0 x 0.25 mm
Beam size at detector(focus)	0.05 x 0.05 mm

Figure 3.6: Beamline 21 Usage parameters report

A B



C D

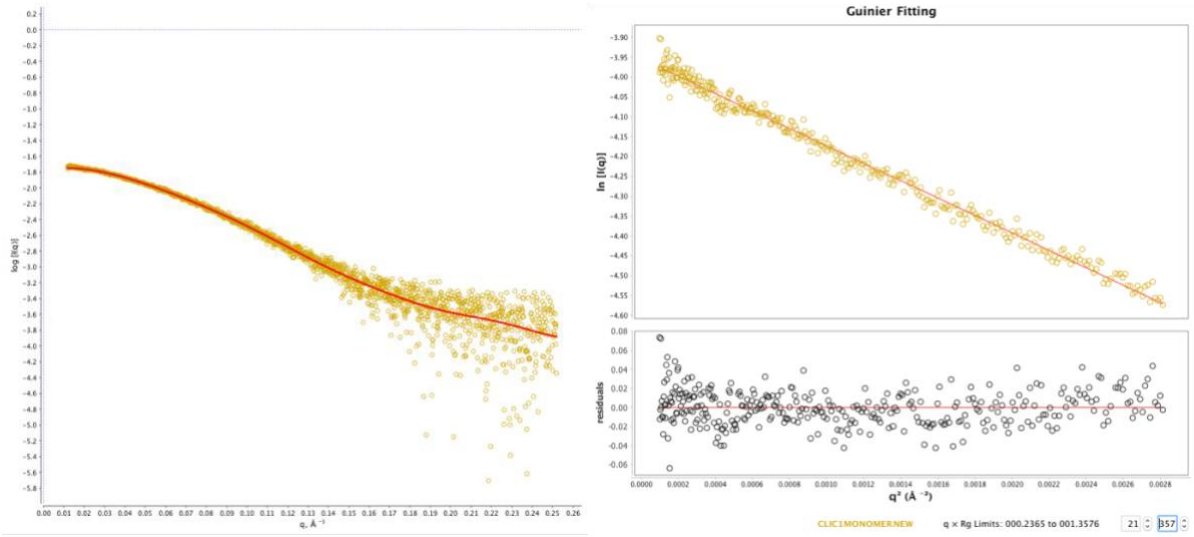


Figure 3.7: Analysis of CLIC1 by small angle x-ray scattering. Processed SAXS data for CLIC1 monomer in Hepes buffer pH 7.4 from Shodex-403 A)Pair distribution function of CLIC1 demonstrates CLIC1 is globular with an extended tail that suggests an elongated conformation B)Kratky-Debeye plot is demonstrated as SAXS data plateaus at Q2 first suggesting CLIC1 is a flexible protein C) Normalised Kratky plot

demonstrates experimental data provides an excellent fit D) Geunier fit demonstrates sample experiences no aggregation or radiation damage and sample fits a linear trend. Scatter to fit the data to model calculations uses a downhill simplex algorithm which precedes a Levenberg-Marquardt algorithm.

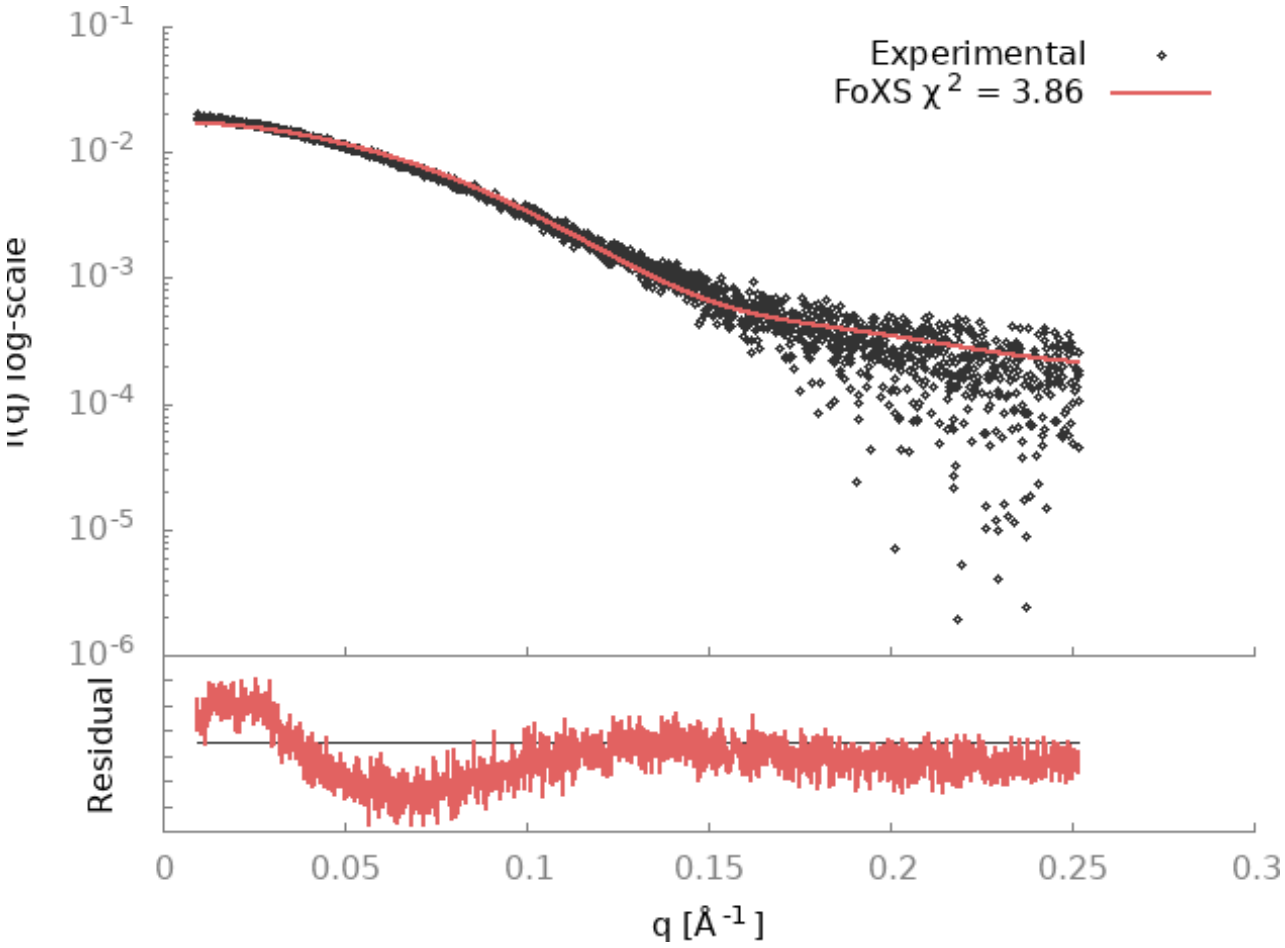


Figure 3.8: FOXS server comparison of CLIC1 crystal structure predicted scattering data against experimental CLIC1 scattering data: Real CLIC1 scattering data is shown in Black and predicted scattering data is shown in red. FOXS is fast x ray scattering that is able to compare and contrast experimental scattering data against predicted scattering data from PDB files. The 1K0N crystal structure

provides a poor fit to the experimental scattering data with a chi squared score of 3.86.

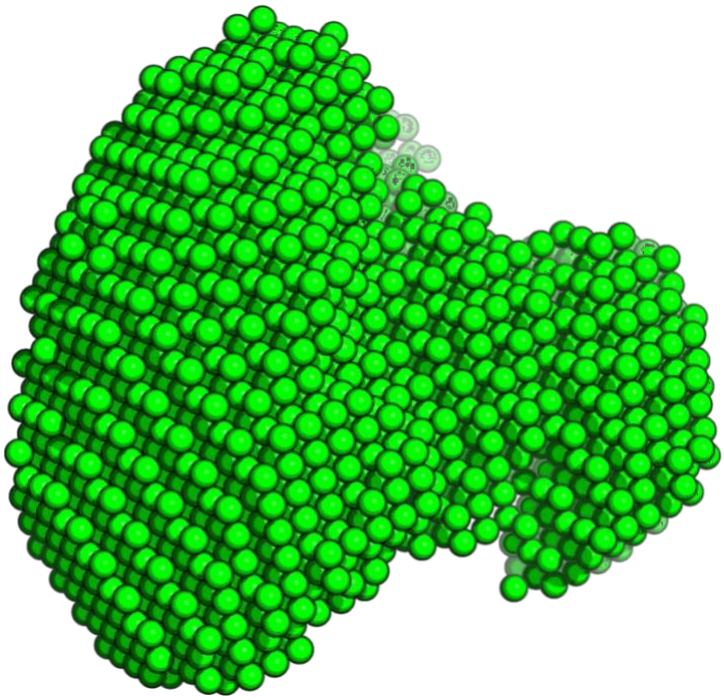


Figure 3.9: PDB bead model of the CLIC1 average monomer structure from the experimental SAXS data. The bead model was calculated using DAMMIF using 10 repetitions on slow mode. DAMMIF provides shape determination of the SAXS data that gives a collection of dense beads within a volume to create a model that would yield a scattering pattern that fits the experimental data. (Franke and Svergun, 2009)

In order to identify the other structures that make up the ensemble in solution, EOM was used. (Petoukhov *et al.*, 2012) EOM stands for ensemble optimisation method and is a program that functions by the user inputting which parts of the protein crystal structure act as rigid bodies and the rest of the sequence is deemed flexible. The rigid bodies can orientate around these flexible regions and the new conformations are

pooled and compared against the x ray scattering curve to create an ensemble that best accounts for the experimental scattering curve. CLIC1 was split into 4 domains to allow movement of all 3 loops identified via NMR to be flexible and to replicate the dynamics of CLIC1 seen in the NMR. The residues allowed to reorientate were 35-45, 90-100 and 150-165, which the rest of the sequence acting as rigid bodies.

The results of EOM identified that the mismatch between the crystal structure and the experimental data was due to elevated flexibility in the loop bridging the N and C terminus. The data provides an ensemble that contains the crystal structure and an elongated CLIC1 structure where the loop has extended This population ensemble when now compared against the experimental SAXS data of the monomer significantly brings the chi squared score down to x^2 and represents a more accurate fit of the scattering data. FOXS suggests the weighting of the two conformers to accurately predict the scattering data. The crystal structure accounts for 80% of the population weighting to act as the major state and the extended CLIC1 structure accounts for 20% to act as the minor state.

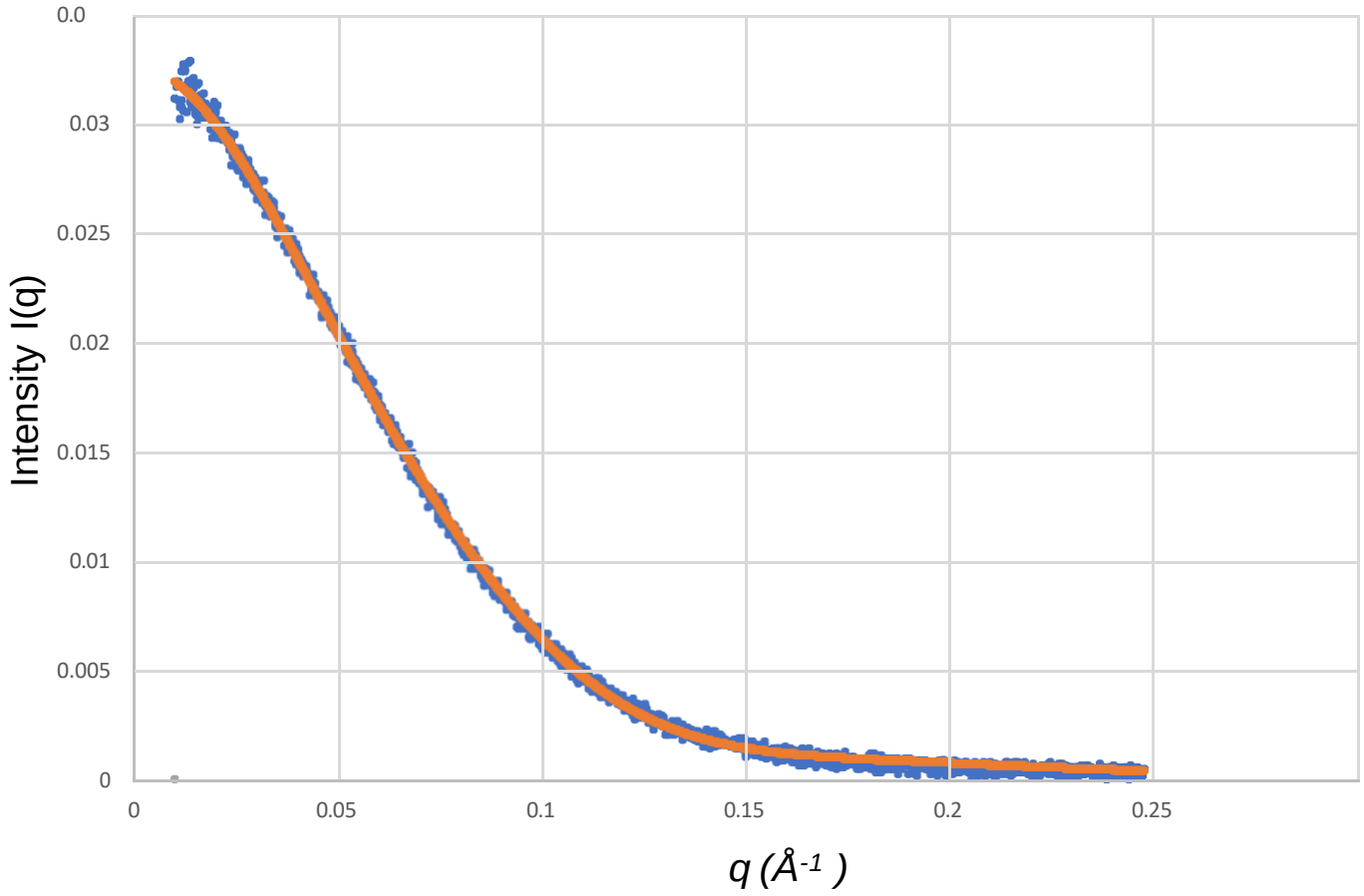


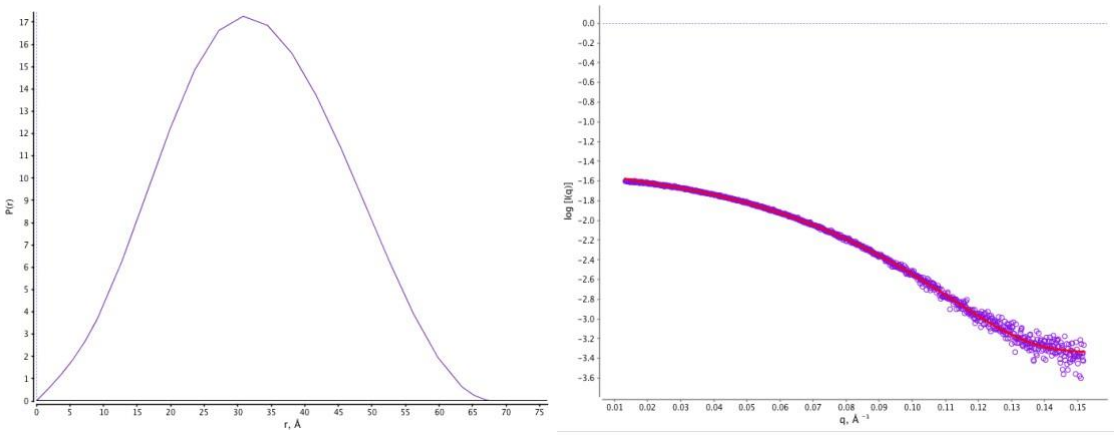
Figure 3.10: Comparison of the EOM ensemble of CLIC1 structures against the experimental scattering data. EOM ensemble was calculated as a weighted profile and then plotted in orange whilst the experimental scattering data for CLIC1 is shown in blue. The ensemble of structures provides a good fit to the experimental data giving a chi squared score of 1.04.

Upon identifying this minor state, the next step was to identify if this minor state existed in other CLIC homologues or was unique to the CLIC family and could potentially play a role in explaining its metamorphic activity. GST O-1 contains the same GST fold that exists in CLIC1 and has the highest sequence similarity score of all structural homologues. The Pr plot of GST is a bell shaped distribution curve shape that indicates a very globular structure prior to further analysis (Koch, Vachette and Svergun, 2003). GST O-1 exists as a natural dimer (Board *et al.*, 2000) and the

experimental SAXS data matches the crystal structure (4yqu) with a chi squared score of 1.05 and hence has only one state seen in figure 3.10.

Although GST 0-1 exists as a dimer and CLIC1 exists as a monomer, the flexibility seen in the loop bridging the N and C terminal domain in CLIC1 is not reciprocated in GST O-1. GST O-1 does not have a flexible loop bridging the N and C terminal domains in each monomeric subunit. This is evident through the almost perfect match between the predicted scattering data of the crystal structure 4yqu and the experimental SAXS data. Hence this additional elongated conformation seems to be unique to the CLIC family.

A B



C D

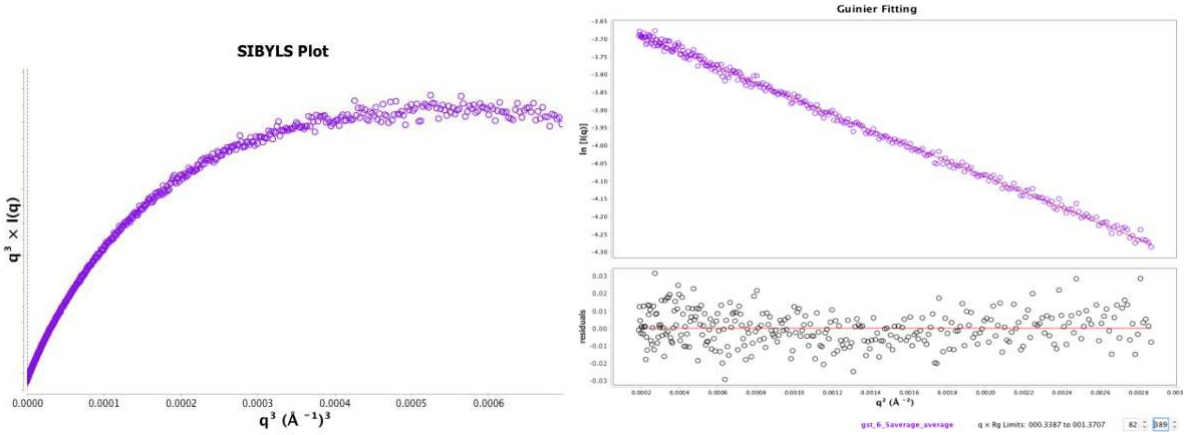


Figure 3.11: Analysis of GST 0-1 by small angle x-ray scattering. Processed SAXS data for GST 0-1 in Hepes buffer pH 7.4 from Shodex-403**.** A) Pair distribution plot demonstrates the structure of the GST Omega-1 is completely globular. B) Normalised Kratky plot C) Siblys plot D) Geunier fitting

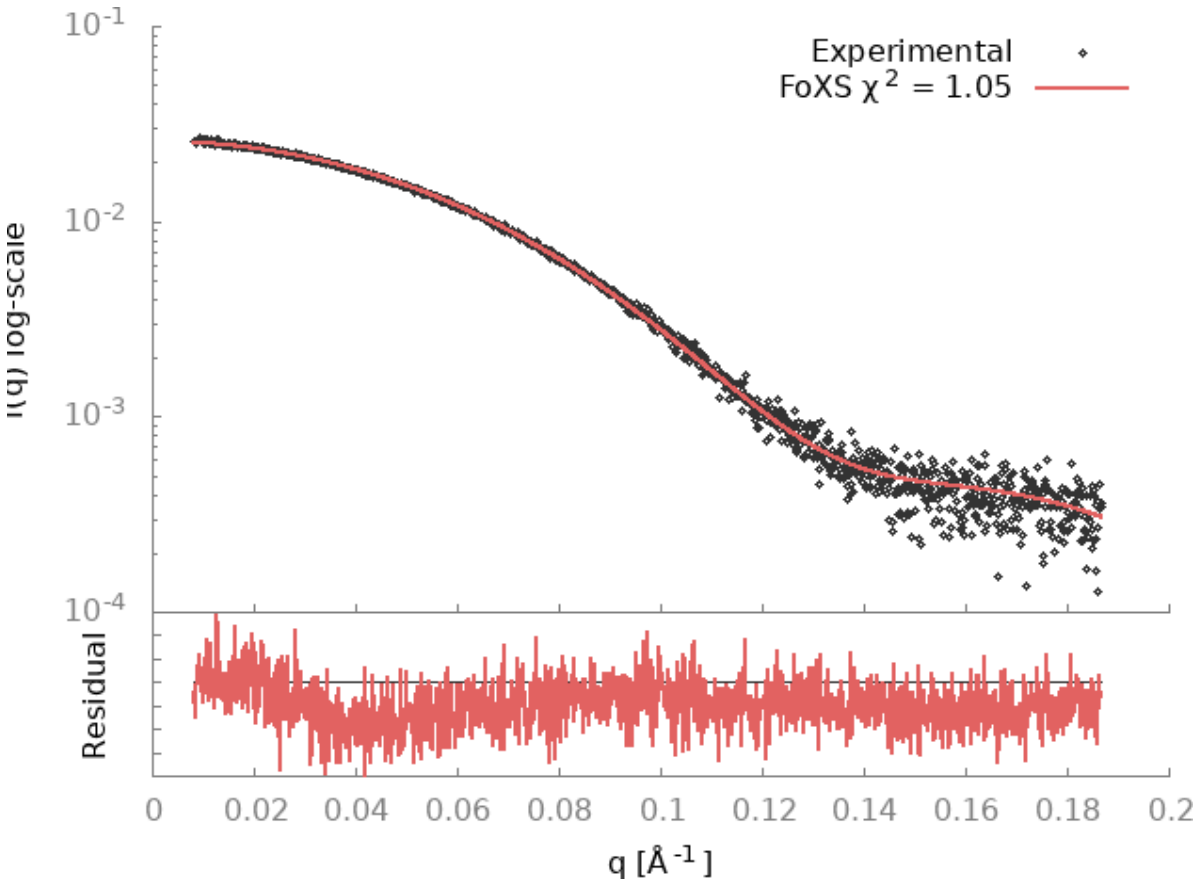


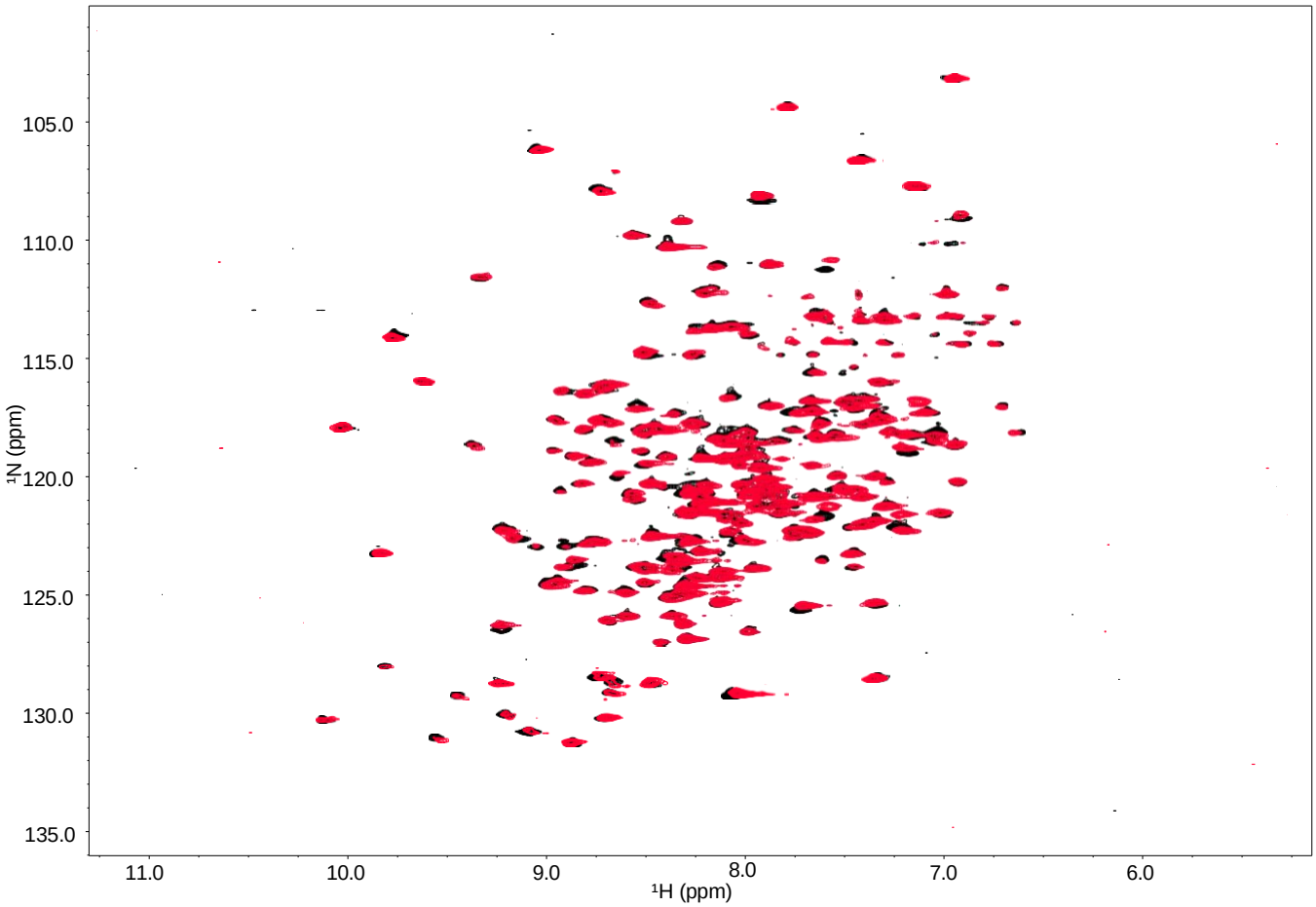
Figure 3.12: FOXS server comparison of GST O-1 crystal structure predicted scattering data against experimental GST O-1 scattering data: Real GST O-1 scattering data is shown in black and predicted scattering data is shown in red. The 4yqu crystal structure provides an excellent fit to the experimental scattering data with a chi squared score of 1.05.

3.3.6- NMR can provide restraints to develop a refined CLIC1 structure

Protein structures have for many years been calculated using methods such as crystallography, cryo-EM, NMR, and more recently Alphafold. For CLIC1 a crystal structure is elucidated but often certain sub-states of protein structure are unable to be crystallised. Residual dipolar couplings can be used to refine structural models to elucidate a structure that samples all states in solution, not only those stable in a crystalline environment (Chen and Tjandra, 2012).

A dipolar coupling is a phenomenon seen in NMR that exists as an interaction through space between two nuclei in a magnetic field. The dipolar couplings provide information about the orientation of a bond in respect to the magnetic field. In solution, dipolar couplings are averaged out to 0 due to the presence of all orientations of a given bond. However in the presence of alignment media, this creates a partial alignment of every molecule to the magnetic field resulting in RDC values that do not average to 0 (Prestegard et al., 2004).

We attempted to measure the RDC value for the amide bond 15N-1H. The alignment media 5% PEG/Hexanol was used to generate all RDC values. In order to check the couplings for the N-H bond are stable, the splitting of Deuterium was measured prior to running and was determined to be stable at 16 Hz. A TROSY and HSQC pair of spectra were measured both in and without the presence of the alignment media to calculate the couplings for each residue. 91 residues out of a total of 241 were calculated experimentally.


105.0
110.0
115.0
120.0
125.0
130.0
135.0
¹N (ppm)
11.0
10.0
9.0
8.0
7.0
6.0
¹H (ppm)

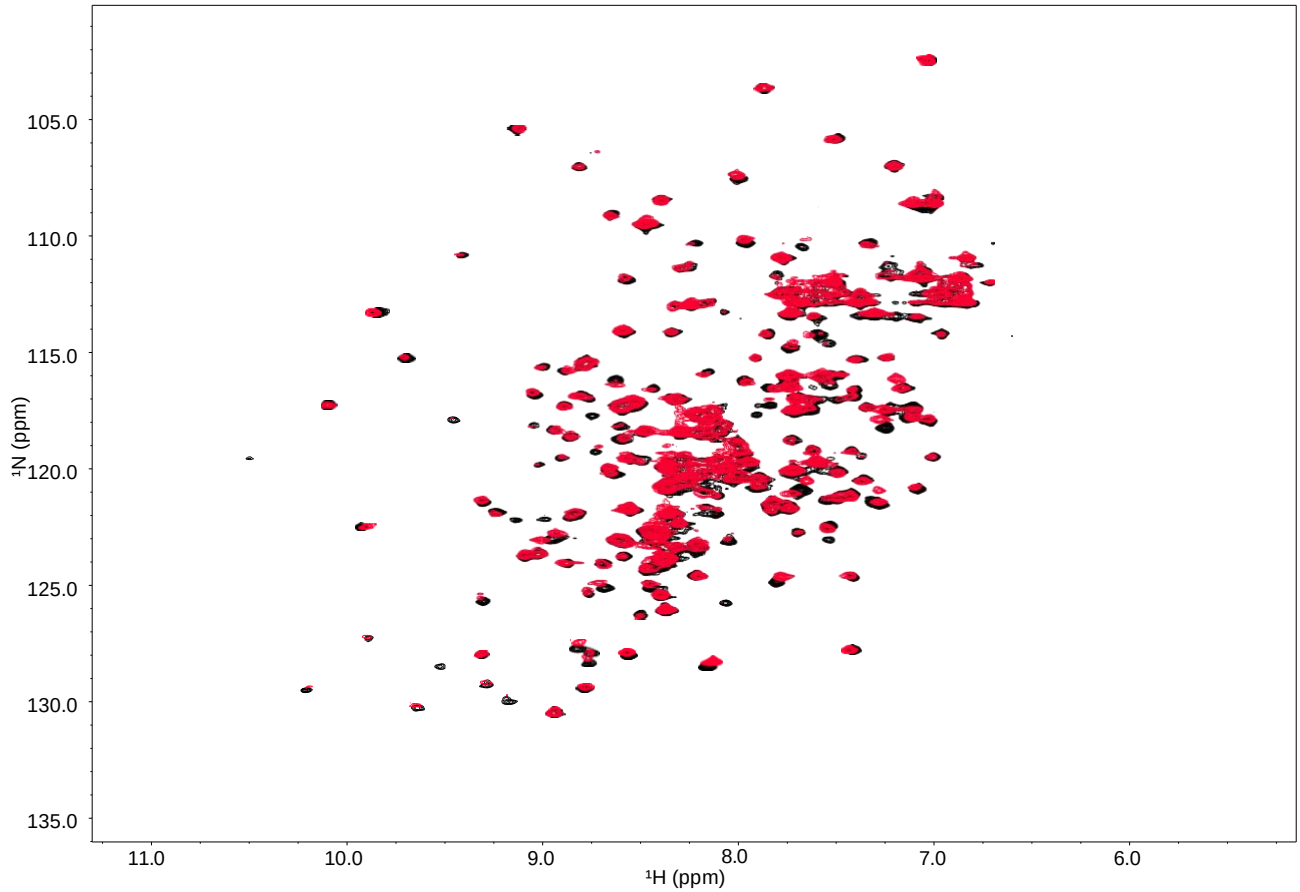

105.0
110.0
115.0
120.0
125.0
130.0
135.0
¹N (ppm)
11.0
10.0
9.0
8.0
7.0
6.0
¹H (ppm)

Figure 3.13: Complete set of Residual Dipolar Coupling Spectra. Spectra were collected using a 400uM single labelled sample on a 800MHz spectrometer at the Crick Institute in pH 7.4 50mM Hepes 50mM NaCl buffer. A) HSQC-TROSY (black) overlaid with TROSY in 5% PEG/Hexanol alignment media (red). B) HSQC (black) overlaid with HSQC in 5% PEG/Hexanol alignment media (red).

We used PALES (Prediction of Alignment from Structure) to then calculate the predicted residual dipolar couplings from the crystal structure- 1K0N(Prestegard *et al.*, 2005) . The experimental RDC values for all 91 residues were compared to the predicted RDC values from PALES and were found to be a poor fit seen in figure 3.14. When a predicted RDC value for a residue does not match the experimental RDC value for that same residue it appears outside of the linear fit.

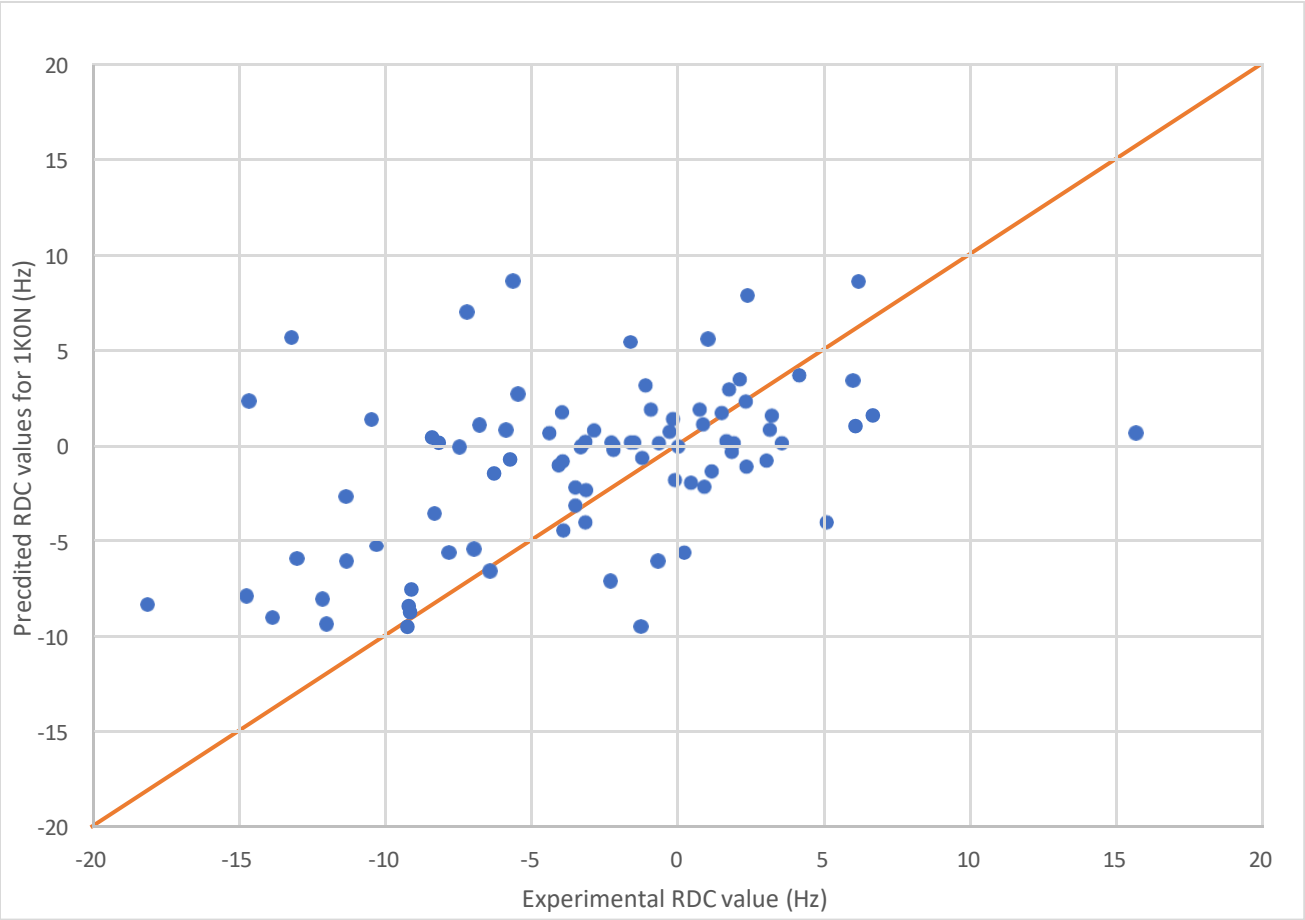


Figure 3.14: RDC values from the crystal structure do not match experimental CLIC1 RDC values- Correlation between predicted residual dipolar couplings of the CLIC1 crystal structure- 1K0N against experimental residual dipolar couplings**.**

This demonstrates that the crystal structure does not represent the structure in solution. Our SAXS data suggested there was flexibility in the linker bridging the N and C terminal domain. Using the software Module2 we calculated a separate alignment tensor for the N and C terminal domains using all RDC values in each of these domains respectively (Dosset *et al.*, 2001). By calculating a separate alignment tensor for each domain, this allows the reorientation of each domain with respect to each other. The

reorientation of each domain in CLIC1 using our experimental RDC values allowed us to generate the model seen in Figure 3.15. Residual dipolar coupings were only used for 91 of 241 residues. In anisotropic conditions, we identified an increase in line broadening for many peaks. In order to reduce the errors of our RDC values, we excluded RDC values where the residues had a low signal to noise or experience significant overlap. S/N is calculated as the linewidth at half height and is calculated automatically by NMRview. When residues have significant overlap with other residues this alters the centre position of the peak of both residues, which creates intrinsic errors in identifying the difference of the peak centre between isotropic and anisotropic conditions. As such these residues were excluded from our calculations. Residues undergoing exchange were also removed from our calculations. Exchange especially in the intermediate regime can lead to line broadening which alters the centre position of the peak in both isotropic and anisotropic conditions, leading to erroneous RDC values. Such regions defined as undergoing exchange where the loop bridging the N and C terminal domain and the foot-loop in the C terminal domain.

Our new model of CLIC1 in solution represents an average of all states seen in solution and differs from the crystal structure of CLIC1 -1K0N with flexibility of the linker bridging the N and C terminal domain.

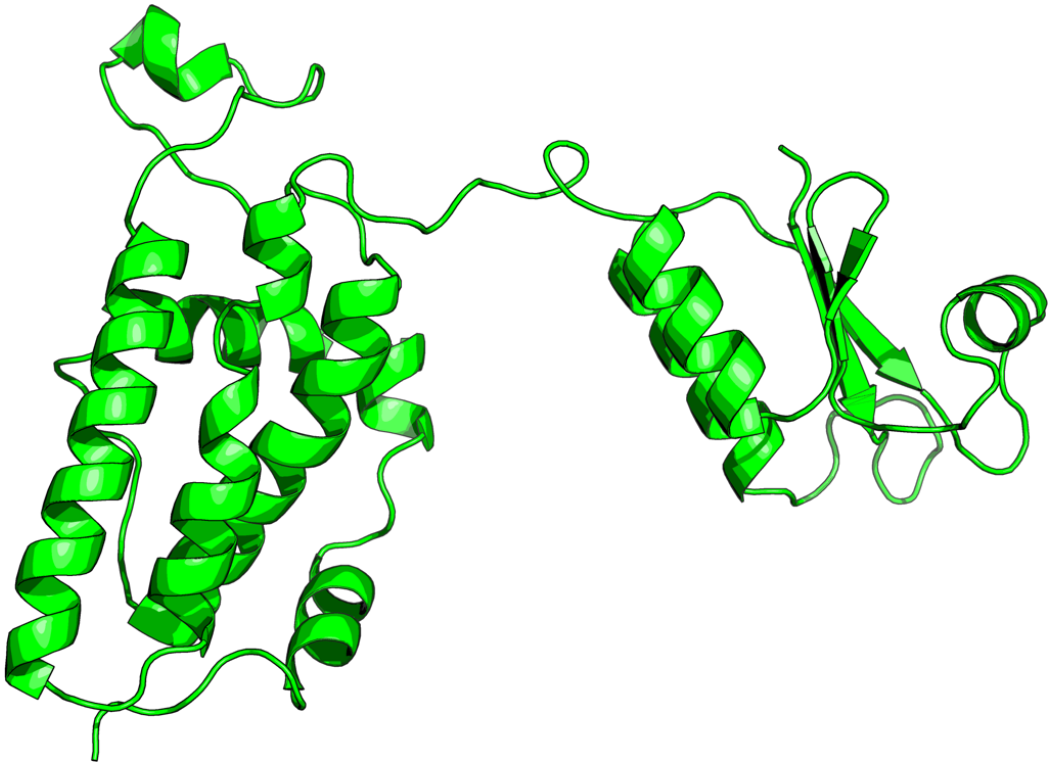


Figure 3.15: PDB structure of CLIC1 in solution fitted using experimental RDC values: 91 residue RDC values were used on Module 2 to create a separate alignment tensor for the N and C terminal domain. The orientation of both domains using the experimental RDC values creates this structure of CLIC1.

3.4- Discussion

All experiments were designed to test the hypothesis that CLIC1 exhibits only one stable state in solution. It became quickly clear from a combination of NMR and SAXS that this wasn't the case, that at least two states existed in solution and the crystal structure was not fully accounting for all states present. CLIC1 has been known for many years to be a flexible protein(Stoychev *et al.*, 2009) although no research could come to a consistent conclusion as to how this aided the metamorphosis of CLIC1 and its insertion into the membrane.

Initial experiments sought to identify specific regions of CLIC1 with enhanced flexibility, identifying the foot loop region, the N terminal region and the domain linking bridging the C terminal domain and the N terminal domain. All three of these regions have been demonstrated to be potentially flexible (Ferofontov *et al.*, 2018) (Hossain *et al.*, 2016) within the literature and our experiments confounded that. But without significant changes to oxidation states or pH, these flexible regions were deemed to have no effect on the structure of CLIC1 in solution.

Small angle X ray scattering experiments and NMR relaxation experiments were carried out at pH 7.4 in HEPES buffer. The SAXS experimental data did not match the predicted SAXS curve of the crystal structure 1K0N, demonstrating that the flexible regions of CLIC1 are having a tangible effect on the structure even at neutral pH with no ligands present. This led to the understanding that an ensemble of structures must be present in solution. Very quickly we identified that the linker region linking the two domains in CLIC1 was causing the two domains to separate temporarily likely aided by the lack of intermolecular interactions compared to its homologues the glutathione S transferase family.

No studies of any of the GST family proteins being run on SAXS as an individual protein could be found in literature, hence we carried out SAXS experiments using GST O-1. The GST 0-1 experimental data provided an almost identical match to the predicted SAXS data from the crystal structure 1EEM. This provided clear evidence that the GST family did not experience elongated states and this elongated state is unique to the CLIC family. This view was corroborated by countless experiments using GST as a fusion tag for proteins in SAXS experiments (Taube, Jarmołowski and Kozak, 2010; Alborghetti *et al.*, 2013). The GST structure fits into the bead models generated and its stability and lack of overall conformational plasticity makes the protein an excellent choice as a fusion tag for these experiments. With the understanding that CLIC1 can exist in a sub-state where both domains are separated from each other, the question arises as to how this aids the function of CLIC1.

The transmembrane domain has been predicted both computationally and experimentally, although the experiments used harsh oxidising conditions in order to trigger the membrane insertion of CLIC1. On the computational side this region was predicted due to this string of residues being largely hydrophobic. So the residues 26-46 are predicted to be the transmembrane region of CLIC1.

Interestingly in the elongated state, the predicted transmembrane is now exposed to the solvent. In the crystal structure, the transmembrane region is occluded from the solvent by other residues in the protein which would prevent contact of the transmembrane region and lipids in the membrane. Now in the elongated state, exposure of hydrophobic residues coupled with unfolding of the N terminal domain could facilitate interaction of CLIC1 with the membrane.

It has been seen using FRET studies that the distance between the N and C terminal domains increases in the membrane bound form of CLIC1 compared to the crystal structure. Intramolecular FRET between residue Trp35 and C223 showed increased distance in the membrane bound form. Based on our data, the separation between the two domains can happen in solution although represents less than >5% of the population weighting and hence would not significantly distort the FRET distance (Goodchild *et al.*, 2011). However our elongated sub state is beginning to match more accurately the membrane bound form. It is possible this extended form could be stabilised through membrane interactions or oligomerisation.

One of the interesting considerations is that this sub state calculated from EOM has been unable to be crystallised. There are a few considerations as to likely why this is. Firstly the sub state exists as a very minor population weighting of sub 5% which creates a probability problem of when sampling a random state in a crystal means you are significantly more likely to sample the major state.

Another major roadblock as to why the minor state is unlikely to have been crystallised is that it temporarily exposes hydrophobic residues to the solvent. It is likely why it's a minor state as this conformation can't be stable for a significant time with exposure of hydrophobic residues to the solvent unless occluded by lipids in a membrane bound form. Protein states which have hydrophobic surfaces such as in the elongated state of CLIC1 are often difficult to crystallise as they promote aggregation in an aqueous solution.

We hypothesise that the flexibility of the domain linker and the separation of the two domains is key to its ability to metamorphically convert from a soluble protein to a

membrane bound chloride ion channel. Hence we wanted to identify if a flexible linker or separation of the N and C terminal domains plays a role in the conversion of many other metamorphic proteins from one state to another.

In the metamorphic protein RfaH, this transcription factor exists in a “closed state” that is held together by an interdomain salt bridge between the residues E48 and R138. Only when this salt bridge is disrupted can RfaH enter the “open” state and this even facilitates a further structural rearrangement of the C terminal domain. In CLIC1 it is likely these intermolecular forces holding the two domains together were disrupted due to mutations during evolution of this protein as opposed to in the case of RfaH where disruption occurs during equilibrium. Interestingly access to the open state and partial separation of the two domains of RfaH causes a change in the secondary structure of the C terminal domain, completely switching from an entirely α-helical N terminal domain to an entirely β-sheet domain. It could be the case in CLIC1 that access to the open state could alter the thermodynamics to promote unfolding of the N terminal region of CLIC1 that would aid interaction with lipids and membrane insertion. In CLIC1 it is also predicted that the transmembrane region that is partially
β-sheet and partially disordered becomes completely α-helical in the presence of lipids. As is the case in RfaH, this structural rearrangement of CLIC1 could be aided by the presence of the open state. RfaH which is a metamorphic protein highlights here in the importance of intermolecular interactions and how the potential loss of interactions can lead to drastic changes in structures seen in proteins.

A similar example seen is the MAD2 protein. MAD2 is a protein that acts as a feedback control for the mitosis cycle through a checkpoint that prevents misassembled

spindles. MAD2 acts as a metamorphic protein similar to CLIC1 and undergoes conformational changes in solution between two different states. Each state having a separate function within the cell context. MAD2 has large loops linking structured regions and domains. These disordered regions will be flexible in order to facilitate conformational rearrangements in solution. This is similar to CLIC1 in that CLIC1 is able to undergo conformational changes largely to flexible disordered regions. Interestingly in this case and many metamorphic proteins, each state has a separate function.

In CLIC1, one would have to suggest that the crystal structure is important for the function of CLIC1 in solution although this is unknown. The elongated state is priming the structure for membrane insertion. Although we can't rule out the possibility the elongated state also has an unknown function in the cell for the soluble version of CLIC1.

One of the conformers in MAD2 is very lowly populated and unstable in solution and mutations can be made to uncouple the two conformers in equilibrium. It is also seen that one of the conformational changes seen is essential for oligomerisation and can promote dimerization. They uncovered the additional state of MAD2 using NMR spectroscopy, however prior to NMR spectroscopy they were able to separate out the two conformers using a mutation to R133 which disrupts one of the conformers.

In CLIC1 the elongated state is lowly populated and future research should look at mutations could disrupt this equilibrium similar to in MAD2. It would allow the separation of the two sub states of CLIC1 which would aid an understanding of the role of the elongated state. In MAD2 we also see that one of the states is important for oligomerisation. Naturally in CLIC1 we see oligomerisation of increasing rates as the

concentration of CLIC1 increases. We are yet to understand the effect of concentration on CLIC1 and the population weightings of the two states within different concentrations. It could be feasible that at higher concentrations of CLIC1, there is a higher proportion of elongated state at equilibrium which drives oligomerisation. Although further studies would be needed to provide evidence for this.

This initial movement within the structure is likely the first step of the metamorphosis of CLIC1 and the elongated form must now be considered as a model when analysing CLIC1 interactions with drugs and ligands. The new sub state completely changes the environment of many residues within the structure which alters the binding sites and pockets seen through computational analysis of drug binding experiments. This could affect the affinity of many pharmaceuticals that were predicted based on affinity to the crystal structure or could lead to the development of new inhibitors that could target the extended sub state if it was proved essential for CLIC1 membrane insertion or metamorphosis.

The new sub state must be considered in drug prediction and in molecular dynamics simulations. Interestingly, alphafold was only able to predict the closed conformation, suggesting that in very dynamic proteins such as CLIC1, experimental data is providing an advantage over some of the new AI structure prediction techniques and can not be completely relied on in the case of metamorphic families such as CLIC.

In summary, we identify CLIC1 exists in solution as an ensemble of structures. CLIC1 due to flexibility of the loop bridging the C and N-terminal domain can exist in both a globular structure that matches the crystal structure and also a more extended structure. In this extended structure, the predicted transmembrane region of CLIC1 is

exposed, which we predict may play an influential role in the unique ability of the CLIC family to insert into the membrane.

3.5- Conclusion

The use of a combination of bioinformatics, small angle x ray scattering and NMR has ultimately derived regions of CLIC1 and conserved in the CLIC family regions of the structure that are inherently highly flexible. We have identified high flexibility in the loop in positions 88-101 linking the N- and C-terminus, and in combination with a reduced number of intermolecular interactions allows a conformational change within the structure. This conformational change results in a minor elongated sub state of CLIC1 to exist and the movement of the protein into this minor sub state is seen on a slow timescale. Such a state is likely involved as an initial step to expose the transmembrane region of CLIC1 to lipids which enables its metamorphic nature and its ability to insert into the membrane and act as a Chloride ion channel.

3.6- Future work

The majority of the future work will come down to determining whether this elongated state is essential to membrane insertion. Mutations that can stabilise the closed form by reintroducing interactions strong enough to prevent separation of the domains is a feasible mechanism. Firstly, SAXS could be repeated with these mutations to determine the structure now matches the crystal structure. Once this is evident, an insertion assay would be undertaken and compared against wild type CLIC1 which would determine whether a closed form of CLIC1 would still insert into the membrane which as it stands seems highly unlikely.

Further studies could also be completed in NMR. Residual dipolar couplings of N-H bonds could be repeated in further alignment media to further refine the structure. Along with other bond angles such as C-H, C-N C-Ha, C-Hb etc, these RDC values could be calculated which would further validate the averaged CLIC1 structure in solution seen in the NMR and provide confidence in the model produced.

Chapter 4: Elucidating the role of Zn^{2+} in aiding the membrane insertion of CLIC1

4.1- Abstract

CLIC1 is able to form a chloride ion channel upon exposure to lipids. However the percentage of CLIC1 that would insert into lipids compared to the percentage of soluble CLIC1 has always been a uncontrolled factor in experiments with this protein to date. Recently it was identified that divalent cations could trigger the switch between the soluble form of CLIC1 and the membrane bound form shifting the equilibrium towards the chloride ion channel. Within the breadth of divalent cations, there was a clear distinction that certain ions promoted membrane insertion more than others with zinc promoting a significantly greater level of membrane insertion than the other divalent cations.

In order to understand the role of zinc in changing the equilibrium between the two forms of CLIC1 we studied the Zn binding affinity and structural changes induced by this interaction using MST and NMR. Analysis using these two techniques identified low-medium affinity binding of zinc to CLIC1. NMR revealed chemical shift perturbations and intensity losses in residues surrounding the predicted transmembrane region. It is likely that Zn binding is disrupting the transmembrane region to promote accessibility of this hydrophobic patch to lipids to facilities the insertion of this transmembrane segment.

4.2- Introduction

To date, the molecular mechanism of the insertion of CLIC1 is unknown. Previous experiments have proposed potential triggers for the membrane insertion of CLIC1, however they are often conflicting and have limitations. One prior hypothesis pointed to oxidation promoting the membrane bound channel form. The study details that Cys24 and Cys59 formed a disulphide bond that stabilised a dimer. However further experiments demonstrated this oxidised dimer was not essential for membrane insertion or channel activity. This is compounded by the evidence that Cys59 is not conserved across the CLIC family which prevented the formation of a disulphide bond in other members of the CLIC family(Littler *et al.*, 2004).

Further studies pointed to activation of CLIC1 as a chloride channel occurring at pH5.5 (Fanucchi, Adamson and Dirr, 2008a) (Stoychev *et al.*, 2009). However a distinction must be made between the trigger for membrane insertion and activity of the CLIC1 chloride ion channel. The lowering of pH has been demonstrated to increase CLIC1 chloride channel activity, however no evidence to date has provided evidence that the lowering of pH promotes membrane insertion. Studies have actually provided evidence that the lowering of pH to 5.5 has no effect on membrane insertion of CLIC1(Varela et al., 2022).

We propose that membrane insertion of CLIC1 is triggered by binding to divalent cations with numerous studies demonstrating that ions can promote the interaction of proteins with lipids. This includes the family of annexins that upon calcium binding an N terminal-helix is expelled from the core of the protein that creates a calcium-induced conformation that preferentially interacts with the membrane(Rosengarth and Luecke, 2003). Further experiments present Ca^{2+} ions promoting membrane insertion of the human islet amyloid polypeptide (hIAAPP)(Sciacca *et al.*, 2013).

When the CLIC1 crystal structure was published there were no ligands found bound to the structure(Harrop *et al.*, 2001). However when the crystal structures of two CLIC1 homologues were published DmCLIC and EXC-4 from Drosophila melanogaster and Caenorhabditis elegans respectively, a Calcium ion was found bound to both proteins in the crystal structure (Berry *et al.*, 2003). The residues that form interactions with the Calcium ion are largely conserved across the entire CLIC family. These residues are also missing from the closest homologue to CLIC, the GST family. This suggests a functional role for this binding site and given that calcium can promote membrane insertion albeit less than zinc, clearly its binding plays an important role in its metamorphosis.

After discovering this calcium binding site, no further studies were conducted on the role of the divalent cations in the structure and function of the CLIC family. We sought to study the binding affinity of zinc and calcium to CLIC1 using MST. NMR can also provide valuable information about changes to the structure and dynamics of CLIC1 in the presence of divalent cations.

Identifying the role of divalent cations in promoting the switch between soluble form and chloride ion channel form could provide information on which regions of CLIC to target for drug binding to prevent this molecular switch and could provide treatment for cancers with a very high level of membrane bound CLIC1 which promotes oxidative stress.

4.3- Results

4.3.1- MST identifies divalent cation binding to CLIC1 and the affinity of the interaction

In order to identify whether divalent cations bind to CLIC1, we used microscale thermophoresis. A protein construct containing a C terminal GFP tag was used in order to act as the fluorophore. MST is useful at identifying binding of a ligand as it can identify changes to the fluorophores microenvironment which will come about as a result of ligand binding if such an event occurs. Thermophoresis describes the event of movement of particles in a temperature gradient. Thermophoresis is dependent on a variety of factors including size, charge and solvent exposure. When proteins bind to a ligand and form a protein-ligand complex this often alters changes in size, charge and solvent exposure. Eventually these ligand induced changes will saturate when the protein is fully saturated with ligand (Jerabek-Willemsen *et al.*, 2014).

CLIC1 was at a concentration of 4um and asolectin lipids were provided at a concentration of 50μm to prevent aggregation of CLIC1 that can occur without lipids in the presence of Zn2+. An increasing concentration of Zn2+ results in an increasing amount of aggregation which would provide anomalous values without lipids. MST identified that both Zn2+ and Ca2+ are able to bind to CLIC1 in the presence of asolectin vesicles. MST demonstrated at this concentration, Zn and Ca have relatively similar binding affinities to CLIC1 with an affinity of 0.3mM. This Kd suggests CLIC1 binds weakly to Zinc and Calcium ions at this concentration of protein and lipids at seen in figure 4.1.

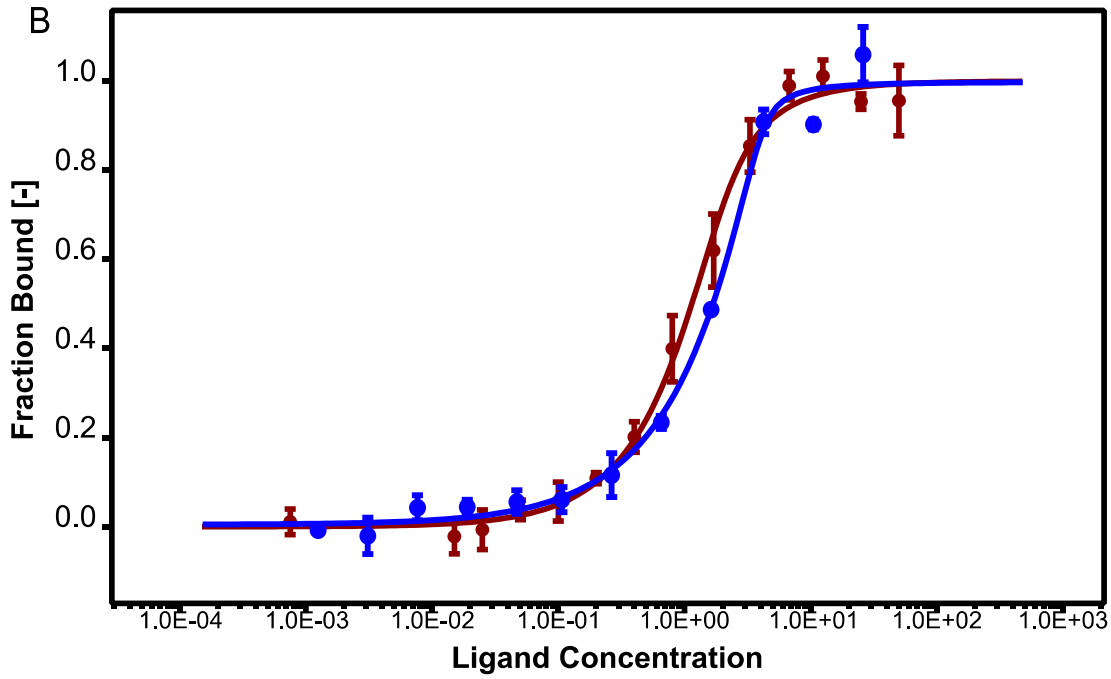
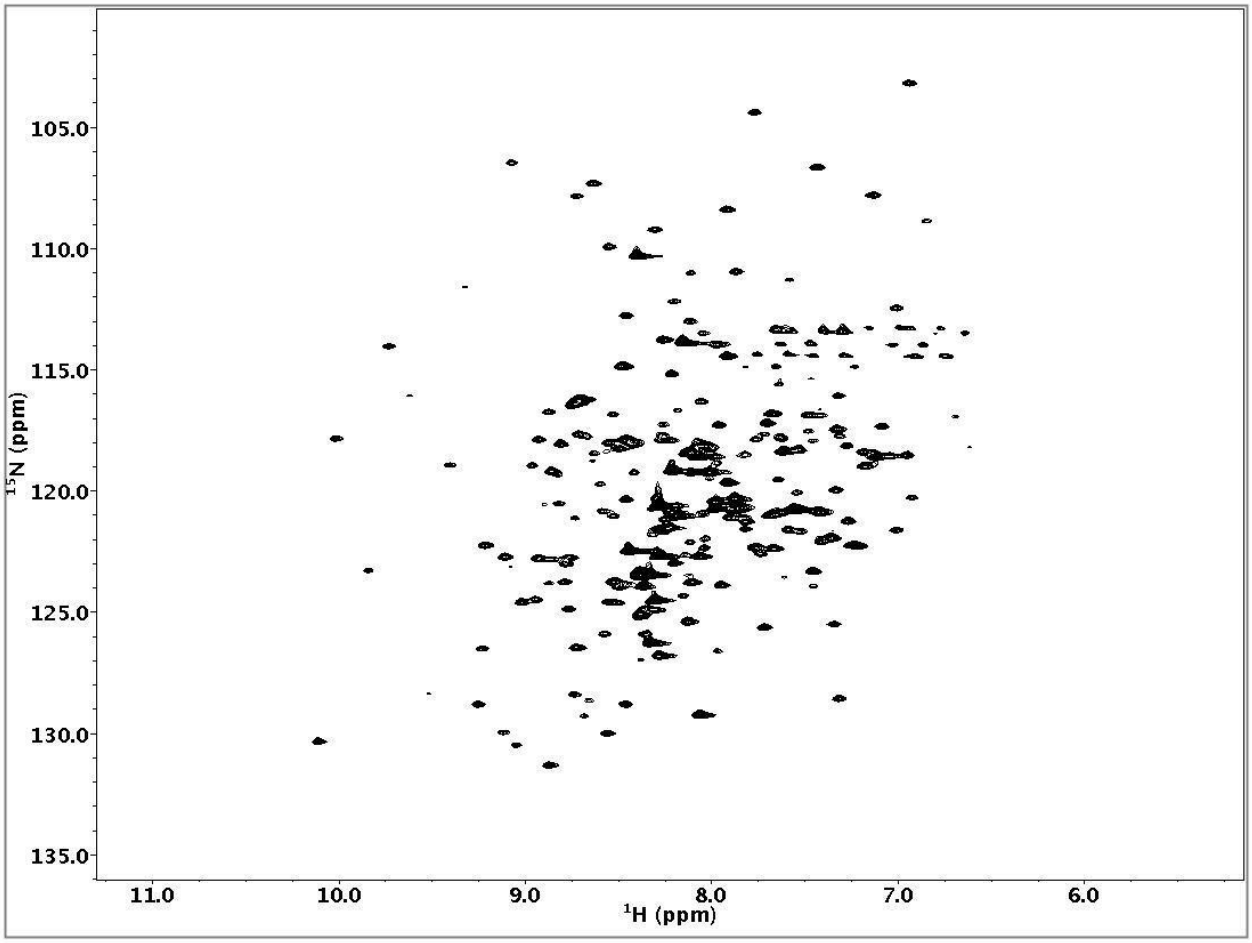


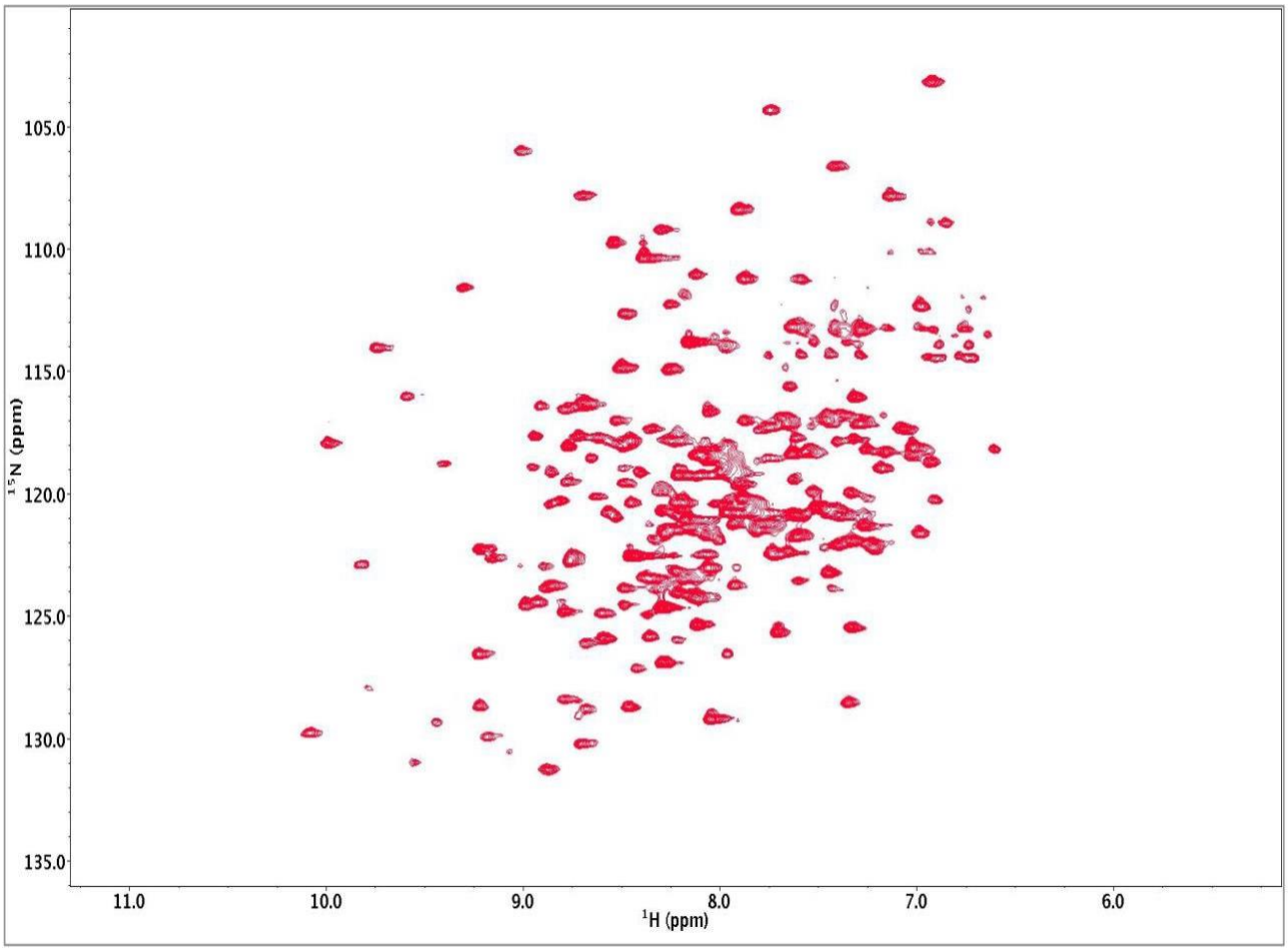
Figure 4.1: CLIC1 binds to Zinc and Calcium demonstrated by MST- Microscale thermophoresis binding curve of CLIC1 in the presence of increasing amount of Zn^{2+} (blue) and Ca^{2+}(red). Standard deviation of each point is represented through error bars.

4.3.2- NMR identifies residue specific changes to CLIC1 upon Zinc binding

Given the previous literature suggesting Zinc promotes membrane insertion and the MST data that demonstrates zinc binds (Varela et al., 2022), NMR is the perfect tool to identify the residues that bind to zinc and the residues that have their environment altered by zinc. (Becker *et al.*, 2018). Solution state NMR was carried out on a 300uM sample of CLIC1 initially with 0 molar ratio Zinc. Molar ratio describes the concentration of ligand proportionally against the concentration of protein, therefore as the protein concentration is 300μM, then 0.5MR would be 150μM. Then increasing amounts of Zn2+ was added until a maximum of 1MR (300um) Zn. In solution state NMR, lipids could not be added as the protein would insert into the membrane in a solid state and would then therefore not be visible by solution state NMR.

The first observation of the data is that the Kd for Zinc binding to CLIC1 seems to be significantly higher than in the MST experiments, as specific residues completely lose any visible intensity after as low as 0.5MR ZN. An increasing number of residues seemed to disappear as the concentration of Zinc increased in figure 4.2, suggesting these residues had their environment altered. The concentration of Zinc was not increased greater than 1MR as this promotes aggregation and would lead to artefacts within the spectrum.




105.0
110.0
115.0
120.0
125.0
130.0
135.0
^{15}N (ppm)
11.0
10.0
9.0
8.0
7.0
6.0
^{1}H (ppm)

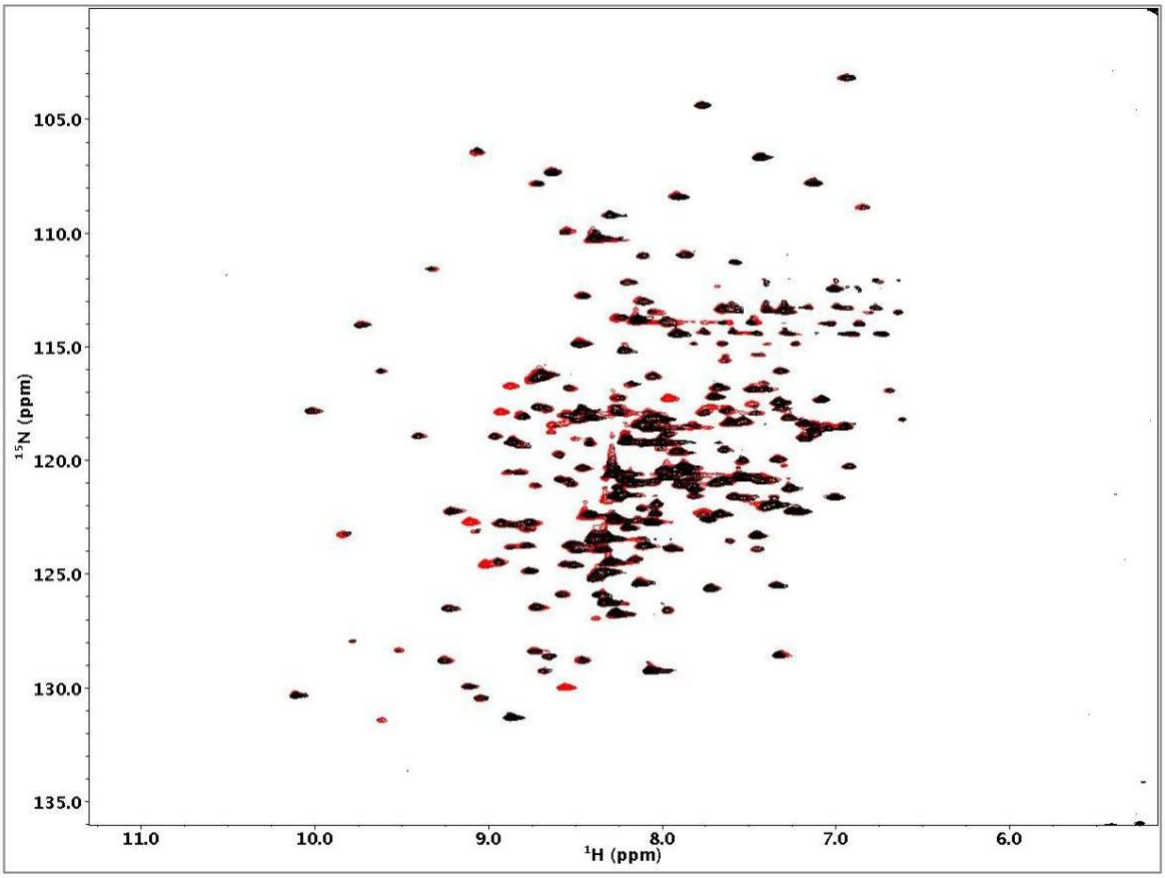


Figure 4.2: TROSY-HSQC of CLIC1 binding to 1MR Zn2+- A) 15N labelled CLIC1 with 1MR Zn^{2+} B) 15N labelled CLIC1 C) Overlay of CLIC1 with 0MR Zn^{2+}(Red) and 1MR Zn^{2+} (Black)

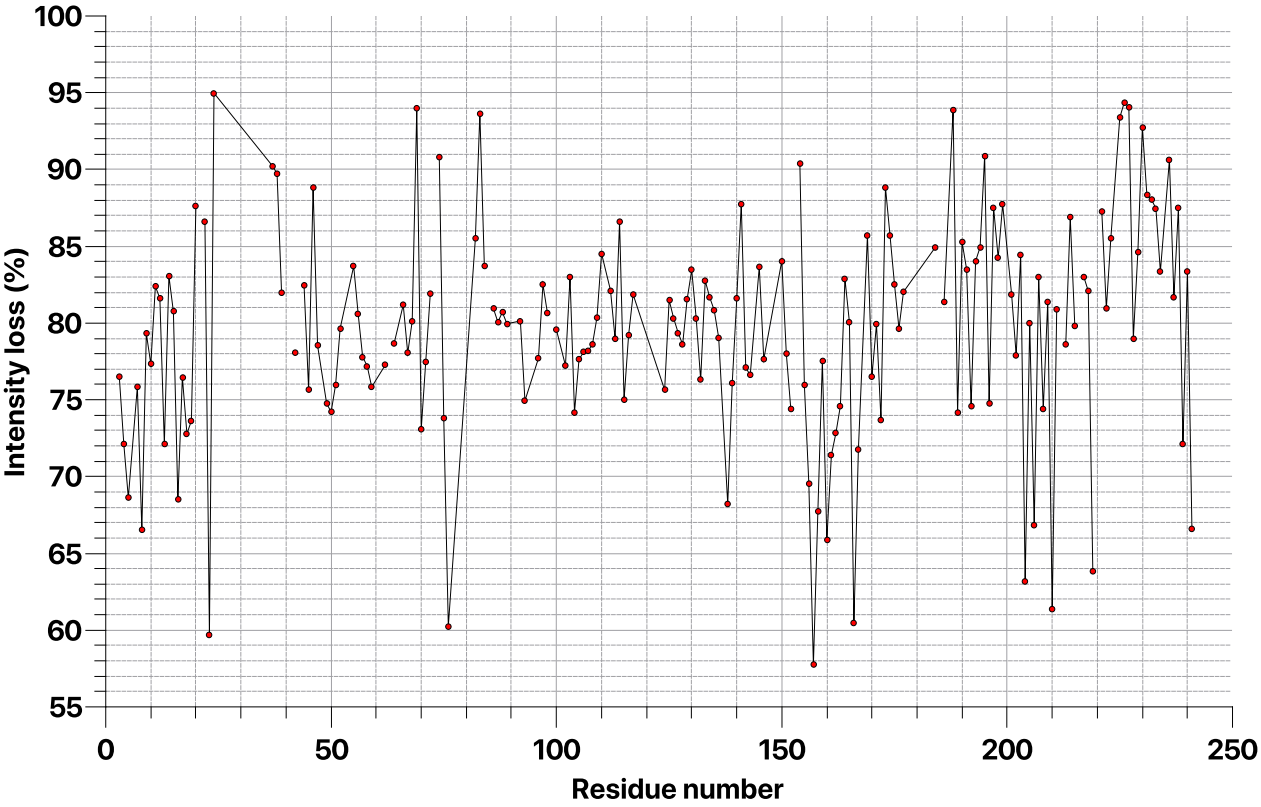
The intensities for all assigned residues were measured and compared against the intensities of the residues without the presence of Zinc. To avoid a bias for decreasing intensity of residues that have high or low initial starting intensities a percentage was used.

$$\frac{\text{(Intensity of residue without Zinc- Intensity of residue with zinc corrected for dilution factor)}}{\text{Intensity of residue without zinc}} \text{X100} = \% \Delta \text{ Of residue x}$$

Figure 4.3: Intensity loss calculation for NMR peaks- This equation determines intensity loss of each peak from one HSQC spectrum to another. By dividing the change in intensity over the original intensity it normalises the values for all peak losses compared to initial intensity. The intensity of a HSQC peak on a spectrum after a ligand addition is also corrected for a dilution factor where the addition of a specific volume of ligand would increase the overall volume of the sample. This increase in volume of sample would result in a proportional loss of intensity for all residues which the dilution factor negates the effect of.

The greatest percentage change in residues intensity was seen in three key places. One in the loop N-terminal to the unassigned transmembrane region spanning residues 20 to 24, one in the region spanning residues 65 to 76 and the final region on the C terminal side spanning residues 225 to 230. These regions have been highlighted as red in the figure 4.3 of CLIC1. The red regions were identified to have a greater than 60% percentage loss of intensity. All other residues were highlighted in green as having a lower percentage intensity loss.

Chemical shift perturbations were not calculated in these results as there were no trackable changes to peak values. A few new peaks appeared however but it was impossible using this data to accurately predict which residues these accounted for as a result of Zinc binding without a backbone assignment of the Zn-bound form. Unassigned residues (represented in grey) may also experience large loss of intensity but can not be accounted for. Also in the presence of zinc, CLIC1 oligomerises and this will have an impact on the spectrum and subsequent data analysis and a further solution NMR zinc binding studies had to be completed CLIC1 constructions designed to prevent oligomerisation. The effect of Zinc on the oligomerisation state of CLIC1 will be looked at later in this chapter specifically in section 4.3.5 which covers this in great detail.


Intensity loss (%)
100
95
90
85
80
75
70
65
60
55
0
50
100
150
200
250
Residue number

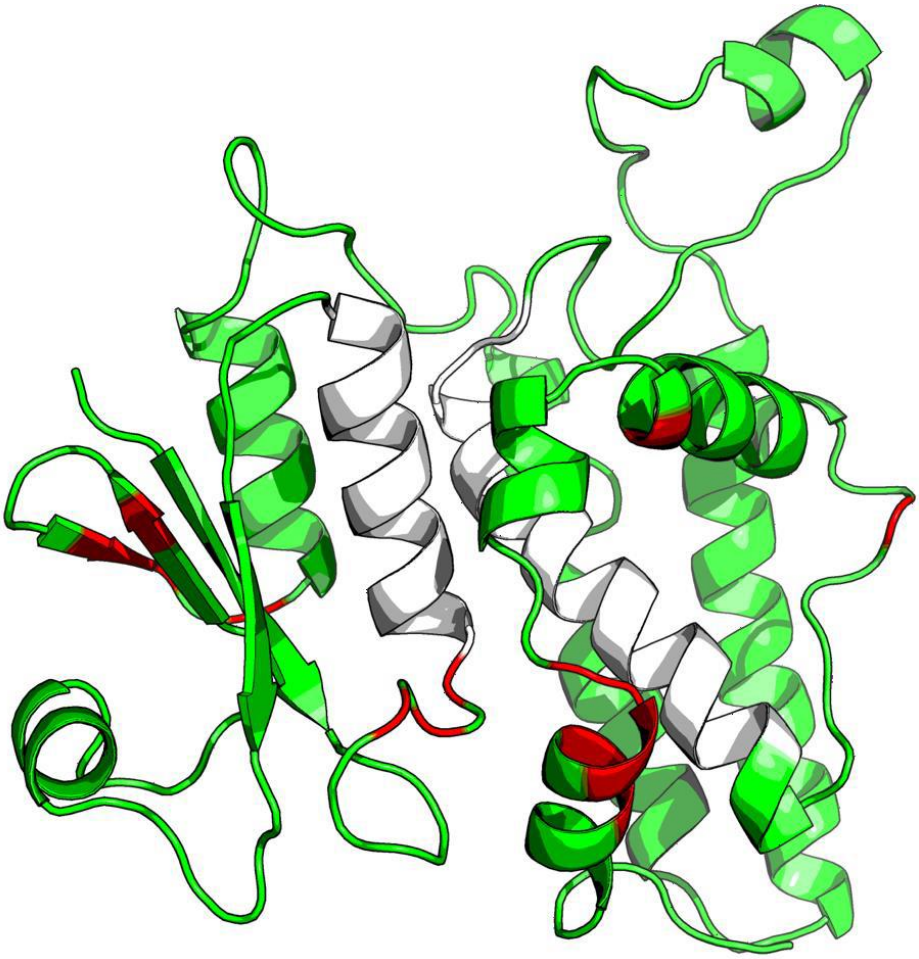
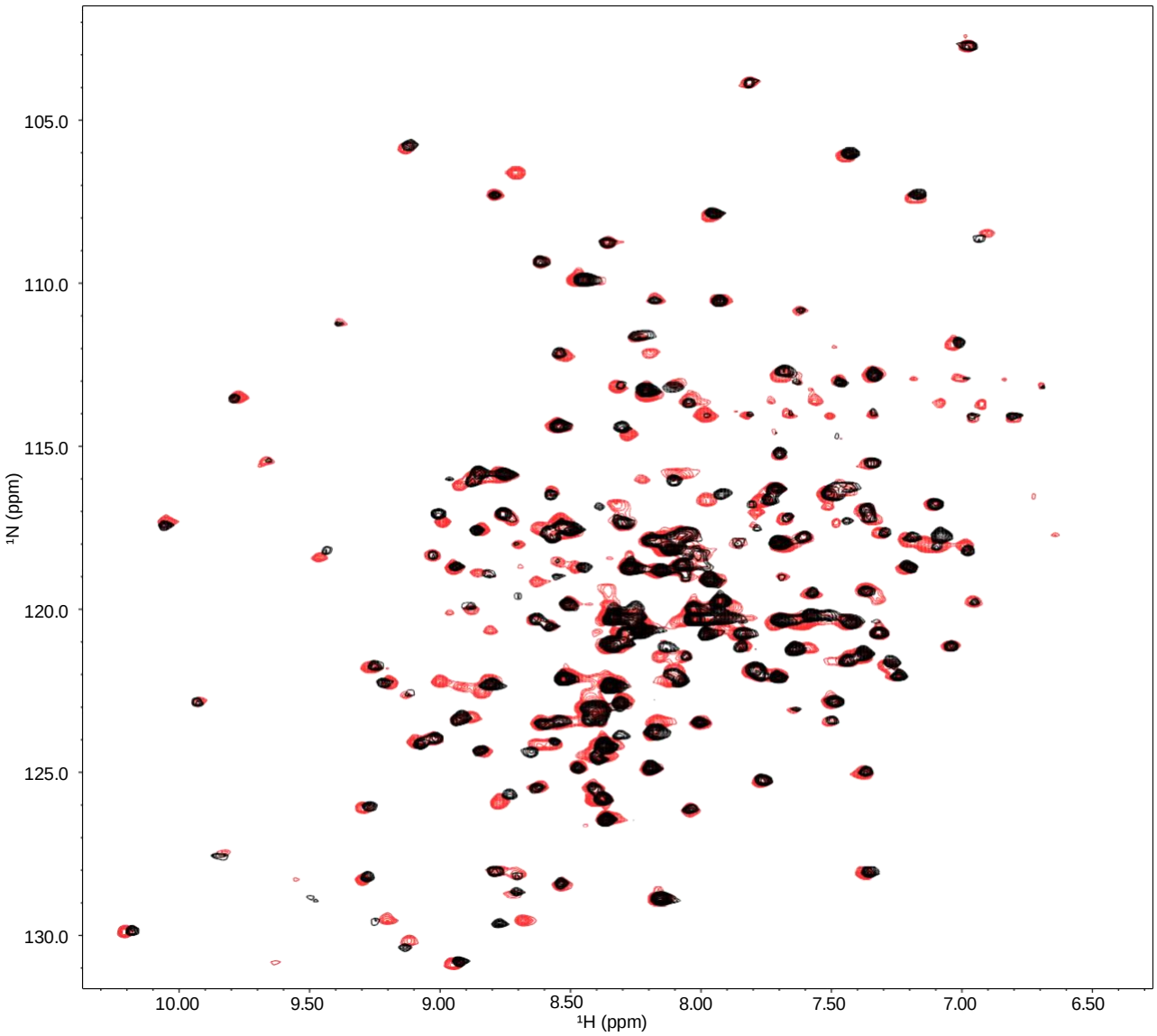


Figure 4.3. CLIC1 peak intensity changes after Zinc binding- A) Graph demonstrating the intensity losses of assigned residues in CLIC1 after zinc binding. Intensities were extracted from a HSQC-TROSY experiment in the presence of 0MR and 1MR(300μM) zinc. B) The residues with the greatest proportional loss of intensity are seen in red. The rest of the molecule is seen in green, with unassigned residues depicted as white. Largest changes occur in three places, residues 20-24, 65-76 and 225-230.

4.3.3- The CLIC1 structure is not impacted by Zinc in the same mechanism as pH

Recent literature was able to insert CLIC1 into the membrane using an excess of zinc(Varela et al., 2022). The question remained whether the excess of zinc was causing a large drop in pH that promoted insertion of CLIC1 into the membrane. Further literature also states CLIC1 chloride ion channel conductance is highest at pH 5.5. Therefore solution NMR was used to collect spectra of CLIC1 at the pH values of 7.4, 7, 6.5 and 5.5 to identify whether residue specific changes occurred and if they are similar or identical to the changes observed upon zinc binding.

Percentage change was again calculated to identify a clear difference in intensity for each residue. All residues experienced some intensity loss at pH 5.5 due to minor amounts of aggregation but the sample was spun and filtered to remove all aggregates prior to the collection of data at pH 6.5 and 5.5.


105.0
110.0
115.0
120.0
125.0
130.0
¹N (ppm)
10.00
9.50
9.00
8.50
8.00
7.50
7.00
6.50
¹H (ppm)

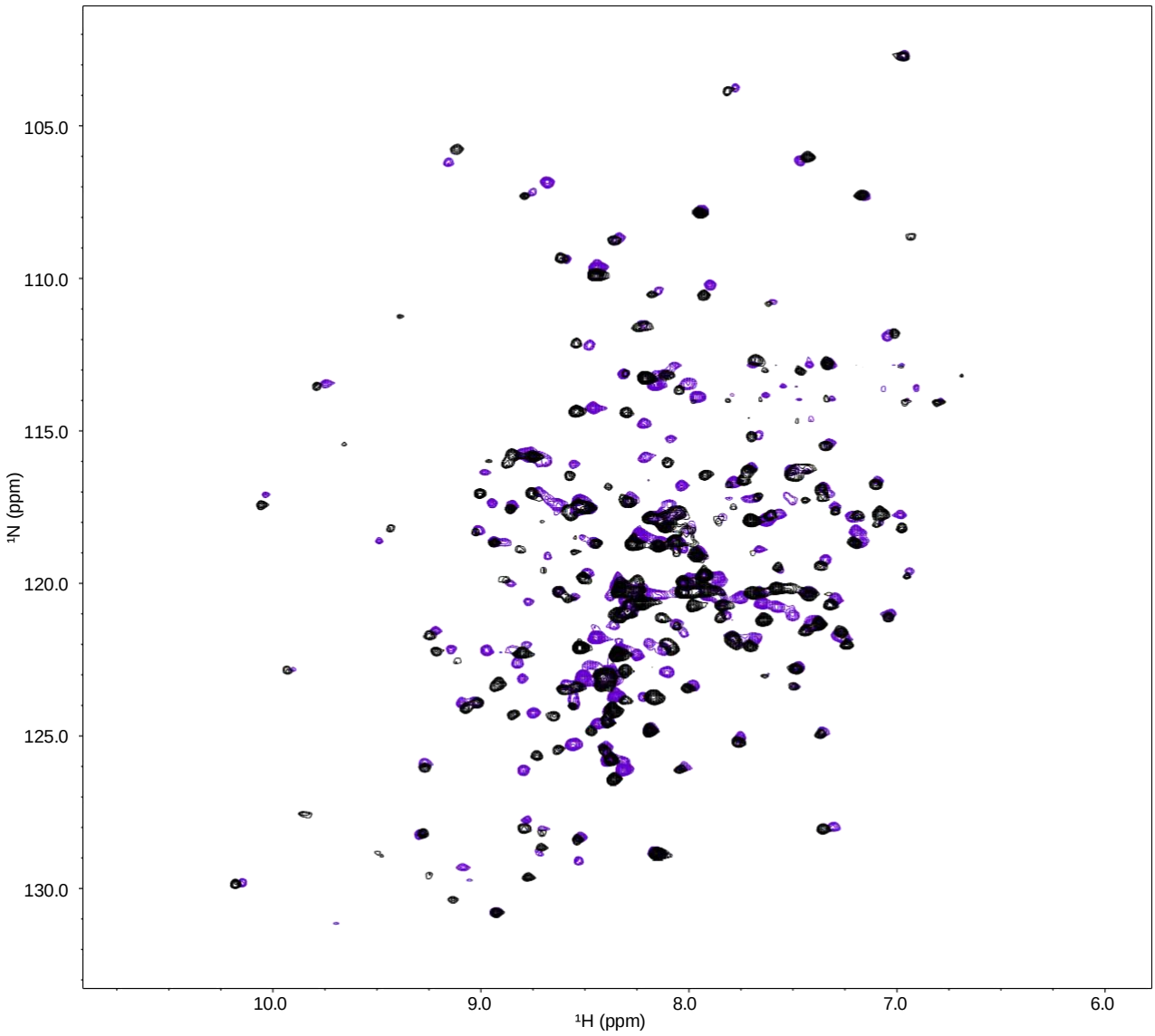


Figure 4.4: NMR pH titration of CLIC1 from pH 7.4 to pH 5.5- TROSY-HSQC was carried out for CLIC1 at these current pH values A) pH 7.4 (Black) overlaid with pH 6.5(red) B) pH 7.4 (Black) overlaid with pH 5.5(purple).

A comparison was made of the intensity of every residue from pH 7.4 to pH 5.5 where CLIC1 is most active in the chloride ion channel form. There is too some extent an intensity loss in almost every assigned residue. There is a large intensity loss of >40%

for many residues in the beginning of the foot loop particularly 165-172 evidenced in figure 4.5.

The results demonstrate the change of environment at pH 5.5 is having a greater impact on this region of the protein than other regions. Although for dynamic regions that experience high T1 relaxation this does not guarantee a drastic change in the structure, it is highly likely to be explained as minor movements of the loop on a fast timescale. Intensity changes to residues could also be caused by being in close proximity to histidine residues that have changed protonation state or alternatively intensity losses could be seen primarily in more solvent exposed regions. However neither of these causes of intensity loss could explain the changes of intensity for the foot loop region.

Overall pH 5.5, does not seem to elicit any large scale changes to specific regions of CLIC1. The intensity losses are scattered across all regions of CLIC1 and represent no real pattern of specific area of enquiry. It is likely the lower pH has changed the environment of almost every residue within CLIC1 which would be expected simply as a change in protonation state of Histidines. This is not indicative of any large scale

conformational changes to CLIC1.

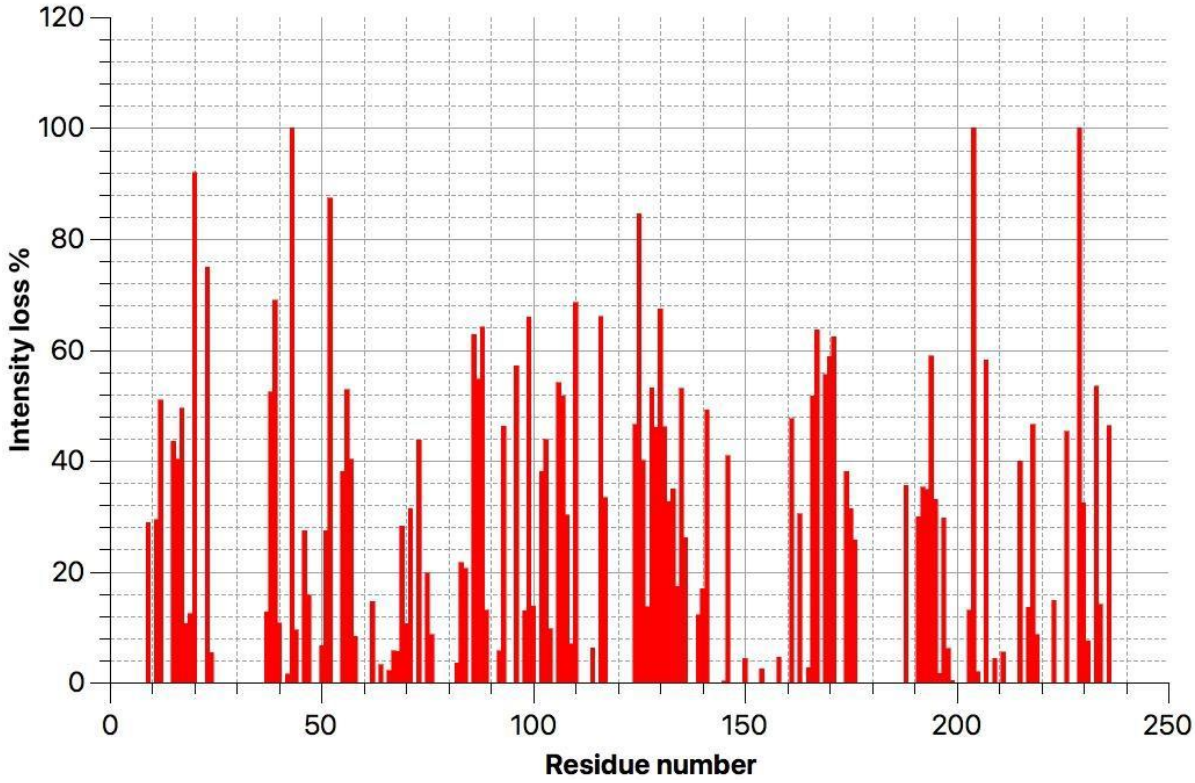
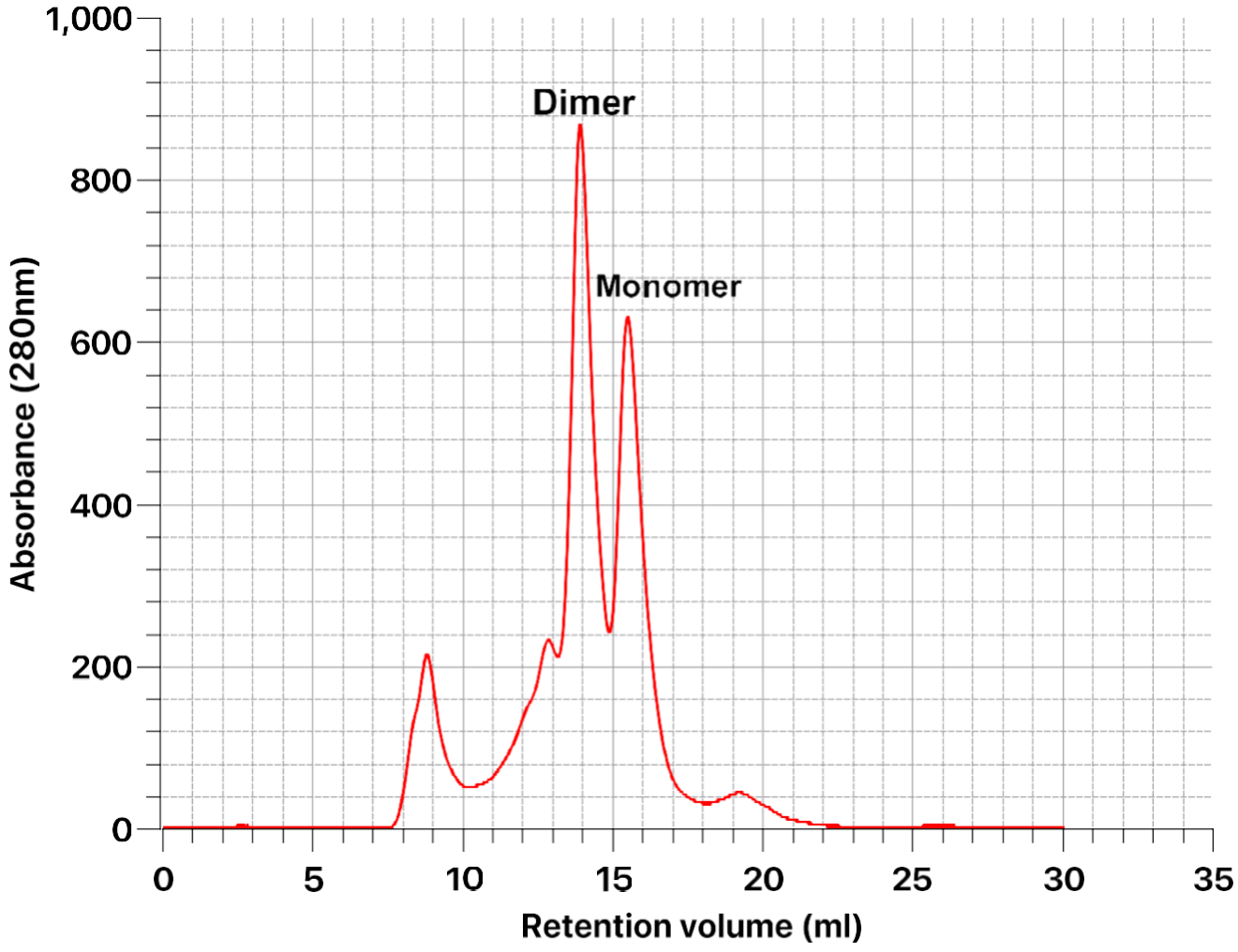


Figure 4.5: Intensity loss of peaks in CLIC1- Intensity losses were calculated from assigned residues spanning pH 7.4 to pH 5.5. Intensity values were extracted from centered peak positions from the TROSY-HSQC spectra. Intensity loss as a percentage against initial intensity was then plotted against residue number

4.3.4- An N terminal his tag prevents oligomerisation effects upon Zn binding

The previous Zinc binding titration to CLIC1 yielded residue specific information as to the impacts of Zinc binding to CLIC1. Although as zinc binding also promotes oligomerisation of CLIC1, the intensity losses and chemical shift perturbations to residues may be a result of changing environments of the oligomerisation in addition to direct zinc binding.

In order to remove this effect, a CLIC1 construct was used which contained a N terminal His-tag. With this tag present oligomerisation is prevented and only monomeric species is observed in solution in comparison to an untagged CLCI1 sample that will contain monomers, dimers and potentially tetramers if the concentration is high enough(Peter *et al.*, 2013). With the tag present and only monomeric species in solution, the changing environment of residues should be more specific to the direct binding event and structural rearrangements of the monomer and not of any higher order species. (Turkewitz *et al.*, 2021a)



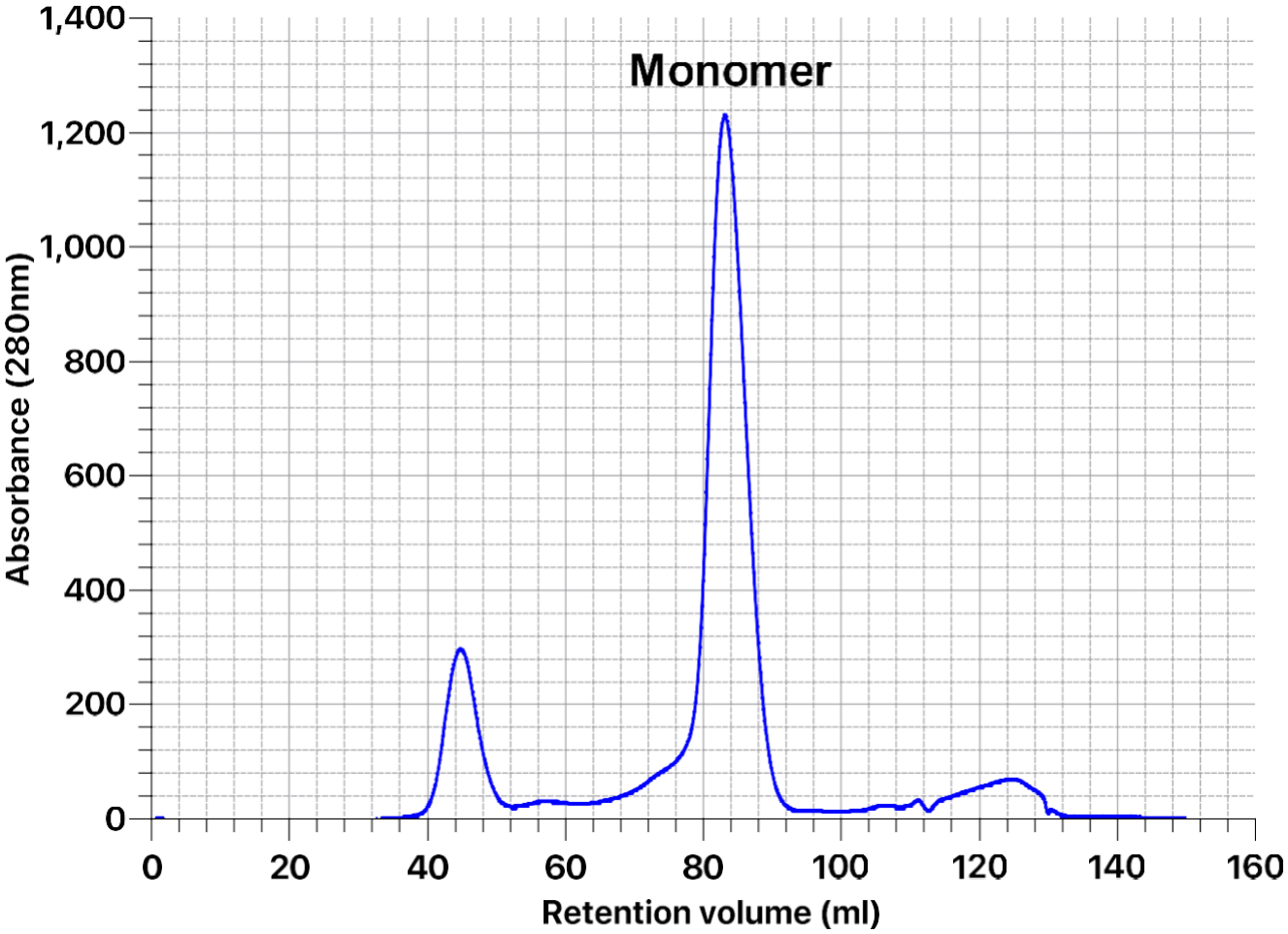
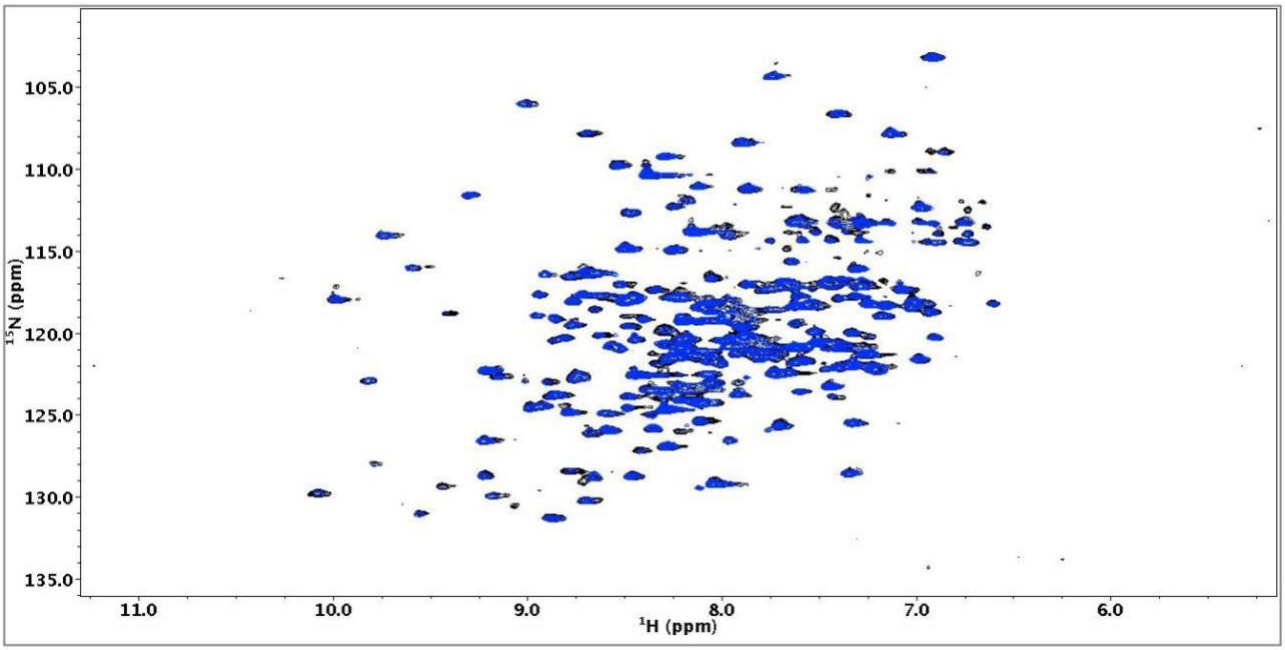


Figure 4.6: A His-tag disrupts the formation of CLIC1 dimer causing CLIC1 to exist exclusively as a monomer-A) Superdex-200 SEC trace of CLIC1 wild-type in buffer 150mM Hepes 50mM NaCl pH 7.4. The dominant species in solution are the monomer and dimer which have respective sizes of 27kDa and 54kDa. **B)**Superdex-200 SEC trace of CLIC1- His-tag in buffer 150mM Hepes 50mM NaCl pH 7.4. The largest elution volume is the monomer which is a size of 27kDa.

To this extent a TROSY-HSQC was collected on a 300uM sample of CLIC1 and zinc was titrated at molar ratios Zn:CLIC1 of 0.1, 0.25, 0.5 and 1, with respective concentrations of 30, 75, 150 and 300uM zinc. A final TROSY-HSQC was collected of

the 1MR zinc titration with 1mM of EDTA added to the sample in an attempt to identify whether zinc binding to CLIC1 is a reversible event in solution (figure 4.7).



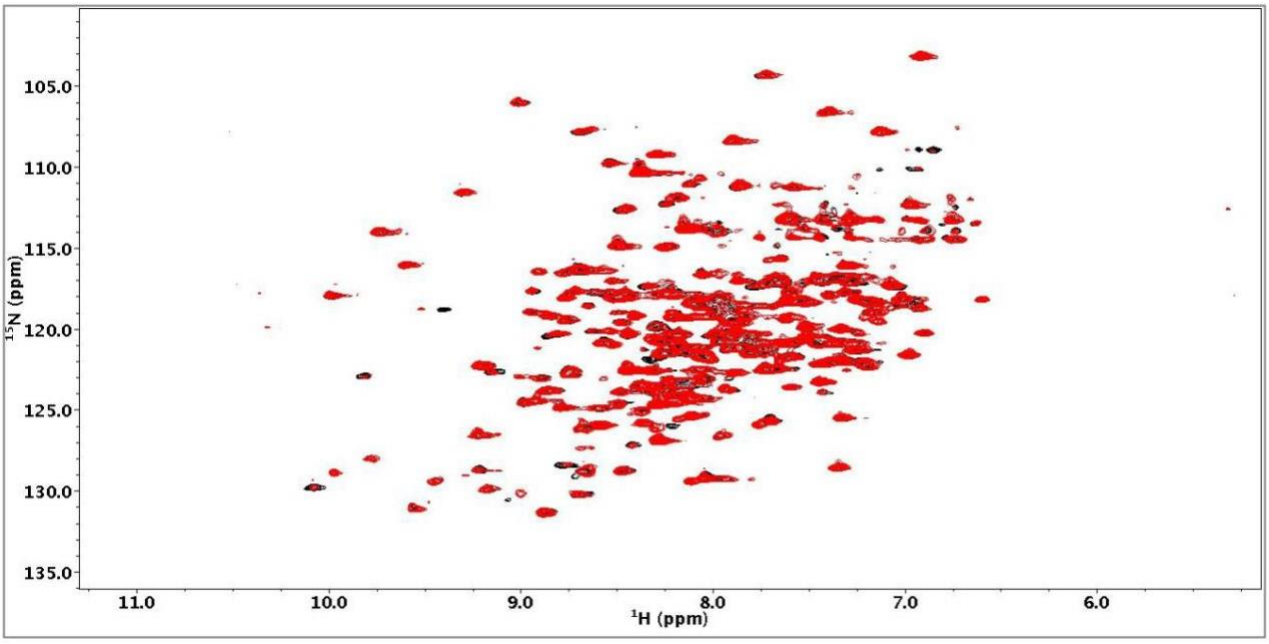


Figure 4.7: TROSY-HSQC of CLIC1 His-Tag with Zn2+ titration- A) CLIC1 His-tag (Black) overlayed with CLIC1 His-tag with 0.5MR Zn^{2+} (Blue) B) CLIC1 His-tag (Black) overlayed with CLIC1 His-tag with 1MR Zn^{2+} (Red) C) CLIC1 His-tag with 1MR Zn^{2+} (Red) overlayed with CLIC1 His-tag with 1MR Zn^{2+} and 1mM EDTA (Purple).

Compared to the zinc titration without the tag, there are intensity losses as low as 0.5MR Zn in addition to chemical shift perturbations and new peaks. The new peaks cannot be identified as to what residue this corresponds to without a backbone assignment although will likely correspond to one of the peaks with a large intensity loss. One notable difference is the observation of the bound state. In figure 4.7, Try35 has two peaks seen on the spectrum. One peak referring to the unbound state without Zinc and one peak referring to the bound state with Zinc present. The two peaks are in slow exchange as when the concentration of Zinc increases it shifts the population towards the bound state.

Without the oligomerisation effect occurring with the tag, it is easier to clearly see the bound and unbound states of many residues. In addition after reaching a maximum of 1MR Zn to fully saturate the binding of Zn to CLIC1, a 1mM sample of EDTA was added to the sample. EDTA is an ion chelator and would chelate the zinc ions present in solution and those bound to CLIC1.

This causes Zn to unbind from the CLIC1 binding site and subsequently we see the spectrum return to its original state before Zinc was added to the sample. Almost every chemical shift perturbation and intensity loss is reversed, matching almost identically the original spectrum. This demonstrates that zinc binding with the CLIC1 monomer is a reversible event although if oligomerisation follows then this event is not reversible.

The intensity losses at 1MR Zn were mapped as a percentage loss compared to the original intensity without zinc as to not bias peaks with low or high starting intensities. In figure 4.8 there is a clear greater intensity loss on the N terminal domain compared to the C terminal domain. Although the far end of the C terminal domain also experiences large intensity losses. Largely the structured domains in the centre of the monomeric species experience only minor intensity losses. The vast majority of the greatest intensity losses >60% are from residues surrounding the transmembrane region, located between residues 26-46. A large proportion of the transmembrane region is shown in grey as it is unassigned in the backbone assignment. The largest intensity losses in the transmembrane region and the regions surrounding it demonstrates these residues are most effected by zinc binding to the monomeric structure.

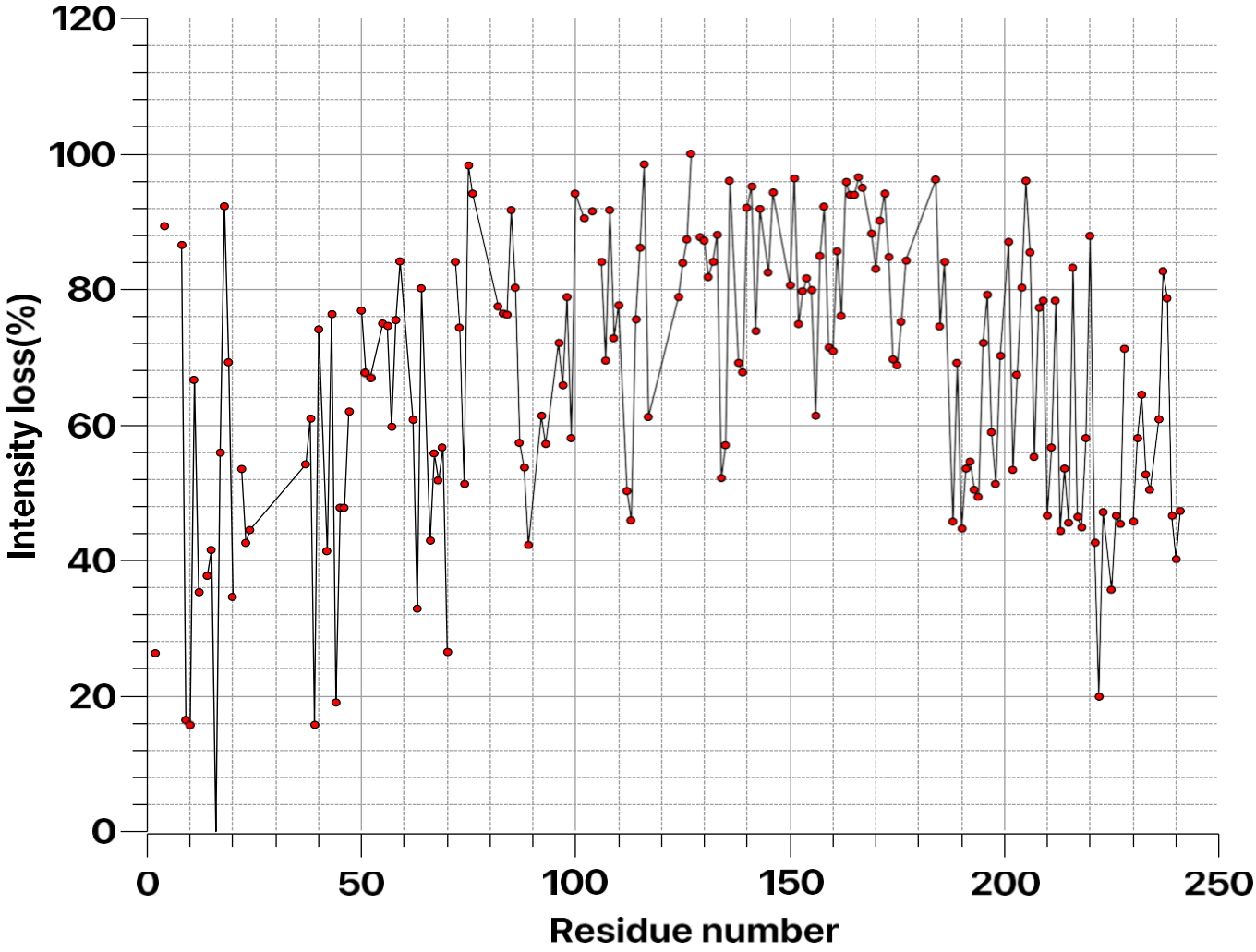


Figure 4.8: CLIC1 experiences greater intensity losses from Zinc in the N terminal domain than the C terminal domains- Peak Intensity was calculated from the TROSY-HSQC of CLIC1 His-tag spectra including 0MR Zinc and 1MR Zinc. These peak intensity differences were plotted as a percentage loss of the original peak intensity and plotted against residue number for all assigned residues with little to no overlap.

This area of CLIC1 surrounding the transmembrane region is experiencing a new environment that could be the result of zinc binding creating a bound state or alternatively due to conformational changes that occur as a result of zinc binding. It is

likely this is both as zinc binding is destabilising this region of the protein. There are some further changes that occur as a result of zinc binding, a large drop in intensity in the N terminal Beta sheets and some residues that occur in the loops of the protein.

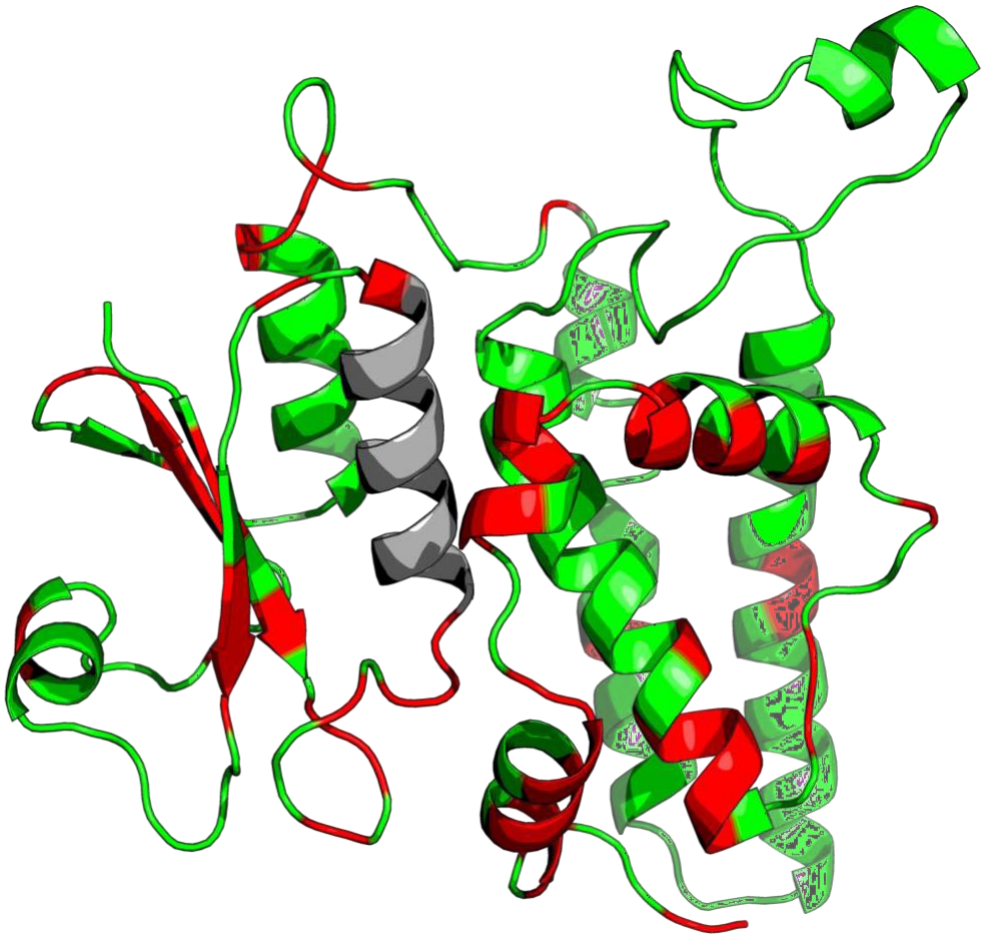


Figure 4.9: Pymol mode of greatest CLIC1 His-tag peak intensity changes after Zinc binding- The residues with the greatest intensity loss are depicted in red. Unassigned residues in the transmembrane domain are depicted in grey and all other residues are depicted as green. The vast majority of large intensity losses are present in and around the predicted TM domain.

4.3.5- Zinc promotes the oligomerisation of CLIC1 and higher order states

In order to determine the true extent to which Zinc binding affects oligomerisation and the production of higher order species, Size Exclusion Chromatography coupled to SAXS detection (SEC-SAXS) was used. SEC-SAXS can separate the individual oligormeric states of and collect individual data for each of them if the peaks are sufficiently separated in the chromatogram. The combination of techniques enable the identification of the CLIC1 oligomeric species, their quantification and the prediction of their size as seen in figure 4.10.

When no zinc was present (trace is shown in blue) CLIC1 exists largely as a monomer in solution with a dimer also present in small amounts that is in equilibrium with the monomer. Trace amounts of tetramer can be likely detected as a small indent rather than a clear peak. This type of chromatogram is consistent with the normal equilibrium seen after every purification of CLIC1 on a Superdex 200 size exclusion column.

When 0.5MR of zinc is added, this drastically increases the rate of oligomerisation and changes the intensity of the original peaks. The monomer peak decreases in intensity for the zinc bound CLIC1 SEC trace. The intensity of the Zinc bound monomer is not visible on the trace. The dimer peak with Zinc bound increases in intensity and becomes the dominant species in solution. In addition an increase in the amount of tetramer is also demonstrated for 0.5MR Zn, since its intensity has increased from trace amounts to a clear observable peak. Additionally we see a very large peak appear that is greater in size than the tetramer. This peak is caused by the aggregation of CLIC1 in solution triggered by zinc binding.

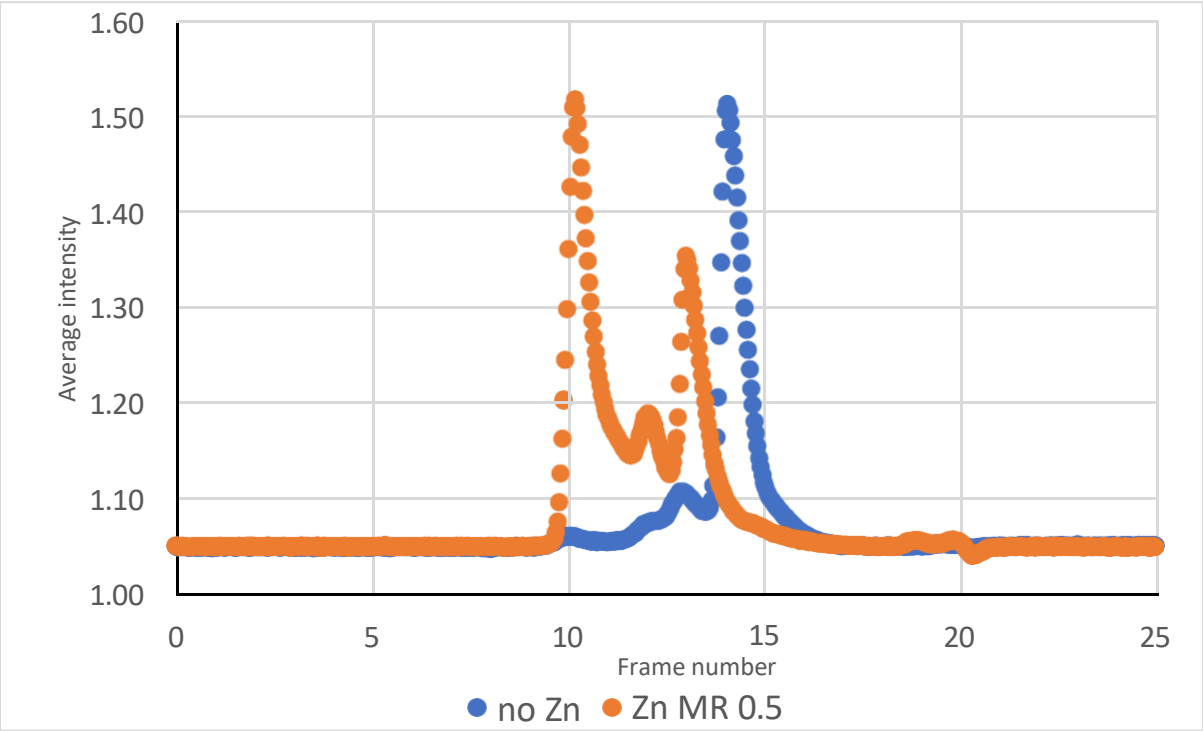
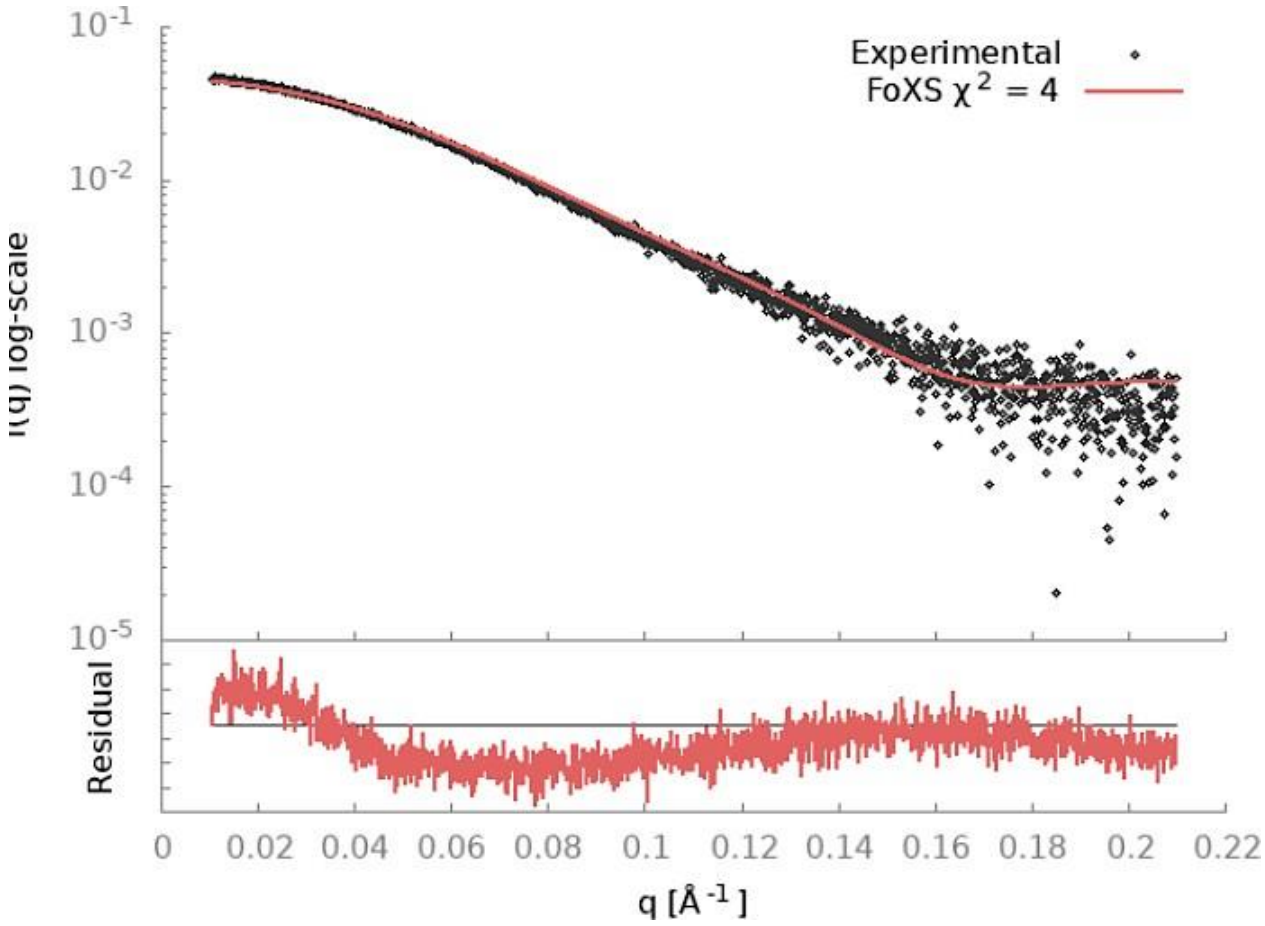


Figure 4.10: Zinc binding promotes oligomerisation of CLIC1- SEC-SAXS profile using Showdex-403 at 15C. The SEC trace for CLIC1 with 0MR(0um) Zinc is shown in blue whilst the SEC trace for CLIC1 with 0.5MR(750um) Zinc is shown in orange.

The membrane bound of CLIC form is predicted to adopt a tetrameric assembly based on chloride ion channel assays (Warton *et al.*, 2002b). The SEC trace suggests that zinc is increasing the presence of the higher oligomer that has the same stoichiometry as the membrane bound form of the chloride ion channel. It is important to note that the dimer and tetramer species observed in the zinc bound form did not match the scattering data of the dimer and tetramer species of the unbound CLIC1, which suggests that CLIC1 can occupy different conformations of higher order species in the presence of zinc compared to without zinc.

4.3.6- Alphafold predicts the structure of the dimer

A structure of the dimer of CLIC1 was published under oxidising conditions. This has been an accepted model of the dimer although recent literature suggested oxidisation was not essential or required for membrane insertion. So the question remained whether the proposed dimer crystal structure was accurate in solution. To that extent SAXS was conducted for a 800uM sample of CLIC1 at pH 7.4. The small angle x ray scattering data for the dimer was analysed and compared using FOXS software against the oxidised dimer.



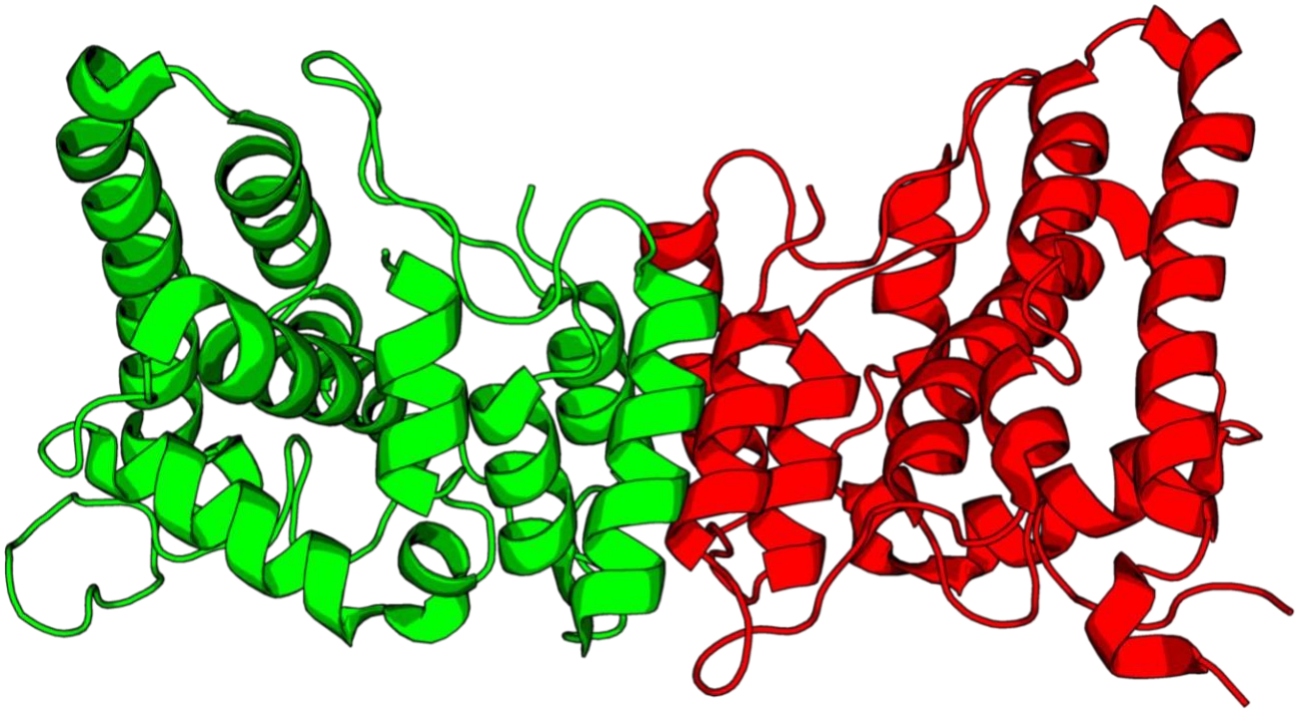
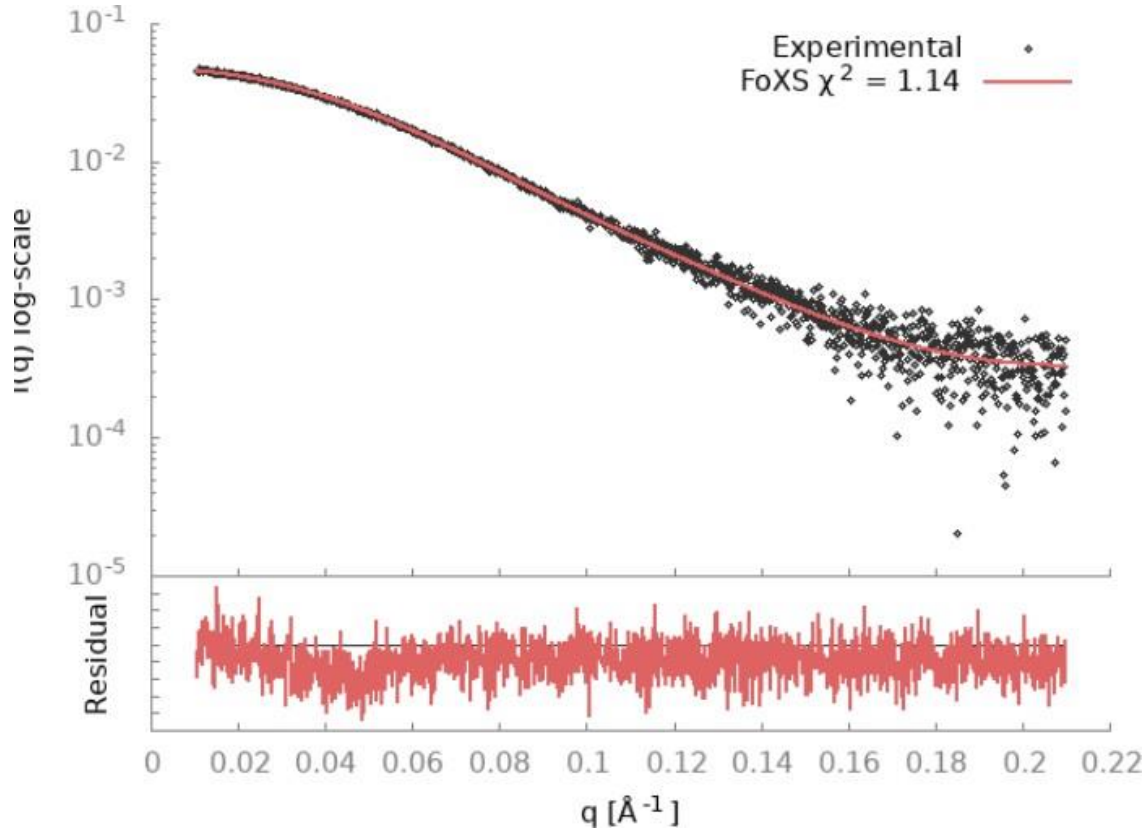


Figure 4.11: FOXS server comparison of CLIC1 oxidised dimer crystal structure predicted scattering data against experimental CLIC1 dimer scattering data: A) Real CLIC1 scattering data is shown in black and the predicted scattering data is shown in red. The 1rk4 crystal structure provides a poor fit to the experimental scattering data with a chi-squared score of 4. B) Pymol image of 1rk4 crystal structure of CLIC1 oxidised dimer. Chain A is coloured green, whilst chain B is coloured red.

The poor fit between the predicted scattering data of the oxidised dimer and the experimental dimer scattering data indicates, this structure is not physiologically relevant in solution.. Alphafold is a machine learning computational method to predict 3D structures of proteins built upon its learning of current protein data bank structures. It is currently the only known computational method to very accurately predict protein structures that match experimental data, with over 200 million protein structure predictions that are openly accessible (Varadi *et al.*, 2022) (Jumper *et al.*, 2021). With the rise of alphafold, this AI program is able to predict the structure of higher order

states due to the development of alphafold multimer. Alphafold multimer v2 predicts a novel dimer structure that significantly and more accurately matches the x ray scattering data. The predicted dimer suggests N terminal interactions exist which are consistent with previous data suggesting an N terminal tag interferes with oligomerisation. N terminal interactions are required to form a dimer and potentially higher order states. However, it is unknown so far whether this dimer plays any role in membrane insertion.



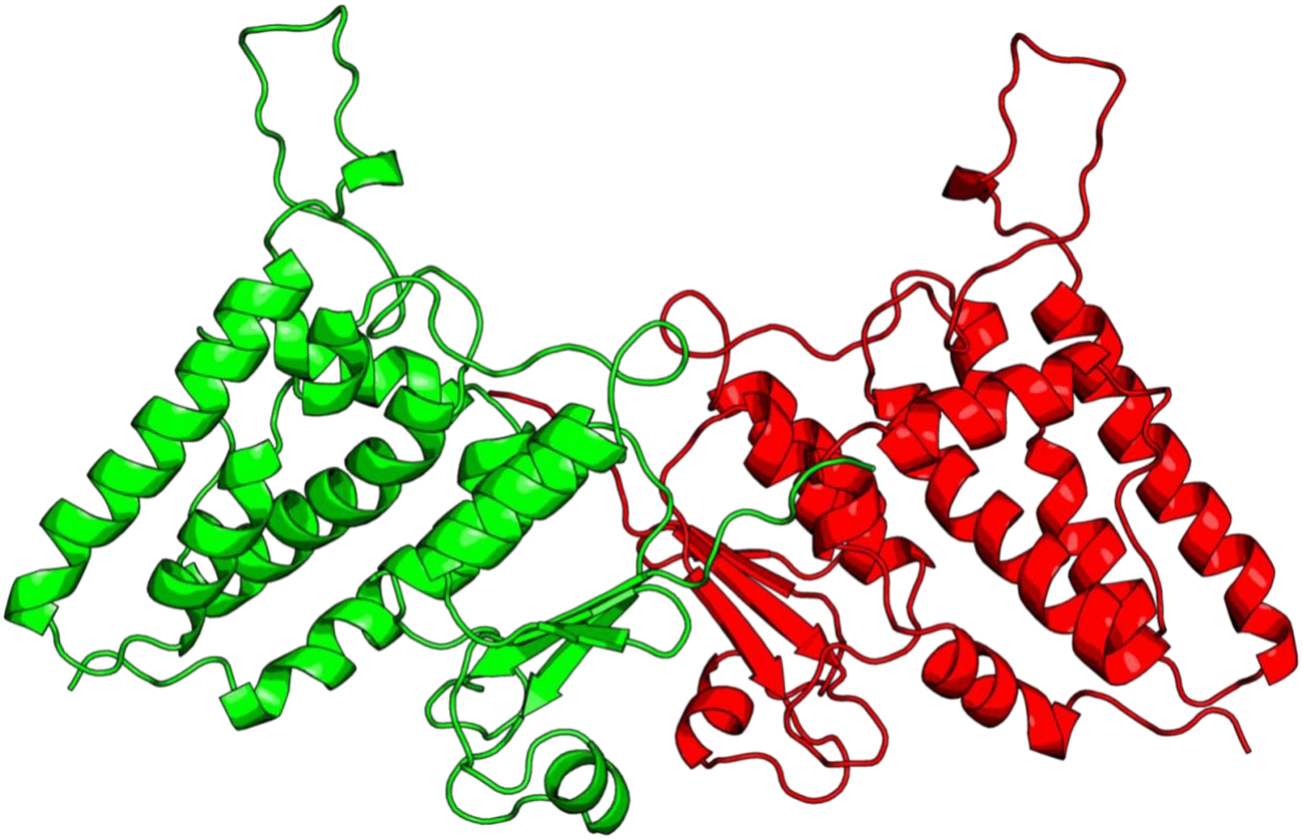


Figure 4.12: FOXS server comparison of alphafold CLIC1 dimer predicted scattering data against experimental CLIC1 dimer scattering data: A) Real CLIC1 scattering data is shown in black and the predicted scattering data is shown in red. The predicted alphafold dimer structure provides a good fit to the experimental scattering data with a chi-squared score of 1.14.

Interestingly, when the experiment was repeated in the presence of 0.5MR zinc. The dimer saxs data was collected and analysed under the same conditions. When this experimental zinc bound saxs data was compared with the alpha fold dimer, it no longer provided a good fit to the data. This suggests the dimer and potentially higher order states differ in structure and interactions when bound to zinc compared to other oligomers that exist in solution with no zinc present.

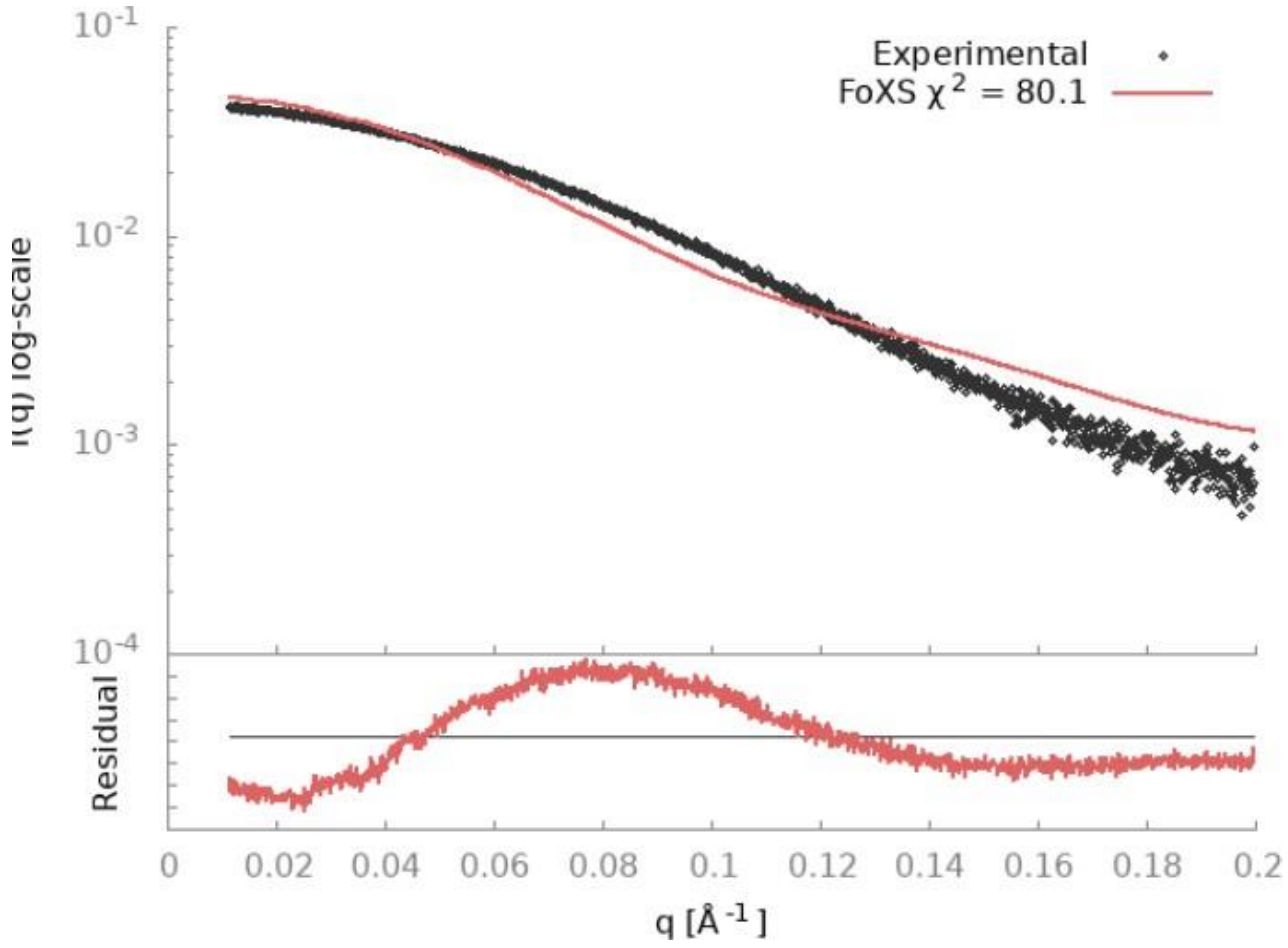


Figure 4.13: FOXS server comparison of the alphafold CLIC1 dimer structure predicted scattering data against experimental CLIC1 zinc bound dimer scattering data: A) Real CLIC1 scattering data is shown in black and represents CLIC1 with an addition of 0.5MR Zn^{2+} (750μM) and the predicted scattering data is shown in red. The predicted alphafold dimer structure provides a poor fit to the experimental scattering data with a chi-squared score of 80.1.

4.3.7- Zinc binding enhances relaxation of N terminal loops in CLIC1

Upon recognising that Zinc is able to bind to CLIC1 in solution, the next consideration was to attempt to understand the role that Zinc binding plays in promoting the formation of the Chloride ion channel. In order to investigate this effect, 500um CLIC1 single labelled sample had 0.5MR Zinc added and T1 and T2 ^{15}N spin relaxation rates were measured. 1/T1 and 1/T2 were calculated to give R1 and R2 which were measured as a ratio to determine the relaxation properties of CLIC1 in the presence of Zinc.

Compared to in the absence of Zinc there were 2 areas of CLIC1 that were highly flexible in both the unbound and now the bound form. Those 2 areas were the loop bridging the N terminal domain and the C terminal domain defined as residues 88-100. Whilst the other loop that was highly flexible in both was the footloop in the C terminal domain that has elevated T1 and is highly flexible on a fast timescale.

However there was also notable differences in the relaxation properties of the bound and unbound form. In the Zinc bound form of CLIC1 we noticed some altered relaxation properties of two regions in the N terminal domain. The first region that changed was residues 58-65 and 74-76 that equate to two small loops very close to each other. Both these loops observed significantly greater flexibility than in the native state CLIC1.

There is also enhanced flexibility in some of the other loops in the N terminal side of CLIC1. There is a cluster of residues 39-41 and residues 12 and 15 have also demonstrated an increase in relaxation which are a result of Zinc binding. Interestingly as an overall molecule, CLIC1 is more dynamic with Zinc bound than without binding.

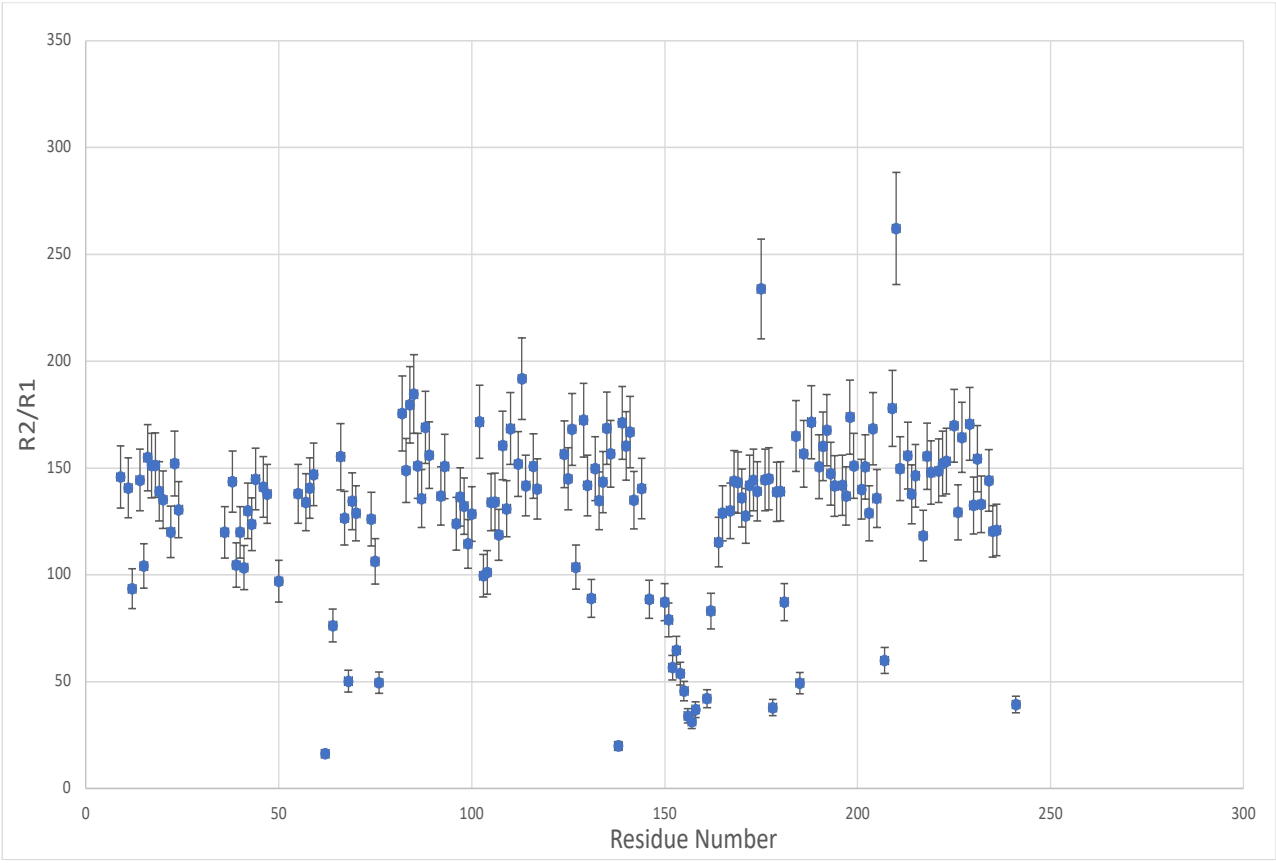


Figure 4.14: CLIC1 exhibits an increase in flexibility of some specific N terminal residues in the presence of 1MR Zinc-^{15}N R2/R1 relaxation rates of CLIC1 at 303K in 800MHz. Specific regions of enhanced flexibility with Zinc are 39-41, 58-65, 74-76. Breaks in the scatter graph are due to missing R2/R1 values from unassigned residues or residues with large amounts of overlap. Error bars are derived from S/N of peaks during the fitting process on NMRview which using the monte carlo approach estimates the standard deviations of the residue intensities

Given the changes in relaxation, the lowest 5% of R2/R1 values of assigned CLIC1 residues were highlighted in red. The rest of the molecules are coloured in green. A specific cluster of residues displayed as sticks in figure 4.14 were located in positions G62, L68 and D76. These residues are highlighted as they all were clustered in close proximity to each other. Relaxation data fitting demonstrated elevated error values

compared to the apo state CLIC1 as a result of increased broadening of peaks. Residues that are broadening in the lineshape demonstrate intermediate exchange and are broadening as a result of likely exchange between species. Increased broadening of peaks increases the errors in the fitting of both R1 and R2 values and subsequently R2/R1 ratios. An increase in errors can also occur directly as a result of the intensity losses seen when zinc binds to CLIC1. Subsequently when relaxation data is collected of the bound state, this reduces the signal to noise of some residues to fit the decay of intensity providing R1 and R2 values.

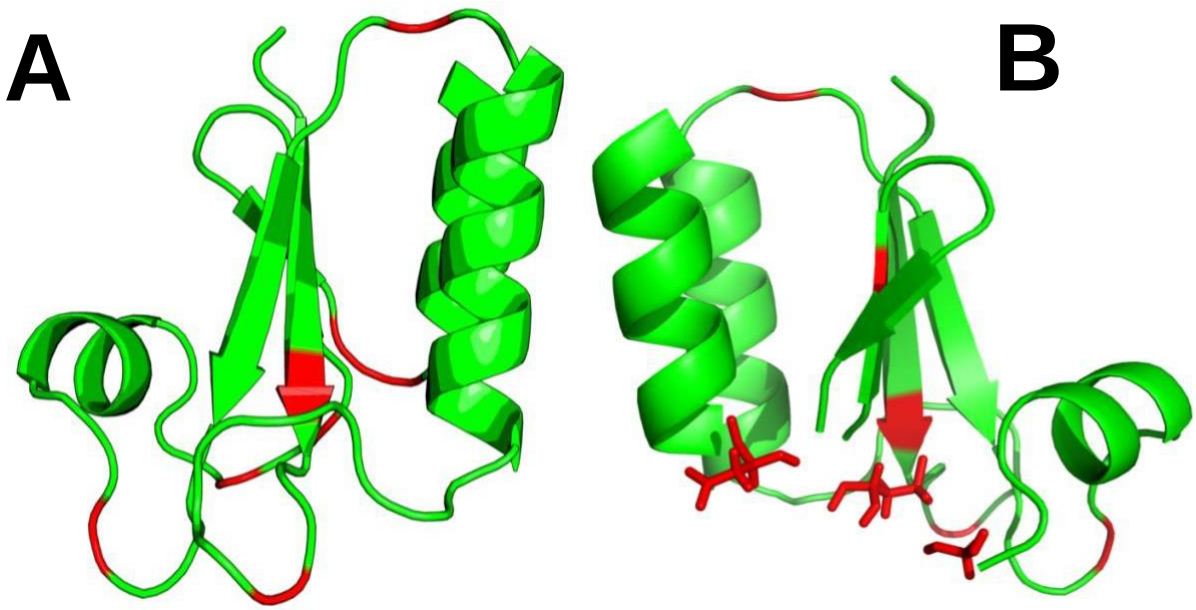


Figure 4.15: Pymol model of the CLIC1 N terminal domain residues with the lowest R2/R1 values when bound to Zinc- Residues in red are peaks that experience the greatest alteration in relaxation rate. A) CLIC1 with residues shown with a large change in relaxation rate in red cartoon view. B) CLIC1 with G62, L68 and D76 shown as red sticks to highlight the close proximity of these residues which experience a large change in relaxation rate.

4.4- Discussion

Research into the mechanism of the metamorphic activity of CLIC1 has been stalled in recent years. Lines of enquiry into CLIC1 research has focused on using oxidation to promote the formation of the oxidised dimer and higher order oxidised states that were believed to be involved in membrane insertion (Goodchild *et al.*, 2010b). However recent literature has determined oxidation to be neither essential for oligomerisation nor membrane insertion(Varela et al., 2022; Ferofontov et al., 2018). In the oxidised dimer of CLIC1, cysteine 59 is involved in forming the disulphide bond was not conserved in the other remaining CLIC members not its structural homologues with membrane insertion capabilities. If the cysteine is not conserved the disulphide bond could not be formed in the other CLIC members. It seemed unlikely that the other members with such strong sequence homology have a drastically different mechanism of insertion to CLIC1.

Recently the discovery of the ability of divalent cations ability to direct membrane insertion of CLIC1 led to a new hypothesis. Ca^{2+} and Zn^{2+} ions were able to cause a shift in the equilibrium between the soluble and membrane bound states of CLIC1. With sufficient concentrations of either of the 2 divalent cations and the presence of lipids, the vast majority of CLIC1 acts as a chloride ion channel and only trace amounts of CLIC1 remain in solution(Varela et al., 2022).

In signalling pathways that occur in cancers where CLIC1 is upregulated as a membrane bound channel, we see large increases in oxidation and oxidative stress within the cell(Peretti *et al.*, 2014). As part of the pathways that promote oxidative stress, there are often large influxes of Zinc and Calcium ions into the cell(Olechnowicz *et al.*, 2018). Within a cellular context, this explains why oxidative stress had been associated with an increase in the activity of the intracellular chloride ion channels.

This new line of enquiry into the role of divalent cations on CLIC1 metamorphosis was birthed but the mechanism through which the ions triggered the structural rearrangement of CLIC1 remained to be elucidated. Through techniques such as MST and NMR we begin to uncover the role of Zinc on promoting the membrane bound form. The MST assay determined at this concentration of CLIC1 (4uM), the affinity of CLIC1 to both ions was largely identical and the binding was very weak with an affinity of 0.3mM(Varela et al., 2022). The weak binding to divalent cations determined in this assay could have been affected nevertheless by interference caused by the presence of a C-terminal green fluorescent protein.

This assay was collected in the presence of a concentration of 50uM asolectin lipids. The presence of the lipids was essential as without their presence, the binding of CLIC1 to divalent cations would cause aggregation. Aggregation of CLIC1 was seen with high levels of divalent cations in both NMR and MST. In order for CLIC1 to insert into the membrane, the transmembrane domain must be exposed to lipids. The predicted transmembrane domains exists as a large hydrophobic patch of residues that is largely occluded in the crystal structure(Peter *et al.*, 2013). The aggregation seems to suggest that the divalent cations are causing the exposure of hydrophobic regions which without the presence of lipids to occlude the TM, we see aggregation as a by product of the reattempt to occlude hydrophobic residues from the solvent.

The NMR spin relaxation data from the NMR suggests the loop surrounding the TM become more flexible and residues within the TM and around the TM have their chemical environment altered upon Zinc binding. All of this data combined is suggesting that Zinc binding enhances flexibility of loops in the N terminal domain of CLIC1 that allows the N terminus to unfold causing exposure of the TM domain. In this partially unfolded state CLIC1 is more readily able to insert into the membrane.

It has well been documented that Ca^{2+} and Mg^{2+} are able to promote protein membrane interactions. Calcium is able to alter the thermodynamics of the process between proteins interacting with lipids(Vasquez-Montes *et al.*, 2022). Bid is a member of the Bcl-2 family with a pro-apoptotic function. In this protein, its hydrophobic transmembrane segment is already surprisingly exposed to the solvent in the crystal structure. Tryptophan fluorescence experiments identified that Calcium promotes favourable membrane insertion of Bid which can even be reversed with the use of divalent ion chelators such as EDTA(Billen, Shamas-Din and Andrews, 2009).

Similar events occurred with the pH-Low Insertion Peptide (pHLIP). Initially named as such due to its insertion being triggered by low pH values of pH 4.0. Recent evidence shows that divalent cations can also play a significant role in promoting membrane insertion of pHLIP. Binding to calcium triggers a conformational change in the structure of the protein that results in the generation of a new sub-state that favourably interacts with the membrane. This new sub-state upon interacting with the membrane forms an alpha helix that becomes the transmembrane segment of pHLIP(Vasquez-Montes *et al.*, 2019).

Given the large chemical shift perturbations and intensity changes of many peaks upon CLIC1 interaction with divalent cations, it seems reasonable to assume that CLIC can form a different sub-state when bound to Zinc or Calcium. This sub-state is largely unstable with hydrophobic residues exposed to the solvent, but when lipids are present the lipids can interact with CLIC1 to occlude hydrophobic regions from the solvent. In pHLIP, it is also seen that a saturation of the level of Calcium ions can promote membrane interactions at only slightly acidic and even neutral pH(Vasquez-Montes *et al.*, 2019). This is largely in agreement with research on CLIC1, where we demonstrated lowering of pH has clear different effects than that of divalent cations.

Within our research, we define 3 clear effects for CLIC1 upon Zinc binding. The increased flexibility of N terminal loops, the structural rearrangement of CLIC1 and increased oligomerisation. All 3 effects are interconnected and likely occur simultaneously within the cell context. Mass spectrometry data of membrane proteins has identified that one of the roles of lipids is to stabilise higher order oligomers of membrane proteins. Within CLIC1 we notice an increased presence of higher order oligomers with Zinc present in sufficient quantities. This effect was however accompanied with the presence of very large amounts of aggregate, increasing as the molar ratio of Zinc to protein increases.

Lipids have been determined to stabilise particularly weak interfaces of oligomers including oligomers where the interface is so unstable, that they simply cannot exist in solution without lipids(Gupta *et al.*, 2017). With many membrane proteins existing as oligomers in the functionally active form we begin to understand the requirement of lipids to shift proteins into their active state. In CLIC1, we experience large levels of aggregate without lipids. However in the MST assay, in the presence of lipids, we do not experience significant aggregation which could explain the role of lipids in stabilising the active form of CLIC1 believed to be the tetramer.

The oligomers detected in solution for CLIC1 with Zinc bound appear not to be in the same conformation that exist within the membrane. But we identify the role of Zinc in promoting higher order oligomers that are then stabilised by lipid interactions. The question remains whether oligomers form first in solution and then we observe the subsequent unfolding of the N terminal domains of the sub units, or whether unfolding of the N terminal domain promotes oligomerisation along with an interaction with lipids. The chronology of the effects of Zinc are hard to decipher and requires more experimentation.

We proposed the hypothesis that structural rearrangement of the N terminus and oligomerisation of CLIC1 promotes the formation of the Chloride ion channel. Other metamorphic proteins seem to adopt a similar mechanism of insertion seen to CLIC1. Triggered by phosphorylation and not Zinc binding but the Mixed Lineage Kinase Domain Like Pseudokinase is a protein that is expressed as a soluble protein but is able to span the membrane to cause pore formation that makes the plasma membrane permeable to trigger cell death.

The mechanism of MLKL involves a trigger event similar to CLIC1. In this case, the protein is activated by phosphorylation, which triggers a conformational change that exposes a “brace region”. This brace region is proximal to the transmembrane segment of MLKL that spans the membrane. The “brace region” is also responsible for triggering oligomerisation as membrane interactions occur through this region. Therefore, the exposure of the brace region is essential for the formation of the higher order oligomers and the active form that acts as a membrane pore(Quarato *et al.*, 2016).

When Zinc binds to CLIC1 and triggers a conformational change that promotes higher order oligomers. It is possible that CLIC1 similarly has a “brace region” that is occluded in the crystal structure of CLIC1 but is now exposed after Zinc binding which would facilitate the oligomerisation of CLIC1. This would explain the enhanced oligomerisation with Zinc compared to without. In MLKL, oligomerisation is also triggered by phosphorylation in the absence of membranes similar to Zinc in CLIC1, but the presence of membranes stabilises the active form and drives membrane localisation.

A further possible consideration is how the role of Zinc interplays with the inherent flexibility seen in the inter domain loop for the native CLIC1. It seems likely that the ability of the two domains to separate from each is a complementary effect to the role of Zinc in causing membrane insertion of CLIC1. Looking at CLIC1 homologues that do not insert such as the Glutathione S transferase family, we identify these proteins are globular in shape and the domains do not dock away from each other.

This means the extended conformational of CLIC1 is a product of evolution for this family. It is unlikely it would have evolved if it was not advantageous for CLIC function. With the extended conformation of CLIC1, this exposes the transmembrane region partially to the solvent. We expect after the separation of the two domains that the flexibility of N terminal loops will allow the N terminal domain to unfold and expose the transmembrane region fully to lipids.

Without the ability of CLIC1 to enter an extended conformation, the structure of CLIC1 would be too condensed and there would not be enough space for the N terminal region to unfold. We expect if CLIC1 had the same number and strength of interactions as its homologue GST. Then Zinc would not be able to trigger unfolding of the structure and CLIC1 would not be able to insert into the membrane.

An alternative hypothesis would imply that the extended conformation is important for CLIC1 function as a soluble protein. The current function for CLIC1 in solution is unknown although some studies have demonstrated oxidoreductase activity(Turkewitz *et al.*, 2021b). The extended conformation may have a role in regulating oxidoreductase activity. However the role of the extended conformation in aiding enzymatic activity of CLIC1 and promoting Zinc-triggered membrane insertion do not have to be mutually exclusive, it may play a role in both mechanisms.

We predict that structural rearrangements and aggregation seen by CLIC1 when bound to Zn^{2+} ions are a result in the loss of stability of the structure in the bound form. Many studies demonstrate the role of Zinc in destabilising protein structures, inducing hydrophobic exposure of residues and unfolding of the structure, as well as large scale aggregation(Brazil, Ybarra and Horowitz, 1998; Campanero-Rhodes *et al.*, 2006). The dimeric arginine kinase (dAK) protein undergoes a conformational change upon zinc binding which results in the formation of an intermediate with an unfolded structure. It is predicted that the formation of an unfolded intermediate then triggers the formation of aggregates in an attempt to occlude the hydrophobic residues of the intermediate. This is similar to the effects seen in CLIC1 where a conformational change is demonstrated upon Zinc binding via NMR and the formation of aggregates are observed. It could be possible that Zinc bound to CLIC triggers this unfolding pathway similar to dAK. In dAK, Urea induced unfolding exerts similar effects to that of Zinc triggered unfolding(Liu and Wang, 2010). Experiments using Urea and CLIC1 could be conducted to investigate whether this is also the case with CLIC1.

We also identify that CLIC1 is more unstable with Zinc bound due to the formation of aggregates. Research should be conducted into whether CLIC1 is able to interact with chaperones. Chaperones are known to prevent aggregation and can modulate hydrophobic surfaces(He *et al.*, 2020). Therefore, the possible effect of chaperones in the stabilisation of CLIC1 conformations with hydrophobic residues exposed prior to membrane insertion could be explore. If chaperone activity is able to stabilise a Zinc bound form of CLIC1 it could also prevent aggregation and aid membrane insertion.

In summary, zinc binding plays a few key roles in promoting the membrane insertion of CLIC1. Zinc promotes oligomerisation of CLIC1, zinc changes the environment of many residues surrounding the transmembrane region. Finally zinc alters the

relaxation properties of N terminal loops. Together these effects, elucidate zinc as the trigger for membrane insertion of CLIC1 as a chloride ion channel.

4.5- Conclusion

The use of a combination of microscale thermophoresis, NMR and SAXS has identified the regions of CLIC1 that are involved in binding to Zinc in solution and the regions impacted by a structural rearrangement that occurs upon binding. This data demonstrates the regions involved in binding and structural rearrangement are the regions surrounding the hydrophobic transmembrane region. The transmembrane region is also likely to be dynamic but the fact that the backbone resonances of this region remain unassigned prevents this from being included in the data. In order for CLIC1 to insert into the membrane, the transmembrane region has to be exposed to enable its insertion into lipids, it seems apparent that the Zinc binding plays a role in exposure of the transmembrane region that causes oligomerisation and aggregation in solution or membrane insertion with the presence of lipids.

4.6- Future work

Future work will involve trying to make attempts to assign the transmembrane region that can allow the inclusion of these residues in future analysis of the effects of zinc and membrane insertion. Mutation to many of the residues involved in oligomerisation and zinc binding would provide further validation of these predicted regions.

Further studies could include completing membrane insertion assays or zinc titrations and monitoring how the mutations affect the spectrum or the tendancy of protein to insert into the membrane.

In addition, further NMR studies could be completed using solid-state NMR to begin to elucidate the structure of the membrane bound chloride ion channel and start to understand the dynamics of the membrane bound form. The spectrum of CLIC1 for the membrane bound form needs to be assigned and hence some of the assignments of the soluble form of CLIC1 could be transferred to a solid-state spectrum. This could be possible for the C terminal side of CLIC1 that does not insert into the membrane. However the N terminal side of CLIC1 is likely to undergo structural rearrangements to facilitate the insertion of the predicted transmembrane region. Therefore these regions of CLIC1 would need to be reassigned. To identify the structure, dynamics and membrane interactions of the membrane bound form of CLIC1, studies could also use saposin-A (SapA) nanodiscs. The use of SapA nanodsics allows membrane proteins to be studied in solution NMR due to their small size. Optimisation is required to determine the optimal protein-lipid ratio but upon successful incorporation of protein into the membrane, SapA nanodiscs provide an environment similar to the native membrane state(Chien *et al.*, 2017).

Chapter 5: Mutations can disrupt the equilibrium of CLIC1 in solution

5.1- Introduction

The literature demonstrates that CLIC1 likely exists as a tetrameric assembly as chloride ion conductance of the native membrane bound form was four times the chloride conductance of a single CLIC1 subunit(Warton *et al.*, 2002b). Further research also determines that CLIC1 exists in solution as largely a monomeric protein with dimer and trace amounts of tetramer also being present(Varela et al., 2022). It has been unknown as to whether the dimer and tetramer structures seen in solution play any role in CLIC1's unique ability to be metamorphic and insert into the membrane as a chloride ion channel. It has been identified that both monomer and dimer forms of CLIC1 are able to insert into the membrane and form functional chloride ion channels. The question remains whether the monomer forms higher order states prior to membrane interaction that unfold or CLIC1 forms oligomers only at the membrane environment in which case the solution higher order states are not required to form chloride ion channels.

One way of identifying whether these higher order species have a role in this metamorphosis is through mutating residues in CLIC1 that can disrupt this equilibrium in solution. The use of a size exclusion column can provide a ratio of monomer, dimer and tetramer seen for each mutation. Mutations that can disrupt this equilibrium can then be used in an insertion assay and see if the increase or decrease in higher order states affects CLIC1's ability to insert into the membrane with a consistent concentration of Zn^{2+}. Our own SEC-SAXS data in figure 4.10 suggests that CLIC1 can oligomerise prior to membrane interaction with the addition of zinc. We have identified residues using our NMR data that undergo large intensity changes with zinc bound and have chosen these residues to mutate in the hope of disrupting the oligomerisation equilibrium.

5.2- Results

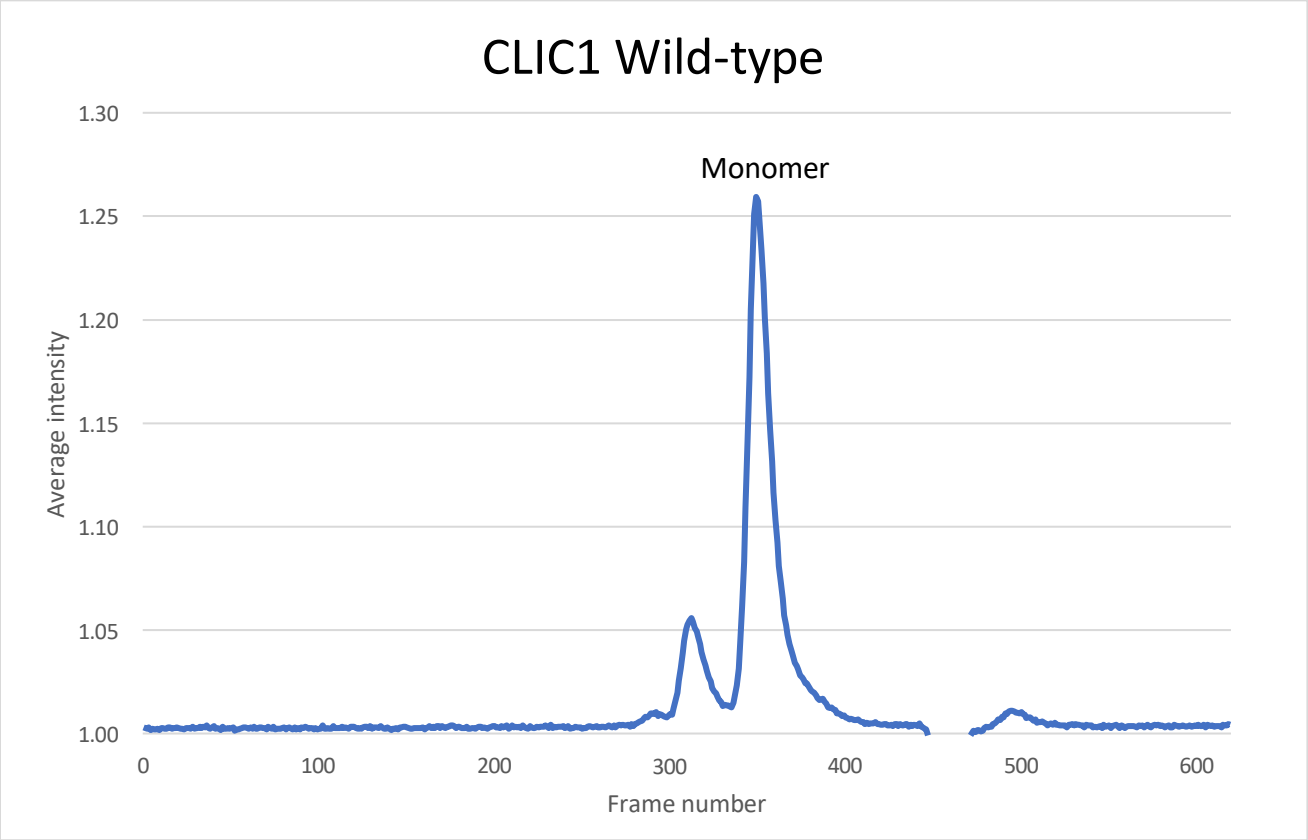
In order to identify how mutations can disrupt the equilibrium of monomer and higher order states of CLIC1 in solution, we first must identified the normal gel filtration trace for wild type CLIC1 at a concentration of 15mg/ml. The concentration of CLIC1 and CLIC1 mutants was kept identical as the oligomerisation process is concentration dependent, and therefore by keeping all samples at the same concentration we can directly correlate the effect of a mutation in the oligomerisation process.

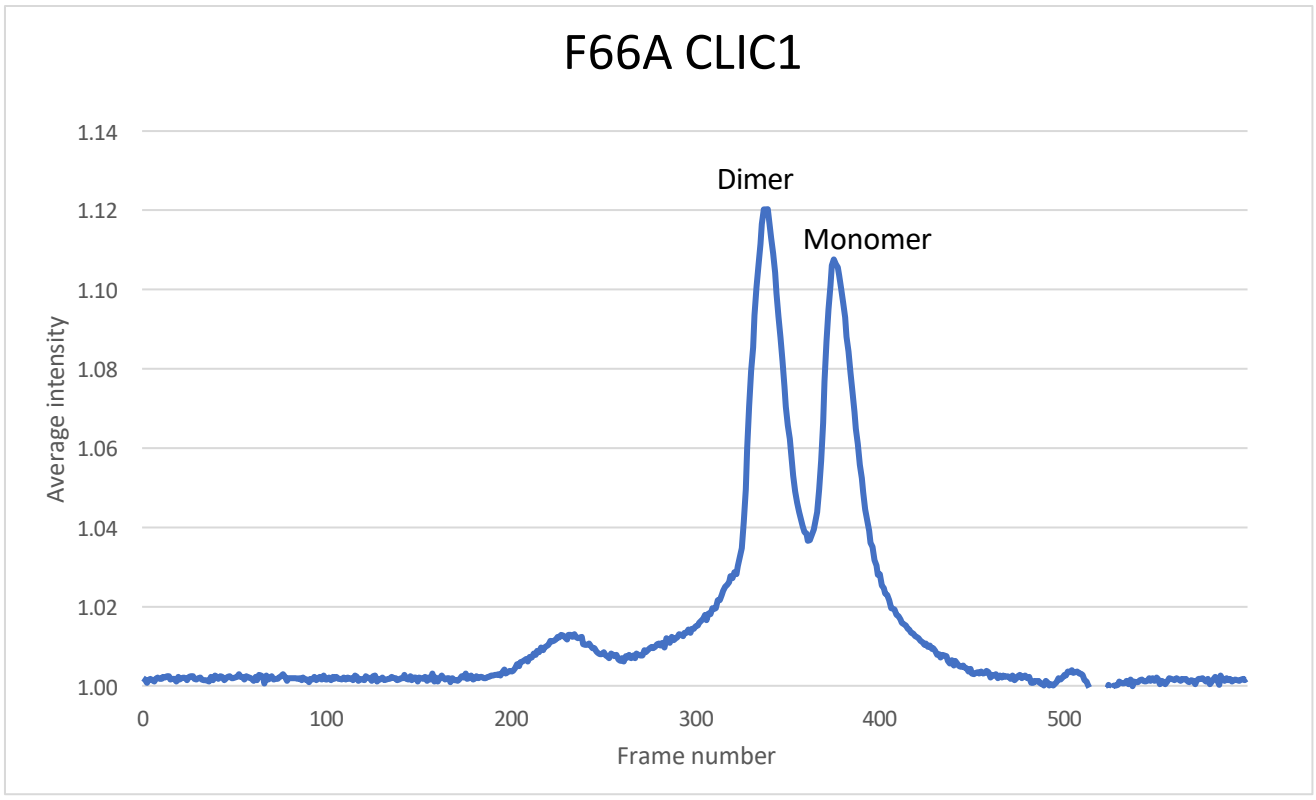
To examine this equilibrium in the wild-type protein and in mutants we used SEC on its own or coupled to SAXS. For wild-type CLIC1 at 15mg/ml the peak with the greatest intensity is the monomer. In addition to the monomer there is 2 further peaks which correspond to the dimer and tetramer peaks predicted by SAXS size estimates, which are of lower intensity than the monomer. For the F66A mutant there is a large contrast of the SEC-SAXS trace compared to the wild-type CLIC1. The highest intensity peaks are the dimer and monomer, with the dimer having a higher absorbance than the monomer. This demonstrates that the F66A mutant is causing a greater proportion of CLIC1 dimer in equilibrium compared to the wild-type CLIC1 which is seen in figure 5.1.

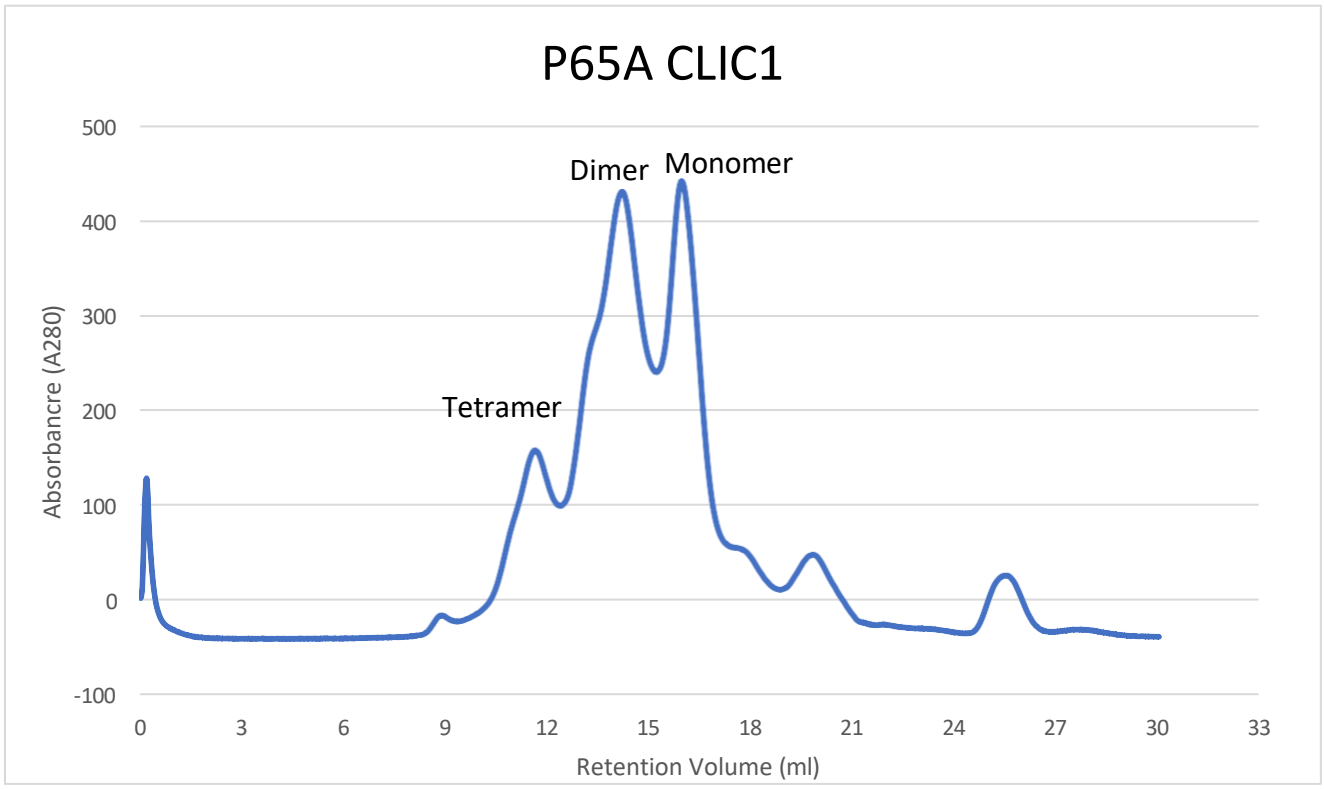
We see that the P65A mutant perturbs the equilibrium of CLIC1 oligomeric states to a greater extent than the F66A mutant. Compared to the wild-type, the proportion of dimer to monomer has significantly increased. In the wild-type CLIC1 there is a trace amount of tetramer, however in the P65A mutant SEC trace we see the tetramer develop as a clear identifiable peak that is distinguishable from the dimeric species.

In addition, we identify a mutation of R29A that can reduce the presence of oligomeric states in solution. In the wild type CLIC1, there is the presence of the dimer. However in contrast with R29A, R29A has no detectable dimer peak in the SEC-SAXS trace.

This demonstrates the mutation has either directly prevented dimer interactions or has caused conformational changes to CLIC1 that prevents dimer interactions in solution.




F66A CLIC1
Dimer
Monomer
Average intensity
1.14
1.12
1.10
1.08
1.06
1.04
1.02
1.00
0
100
200
300
400
500
Frame number


P65A CLIC1
Dimer
Monomer
Tetramer
Absorbancre (A280)
500
400
300
200
100
0
-100
0
3
6
9
12
15
18
21
24
27
30
33
Retention Volume (ml)

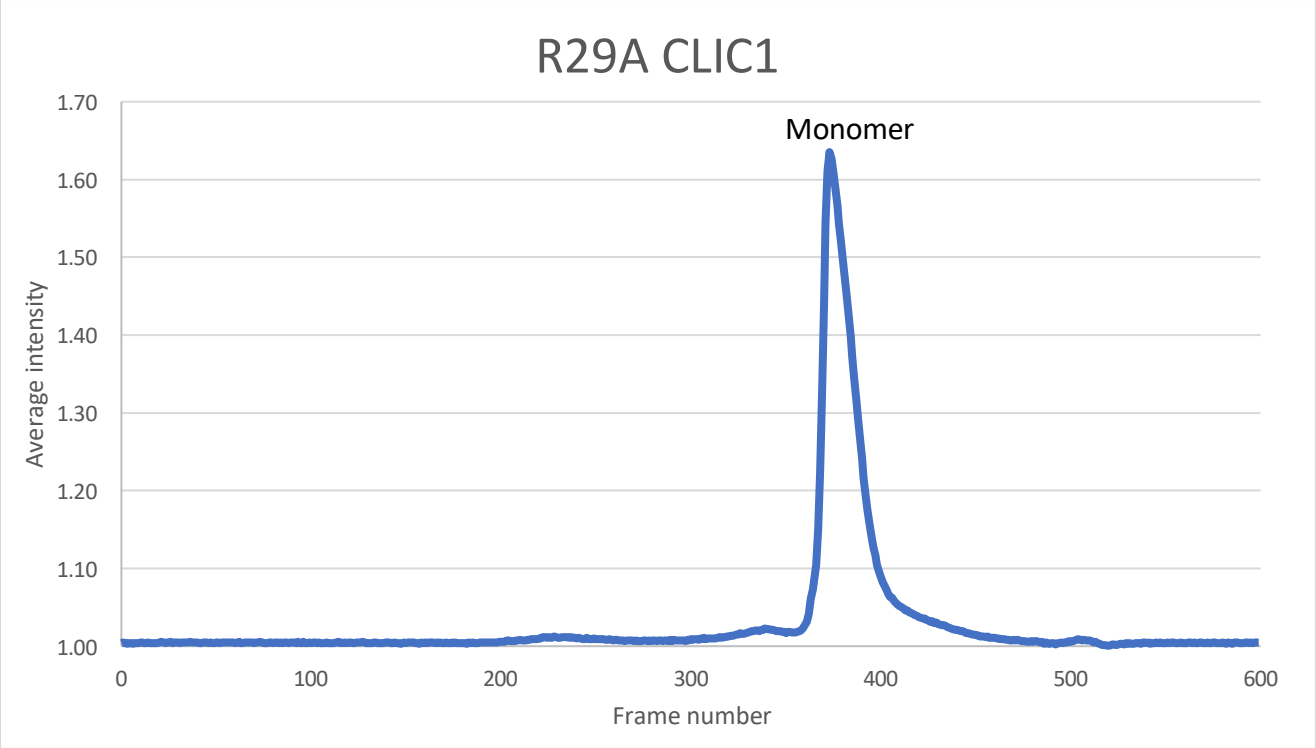
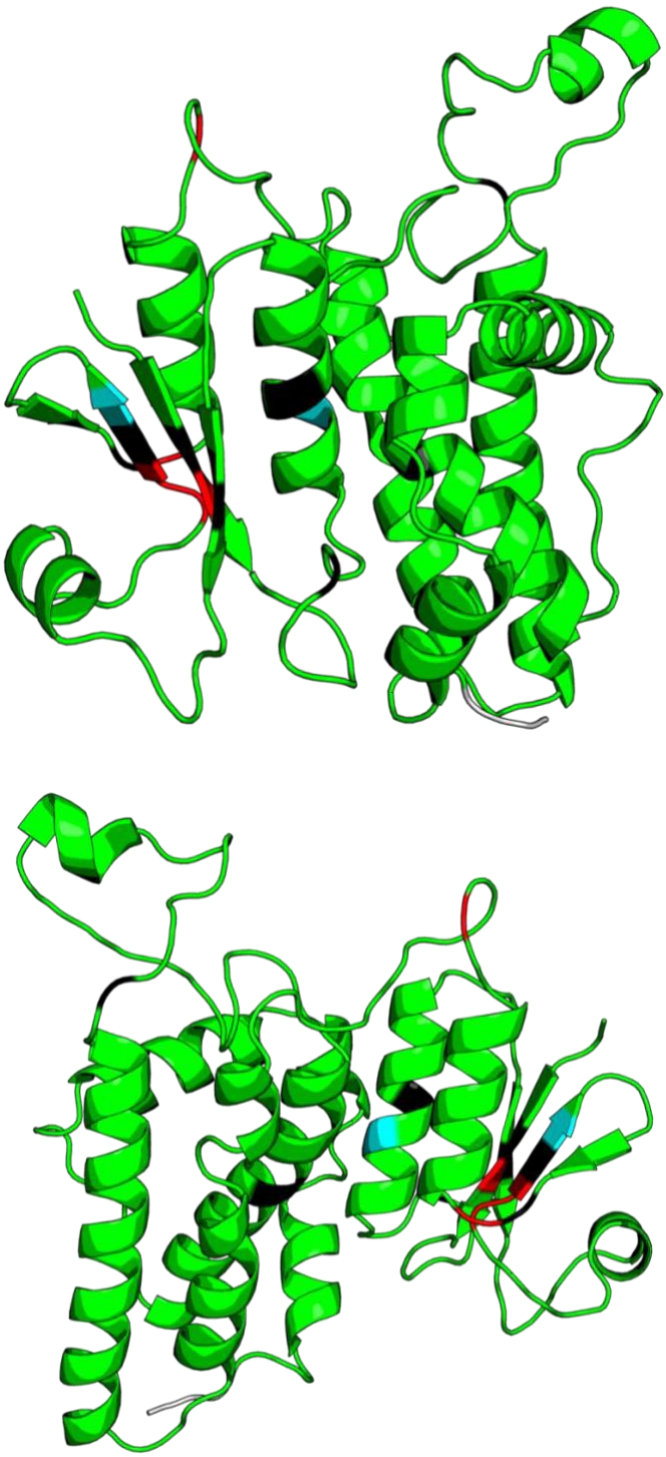


Figure 5.1: P65A, F66A and R29A CLIC1 mutants disrupt the equilibrium of CLIC1 oligomeric states- All samples were produced at 15mg/ml and in the buffer 150mM Hepes 50mM NaCl pH 7.4 A) SEC-SAXS profile of CLIC1 wild-type using the size exclusion column Showdex-403 at 15C. B) SEC-SAXS profile of F66A using the size exclusion column Showdex-403 at 15C. C) Superdex-200 SEC trace of P65A CLIC1. D) SEC-SAXS profile of R29A using the size exclusion column Showdex-403 at 15C

The proline that is mutated in the P65A mutant is conserved across the entire CLIC1 family and including the DmCLIC and EXC-4 homologues that have a calcium binding site which is demonstrated in figure 1.7. In contrast the phenylalanine in the F66A mutant is not conserved although CLIC2 and CLIC4 share the amino acid. In CLIC3 and the CLIC homologues DmCLIC and EXC-4, we see the phenylalanine has been substituted for an isoleucine. Both phenylalanine and isoleucine are hydrophobic amino acids. Therefore the substitution from phenylalanine to isoleucine does not

drastically alter the properties of the amino acid and the amino acid may still play an important functional role.

In total 14 mutations were made to CLIC1, with R29, P65A and F66A having the most notable effects on the equilibrium of CLIC1 oligomerisation. However other CLIC1 mutations did partially alter this equilibrium. D76A, F11A and P90A increased the presence of oligomeric states compared to the wild-type CLIC1. L68A decreased the presence of dimer in the CLIC gel filtration trace. Finally, F31A, K20A, K183A, L10A, L67A, P147A, T44A and T75A had no observable effect on the oligomeric states of CLIC1 compared to the wild-type protein. The position of all these mutations within the 1K0N crystal structure are presented on figure 5.2.



```
sp|O95833|CLIC3_HUMAN       FTLTTVDTRRSPDVLKDFAPGSQLPILLYDSDAK--TDTLQIEDFLEETLGPPDFPSLAP   96
sp|O15247|CLIC2_HUMAN       FNVTTVDMTRKPEELKDLAPGTNPPFLVYNKELK--TDFIKIEEFLEQTLAPPRYPHLSP  104
sp|Q9Y696|CLIC4_HUMAN       FSVTTVDLKRKPADLQNLAPGTHPPFITFNSEVK--TDVNKIEEFLEEVLCPPKYLKLSP  109
sp|O00299|CLIC1_HUMAN       FNVTTVDTKRRTETVQKLCPGGQLPFLLYGTEVH--TDTNKIEEFLEAVLCPPRYPKLAA   98
tr|Q9VY78|Q9VY78_DROME     LKVTTVDMQKPPPDFRTNFEATHPPILIDNGLAI--LENEKIERHIMKNI-PGGYNL-FV  116
sp|Q8WQA4|EXC4_CAEEL        VEVKTVNV--NSEAFKKNFLGAQPPIMIEEEKELTYTDNREIEGRIFHLAKEFNVPL-FE  113
                            . :.**:       .:    . : *::          :  :**  :
```

Figure 5.2: Position and conservation of mutations in the CLIC1 structure: A) Pymol images of the crystal structure 1K0N. Mutations that promote oligomerisation are coloured in red whilst mutations that decrease oligomerisation are coloured in cyan. Mutations that affect no effect on oligomerisation properties of CLIC1 are depicted in black. B) Conservation analysis of P65 and F66 that promote oligomerisation after mutation. The sequence of CLIC1 is compared against CLIC2-4 and DmCLIC and EXC-4 which are structural homologues with chloride ion channel activity that bind to Calcium.

5.3- Discussion and future work

The data presented of the P65A and F66A CLIC1 mutants represent some interesting preliminary data towards understanding the mechanism of CLIC1 insertion into the membrane. Both mutants altered the equilibrium of CLIC1 and its oligomeric states in solution with the P65A mutant increasing the ratio of dimer and tetramer to monomer. For the F66A mutant we saw an increase in ratio of dimer to monomer.

We saw in previous data that Zinc is able to bind to CLIC1 and increase the presence of oligomeric states in solution. The proline mutated in CLIC1 has an equivalent conserved proline in DmCLIC and EXC-4 that is identified to interact with Ca^{2+} ions determined by the crystal structure of both of these proteins. If this proline is able to interact with divalent cations, and it is mutated it could disrupt this region in a similar mechanism to divalent cation binding. The mutation to P65A promotes the oligomerisation of CLIC1 which creates a SEC trace that is very similar to CLIC1 bound to zinc ions.

When Zinc binds it alters the relaxation properties of P65 in CLIC1. It seems clear that disruption of this region is essential for oligomerisation and may potentially be important to the insertion of CLIC1 into the membrane. Future studies should examine the relaxation properties of the P65A and F66A mutant to determine if the mutation alters the relaxation properties in a similar mechanism to zinc binding. Studies must also be conducted on the ability of both mutants to bind to divalent cations which could be studied using MST. This proline residue interacts with calcium in CLIC homologues, these mutants could reduce the binding affinity of CLIC1 to calcium and zinc. An insertion assay should also be conducted with and without the presence of zinc to determine whether the mutations alter the insertion properties of CLIC1.

Chapter 6: Final discussion

6.1- Updated model of CLIC1 membrane insertion

The metamorphosis and translocation of CLIC1 into the membrane in cancer cells presents the protein as a potential therapeutic target particularly in cancers where CLIC1 is overexpressed such as breast, gastric, colorectal etc. For many years the trigger of the molecular switch from cytosolic CLIC1 to the membrane chloride ion channel remained to be elucidated. However novel research identified divalent cations as a trigger for the translocation of the protein into the lipid environment. Within the divalent cation family there was a preference for the ability of the ion to shift the equilibrium towards the membrane bound state. Calcium and Zinc caused the greatest translocation of CLIC1 into lipids and Zinc had the greatest effect of the two.

The purpose of these thesis was to attempt to define the role of Zinc in triggering this molecular switch. This will enable us to understand the structural properties of CLIC1 in solution and how Zinc plays a role in changing the structural properties of the cytosolic form facilitating its insertion into the membrane. It is important to note that this thesis provides no information about activity of the protein in the membrane bound form. All the experiments described here attempted to understand structural changes that trigger metamorphosis of CLIC1. Once present in the membrane, CLIC1 is affected by different processes and mechanisms that will affects its activity that is not the focus of these experiments.

Once CLIC1 was expressed and purified successfully, the initial goal was to identify if the only structure of CLIC1 present in solution was that of the crystal structure. In order for CLIC1 to be metamorphic it is likely to have highly dynamic regions that are able to undergo conformational changes to facilitate the formation of a chloride ion channel.

To that extent NMR was initially used to identify regions of the protein with high flexibility. This identified a few key regions, the C terminal footloop, loops surrounding the transmembrane region and potentially the transmembrane region as it is unassigned. The final region identified to be highly flexible is the loop bridging the C and N terminal domain.

Using this information, the next logical experiment was small angle x ray scattering to determine the structure in solution. It was evident that the experimental scattering data of the monomer did not match the predicted scattering data of the crystal structure 1K0N. To this extent, the flexible regions from the NMR analysis were used in order to allow flexibility within the structure for an ensemble optimisation method. It became clear that within solution, CLIC1 exhibits a minor elongated structure which allows separation of the N and C terminal domains via the flexible linker bridging the two domains. However the major structure within solution is the crystal structure.

The new understanding of CLIC1 in solution is that the structure can now exist as an elongated separation of the two domains naturally in solution without the need for divalent cations. This has also been seen to some extent in CLIC6 which also contains a flexible linker that enabled further conformations of the structure that differed from the crystal structure. This minor conformation causes exposure of the predicted transmembrane domain in CLIC1 whereas previously the only known structure in solution completely sequesters this hydrophobic region away from any solvent exposure.

It seems highly important that in solution CLIC1 can allow exposure of the transmembrane region. This would allow the transmembrane region and N terminal domain to undergo conformational changes that would facilitate interactions with

lipids. In the crystal structure the transmembrane domain is so sequestered in the centre of the structure it would provide no space for conformational rearrangement and would prevent metamorphosis.

This unique ability for the two domains to separate away from each other is likely to differentiate the CLIC family from other proteins that share the GST fold but lack the ability to insert into the membrane. Such an example is the Glutathione S transferase family, which are structural homologs of the CLIC family. We collected SAXS data for GST O-1 which was identical to the predicted SAXS data from the GST O-1 crystal structure. Bioinformatic analysis identified a significantly reduced number of interactions between the N and C terminal domain of the CLIC family compared to the GST family, which could explain the more compact structure of GST O-1 in solution.

It is likely the reduced number of interactions in CLIC1 allows the N terminal domain and C terminal domain to separate via the flexible linker and is a key understanding as to why the CLIC family is unique in its metamorphosis and ability to insert into the membrane. The exposure of the transmembrane region to the solvent is the first initial step in the conversion of cytosolic CLIC1 to a chloride ion channel.

Combining this work we wanted to identify the role of Zinc in converting this ensemble of structures in solution to a chloride ion channel. Initially the discussion was as to whether Zinc specifically binds to CLIC1 or plays an alternative role in this metamorphosis. To determine this initially microscale thermophoresis was used and it was identified that both zinc and calcium bind to CLIC1 although both were determined to have a very similar low affinity.

The zinc titration binding experiment suggested the affinity of zinc to CLIC1 was different from the affinity of zinc to CLIC1 measured by MST . In both the presence

and absence of a his-tag Zinc bound with significantly higher affinity that was demonstrated by the MST. The only two difference being that CLIC1 was at a much higher concentration in the NMR experiments and lacked a GFP molecule. Hence there are two potential conclusions. That zinc binding is concentration dependent, although a change in the CLIC1 concentration in the NMR experiments had no impact on the binding so this seems unlikely. Alternatively and the more likely option is that the C terminal GFP molecule is affecting the fold or structure of CLIC1 in such a way that it reduces the affinity of this construct to Zinc and Calcium. Without the presence of this GFP molecule the affinity for Zinc increases dramatically.

Understanding that Zinc can bind to CLIC1, the next objective was to start to understand some of the structural changes that Zinc is causing to the structure of CLIC1 to facilitate its insertion into the membrane. In order to identify specific residues that have their environment changed upon Zinc binding we analysed the chemical shift perturbations. The CSP data demonstrated that residues that are assigned within the transmembrane region experienced a large change in environment. Large changes in environment were seen also by a large number of residues surrounding the transmembrane region including residues on the C terminal side that do come in close proximity to the predicted transmembrane region.

This provides clear evidence that Zinc binding to CLIC1 induces conformational changes to the CLIC1 structure prior to its insertion into the membrane. Relaxation data from the NMR further identified that there is enhanced relaxation properties for the some of the loops surrounding the transmembrane region. This indicates that the loops surrounding the transmembrane region are more flexible with Zinc bound to the structure. It is likely that Zinc binding increases flexibility of loops surrounding the

transmembrane region that facilitates the structural rearrangement of the N terminal domain.

One of the concerns was that previous experiments had implicated pH as a factor in triggering insertion of CLIC1 and the original research had used a large amount of Zinc that could cause a reduction in pH triggering the formation of the chloride ion channel. NMR studies determined quickly that the chemical shift perturbations present when Zinc is bound and the pH is reduced are drastically different. This suggests the two factors have different roles on affecting the protein. It is more likely that pH plays a role in a gating mechanism rather than insertion into the membrane.

The use of SEC-SAXS also identified that the presence of Zinc can trigger oligomerisation in solution and promotes the formation of an increased amount of tetramer and dimer species. Preliminary data in our laboratory suggest that the tetrameric state is the oligomeric species that is active as a chloride ion channel. Although we have identified a tetramer present in solution, it is unlikely that it represents the conformation of the chloride ion channel present in lipids. However it may share in common a similar architecture on the interior side of the channel form. In addition, it shows the role of zinc in promoting the formation of higher order states and confirms its function in triggering CLIC1 membrane insertion.

Specific residues undergo large intensity losses upon CLIC1 binding to zinc. The chemical environment of these residues is altered either due to direct contact with the zinc ion or due to conformational changes of CLIC1. Upon identifying the most impacted residues for zinc binding, we mutated 14 of these residues to alanine in separate constructs. P65A and F66A increased the presence of oligomeric states in solution similar to the effect of zinc binding on the oligomeric states of CLIC1. This

suggests that mutations to this loop region of CLIC1 can alter the dynamics of this region in a similar mechanism to zinc. The NMR relaxation data combined with our mutagenesis experiments show this N terminal loop to be of great importance for both oligomerisation and likely membrane insertion of CLIC1.

Overall the mechanism of CLIC1 insertion given our data is expected to follow this three step process:

1. In solution, the N and C terminal domain can separate from each other via flexibility in the linker and a lack of inter domain interactions which exposes the transmembrane domain
2. Zinc binds to CLIC1 which causes a conformational rearrangement of the N terminal domain and transmembrane domain so that it can interact with oligomerise and interact with lipids.
3. The tetrameric assembly of CLIC1 inserts into the membrane and has chloride ion conductance activity at low pH.

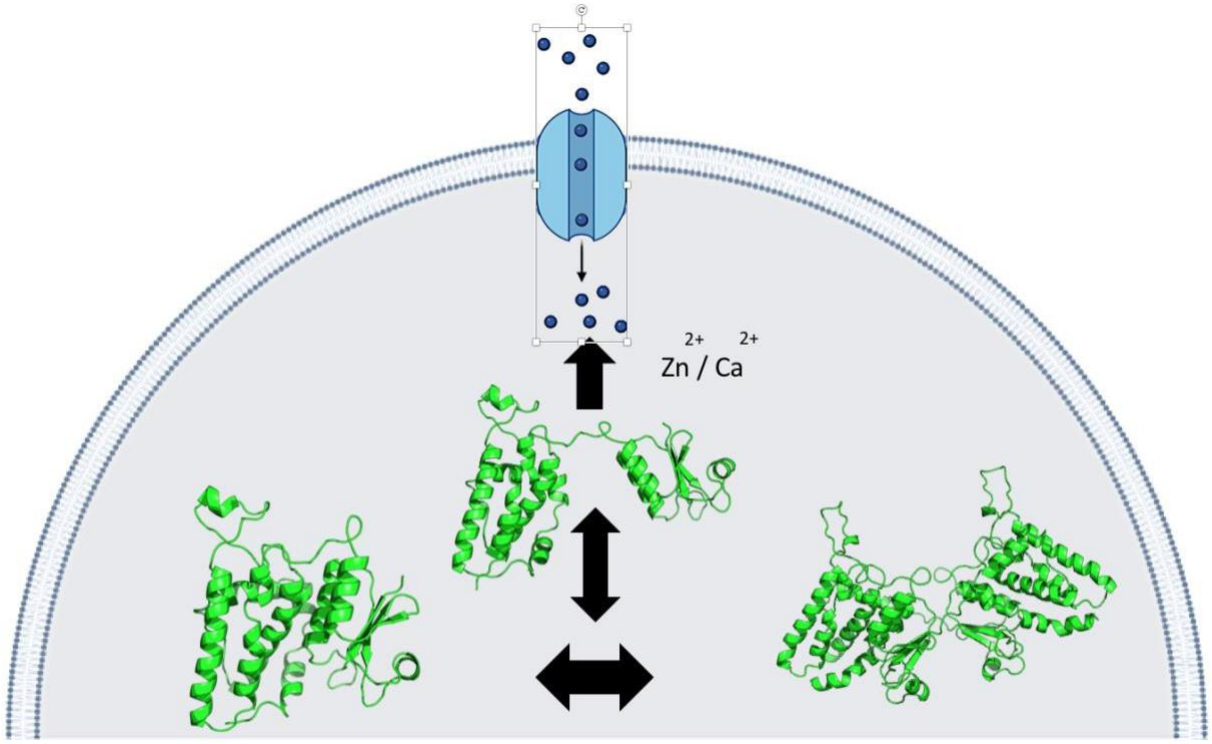


Figure 6.1: A multi-step CLIC1 mechanism of insertion model: CLIC1 in solution exists as an ensemble of two states, an open and closed form. The open form of CLIC1 binds to Zn^{2+}, oligomerises and partially unfolds the N-terminal domain. The tetrameric assembly of CLIC1 interacts with lipids and forms a chloride ion channel. This channel is active at low pH.

6.2- Limitations of the research

The role of Zinc in binding and causing conformational changes to CLIC1 is thoroughly evidenced. However there is a slight concern in regards to some of the important residues missing assignments. In an ideal world 100% of the protein would be assigned and a large number of residues within the predicted transmembrane are missing leaving assumptions to be made by a few reporter residues within this area.

If all residues were assigned for the entire protein, it would become more clear the distinct regions that are affected by Zinc binding and whether specific parts of the transmembrane region are more flexible than others. Also when measuring flexibility of the system, it may be possible that conformational changes that are more nuanced or more extreme are missed simply because we have no provided experimental data on the timescales through which the movement exists.

In regards to the SAXS data, it seems likely the separation of the N and C terminal domain and exposure of the TM region is likely to have a functional role given the requirement of the TM region to insert into lipids. However this is not experimentally validated whether if CLIC1 was refined to strictly its globular structure whether it would then be unable to insert. Further mutations and structural data is required to confirm this hypothesis.

Finally all of the results and data were conducted in solution which is an environment devoid of lipids. CLIC1 is unable to convert into a chloride ion channel in the absence of lipids. Hence some structural states that can occur with Zinc binding and lipids are simply invisible in solution. Without the lipids, the protein still attempts to prevent exposure of hydrophobic residues to solvent which could explain the presence of aggregation in high amounts of Zinc. In addition with Zinc there is a higher presence

of high order oligomers in solution. This could simply be an attempt by CLIC1 to sequester hydrophobic patches away from solution that in the presence of lipids would be protected by the membrane.

The studies were also not conducted in vivo studies. When bound to Zinc, CLIC1 may then interact with other binding partners that is essential for activity or correct folding in a cellular environment. These would be absent in a solution environment. Previous literature demonstrates CLIC1 is active after zinc binding and insertion into the membrane without the presence of additional binding partners however we have no data to suggest whether the process of insertion or activity could be enhanced by interaction with other factors in vivo.

6.3- The CLIC1 insertion mechanism draws similarities with the annexin family

We present in our findings a model of CLIC1 membrane insertion that is a novel mechanism for CLIC1. In contrast, we can draw similarities with other proteins that adopt similar mechanisms that can aid our understanding of the insertion of CLIC1 into the membrane(Grewal *et al.*, 2017).

The annexin family are a group of calcium-binding scaffolding proteins that function to anchor other proteins to the cell membrane. Increasing levels of intracellular calcium have been shown to promote annexin binding to the membrane. Annexin has an N-terminal region that interacts with lipids and this N terminal region undergoes a conformational change upon binding to calcium. Further analysis of the annexin family determined that annexins 1,2,4 and 6 all had different affinities for calcium in solution, however calcium was essential for promoting membrane insertion in all cases(Monastyrskaya *et al.*, 2007).

This mechanism is largely similar to the one that we propose for CLIC1, we identify conformational changes particularly to the N terminal domain upon zinc binding. Previous literature determines zinc to promote insertion of CLIC1 into the membrane, therefore we determine that the conformation switch of the zinc bound form interacts more readily with lipids. Interestingly the affinity for calcium differs among members of the annexin family. Preliminary lab data suggests the affinity for zinc differs for CLIC4 than CLIC1. The authors of the annexin papers propose the varying lengths of N terminal regions of annexin as a potential cause of different affinities to the cations. In the CLIC family, each member has significant differences in the disordered N terminal region, which could account for the changes in affinity to zinc seen in preliminary NMR data.

6.4- Future development of research into CLIC1

We propose a multi-step insertion mechanism for CLIC1 and further research can be conducted to understand this process in greater detail. The impact of the ensemble in solution upon which the transmembrane region is exposed needs to be explored. Attempts must be made to either stabilise the crystal structure completely preventing opening or completely stabilise the extended structure. Given the hydrophobic properties of the transmembrane region it suggests there might be great difficulty in attempting to stabilise this form of CLIC1.

It seems reasonable to assume attempting to stabilise the crystal structure so that it shifts 100 percent of the population towards the closed state is more manageable. GST has an increased number of intermolecular interactions between the two domains and is unable to separate out the N and C terminal. Given this knowledge within CLIC1, mutations should be made to attempt to mirror GST and increase the number of interdomain interactions. SAXS data can then be measured and the resulting data then compared to the crystal structure. If the mutations are successful in preventing separation of the two domains then the experimental data will now exactly match that of the crystal structure.

Once confirmation of the single structure is solution is identified. A membrane insertion assay should be recompleted and compared to wild type CLIC1. If the presence of the extended minor state is required for membrane insertion or plays an impactful role then the vast majority of CLIC1 should remain in solution and not insert into lipids even in the presence of high concentrations of Zinc. If the protein still inserts with Zinc bound then it suggests an alternative possibly functional role of this minor state.

After identifying that Zinc binds to CLIC1 via initially MST and then further evidence from NMR the next step would be to attempt to perturb Zinc binding. Mutations should be made to residues seen in the NMR that drastically change their chemical environment. Residues with large chemical shift perturbations should be mutated. NMR should identify whether these mutations prevent or reduce the affinity of zinc to bind to CLIC1.

It is highly likely that some of the residues have a chemical shift perturbation because of a conformational change to CLIC1 and are not directly interacting with the Zinc atom. Therefore some mutations may not alter the affinity of Zinc to bind. But if they are important for the structural rearrangement of CLIC1 into a chloride ion channel then a membrane insertion assay should see differences compared to wild type CLIC1.

Almost all experimental data in this thesis has been conducted on changes to CLIC1 in solution. This environment is devoid of lipids which are essential for the conversion of CLIC1 from a cytosolic protein to a chloride ion channel. Therefore further studies must be conducted on the membrane bound form.

To study the chloride ion channel via NMR a solid state probe must be used. In order to achieve a solid-state spectrum that is of a high enough quality to be analysed there requires a lot of optimisation. Sample prep will be altered with the concentration of protein and the lipid protein ratio. The amount of Zinc added will also need to be optimised. If a solid state sample was produced, distance restraints could be calculated to determine roughly the structure of the membrane bound form.

In a similar way to the solution form of CLIC1, relaxation parameters can be calculated to determine the flexible regions of CLIC1 within the membrane bound form. In order

to determine these features for the membrane bound form, then CLIC1 will have to be assigned as the chloride ion channel. It is likely given the size of the membrane bound form of 108kDa that this will be likely too large to feasibly assign. As such for a protein this size, a few reporter residues should be used to report on interactions and flexibility for different regions of CLIC1. An example of how this could be undertaken is using ILV labelling. The isoleucine, leucine and valine residues could act as these reporter residues. This would massively reduce the number of peaks, reducing overcrowding of the spectrum and limiting overlap of peaks. In the membrane bound form, peaks can be very broad and with so many residues, one would expect very large amounts of overlap making the spectrum messy. The reporter residues will attempt to negate some of these problems.

In this research, the structure of CLIC1 in solution has been determined to exist as an ensemble and not exclusively as the x ray structure. In addition the role of divalent cations has been determined. It would be expected that these mechanisms are consistent for the entire CLIC family. Therefore the experiments would have to be repeated with CLIC2-6. If the experiments provided results that completed the work on CLIC1, then a more general mechanism for the entire CLIC family can be hypothesised. The residues that bind Zinc and calcium are highly likely to be completed conserved across all the CLIC proteins, similarly residues essentially for metamorphosis are likely to be highly conserved if not share similar charges.

Further study needs to be carried out on the function of the soluble CLIC1 form. In addition, some consideration is required to understand then how the dynamic

equilibrium of monomer, dimer and small amounts of tetramer would impact the role of soluble CLIC1.

6.5- Impact of this research in the field

In determining that CLIC1 in solution can exist as an ensemble, an additional conformation of CLIC1 has been determined. If this sub state is essential for membrane insertion or the activity of the soluble form then the sub state has a functional role. By knowing this sub state, then future drug development can be targeting this structure and not the crystal structure. All current drug development efforts are calculating affinity of the drug bound to the crystal structure. By not considering its alternative state, this would not only affect the affinity of the drug but also its efficacy. Understanding there is a sub state could open up new pockets for drug binding and this state should be considered in computational modelling.

If the additional sub-state is important for membrane insertion then inhibiting this conformation could inhibit the membrane bound form. This would be a very important therapeutic for cancer drug developments. CLIC1 is overexpressed in cancers such as lung, gastric, liver and glioblastomas. A diagnosis of Glioblastoma has a very poor prognosis and such significant developments in therapeutics to target this rare and aggressive cancer form have so far remained elusive. Inhibition of CLIC1 in vitro has already been demonstrated to impair glioblastoma cell viability and as such inhibition of the membrane bound form of CLIC1 presents a very good drug target to potentially improve the prognosis of those diagnosed with the disease.

This research also advanced knowledge on the understanding of the mechanism of CLIC1 translocation from the cytosol to the membrane environment through binding to zinc ions. As such it would important to see if this mechanism extends to the entire CLIC family. Research can then be conducted to see if a ligand binding triggered metamorphosis from cytosol to membrane bound is exclusive to the CLIC family or a more general mechanism that is utilised by many metamorphic proteins.

6.6- Final conclusion

This thesis has utilised biophysical techniques such as SAXS and NMR to understand the ensemble of structures that exist in solution and provide a mechanism as to how zinc binding to the solution state of CLIC1 triggers insertion into the membrane and the formation of a chloride ion channel. Given the conservation of key residues involved in this mechanism throughout the CLIC family, this mechanism is likely to be consistent for CLIC2-6 in humans and CLIC family members in other species including DmCLIC and EXC-4 in *Drosophila melanogaster* and *Caenorhabditis elegans* respectively.

Bibliography

Alborghetti, M.R. *et al.* (2013) ‘Structural Analysis of Intermolecular Interactions in the Kinesin Adaptor Complex Fasciculation and Elongation Protein Zeta 1/ Short Coiled-Coil Protein (FEZ1/SCOCO)’, *PLoS ONE*, 8(10). Available at: https://doi.org/10.1371/JOURNAL.PONE.0076602.

Averaimo, S. *et al.* (2013) ‘Point Mutations in the Transmembrane Region of the Clic1 Ion Channel Selectively Modify Its Biophysical Properties’, *PLoS ONE*, 8(9). Available at: https://doi.org/10.1371/journal.pone.0074523.

Becker, W. *et al.* (2018) ‘Investigating Protein–Ligand Interactions by Solution Nuclear Magnetic Resonance Spectroscopy’, *ChemPhysChem*. Wiley-VCH Verlag, pp. 895–906. Available at: https://doi.org/10.1002/cphc.201701253.

Berjanskii, M. v. and Wishart, D.S. (2005) ‘A simple method to predict protein flexibility using secondary chemical shifts’, *Journal of the American Chemical Society*, 127(43), pp. 14970–14971. Available at: https://doi.org/10.1021/ja054842f.

Bernadó, P., Mylonas, E., Petoukhov, M. v., *et al.* (2007) ‘Structural characterization of flexible proteins using small-angle X-ray scattering’, *Journal of the American Chemical Society*, 129(17), pp. 5656–5664. Available at: https://doi.org/10.1021/ja069124n.

Berry, K.L. *et al.* (2003) ‘A C. elegans CLIC-like Protein Required for Intracellular Tube Formation and Maintenance’, *Science*, 302(5653), pp. 2134–2137. Available at: https://doi.org/10.1126/science.1087667.

Berry, K.L. and Hobert, O. (2006) ‘Mapping Functional Domains of Chloride Intracellular Channel (CLIC) Proteins in Vivo’, *Journal of Molecular Biology*, 359(5), pp. 1316–1333. Available at: https://doi.org/10.1016/j.jmb.2006.04.046.

Billen, L.P., Shamas-Din, A. and Andrews, D.W. (2009) ‘Bid: a Bax-like BH3 protein’, *Oncogene 2009 27:1*, 27(1), pp. S93–S104. Available at: https://doi.org/10.1038/onc.2009.47.

Board, P.G. *et al.* (2000) ‘Identification, characterization, and crystal structure of the omega class glutathione transferases’, *Journal of Biological Chemistry*, 275(32), pp. 24798–24806. Available at: https://doi.org/10.1074/jbc.M001706200.

Board, P.G. *et al.* (2004) ‘CLIC-2 modulates cardiac ryanodine receptor Ca2+ release channels’, *International Journal of Biochemistry and Cell Biology*, 36(8), pp. 1599–1612. Available at: https://doi.org/10.1016/j.biocel.2004.01.026.

Brazil, B.T., Ybarra, J. and Horowitz, P.M. (1998) ‘Divalent Cations Can Induce the Exposure of GroEL Hydrophobic Surfaces and Strengthen GroEL Hydrophobic Binding Interactions: NOVEL EFFECTS OF Zn2+ GroEL INTERACTIONS’, *Journal of Biological Chemistry*, 273(6), pp. 3257–3263. Available at: https://doi.org/10.1074/JBC.273.6.3257.

Campanero-Rhodes, M.A. *et al.* (2006) ‘Zinc ions induce the unfolding and self-association of boar spermadhesin PSP-I, a protein with a single CUB domain architecture, and promote its binding to heparin’, *Biochemistry*, 45(27), pp. 8227–8235.https://doi.org/10.1021/BI052621G/ASSET/IMAGES/LARGE/BI052621GF00008.JPE G.

Chao, F.A. and Byrd, R.A. (2018) ‘Protein dynamics revealed by NMR relaxation methods’, *Emerging Topics in Life Sciences*. Portland Press Ltd, pp. 93–105. Available at: https://doi.org/10.1042/ETLS20170139.

Chen, K. and Tjandra, N. (2012) ‘The use of residual dipolar coupling in studying proteins by NMR’, *Topics in Current Chemistry*, 326, pp. 47–67. Available at: https://doi.org/10.1007/128_2011_215/COVER.

Chien, C.T.H. *et al.* (2017) ‘An Adaptable Phospholipid Membrane Mimetic System for Solution NMR Studies of Membrane Proteins’, *Journal of the American Chemical Society*, 139(42), pp. 14829–14832. Available at: https://doi.org/10.1021/JACS.7B06730/ASSET/IMAGES/LARGE/JA-2017-067305_0004.JPEG.

Davies, K.A. *et al.* (2020) ‘Distinct pseudokinase domain conformations underlie divergent activation mechanisms among vertebrate MLKL orthologues’, *Nature Communications*, 11(1). Available at: https://doi.org/10.1038/s41467-020-16823-3.

Delaglio ~’, F. *et al.* (1995) *NMRPipe: A multidimensional spectral processing system based on UNIX pipes**, *Journal of Biomolecular NMR*.

Dishman, A.F. and Volkman, B.F. (2018) ‘Unfolding the Mysteries of Protein Metamorphosis’, *ACS Chemical Biology*, 13(6), pp. 1438–1446. Available at: https://doi.org/10.1021/acschembio.8b00276.

Dondelinger, Y. *et al.* (2014) ‘MLKL Compromises Plasma Membrane Integrity by Binding to Phosphatidylinositol Phosphates’, *Cell Reports*, 7(4), pp. 971–981. Available at: https://doi.org/10.1016/j.celrep.2014.04.026.

Dosset, P. *et al.* (2001) ‘A novel interactive tool for rigid-body modeling of multi-domain macromolecules using residual dipolar couplings’, *Journal of Biomolecular NMR 2001 20:3*, 20(3), pp. 223–231. Available at: https://doi.org/10.1023/A:1011206132740.

Dulhunty, A. *et al.* (2001) ‘The Glutathione Transferase Structural Family Includes a Nuclear Chloride Channel and a Ryanodine Receptor Calcium Release Channel Modulator’, *Journal of Biological Chemistry*, 276(5), pp. 3319–3323. Available at: https://doi.org/10.1074/jbc.M007874200.

Duran, C. *et al.* (2009) ‘Chloride channels: Often enigmatic, rarely predictable’, *Annual Review of Physiology*, pp. 95–121. Available at: https://doi.org/10.1146/annurev-physiol-021909-135811.

Fanucchi, S., Adamson, R.J. and Dirr, H.W. (2008a) ‘Formation of an unfolding intermediate state of soluble chloride intracellular channel protein CLIC1 at acidic pH’, *Biochemistry*, 47(44), pp. 11674–11681. Available at: https://doi.org/10.1021/bi801147r.

Fanucchi, S., Adamson, R.J. and Dirr, H.W. (2008b) ‘Formation of an unfolding intermediate state of soluble chloride intracellular channel protein CLIC1 at acidic pH’, *Biochemistry*, 47(44), pp. 11674–11681. Available at: https://doi.org/10.1021/bi801147r.

Fernández, C. and Wider, G. (2003) ‘TROSY in NMR studies of the structure and function of large biological macromolecules’, *Current Opinion in Structural Biology*, 13(5), pp. 570–580. Available at: https://doi.org/10.1016/J.SBI.2003.09.009.

Ferofontov, A. *et al.* (2018) ‘Inherent flexibility of CLIC6 revealed by crystallographic and solution studies’, *Scientific Reports*, 8(1). Available at: https://doi.org/10.1038/s41598-018-25231-z.

Franke, D. and Svergun, D.I. (2009) ‘DAMMIF, a program for rapid ab-initio shape determination in small-angle scattering’, *Journal of Applied Crystallography*, 42(2), pp. 342–346. Available at: https://doi.org/10.1107/S0021889809000338.

Gagnon, L.H. *et al.* (2006) ‘The chloride intracellular channel protein CLIC5 is expressed at high levels in hair cell stereocilia and is essential for normal inner ear function’, *Journal of Neuroscience*, 26(40), pp. 10188–10198. Available at: https://doi.org/10.1523/JNEUROSCI.2166-06.2006.

Goodchild, S.C. *et al.* (2010a) ‘Metamorphic response of the CLIC1 chloride intracellular ion channel protein upon membrane interaction’, *Biochemistry*, 49(25), pp. 5278–5289. Available at: https://doi.org/10.1021/bi100111c.

Goodchild, S.C. *et al.* (2011) ‘Transmembrane extension and oligomerization of the CLIC1 chloride intracellular channel protein upon membrane interaction’, *Biochemistry*, 50(50), pp. 10887–10897. Available at: https://doi.org/10.1021/bi2012564.

Grewal, T. *et al.* (2017) ‘Annexin A6—A multifunctional scaffold in cell motility’, *Cell Adhesion and Migration*, 11(3), pp. 288–304. Available at: https://doi.org/10.1080/19336918.2016.1268318.

Gritti, M. *et al.* (2014) *Metformin repositioning as antitumoral agent: selective antiproliferative effects in human glioblastoma stem cells, via inhibition of CLIC1-mediated ion current*. Available at: www.impactjournals.com/oncotarget.

Gupta, K. *et al.* (2017) ‘The role of interfacial lipids in stabilizing membrane protein oligomers’. Available at: https://doi.org/10.1038/nature20820.

Gururaja Rao, S. *et al.* (2018) 'Three decades of chloride intracellular channel proteins: From organelle to organ physiology', *Current Protocols in Pharmacology*, 80(1), pp. 11.21.1-11.21.17. Available at: https://doi.org/10.1002/cpph.36.

Hare, J.E. *et al.* (2016) 'Interaction of Human Chloride Intracellular Channel Protein 1 (CLIC1) with Lipid Bilayers: A Fluorescence Study', *Biochemistry*, 55(27), pp. 3825–3833. Available at: https://doi.org/10.1021/acs.biochem.6b00080.

Harrop, S.J. *et al.* (2001) 'Crystal Structure of a Soluble Form of the Intracellular Chloride Ion Channel CLIC1 (NCC27) at 1.4-Å Resolution', *Journal of Biological Chemistry*, 276(48), pp. 44993–45000. Available at: https://doi.org/10.1074/jbc.M107804200.

Harrop, S.J. *et al.* (2007) 'Comparison of vertebrate and invertebrate CLIC proteins: The crystal structures of *Caenorhabditis elegans* EXC-4 and *Drosophila melanogaster* DmCLIC ', *Proteins'*,364-78. Available at: https://doi.org/10.1002/prot.21704

He, W. *et al.* (2020) 'Increased surface charge in the protein chaperone Spy enhances its anti-aggregation activity', *Journal of Biological Chemistry*, 295(42), pp. 14488–14500. Available at: https://doi.org/10.1074/JBC.RA119.012300.

Hildebrand, J.M. *et al.* (2014) 'Activation of the pseudokinase MLKL unleashes the four-helix bundle domain to induce membrane localization and necroptotic cell death', *Proceedings of the National Academy of Sciences of the United States of America*, 111(42), pp. 15072–15077. Available at: https://doi.org/10.1073/pnas.1408987111.

Hossain, K.R. *et al.* (2016) 'Cholesterol Promotes Interaction of the Protein CLIC1 with Phospholipid Monolayers at the Air–Water Interface', *Membranes 2016, Vol. 6, Page 15*, 6(1), p. 15. Available at: https://doi.org/10.3390/MEMBRANES6010015.

Howell, S., Duncan, R.R. and Ashley, R.H. (1996) *Identification and characterisation*

of a homologue of p64 in rat tissues, *FEBS 17285 FEBS Letters*.

Iacovache, I., Bischofberger, M. and van der Goot, F.G. (2010) ‘Structure and assembly of pore-forming proteins’, *Current Opinion in Structural Biology*, pp. 241–246. Available at: https://doi.org/10.1016/j.sbi.2010.01.013.

Jeffries, C.M. *et al.* (2015) ‘Limiting radiation damage for high-brilliance biological solution scattering: Practical experience at the EMBL P12 beamline PETRAIII’, in *Journal of Synchrotron Radiation*. International Union of Crystallography, pp. 273–279. Available at: https://doi.org/10.1107/S1600577515000375.

Jerabek-Willemsen, M. *et al.* (2014) ‘MicroScale Thermophoresis: Interaction analysis and beyond’, *Journal of Molecular Structure*, 1077, pp. 101–113. Available at: https://doi.org/10.1016/j.molstruc.2014.03.009.

Jiang, Y.Y. *et al.* (2017) ‘Chloride Channels are Involved in the Development of Atrial Fibrillation - A Transcriptomic and proteomic Study’, *Scientific Reports*, 7(1). Available at: https://doi.org/10.1038/s41598-017-10590-w.

Jin, H.K. *et al.* (2009) ‘Structure and dynamics of the iron-sulfur cluster assembly scaffold protein IscU and its interaction with the cochaperone HscB’, *Biochemistry*, 48(26), pp. 6062–6071. Available at: https://doi.org/10.1021/bi9002277.

Johnsona, B.A. and Blevinsb, R.A. (1994) *NMRView: A computer program for the visualization and analysis of NMR data**, *Journal of Biomolecular NMR*.

Jones, P.M. *et al.* (2013) ‘Computational analysis of the soluble form of the intracellular chloride ion channel protein CLIC1’, *BioMed Research International*, 2013. Available at: https://doi.org/10.1155/2013/170586.

Jumper, J. *et al.* (2021) ‘Highly accurate protein structure prediction with AlphaFold’, *Nature*, 596(7873), pp. 583–589. Available at: https://doi.org/10.1038/s41586-021-03819-2.

Koch, M.H.J., Vachette, P. and Svergun, D.I. (2003) ‘Small-angle scattering: A view on the properties, structures and structural changes of biological macromolecules in solution’, *Quarterly Reviews of Biophysics*, pp. 147–227. Available at: https://doi.org/10.1017/S0033583503003871.

Lee, J.R. *et al.* (2019) ‘The inhibition of chloride intracellular channel 1 enhances Ca2+ and reactive oxygen species signaling in A549 human lung cancer cells’, *Experimental and Molecular Medicine*, 51(7). Available at: https://doi.org/10.1038/s12276-019-0279-2.

Lella, M. and Mahalakshmi, R. (2017) ‘Metamorphic Proteins: Emergence of Dual Protein Folds from One Primary Sequence’, *Biochemistry*, 56(24), pp. 2971–2984. Available at: https://doi.org/10.1021/acs.biochem.7b00375.

Littler, D.R. *et al.* (2004) ‘The Intracellular Chloride Ion Channel Protein CLIC1 Undergoes a Redox-controlled Structural Transition’, *Journal of Biological Chemistry*, 279(10), pp. 9298–9305. Available at: https://doi.org/10.1074/jbc.M308444200.

Littler, D.R. *et al.* (2008) ‘Comparison of vertebrate and invertebrate CLIC proteins: The crystal structures of Caenorhabditis elegans EXC-4 and Drosophila melanogaster DmCLIC’, *Proteins: Structure, Function and Genetics*, 71(1), pp. 364–378. Available at: https://doi.org/10.1002/prot.21704.

Liu, T. and Wang, X. (2010) ‘Zinc induces unfolding and aggregation of dimeric arginine kinase by trapping reversible unfolding intermediate’, *Acta Biochimica et*

Biophysica Sinica, 42(11), pp. 779–786. Available at: https://doi.org/10.1093/ABBS/GMQ092.

Lõpez-Pelegrín, M. *et al.* (2014) 'Multiple stable conformations account for reversible concentration-dependent oligomerization and autoinhibition of a metamorphic metallopeptidase', *Angewandte Chemie - International Edition*, 53(40), pp. 10624–10630. Available at: https://doi.org/10.1002/anie.201405727.

Lu, J. *et al.* (2015) 'Chloride intracellular channel 1 (CLIC1) is activated and functions as an oncogene in pancreatic cancer', *Medical Oncology*, 32(6). Available at: https://doi.org/10.1007/s12032-015-0616-9.

Madhurima, K., Nandi, B. and Sekhar, A. (2021) 'Metamorphic proteins: The Janus proteins of structural biology', *Open Biology*. Royal Society Publishing. Available at: https://doi.org/10.1098/rsob.210012.

Maity, S., Gundampati, R.K. and Kumar, T.K.S. (2019) 'NMR methods to characterize protein-ligand interactions', *Natural Product Communications*, 14(5). Available at: https://doi.org/10.1177/1934578X19849296/ASSET/IMAGES/LARGE/10.1177_1934578X19849296-FIG2.JPEG.

Marion, D. (2013) 'An Introduction to Biological NMR Spectroscopy', *Molecular & Cellular Proteomics : MCP*, 12(11), p. 3006. Available at: https://doi.org/10.1074/MCP.O113.030239.

Markley, J.L. *et al.* (2013) 'Metamorphic protein IscU alternates conformations in the course of its role as the scaffold protein for iron-sulfur cluster biosynthesis and delivery', *FEBS Letters*, pp. 1172–1179. Available at: https://doi.org/10.1016/j.febslet.2013.01.003.

Milton, R.H. *et al.* (2008) 'CLIC1 function is required for β-amyloid-induced generation of reactive oxygen species by microglia', *Journal of Neuroscience*, 28(45), pp. 11488–11499. Available at: https://doi.org/10.1523/JNEUROSCI.2431-08.2008.

Mlynárik, V. (2017) 'Introduction to nuclear magnetic resonance', *Analytical Biochemistry*, 529, pp. 4–9. Available at: https://doi.org/10.1016/J.AB.2016.05.006.

Monastyrskaya, K. *et al.* (2007) 'Annexins as intracellular calcium sensors', *Cell Calcium*, 41(3), pp. 207–219. Available at: https://doi.org/10.1016/J.CECA.2006.06.008.

Novarino, G. *et al.* (2004) 'Involvement of the intracellular ion channel CLIC1 in microglia-mediated β-amyloid-induced neurotoxicity', *Journal of Neuroscience*, 24(23), pp. 5322–5330. Available at: https://doi.org/10.1523/JNEUROSCI.1170-04.2004.

Olechnowicz, J. *et al.* (2018) 'Zinc status is associated with inflammation, oxidative stress, lipid, and glucose metabolism', *Journal of Physiological Sciences*, 68(1), pp. 19–31. Available at: https://doi.org/10.1007/S12576-017-0571-7/FIGURES/3.

Peretti, M. *et al.* (2014) *Chloride channels in cancer: Focus on chloride intracellular channel 1 and 4 (CLIC1 AND CLIC4) proteins in tumor development and as novel therapeutic targets ☆*.

Peter, B. *et al.* (2013) 'Membrane mimetics induce helix formation and oligomerization of the chloride intracellular channel protein 1 transmembrane domain', *Biochemistry*, 52(16), pp. 2739–2749. Available at: https://doi.org/10.1021/bi4002776.

Petoukhov, M. v. *et al.* (2012) ‘New developments in the ATSAS program package for small-angle scattering data analysis’, *Journal of Applied Crystallography*, 45(2), pp. 342–350. Available at: https://doi.org/10.1107/S0021889812007662.

Prestegard, J.H. *et al.* (2005) ‘Determination of Protein Backbone Structures from Residual Dipolar Couplings’, *Methods in Enzymology*, 394, pp. 175–209. Available at: https://doi.org/10.1016/S0076-6879(05)94007-X.

Prestegard, J.H. *et al.* (no date) *Determination of Protein Backbone Structures from Residual Dipolar Couplings*.

Qu, L. *et al.* (2022) ‘CLIC1 promotes the progression of cervical cancer through the PTEN/PI3K/AKT pathway’, *Panminerva Medica*. Edizioni Minerva Medica, pp. 294–295. Available at: https://doi.org/10.23736/S0031-0808.21.04430-X.

Quarato, G. *et al.* (2016) ‘Sequential Engagement of Distinct MLKL Phosphatidylinositol-Binding Sites Executes Necroptosis’, *Molecular Cell*, 61(4), pp. 589–601. Available at: https://doi.org/10.1016/J.MOLCEL.2016.01.011.

Rao, S.G. *et al.* (2017) ‘Identification and Characterization of a Bacterial Homolog of Chloride Intracellular Channel (CLIC) Protein’, *Scientific Reports*, 7(1). Available at: https://doi.org/10.1038/s41598-017-08742-z.

Rosengarth, A. and Luecke, H. (2003) ‘A Calcium-driven Conformational Switch of the N-terminal and Core Domains of Annexin A1’, *Journal of Molecular Biology*, 326(5), pp. 1317–1325. Available at: https://doi.org/10.1016/S0022-2836(03)00027-5.

Schneidman-Duhovny, D. *et al.* (2016) ‘FoXS, FoXSDock and MultiFoXS: Single-state and multi-state structural modeling of proteins and their complexes based on SAXS

profiles', *Nucleic Acids Research*, 44(1), pp. W424–W429. Available at: https://doi.org/10.1093/nar/gkw389.

Schneidman-Duhovny, D., Hammel, M. and Sali, A. (2010) 'FoXS: a web server for rapid computation and fitting of SAXS profiles', *Nucleic Acids Research*, 38(SUPPL. 2). Available at: https://doi.org/10.1093/nar/gkq461.

Sciacca, M.F.M. *et al.* (2013) 'Cations as Switches of Amyloid-Mediated Membrane Disruption Mechanisms: Calcium and IAPP', *Biophysical Journal*, 104(1), pp. 173–184. Available at: https://doi.org/10.1016/J.BPJ.2012.11.3811.

Seco, C.Z. *et al.* (2015) 'Progressive hearing loss and vestibular dysfunction caused by a homozygous nonsense mutation in CLIC5', *European Journal of Human Genetics*, 23(2), pp. 189–194. Available at: https://doi.org/10.1038/ejhg.2014.83.

Setti, M. *et al.* (2013) 'Functional role of CLIC1 ion channel in glioblastoma-derived stem/progenitor cells', *Journal of the National Cancer Institute*, 105(21), pp. 1644–1655. Available at: https://doi.org/10.1093/jnci/djt278.

Singh, H. and Ashley, R.H. (2006) 'Redox regulation of CLIC1 by cysteine residues associated with the putative channel pore', *Biophysical Journal*, 90(5), pp. 1628–1638. Available at: https://doi.org/10.1529/biophysj.105.072678.

Singh, H., Cousin, M.A. and Ashley, R.H. (2007a) 'Functional reconstitution of mammalian "chloride intracellular channels" CLIC1, CLIC4 and CLIC5 reveals differential regulation by cytoskeletal actin', *FEBS Journal*, 274(24), pp. 6306–6316. Available at: https://doi.org/10.1111/j.1742-4658.2007.06145.x.

Singh, H., Cousin, M.A. and Ashley, R.H. (2007b) 'Functional reconstitution of mammalian "chloride intracellular channels" CLIC1, CLIC4 and CLIC5 reveals

differential regulation by cytoskeletal actin', *FEBS Journal*, 274(24), pp. 6306–6316. Available at: https://doi.org/10.1111/j.1742-4658.2007.06145.x.

Tina KG, Bhadra R, Srinivasan N. PIC: Protein Interactions Calculator. Nucleic Acids Res. 2007 Jul;35(Web Server issue):W473-6. doi: 10.1093/nar/gkm423. Epub 2007 Jun 21.

Stoychev, S.H. *et al.* (2009) 'Structural dynamics of soluble chloride intracellular channel protein CLIC1 examined by amide hydrogen-deuterium exchange mass spectrometry', *Biochemistry*, 48(35), pp. 8413–8421. Available at: https://doi.org/10.1021/bi9010607.

Taube, M., Jarmołowski, A. and Kozak, M. (2010) 'Low Resolution Structure of RAR1-GST-Tag Fusion Protein in Solution', 117.

Thuringer, D. *et al.* (2018) *The vesicular transfer of CLIC1 from glioblastoma to microvascular endothelial cells requires TRPM7*. Available at: www.oncotarget.com.

Tilley, S.J. and Saibil, H.R. (2006) 'The mechanism of pore formation by bacterial toxins', *Current Opinion in Structural Biology*, pp. 230–236. Available at: https://doi.org/10.1016/j.sbi.2006.03.008.

Tonini, R. *et al.* (2000a) 'Functional characterization of the NCC27 nuclear protein in stable transfected CHO-K1 cells', *The FASEB Journal*, 14(9), pp. 1171–1178. Available at: https://doi.org/10.1096/fasebj.14.9.1171.

Tonini, R. *et al.* (2000b) 'Functional characterization of the NCC27 nuclear protein in stable transfected CHO-K1 cells', *The FASEB Journal*, 14(9), pp. 1171–1178. Available at: https://doi.org/10.1096/fasebj.14.9.1171.

Townsend, D.M. and Tew, K.D. (2003) 'The role of glutathione-S-transferase in anti-cancer drug resistance', *Oncogene*, 22(47), pp. 7369–7375. Available at:

https://doi.org/10.1038/sj.onc.1206940.

Tria, G. *et al.* (2015) ‘Advanced ensemble modelling of flexible macromolecules using X-ray solution scattering’, 2, pp. 207–217. Available at: https://doi.org/10.1107/S205225251500202X.

Tugarinov, V., Kanelis, V. and Kay, L.E. (2006) ‘Isotope labeling strategies for the study of high-molecular-weight proteins by solution NMR spectroscopy’, *Nature Protocols 2006 1:2*, 1(2), pp. 749–754. Available at: https://doi.org/10.1038/nprot.2006.101.

Tulk, B.M. *et al.* (2002a) ‘CLIC1 inserts from the aqueous phase into phospholipid membranes, where it functions as an anion channel’, *J Physiol Cell Physiol*, 282, pp. 1103–1112. Available at: https://doi.org/10.1152/ajpcell.00402.2001.-CLIC1.

Turkewitz, D.R. *et al.* (2021a) ‘Comparative study of His- and Non-His-tagged CLIC proteins, reveals changes in their enzymatic activity’, *Biochemistry and Biophysics Reports*, 26. Available at: https://doi.org/10.1016/j.bbrep.2021.101015.

Turkewitz, D.R. *et al.* (2021b) ‘Comparative study of His- and Non-His-tagged CLIC proteins, reveals changes in their enzymatic activity’, *Biochemistry and Biophysics Reports*, 26, p. 101015. Available at: https://doi.org/10.1016/J.BBREP.2021.101015.

Ulmasov, B. *et al.* (2007) ‘Tissue and subcellular distribution of CLIC1’, *BMC Cell Biology*, 8. Available at: https://doi.org/10.1186/1471-2121-8-8.

Valenzuela, S.M. *et al.* (1997) ‘Molecular cloning and expression of a chloride ion channel of cell nuclei’, *Journal of Biological Chemistry*, 272(19), pp. 12575–12582. Available at: https://doi.org/10.1074/jbc.272.19.12575.

Valenzuela, S.M. *et al.* (2013) ‘Regulation of the Membrane Insertion and Conductance Activity of the Metamorphic Chloride Intracellular Channel Protein CLIC1

by Cholesterol', *PLoS ONE*, 8(2). Available at: https://doi.org/10.1371/journal.pone.0056948.

Varadi, M. *et al.* (2022) 'AlphaFold Protein Structure Database: Massively expanding the structural coverage of protein-sequence space with high-accuracy models', *Nucleic Acids Research*, 50(D1), pp. D439–D444. Available at: https://doi.org/10.1093/nar/gkab1061.

Varela, L. *et al.* (2022) 'The membrane insertion of soluble CLIC1 into active chloride channels is triggered by specific divalent cations'. Available at: https://doi.org/10.1101/638080.

Vasquez-Montes, V. *et al.* (2019) 'Divalent Cations and Lipid Composition Modulate Membrane Insertion and Cancer-Targeting Action of pHLIP', *Journal of Molecular Biology*, 431(24), pp. 5004–5018. Available at: https://doi.org/10.1016/J.JMB.2019.10.016.

Vasquez-Montes, V. *et al.* (2022) 'Ca2+ and Mg2+ Influence the Thermodynamics of Peptide-Membrane Interactions', *Journal of Molecular Biology*, 434(21). Available at: https://doi.org/10.1016/J.JMB.2022.167826.

Warton, K. *et al.* (2002a) 'Recombinant CLIC1 (NCC27) assembles in lipid bilayers via a pH-dependent two-state process to form chloride ion channels with identical characteristics to those observed in Chinese hamster ovary cells expressing CLIC1', *Journal of Biological Chemistry*, 277(29), pp. 26003–26011. Available at: https://doi.org/10.1074/jbc.M203666200.

Warton, K. *et al.* (2002b) 'Recombinant CLIC1 (NCC27) assembles in lipid bilayers via a pH-dependent two-state process to form chloride ion channels with identical characteristics to those observed in Chinese hamster ovary cells expressing CLIC1',

Journal of Biological Chemistry, 277(29), pp. 26003–26011. Available at: https://doi.org/10.1074/jbc.M203666200.

Wilkins (2014) 'Aberrant CLIC4 expression in Pulmonary hypertension'.

Williamson, M.P. (2013) 'Using chemical shift perturbation to characterise ligand binding', *Progress in Nuclear Magnetic Resonance Spectroscopy*, 73, pp. 1–16. Available at: https://doi.org/10.1016/J.PNMRS.2013.02.001.

Wilson, R.J. *et al.* (2004) 'Spatial patterns in species distributions reveal biodiversity change', *Nature*, 432(7015), pp. 393–396. Available at: https://doi.org/10.1038/nature03031.

Wulfkuhle, J.D. *et al.* (no date) *Proteomics of Human Breast Ductal Carcinoma in Situ 1*. Available at: www.ncbi.nlm.nih.gov/SAGE/sagexpsetup.cgi.

Würth, R. *et al.* (2013) 'Metformin selectively affects human glioblastoma tumor-initiating cell viability: A role for metformin-induced inhibition of Akt', *Cell Cycle*, 12(1), pp. 145–156. Available at: https://doi.org/10.4161/cc.23050.

Xu, Y. *et al.* (2016) 'CLIC1 inhibition attenuates vascular inflammation, oxidative stress, and endothelial injury', *PLoS ONE*, 11(11). Available at: https://doi.org/10.1371/journal.pone.0166790.

Appendix

© 2022. Published by The Company of Biologists Ltd | Journal of Cell Science (2022) 135, jcs259704. doi:10.1242/jcs.259704

RESEARCH ARTICLE

A Zn^{2}+-triggered two-step mechanism of CLIC1 membrane insertion and activation into chloride channels

Lorena Varela[1,*], Alex C. Hendry[1,*], Joseph Cassar\ Ruben Martin-Escolano1, Diego Cantoni[2], Felipe Ossa[3], John C. Edwards4, Vahitha Abdul-Salam[3] and Jose L. Ortega-Roldan[1,t]

ABSTRACT

The chloride intracellular channel (CLIC) protein family displays the unique feature of altering its structure from a soluble form to a membrane-bound chloride channel. CLIC1, a member of this family, is found in the cytoplasm or in internal and plasma membranes, with membrane relocalisation linked to endothelial disfunction, tumour proliferation and metastasis. The molecular switch promoting CLIC1 activation remains under investigation. Here, cellular c1- efflux assays and immunofluorescence microscopy studies have identified intracellular Zn^{2}· release as the trigger for CLIC1 activation and membrane insertion. Biophysical assays confirmed specific binding to Zn^{2}+, inducing membrane association and enhancing c1- efflux in a pH-dependent manner. Together, our results identify a two-step mechanism with Zn^{2}· binding as the molecular switch promoting CLIC1 membrane insertion, followed by pH-mediated activation of c1- efflux.

KEY WORDS: Membrane protein, Chloride channel, Channel activation, Lipid-protein interaction, Biophysics

INTRODUCTION

The chloride inrracellular channel (CUC) family consists of a group of highly homologous human proteins with a striking feature, their ability to change their structure upon activation from a soluble form into a membrane-bound chloride channel, translocating from the cytoplasm to inrracellular membranes (Tulk et al., 2000; Valenzuela et al., 1997). CUC 1 is the best characterised of the CUC protein family. It is expressed intracellularly in a variety of cell types, being especially abundant in heart and skeletal muscle (Valenzuela et al., 1997). The integral membrane form ofCLICI has been found to be localised mostly in the nuclear membrane, although it is present in the membranes of other organelles and transiently in the plasma membrane (Valenzuela et al., 2000). Jt has also been shown to function as an active chloride channel in phospholipid vesicles when expressed and purified from bacteria, showing clear single channel properties (Tulk et al., 2000, 2002).

CLICI has been implicated in the regulation of cell volume, electrical excitability (Averaimo et al., 2014), differentiation (Wang et al., 20 I 1), cell cycle (Valenzuela et al., 2000) and cell growth and proliferation (Tung and Kitajewski, 2010). High CLICI expression has been reported in a range of malignant tumours (Grilli et al., 2014; Setti et al., 2015; Tian et al., 2014; Wang et al., 20 I 1; Zhang et al., 2015; Zhao et al., 2015) and cardiovascular diseases such as pulmonary hypertension (Abdul- Salam et al., 2010) and ischaemic cardiomyopathy (Gronich et al., 2010). One common effect ofCLICI in these disease mechanisms is its effect on endothelial function (Gurski et al., 2015; Xu et al., 2016). CUC I compromises endothelial barrier function and mediates cell growth, angiogenesis and migration (Knowles et al., 2012; Tung and Kitajewski, 2010). These vascular malformations *have* been linked to electrophysiological alterations in the cells caused, at least in part, by the CUC 1 chloride channel activity (Gurski et al., 2015). The activity and deleterious function of CLICI is modulated by its equilibrium between the soluble cytosolic form and its membrane-bound form. Only CLICI in its channel form has been shown to have pro-proliferative and angiogenic activity, and specific inhibition of CUC 1 channel halts endothelial injury, tumour angiogenesis and progression and vascular inflammation.

Despite its clinical importance, to date only conflicting infom1ation is available on the mechanism of CLICl membrane insertion, and a high-resolution structure of the channel form has not been detennined. *in vitro* oxidation with hydrogen peroxide causes a conformational change due to the formation of a disulfide bond between Cys24 and the non-conserved Cys59, exposing a hydrophobic patch that promotes the fonmation of a dimer (Littler et al., 2004) in a process that has been proposed to lead to membrane insertion (Goodchild et al., 2009). However, numerous studies have shown that oxidation does not promote membrane insertion (Singh and Ashley, 2006), with evidence pointing at pH (Fanucchi et al., 2008; Stoychev et al., 2009) or cholesterol (Hossain et al., 2016; 2017) as the likely activation factors. Thus, long standing inconsistencies in the data surrounding the molecular switch that transforms CUC I from its soluble fonn into a membrane-bound channel, and the complex nature of its regulation, have prevented further advances in the understanding of CLICI function.

In this study, we have explored the membrane insertion activation mechanism ofCLICl. We have discovered the activation ofCUCl Cl- effiux by intracellular Zn^{2}+ in glioblastoma cells, which also causes CLICI relocalisation to the plasma membrane. Finally, *in vitro* studies with purified CUC! showed zn2+-driven activation of c1- effiux, membrane association, as well as CUC I-specific binding to both Zn^{2}+ and Ca^{2}+.

[1]School of Biosciences, University of Kent, Canterbury CT2 7NJ, UK. [2]Medway School of Pharmacy, The Universities of Kent and Greenwich at Medway, Chatham ME7 4TB, UK. [3]Centre for Cardiovascular Medicine and Device Innovation, William Harvey Research Institute (WHRI), Faculty of Medicine and Dentistry, Queen Mary University of London, Room 213, John Vane Science Centre, Charterhouse Square, London EC1M 6BQ, UK. [4]Department of Internal Medicine, St Louis University, 3635 Vista Ave., St Louis, MO 63110, USA.
•These authors contributed equally to this work

:f:Author for correspondence (j.l.ortega-roldan@kent.ac.uk)

e L.V., 0000-0002-0743-9441; J.L.O.-R., 0000-0002-6316-4390

This is an Open Access article distributed under the terms of the Creative Commons Attribution License (https://creativecommons.org/licenses/by/4.0), which pem,its unrestricted use, distribution and reproduction in any medium provided that the original work is properly attributed.

Handling Editor: Giampietro Schiavo
Received 19 January 2022; Accepted 4 July 2022

Journal of Cell Science (2022) 135, jcs259704. doi:10.1242/jcs.259704

RESULTS

Divalent cation binding, specifically Ca^{2+}, is involved in the membrane interactions of other protein families (Dube et al., 2016; Rosengarth and Luecke, 2003; Sciacca et al., 2013). Interestingly, the CLIC C. *elegans* and *Drosophila* homologs EXC-4 and *DmCLICI* (also known as Clic) both contain a bound Ca^{2+} ion that is trapped during the expression and purification process. We therefore sought to understand if divalent cations may have a role in CLICI activation as a chloride channel.

The effect of divalent cation-driven membrane localisation on the c1- effiux activity ofCLICI was tested in U87G cells using MQAE as a fluorescent reporter of the intracellular concentration of c1-. With no treatment, the c1- effiux activity is not affected by the chloride channel inhibitors DIDS and NPPB, in line with previous results (Warton et al., 2002), and is only modestly inhibited by the CLJC inhibitor IAA-94 or the Zn^{2+} chelator TPEN, and thus is likely not CLJC mediated. Ionomycin, an ionophore previously shown to increase both Ca^{2+} and Zn^{2+} intracellular concentrations (Ackland and McArdle, I996), induced a significant increase *(P=O.O* 123) of the c1- effiux, as seen by the increase in MQAE **fluorescence, that was reversed upon treatment with the Zn^{2+}** chelator TPEN or with the CLIC inhibitor IAA-94 *(P<0.005)* (Xu et al., 2016) (Fig. I; Fig. SI). Interestingly, TPEN inhibits the CJ- conductance of the control cells to a level similar to that seen upon JAA-94 treatment, suggesting the involvement of Zn^{2+} in the activation ofCLICI c1- effiux. Again, DIDS and NPPB showed no effect on CLICI effiux after treatment with ionomycin.

In light of these results, we questioned whether Zn^{2+}could tTigger CLJC I membrane relocalisation in cells. Endogenous CLJC I localisation was monitored in HeLa and glioblastoma cells (U87G) using immunostaining. CLICI typically exists in the cytosol in untreated HeLa cells, and the addition of the ionophore ionomycin promoted the presence of CLJC I at the plasma membrane (Fig. 2). A similar effect was observed in U87G cells.

Addition of ionomycin increased the degree of CUC I plasma membrane localisation. For both cell lines, this effect was reversed by the addition of TPEN, confirming that Zn^{2+} triggers the activation and membrane relocalisation ofCLICI.

Previous studies have indicated the importance of low pH for CLICI chloride channel activity. We used the previously reported vesicle-based c1- effiux assay to assess effect of either Ca^{2+} or Zn^{2+} ions on CLICI chloride channel activity *in vitro* (Tulk et al., 2002). The CLICI chloride channel shows strong pH dependence, with little activity above pH 6.5 (Warton et al., 2002). We measured channel activity at pH 5.5 and pH 7.5 in the nominal absence of divalent cations, or in the presence of I µM Ca^{2+} or Zn^{2+} (Fig. 3A), using vesicles from the soya bean lipid extract asolectin. This divalent cation concentration was chosen to be equimolar with the **protein concentration in the reaction mix. Protein was mixed with** cations prior to addition of vesicles. We found virtually no activity at pH 7.5 in the presence or absence of divalent cation. At pH 5.5, we found significant c1- permeability conferred by CLICI that was enhanced ~25% by the presence ofZn^{2+} (P 0.024), but not by the presence of Ca^{2+}. We repeated the experiment using purified phospholipid vesicles rather than asolectin because of concern that the activity in the nominal absence of Zn^{2+} might be due to small amounts of Zn^{2+} contaminating the lipids. With purified phospholipids, the activity in the absence of Zn^{2+} was 35% lower than with asolectin vesicles, but the activation with I µM Zn^{2+} was greater and amounted to a statistically significant 40% increase (P 0.0044).

We subsequently attempted to separate activation of the CLICI chloride channel effiux activity from its insertion in the membrane. To this end, we explored the effect of Zn^{2+} and pH on membrane association of recombinantly expressed and purified GFP-tagged CLICI by incubating CLICI-GFP with and without Zn^{2+} at pH 7.4 and 5.5 with giant unilamellar vesicles (GUVs). We used the fluorescence of Red Nile dye, which binds to the GUVs lipids, and

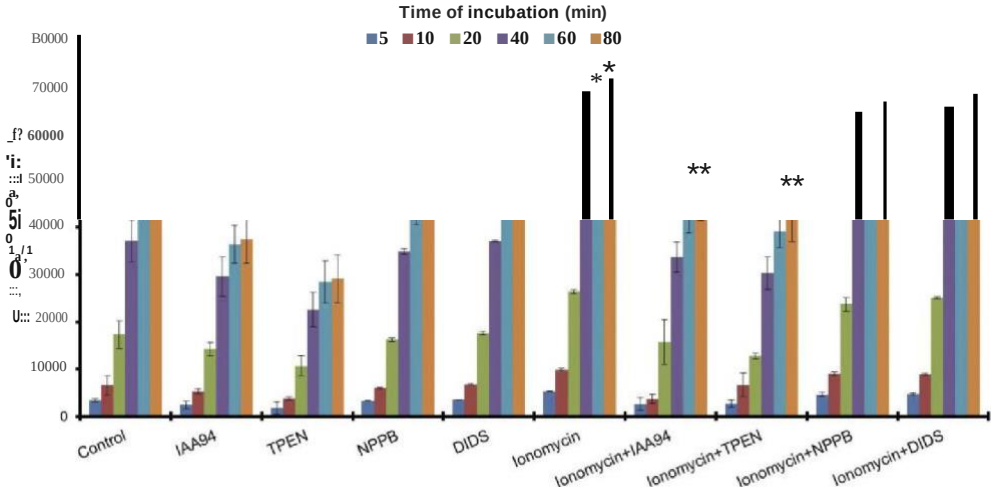


Fig. 1. Effect of different treatments on c1- efflux. Results are in fluorescence intensity units for the dye MQAE from MQAE-stained U87G cells exposed to IAA94 (10 µM), TPEN (5 µM), NPPB, DIOS and ionomycin (all 10 µM) for 80 min. Values constitute mean±s.d. of six independent determinations. Ionomycin treatment resulted in statistically significant differences from 60 min compared to the control samples (P<0.0123) (*P<0.05) and to all other treatments (.. P<0.005) (n=6) (two-tailed I-test).

Journal of Cell Science

Journal of Cell Science (2022) 135, jcs259704. doi:10.1242/jcs.259704

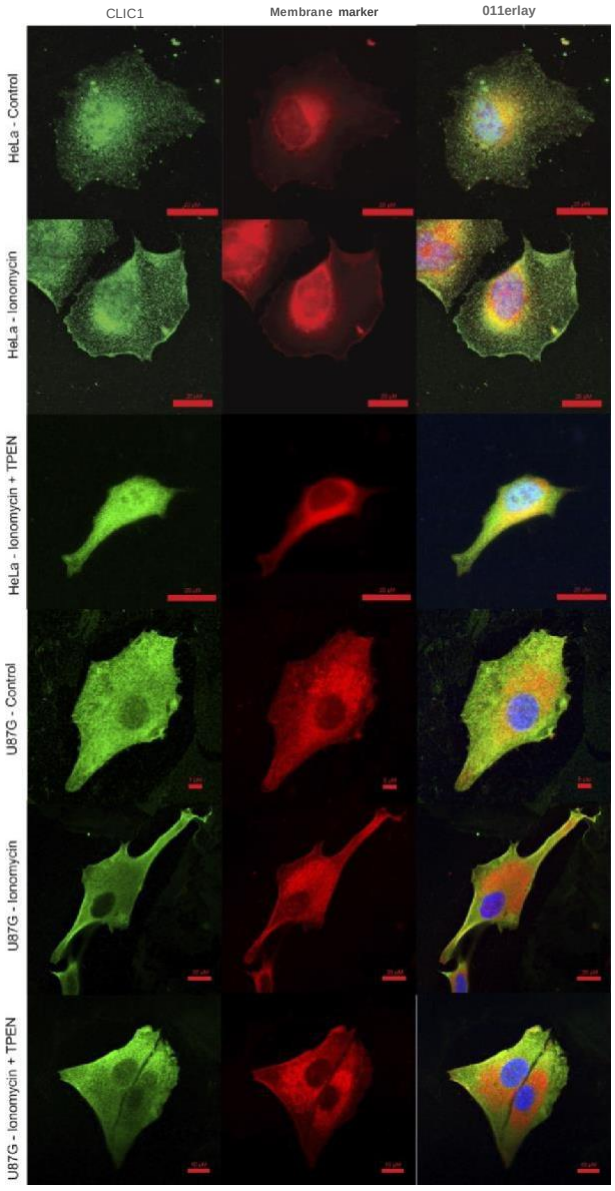


Fig. 2. Divalent cations promote membrane insertion. CLIC1 localisation in Hela and U87G cells. Hela and glioblastoma cells (U87G) were either untreated (1st and 4th row), treated for 3 h with 10 µM ionomycin {2nd and 5th row) or treated with 10 µM ionomycin and the Zn^{2+} chelator TPEN (3rd and 6th row). CLIC1 typically exists in the cytosol and the ionomycin-driven release of Ca^{2+} and Zn^{2+} promoted the presence of CLIC1 at plasma membrane. This effect was reversed upon chelation of intracellular Zn^{2+} by TPEN. Samples were stained with an anti-CLIC1 antibody (green), a CellMASK membrane dye (red) and DAPI (blue). Scale bars **indicated in all images correspond to 5--20 µm.**

GFP, to investigate the degree of colocalisation of CUC 1-GFP with the GUVs. fluorescence microscopy images collected showed CUC! colocalisation in the membrane only in the presence ofZn^{2+} irrespective of the pH value, indicating that Zn^{2+} has a direct effect on CUC I, triggering its membrane insertion (Fig. JC). Ca^{2+} on the other hand only induced partial insertion in the membrane at the **same protein and cation concentrations, in agreement with its** neglectable effect on CUC I c1- effiux (Fig. S2).

Microscale thermophoresis (MST) can be used to identify specific divalent cation binding to CLICl and to detennine the affinity of these interactions. We used a C-terminal GFP tagged CUC I construct at a concentration of I µM and at pH 7.4 to compare the

Journal of Cell Science (2022) 135, jcs259704. doi:10.1242/jcs.259704

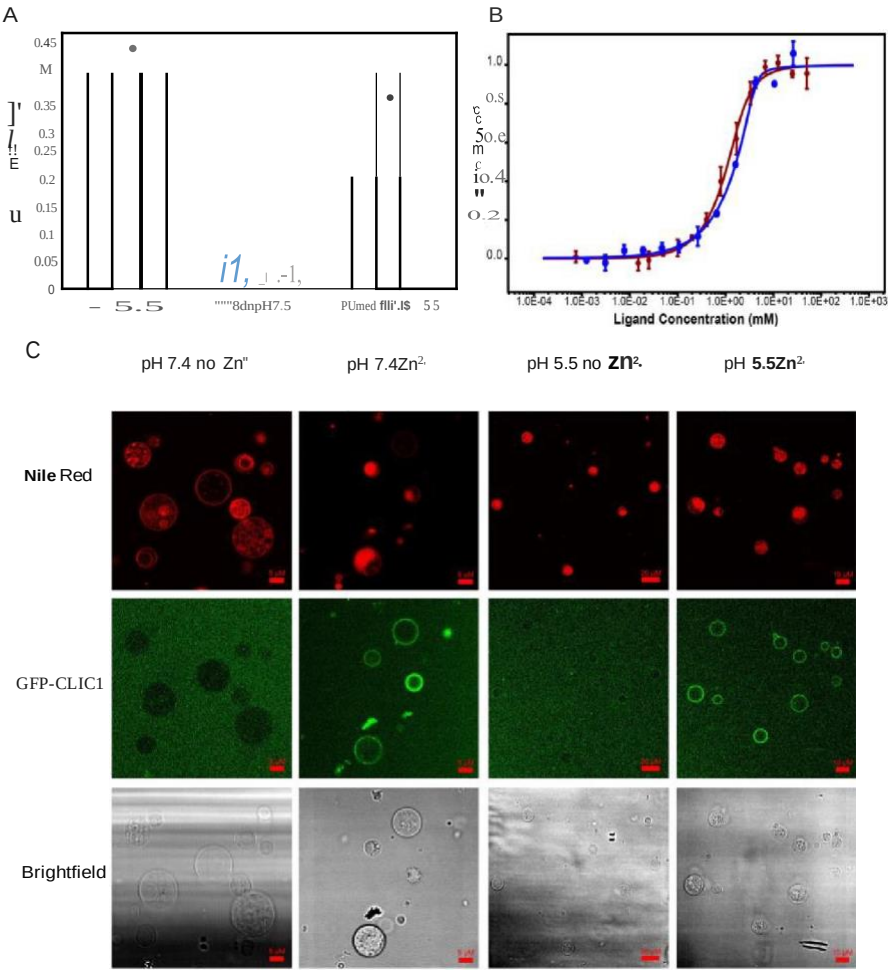


Fig. 3. CLIC1 binds to zn2+, triggering membrane insertion and pH-dependent cl- conductance. (A) zn2, dependence of the CLIC1 cl- efflux rate. cl- effiux rates of CLIC1 in the absence of divalent cations (blue) or in the presence of stochiometric amounts of Zn2, (orange) or Ca2, (grey). Results are mean±s.d. (n=4). Zn2, treatment resulted in statistically significant differences (*P<0.05, two-tailed !-test) compared to the control samples in asolectin vesicles and using purified lipids at pH 5.5. (B) MST binding curves for CLIC1 titrations with Ca2, (red) or Zn2, (blue), displaying a Kd of 0.3±0.1 mM for Ca2, and 0.7±0.2 mM for Zn2,. Results are mean±s.d. (n;3). {C) Fluorescence microscopy images of asolectin. Asolectin GUVs labelled with Nile Red dye incubated with GFP•labelled CLIC1 at pH 7.4 {columns 1 and 2) and pH 5.5 {columns 3 and 4) in the absence {columns 1 and 3) and presence {columns 2 and 4) of Zn2,. Row 1 displays Nile Red fluorescence, row 2 CLIC1-GFP fluorescence and row 3 shows the brightfield images of the GUVs. Images representative of two experiments. Scale bars indicated in all images correspond to 5-20 µm.

binding affinities of Ca^{2+} and Zn^{2+} ions in the presence of asolectin vesicles, as CLICl can aggregate at molar ratios of Ca^{2+} and Zn^{2+} higher than l in theabsenceoflipids. CLICl showed specific binding to both ions, with Zn^{2+} and Ca^{2+} having a similar apparent affinity at 300-700 µM (Fig. 3B).

DISCUSSION

A model for CLIC1 membrane insertion

ln this study, we demonstrate that CUC I binds to Zn^{2+}, promoting membrane insertion in both model membranes and in a cellular environment. Once inserted, c1- effiux is only activated at low pH values. Combining our data, we propose a new two-step activation mechanism ofCLICI whereby CLICI exists in a soluble state, and upon intracellular Zn^{2+} release CUC I binds to it, alters its structure and inserts into the membrane (Fig. 4). The channel is only activated at low pH, suggesting either a pH gating mechanism ora conformational rearrangement within the membrane at low pH values, since pH had no effect on CLICI interaction with the membrane. CLICI has been shown to regulate phagosomal acidification (Salao et al., 2016), supporting the role of pH in the activation of the channel.

Journal of Cell Science

Journal of Cell Science (2022) 135, jcs259704. doi:10.1242/jcs.259704

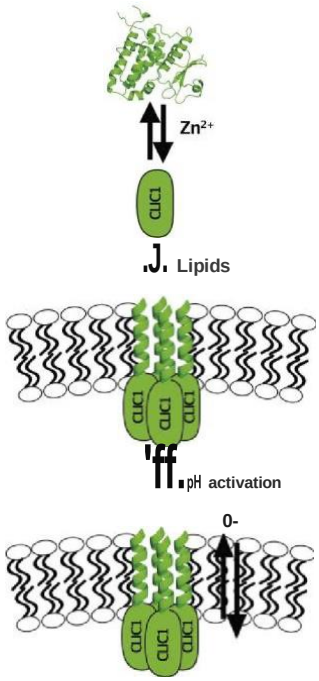


Fig. 4. A two-step model for CLIC1 activation and membrane insertion. CLIC1 binds to Zn^{2+}, inducing a conformational change that triggers membrane insertion. The CLIC1 c1- efflux activity is then activated at low pH.

An increase in the cellular Ca^{2+} and Zn^{2+} concentration has been linked to upstream and downstream changes of the reactive oxygen species (ROS) signalling pathway (Gi:irlach et al., 2015), explaining previous studies on the relationship between CLIC activity and ROS **production and oxidative stress. Ionomyci.n is known to increase** both intracellular levels of Zn^{2+} and Ca^{2+} (Ackland and McArdle, 1996). We show that although ionomycin treatment could result in CLJC I binding to both Zn^{2+} and Ca'+ with similar affinity, only Zn^{2+} is able to induce membrane association (Fig. S2) and c1- efflux (Fig. 3A). This is further supported by treatment with the Zn^{2+} chelator TPEN, which is able to suppress CLIC I membrane relocalisation and its c1- conductance. The higher activation potential of Zn^{2+} over Ca^{2+} must therefore be a result of a higher degree of structural changes resulting from the interaction with Zn^{2+}. The apparent affinity of CLIC I towards Zn^{2+} and Ca^{2+} determined by MST is weak, whereas at molar ratios of I: I Zn^{2+} significantly increases CLIC I c1- conductance. MST relies on the presence of a fluorescent molecule attached to the protein, and in this case, we used a GFP fused to the C-tenninus of CLIC I. We hypothesise that the presence of this C-tenninal GFP might be interfering with the structural changes that need to occur for CUC I to bind to Zn^{2+} and to insert in the membrane, lowering the affinity for this interaction.

Divalent cations have been related to the membrane insertion properties of proteins of the annexin family (Rosengarth and Luecke, 2003), as well as the El membrane protein of rubella virus (Dube et al., 2016) and the amyloidogenic peptide amyl in (Sciacca et al., 2013), promoting the interactions of the soluble forms of these proteins with negatively charged lipids. CLICI has been shown to have maximal c1- effiux activity in the extract of soya bean lipid asolectin, which is rich in the lipid phosphatidylethanolamine (PE), phosphatidylcholine (PC) and the negatively charged phosphatidylinositol (Pl) classes (Tulk et al., 2002), supporting the role of divalent cations in CUCI membrane **insertion. Annexin membrane association is expected to occur due** to the exposure of an otherwise buried amphipathic segment upon binding to Ca^{2+} ions. CUC I contains a region (residues 24-41) with moderate hydrophobicity and a moderate hydrophobic moment that could, in a similar mechanism, detach from the globular structure of the protein upon divalent cation binding, become exposed to the solvent and mediate association with the membranes, likely forming a helix. The hydrophobicity of this segment would also explain the aggregation of the protein at higher concentrations of Ca^{2+} and Zn^{2+} ions in the absence of lipids. Interestingly, the same region in the structurally homologous glutathione S- transferase is not hydrophobic, suggesting that this helix plays a different role in the CLIC family.

Although the structural rearrangements involved in this process are not yet fully understood, the molecular switch between the soluble and membrane-bound forms is now elucidated, complementing the previously known effects of pH and cholesterol. This enables, for the first time, the manipulation of CLICI localisation in cellular systems and the recombinant production of CUC! samples in the chloride channel fonn in membrane mimetic systems (Medina-Carmona et al., 2020), and provides a clear mechanism for the channel formation process of this unusual and clinically important protein.

MATERIALS AND METHODS

Protein expression and purification

The human *CLJCJ* gene (clone HsCD003382 I(*J* from the plasmid service at Harvard Medical School) was cloned into a pASG vector (IBA) containing **an N-ten11inal twin strep tag and a TEV cleavage site, and into a pWaldo** vector (Drew et al., 2001) containing a C-terminal GFP and a TEV cleavage site. **CLICI** was expressed recombinantly in the C43 *E. coli* strain (Lucigen). The cells were lysed by sonication, and the membrane and soluble fractions were separated by ultracentrifugation using a 70Ti or 45Ti rotor (Beckman) at 117,734 *g*. Membrane-bound CUC I can be extracted using a mixture of I% DDM (n-dodecyl- -D-maltopyranoside) (Glycon) and 1% Triton X-100, resulting in solutions with the CLICI soluble fonn. Both fractions were purified separately in the absence of any detergent using affinity chromatography with a Strep-Tactin XT column. The elutions were pooled and cleaved with TEV protease (produced in-house), and subsequently gel filtrated using a Superdex200 Increase column (GE Healthcare) in either 20 mM HEPES buffer with 20 mM NaCl at pH 7.4 or 20 mM potassium phosphate buffer with 20 mM NaCl at pH 7.4.

c1- efflux assays

U87G cells (courtesy of Prof. Martin Michaelis, University of Kent, VK) were maintained in Dulbecco's modified Eagle's medium (DMEM) supplemented with 10% fetal bovine serum (FBS) (both Pan-Biotech) and 1% penicillin/streptomycin (Thenno Fisher Scientific) at 37°C, 95% humidity and 5% CO_2.

For N-(Ethoxycarbonylmethyl)-6-Methoxyquinolinium Bromide (MQAE; Thenno Fisher Scientific) assays U87G cells were seeded into dark 96-well microtiter flat-bottom plates at 4x I 0^4 cells/well in I00 µl volumes DMEM supplemented with I 0% FBS and I% penicillin/ streptomycin and incubated overnight at 37°C, 95% humidity and 5% CO_2. Cells were then stained with 8 mM MQAE for 2 h (Andersson et al.,

2003), and subsequently washed three times with PBS. Non-stained cells were also included. A variety of conditions were evaluated after MQAE loading. In conditions where inhibitors were used, these - 5 µM TPEN or IO µM IAA-94, DIDS or NPPB (Abeam) - were added and incubated for 10 min. Finally, 10 µM ionomycin was added and repetitive fluorescence measurements (every I min for 80 min) were initiated immediately using an Omega fluorescence plate reader (excitation, 355 nm; emission, 460 nm). Six separate wells were used for each biological repeat. The mean±s.d. was calculated for each condition and time.

c1- efflux assays with purified CLIC1

CLJCI chloride channel activity was assessed using the c1--se1ective electrode assay described previously (Tulk et al., 2002). Recombinant CLICI was purified as previously described (Tulk et al., 2002) except EDTA was included at I mM in all steps following the thrombin digestion until the final dialysis change. Unilamellar asolectin or purified lipid (consisting of 80% palmitolyloleolyl phophotidylcholine, I0% palmitoyloleoyl phosphotidylserine and I 0% cholesterol) vesicles (Tulk el al., 2002) were prepared at 20 mg/ml in 200 mM KCI, 5 mM HEPES (pH 7.4). CLICI protein at I µM final concentration was incubated in the presence or absence of divalent cation as indicated in 380 µI volume of200 mM KCI, and 10 mM MES pH 5.5 or HEPES pH 7.5. 20 µI of lipid suspension were added to the protein mixture with vortexing and incubated for 5 min at mom temperature. The lipid mixture was then applied to a 3.5 ml Biogel-P6DG spi.n column previously equilibrated in 330 mM sucrose. The eluate fium the spin column was added to a cup containing 330 mM sucrose, 10 µM KC!, IO mM MES pH 5.5 or HEP.ES pH 7.5 as appropriate, with continuous monitoring of extravesicular c1- concentration with an ion-selective electrode. Valinomycin (Sigma-Aldrich) was added to 1 µM to initiate voltage driven c1- efflux, followed by Triton X-100 to 1% to release remaining intravesicular c1-. The initial rate of fractional c1- efflux after addition of valinomycin is taken as the c1- permeability.

Fluorescence microscopy

GUY fonnation was carried out using a protocol adapted from Manley and Gordon (2008) and Veatch (2007). An asolectin lipid stock was prepared in 50 mM HEPES, 50 mM NaCl pH 7.4 buffer. 2 µl/cm^2 of I mg/ml lipid mixed with 1 mM Nile Red lipophilic stain (ACROS Organic) was applied to two rTO slides and dried under vacuum for 2 h. I00 mM sucrose, 1 mM HEPES pH 7.4 buffer was used to rehydrate the lipids in the described chamber. IO Hz frequency sine waves at 1.5 V were applied to the chamber for 2 h. Liposomes were recovered and diluted into I00 mM glucose, 1 mM HEPES, pH 7.2 buffer. For all four assays, 90 nM CLICI-GFP was incubated with the GUVs with 0.5 mM $ZnCl_2$, 0.5 rnM $CaC1_2$, or without ions, at room temperature for IO min. Microscopy for each assay was perfonned in an 8-well Lab-Tek Borosilicate Coverglass system (Nun) with a Zeiss LSM-880 confocal microscope using 488 nm and 594 nm lasers. All images were processed with Zen Black software.

For immunofluorescence assays, cells were seeded into 24-well plates onto sterile microscopy slides for next day treatment. At 24 h post seeding cells were washed with Tris-buffered saline (TBS), cells were transferred to phosphate-free medium and left untreated or treated with IO µM ionomycin or IO µM *N,N,N′*,N′-Tetrakis(2-pyridylmethyl)ethylenediamine (TPEN) as required. Fixation with 4% formaldehyde for 15 min was carried out m 2 h post treatment. The cells were then washed and penneabilised for I*(J* min with 0.1% Triton X-1*()()* in TBS and washed twice with TBS to remove any detergent. Cells were incubated with CellMASK Deep Red plasma membrane stain (lnvitrogen) for 15 min. Following a TBS wash step, the cells were blocked at room temperature with 2% BSA for 1 h. Primary antibody GFP incubation was carried out overnight at 4°C with a I:50 dilution of monoclonal mouse anti-CUC I antibody (Santa Cruz Biotechnology, clone 356.1). After primary incubation, three wash steps were carried out, prior to a 1 h incubation with secondary antibody at a I: I 000 dilution (Alexa Fluor 488-conjugated donkey anti-mouse-lgG, Life Technologies). A further three washes followed, then nucleus staining with NucBlu Live Cell Stain (lnvitrogen) for 20 min. The slides were washed a final time and mounted with PmLong Gold Antifade (lnvitrogen). All microscopy slides were viewed with a Zeiss LSM-880 confocal microscope using 405 nm, 488 nm and 633 nm lasers. All images were processed with Zen Black and Zen Blue software.

Microscale thermophoresis

A recombinantly expressed C-terminal GFP tag construct of CLJC l was used. Titrations were perfonned at a constant protein concentration of 0.8 µM in HEPES buffer (20 mM HEPES, 20 mM NaCl, pH 7.4) in the presence of 80 µM asolectin vesicles, with increasing concentration of a solution of Zn_2SO_4 in the HEPES buffer and a final volume of 20 µI. Prepared samples were filled into Monolith NT.115 capillaries (NanoTemper). Measurements were recorded on a Monolith NT.115 at 30°C, excited under blue light, medium MST power and 15% excitation power. The data were analysed using MO Affinity Analysis software (NanoTemper) and fitted using the Ku model.

Acknowledgements

We thank Dr N. Fili and Dr J. Rossman for help with confocal imaging, and Dr G. S. Thompson and Dr D. A. I. Mavridou for feedback on the manuscript. Some of the data in this paper formed part of Alexandra Hendry's PhD thesis in the Department of Biosciences at the University of Kent in 2022.

Competing interests

The authors declare no competing or financial interests.

Author contributions

Conceptualization: J.L.0.-R.; Methodology: L.V., D.C.; Validation: J.C.; Formal analysis: L.V., A.C.H.; Investigation: L.V.,A.C.H., J.C., R.M.-E., F.O., J.C.E., V.A.-S.; Writing-original draft: J.L.0.-R.; Visualization: A.C.H., D.C., F.O.; Supervision: L.V., J.L.0.-R.; Project administration: J.L.0.-R.; Funding acquisition: J.L.0.-R.

Funding

We acknowledge support from the Wellcome Trust Seed Award (207743/Z/17/Z). R.M.-E. is supported by a fellowship from the Alfonso Martin Escudero Foundation. V.A.-S. is supported by Barts Charity's Rising Star programme. Open Access funding provided by University of Kent. Deposited in PMC for immediate release.

Peer review history

The peer review history is available online at https://journals.biologists.com/jcs/article-lookup/doi/10.1242/jcs.259704.

References

Abdul-Salam, V. B., Wharton, J., Cupitt, J., Berryman, M., Edwards, R. J. and Wilkins, M. R. (2010). Proteomic analysis of lung tissues from patients with pulmonary arterial hypertension. *Circulation* 122, 2058-2067. doi:10.1161/CIRCULATIONAHA.110.972745

Ackland, M. L. and McArdle, H. J. (1996). Cation-dependent uptake of zinc in human fibroblasts. *Biometals* 9, 29-37. doi:10.1007/bf00188087

Andersson, C., Servetnyk, Z. and Roomans, G. M. (2003). Activation of CFTR by genistein in human airway epithelial cell lines. *Biochem. Biophys. Res. Commun.* **308**, 518-522. doi:10.1016/S0006-291X(03)01436-0

Averaimo, 5., Gritti, M., Barini, E., Gasparini, L. and Mazzanti, M. (2014). CLIC1 functional expression is required for cAMP-induced neurite elongation in post-natal mouse retinal ganglion cells. *J. Neurochem.* 131, 444-456. doi:10.1111/jnc.12832

Drew, 0. E., von Heijne, G., Nordlund, P. and de Gier, J. W. (2001). Green fluorescent protein as an indicator to monitor membrane protein overexpression in Escherichia coli. *FEBS Lett.* **507**, 220-224. doi:10.1016/S0014-5793(01)02980-5

Dube, M., Etienne, L., Fels, M. and Kielian, M. (2016). Calcium-dependent rubella virus fusion occurs in early endosomes. *J. Virol.* 90, 6303-6313. doi:10.1128/JVI.00634-16

Fanucchi, S., Adamson, R. J. and Dirr, H. (2008). Formation of an unfolding intermediate state of soluble chloride intracellular channel protein CLIC1 at acidic pHt. *Biochemistry 41*, 11674-11681. doi:10.1021/bi801147r

Goodchild, S. C., Howell, M. W., Cordina, N. M., Littler, D. R., Breit, S. N., Curmi, P. M. G. and Brown, L. J. (2009). Oxidation promotes insertion of the CLIC1 chloride intracellular channel into the membrane. *Eur. Biophys. J.* 39, 129-138. doi:10.1007/s00249-009-0450-0

GOrlach, A., Bertram, K., Hudecova, 5. and Krizanova, 0. (2015). Calcium and ROS: a mutual interplay. *Redox Biol.* 6, 260-271. doi:10.1016/j.redox.2015.08.010

Gritti, M., WUrth, R., Angelini, M., Barbieri, F., Peretti, M., Pizzi, E., Pattarozzi, A., Carra, E., Sirito, R., Oaga, A. et al. (2014). Metformin repositioning as antitumoral agent: selective antiproliferative effects in human glioblastoma stem cells, via

inhibition of CLIC1-mediated ion current. *Oncotarget* 5, 11252-11268. doi:10.18632/oncotarget.2617
Gronich, N., Kumar, A., Zhang, Y., Efimov, I. R. and Soldatov, N. M. (2010). Molecular remodeling of ion channels, exchangers and pumps in atrial and ventricular myocytes in ischemic cardiomyopathy. *Channels* 4, 101-107. doi:10.4161/chan.4.2.10975
Gurski, L.A., Knowles, L. M., Basse, P.H., Maranchie, J. K., Watkins, S. C. and Pilch, J. (2015). Relocation of CLIC1 promotes tumor cell invasion and colonization of fibrin. *Mo/. Cancer* Res. 13, 273-280. doi:10.1158/1541-7786.MCR-14-0249
Hossain, K. R., Al Khamici, H., Holt, S. A. and Valenzuela, S. M. (2016). Cholesterol promotes interaction of the protein CLIC1 with phospholipid monolayers at the air-water interface. *Membranes* 6, 15. doi:10.3390/membranes6010015
Hossain, K. R., Holt, 5. A., Le Brun, A. P., Al Khamici, H. and Valenzuela, 5. M. (2017). X-ray and neutron reflectivity study shows that CLIC1 undergoes cholesterol-dependent structural reorganization in lipid monolayers. *Langmuir* 33, 12497-12509. doi:10.1021/acs.langmuir.7b02872
Knowles, L. M., Malik, G., Hood, B. L., Conrads, T. P. and Pilch, J. (2012). CLT1 targets angiogenic endothelium through CLIC1 and fibronectin. *Angiogenesis* 15, 115-129. doi:10.10071s10456-011-9247-8
Littler, D. R., Harrop, S. J., Fairlie, W. D., Brown, L. J., Pankhurst, G. J., Pankhurst, S., DeMaere, M. Z., Campbell, T. J., Bauskin, A. R., Tonini, R. et al. (2004). The intracellular chloride ion channel protein CLIC1 undergoes a redox-controlled structural transition. *J. Biol. Chem.* 279, 9298-9305. doi:10.1074/jbc.M308444200
Manley, S. and Gordon, V. D. (2008). Making giant unilamellar vesicles via hydration of a lipid film. *Cull. Protoc. Cell Biol.* 24, Unit 24.3. doi:10.1002/0471143030.cb2403s40
Medina-Carmona, E., Varela, L., Hendry, A. C., Thompson, G. S., White, L. J., Boles, J. E., Hiscock, J. R. and Ortega-Roldan, J. L. (2020). A quantitative assay to study the lipid selectivity of membrane-associated systems using solution **NMR** *Chem. Commun.* **56,** 11665-11668. doi:10.1039/D0CC03612A
Rosengarth, A. and Luecke, H. (2003). A calcium-driven conformational switch of the N-terminal and core domains of annexin A1. *J. Mo/. Biol.* 326, 1317-1325. doi:10.1016/S0022-2836(03)00027-5
Sala□, K., Jiang, L., Li, H., Tsai, V. W.-W., Husaini, Y., Curmi, P. M. G., Brown, L. J., Brown, D. A. and Breit, S. N. (2016). CLIC1 regulates dendritic cell antigen processing and presentation by modulating phagosome acidification and proteolysis. *Biol. Open* 5, 620-630. doi:10.1242/bio.018119
Sciacca, M. F. M., Milardi, D., Messina, G. M. L., Marietta, G., Brender, J. R., Ramamoorthy, A. and La Rosa, C. (2013). Cations as switches of amyloid-mediated membrane disruption mechanisms: calcium and IAPP. *Biophys. J.* 104, 173-184. doi:10.1016/j.bpj.2012.11.3811
Setti, M., Osti, D., Richichi, C., Ortensi, B., Del Bene, M., Fornasari, L., Beznoussenko, G., Mironov, A., Rappa, G., Cuomo, A. et al. (2015). Extracellular vesicle-mediated transfer of CLIC1 protein is a novel mechanism for the regulation of glioblastoma growth. *Oncotarget* 6, 31413-31427. doi:10.18632/oncotarget.5105
Singh, H. and Ashley, R.H. (2006). Redox regulation ofCLIC1 bycysteine residues associated with the putative channel pore. *Biophys. J.* 90, 1628-1638. doi:10.1529/biophysj.105.072678
Stoychev, S. H., Nathaniel, C., Fanucchi, S., Brock, M., Li, S., Asmus, K., Virgil, L., Woods, J. and Dirr, H. (2009). Structural dynamics of soluble chloride intracellular channel protein CLIC1 examined by amide hydrogen-deuterium exchange mass spectrometry. *Biochemistry* 48, 8413-8421. doi:10.1021/bi9010607
Tian, Y., Guan, Y., Jia, Y., Meng, Q. and Yang, J. (2014). Chloride intracellular channel 1 regulates prostate cancer cell proliferation and migration through the MAPK/ERK pathway. *CancerBiother. Radiopharm.* 29, 339-344. doi:10.1089/cbr.2014.1666
Tulk, B. M., Schlesinger, P.H., Kapadia, S. A. and Edwards, J.C. (2000). CLIC-1 functions as a chloride channel when expressed and purified from bacteria. *J. Biol. Chem.* **275,** 26986-26993. doi:10.1016/S0021-9258(19)61469-9
Tulk, B. M., Kapadia, 5. and Edwards, J. C. (2002). CLIC1 inserts from the aqueous phase into phospholipid membranes, where it functions as an anion channel. *Am. J. Physiol. Cell Physiol.* 282, C1103-C1112. doi:10.1152/ajpcell.00402.2001
Tung, J. J. and Kitajewski, J. (2010). Chloride intracellular channel 1 functions in endothelial cell growth and migration. *J. Angiogenes. Res.* 2, 23. doi:10.1186/2040-2384-2-23
Valenzuela, S. M., Martin, D. K., Per, S. B., Robbins, J.M., Warton, K., Bootcov, M. R., Schofield,P.R., Campbell, T.J. and Breit, S. N. (1997). Molecular cloning and expression of a chloride ion channel of cell nuclei. *J. Biol. Chem.* 272, 12575-12582. doi:10.1074/jbc.272.19.12575
Valenzuela, 5. M., Mazzanti, M., Tonini, R., Qiu, M. R., Warton, K., Musgrove, E. A., Campbell, T. J. and Breit, S. N. (2000). The nuclear chloride ion channel NCC27 is involved in regulation of the cell cycle. *J. Physiol.* 529, 541-552. doi:10.1111/j.1469-7793.2000.00541.x
Veatch, S. L. (2007). Electro-formation and fluorescence microscopy of giant vesicles with coexisting liquid phases. *Methods Mal. Biol.* 398, 59-72. doi:10.1007l978-1-59745-513-8_6
Wang, W., Xu, X., Wang, W., Shao, W., Li, L., Yin, W., Xiu, L., Mo, M., Zhao, J., He, Q, et al. (2011). The expression and clinical significance of CLIC1 and HSP27 in lung adenocarcinoma. *Tumour Biol.* 32, 1199-1208. doi:10.1007/s13277-011-0223-0
Warton, K., Tonini, R., Douglas Fairlie, W., Matthews, J. M., Valenzuela, 5. M., Qiu, M. R., Wu, W. M., Pankhurst, S., Bauskin, A. R., Harrop, S. J. et al. (2002). Recombinant CLIC1 (NCC27) assembles in lipid bilayers via a pH-dependent two-state process to form chloride ion channels with identical characteristics to those observed in Chinese hamster ovary cells expressing CLIC1. *J. Biol. Chem.* **277,** 26003-26011. doi:10.1074/jbc.M203666200
Xu, Y., Zhu, J., Hu, X., Wang, C., Lu, D., Gong, C., Yang, J. and Zang, L. (2016). CLIC1 inhibition attenuates vascular inflammation, oxidative stress, and endothelial injury. *PLoS One* 11, e0166790. doi:10.1371/journal.pone.0166790
Zhang, J., Li, M., Song, M., Chen, W., Mao, J., Song, L., Wei, Y., Huang, Y. and Tang, J. (2015). Clic1 plays a role in mouse hepatocarcinoma via modulating Annexin A7 and Gelsolin in vitro and in vivo. *Biomed. Pharmacother.* 69, 416-419. doi:10.1016/j.biopha.2014.11.019
Zhao, W., Lu, M. and Zhang, Q. (2015). Chloride intracellular channel 1 regulates migration and invasion in gastric cancer by triggering the ROS-mediated p38 MAPK signaling pathway. *Mo!. Med. Rep.* 12, 8041-8047. doi:10.3892/mmr.2015.4459

bioRxiv preprint doi: https://doi.org/10.1101/2022.10.01.510446; this version posted October 3, 2022. The copyright holder for this preprint (which was not certified by peer review) is the author/funder, who has granted bioRxiv a license to display the preprint in perpetuity. It is made available under aCC-BY-NC-ND 4.0 International license.

Elucidation of small molecule passive permeation across lipid membranes using conventional solution state NMR methods

Angela Serrano-Sanchez[1,1], Joseph Cassar[1,1], Lisa J. White,lbJ Precious I. A. Popoola,lbJ Jennifer R. HiscocklbJ and Jose L. Ortega-Roldan*[1,1]

Author information:

[a] School of Biosciences. University of Kent, Canterbury, UK. CT2 ?NJ
[b] School of Chemistry and Forensic Science. University of Kent, Canterbury, UK. CT2 ?NH

Corresponding author/Lead contact: j.l.ortega-roldan@kent.ac.uk

Keywords: membrane permeability• antimicrobials• Solution NMR • membrane interaction

Abstract: Quantifying small molecule uptake across a biological membrane in any cell system is crucial for the development of efficacious and selective drugs. However, obtaining such data is not trivial, especially in bacterial systems. Herein, we present an assay which enables the determination of the degree of passive permeation and membrane interaction of mixtures of small molecules in vesicles of a desired lipid composition, including that of bacterial membranes. The assay employs highly accessible conventional solution NMR experiments, exploiting the paramagnetic relaxation enhancement effect, and allows the measurement of membrane permeation on mixtures of any number of small molecules which do not exhibit heterogeneous molecular signal overlap in under 20 minutes. As a proof-of -principle we apply this methodology to candidates from a class of supramolecular self-associating amphiphiles, members from which have been shown to interact with biological phospholipid membranes and elicit an antimicrobial effect, allowing the determination and comparison of their membrane permeability and membrane interaction properties.

Introduction

Antimicrobial resistance (AMR) is one of the greatest global health threats, with a recent study reporting that in 2019 a greater number of people died from the primary effects of AMR than malaria or HIV/AIDS[111]. Therefore, novel therapeutic agents with innovative modes of action are required to address this major health threat. We believe that a significant limitation for novel antimicrobial agents translating into the clinic maybe related to the inability of these compounds to reach a site of action within the organism itself due to penetrate to the organism and achieve their site of action[121]. One of the biggest challenges in developing antibiotics against multi-drug resistant bacterial pathogens is their small-molecule uptake as their membrane composition differ substantially from mammalian cells membranes[13,41], and therefore, assays able to monitor small molecule uptake in any lipid composition are required.

Currently, several in vitro experimental models provide a permeability evaluation and transport of pharmaceutical molecules across at least one cellular membrane to reach their target[151]. Among the high throughputs in vitro techniques, those based in artificial membranes such as parallel artificial membrane permeability assay (PAMPA)[16], and the cell based Caco-2 assay[171]

bioRxiv preprint doi: https://doi.org/10.1101/2022.10.01.510446; this version posted October 3, 2022. The copyright holder for this preprint (which was not certified by peer review) is the author/funder, who has granted bioRxiv a license to display the preprint in perpetuity. It is made available under aCC-BY-NC-ND 4.0 International license.

are the most widely used. These models are important in the initial stages of drug discovery in mammalian cells, but are not available for bacterial systems, do not allow therapeutic mode of action or selectivity analysis, and typically involve long assay times, cell culturing and specialised equipment, hence resulting in an elevated cost.

Herein, we present an accessible, novel approach able to assess small molecule passive permeability through vesicles composed of any type of lipid composition using solution NMR spectroscopy, widely accessible in chemistry and biological laboratories. This methodology is considerably quicker (1 mixture of small molecules/20 minute) and allows the study of any membrane composition in an affordable way.

We have used this methodology to compare the permeabilities and degree of membrane interaction of a set of reference compounds, glucose, which cannot permeate through the membrane, and the membrane permeable indole, and a set of test compounds from the Supramolecular Self-associating Amphiphile (SSA) family 1a-10l(Figure 1). This technology has already shown antimicrobial efficacy against clinically relevant Gram-positive methicillin resistant *Staphylococcus aureus* (MRSA) and Gram-negative *Escherichia Coli (E. coli),* it exhibits a druggable profile in vivo, and enhances antimicrobial and anticancer activities of different commercial drugs11[1-12]i_

Proton NMR T1 and T2 relaxation rates depend, amongst other parameters, on the rotational correlation time of the molecule. For larger molecules which are characterized by longer T1 values this that can modulate the intensity of ^{1}H NMR signals if the sum of the acquisition time and the relaxation delay is not long enough to return to equilibrium during the relaxation delay in a multi transient experiment. The addition of solvent PRE reagents has been shown to induce a much larger reduction of T1 than T2 values for small molecules[113]_ However, the measured effect of the PRE on T2, which lead to a decrease in the ^{1}H intensities, can be maximized employing CPMG pulse sequences[114]l_

We sought to test if the addition of a solvent PRE reagent only in the outside compartment of a vesicle will exert a different effect in the ^{1}H NMR peak intensities of molecules with different permeation rates due to the different modulation of T1 and T2 values. We measured ^{1}H 1D CPMG spectra for the non membrane-permeable glucose and the highly membrane-permeable indole in the absence and presence of vesicles prepared with the gram negative model bacteria *E. coli* lipids with and without the PRE reagent Mn^{2+}. Three different CPMG spin-lock times, 20, 50 and 150 mS, were used to maximise the PRE effect on T2, and hence improve differentiation between molecules with different permeation rates.
Glucose, which cannot permeate through the membrane unaided, shows a significant drop of intensity of its ^{1}H resonances in the presence of Mn^{2+} both in the presence and absence of lipid vesicles, consistent with PRE-induced broadening of the signals. Indole, on the other hand, showed an opposite effect. While in the absence of vesicles Mn^{2+} induced line broadening, in the presence of vesicles we saw the opposite effect, with an increase in the signal intensities upon addition of Mn^{2+}. As previously discussed, this effect can be attributed to the reduction of T1 values of soluble indole molecules which have spent some time associated with the lipid vesicle (Figure 2) counteracting the effects of the increase in T1 due to the molecular mass of the vesicle-indole complex during the CPMG period.
The effect of permeation rates on the PRE modulation of 1H intensities can be parametrised by comparing the intensity ratios of ^{1}H resonances in ^{1}H 1D NMR CPMG experiments with the same spin lock times with and without Mn^{2+} in the presence and absence of lipid vesicles. A value of 1 implies no detectable permeation through the vesicles and values higher than one imply detectable permeation through the vesicles (Equation 1).

$$PF = \frac{(IPRE/\ InoPRE)vesicles}{(IPRE/\ InoPRE)no\ Vesicles}$$

bioRxiv preprint doi: https://doi.org/10.1101/2022.10.01.510446; this version posted October 3, 2022. The copyright holder for this preprint (which was not certified by peer review) is the author/funder, who has granted bioRxiv a license to display the preprint in perpetuity. It is made available under aCC-BY-NC-ND 4.0 International license.

Equation 1. The Permeability Factor (PF) depends on the intensity ratio of ^{1}H 1D CPMG NMR signals of small molecules in the presence and absence of vesicles and a solvent PRE reagent.

This permeability factor, and its change with different CPMG times, can be used to compare the permeability of different compounds in vesicles of the same composition or to assess the permeability of a single compound in vesicles with different lipid compositions (i.e. extracted from different cell strains) (Table 1).

Similarly, the intensity ratio between ^{1}H resonances in ^{1}H 1D NMR CPMG experiments with the same spin lock times in the presence and absence of lipid vesicles reports on the degree of interaction between small molecules and the membrane. A value of 1 signifies no detectable membrane interaction and a value below 1 indicates detectable membrane interaction (Equation 2), with the affinity being related to the CPMG spin-lock time at which the deviation from 1 is observed (Table **1**).

$$M/F = \frac{I_{vesicles}}{I_{no\ Vesicles}}$$

Equation 2. The Membrane Interaction Factor (MIF) depends on the intensity ratio of ^{1}H 1D CPMG NMR signals of small molecules in the presence and absence of vesicles.

It is important to note that PF and MIF values rely on intensities extracted from unbound ligand in the ^{1}H 1D NMR CPMG spectra, and therefore the molecules studied must not fully self-associate in solution at the concentrations used for the assay. The degree of molecular self-association can be obtained easily through comparing the intensity ratio between ^{1}H 1D NMR CPMG spectra collected at 150mS and 20mS spin-lock times, with a value of 1 indicating no self-association and a value below **1** indicating the presence of self-association.

We subsequently used this methodology to assess and classify the permeation rates and membrane-interaction affinities of the control substances indole and glucose and a set of 5 representative compounds from a novel class of supramolecular self-associating amphiphile (SSAs), using vesicles prepared with the same *E. coli* lipids as those prepared previously for the control experiments (Figure 3). The hypothesised basis for the therapeutic activity of this class of related compounds includes their ability to selectively coordinate with phospholipids of different head group composition and permeate into the cell[115,161].

Table 1. Permeability and membrane interaction factors of Glucose, Indole and a subset of compounds from the SSA family. **PF and MIF values were calculates using Equations 1 and 2, respectively. All values given with a** ±0.1 **uncertainty unless** specified in the table.

Compound	PF (20ms)	PF (50ms)	PF (150ms)	MIF (20mS)	MIF (50mS)	MIF (150mS)
Glucose	0.8	0.5	0.4	0.8	0.8	0.8
Indole	2.3	4.5	8.6	0.3	0.1	0.0
C29	0.8	0.7	0.5	1.0	1.0	0.9
C30	1.1	1.2	1.1	1.1	1.1	1.0
C32	1.4	1.2	0.9	1.0	1.0	0.9
C57	0.9	1.0	1.0	0.9	0.9	0.9
C60	5.3±0.2	5.5±0.3	6.6±1.2	0.6	0.4	0.2

The intensity ratios of all aromatic peaks of indole and SSA compounds and the aliphatic peaks of glucose, collected in the absence or presence of lipid vesicles and Mn^{2+}, were used for the permeability analysis. The permeability and membrane interaction factors for these molecules were calculated using Equations 1 and 2 (Table 1). As expected, indole showed high permeability factors (PF) and low membrane interaction factors (MIF), indicative of high

bioRxiv preprint doi: https://doi.org/10.1101/2022.10.01.510446; this version posted October 3, 2022. The copyright holder for this preprint (which was not certified by peer review) is the author/funder, who has granted bioRxiv a license to display the preprint in perpetuity. It is made available under aCC-BY-NC-ND 4.0 International license.

permeability and high membrane interaction affinity. Glucose, on the other hand, showed permeability factors below 1, consistent with its lack of membrane permeability, and MIF of 0.8, indicating a weak membrane interaction affinity consistent with previous findings[1171]. Significant differences can be observed in the permeability of SSA compounds. C60 showes the highest PF and MIF, resembling the properties of indole. C32 shows some slight permeability, although no detectable membrane interaction, an indication of its low affinity for *E. coli* lipid vesicles. C57 shows no detectable permeation, but noticeable membrane interaction. C29 and C30 show no detectable membrane permeation or interaction.

Discussion

Herein, we present a new assay using solution NMR, a methodology accessible to most chemistry and biological laboratories, able to determine the membrane permeability and degree of membrane interaction of small molecules. The method exploits the **NMR** solvent PRE effect using CPMG experiments, and the ability of membrane permeable molecules to travel to the interior of lipid vesicles, shielding themselves from the solvent PRE reagent. The assay consists in the measurement of ^{1}H 1D CPMG NMR spectra in four different samples all containing the mix of drugs: 1 - without vesicles, 2 - without vesicles with 0.5mM Mn2+ added to the buffer, 3 - with vesicles, and 4 - with vesicles with 0.5mM Mn2+ added to the buffer.

This method relies on the elevation of ^{1}H 1D CPMG intensities for molecules permeating through the membrane, which is caused by the bidirectional equilibrium into and out of the vesicles due to the lack of asymmetry in the lipid composition of the vesicles used. As a result, these molecules spend a large time bound to the vesicle, hence the increase in intensity due to PRE effects on T1, and they are partially protected from the PRE effect on T2 in the extravesicular space. A similar effect would result if a molecule was only able to interact with the membrane but could not permeate, likely due to interactions with the headgroup region of the lipids. This region is in close contact with the solvent, and therefore is more exposed to the solvent PRE. To assess if the molecules under study are permeating or only interacting with the membrane, a comparison between the MIF, which is obtained in the absence of PRE, and the PF is needed. C60 shows a high PF and MIF values in the range of 0.6-0.2, while indole shows equally high PF and MIF values of 0.3 - 0. The higher MIF values of C60 suggest that these compounds are able to permeate more that indole, and that indole has a higher affinity to the lipid membrane and stays closely associated to it.

Glucose, a membrane-impermeable molecule was also used as a control. While indole showed high PF and low MIF values, glucose showed low PF and values of MIF close to 1. The deviations found for glucose from the ideal values for a non-permeable molecule (PF and MIF =1) arise from a degree of self-association, as indicated by the intensity ratio between glucose peaks in CPMG experiments collected with low (20mS) and high (150mS) spinlock times in the absence of vesicles and solvent PRE. Self-association needs to be measured and considered for accurate PF measurements, as high degrees of self-association would lower PFs and hinder the detection of permeation.

SSAs are amphiphilic compounds and thus could present surfactant properties. To explore the interaction of SSAs with all types of lipid membranes, Boles and co-workers explored the relation between membrane lysis/permeation and interaction values to support the hypothesis that the increase in antimicrobial efficacy depends on the general surfactant properties of the SSA compound[1151]. Herein, we can also analyse the relation between permeation and membrane interaction with the lysis of lipid vesicles obtained by the previous study. Their results revealed that C48 could not disrupt the lipid membrane from *E. coli* which supports our finding that this compound did not permeate the lipid vesicles in our assay. C30 presented

bioRxiv preprint doi: https://doi.org/10.1101/2022.10.01.510446; this version posted October 3, 2022. The copyright holder for this preprint (which was not certified by peer review) is the author/funder, who has granted bioRxiv a license to display the preprint in perpetuity. It is made available under aCC-BY-NC-ND 4.0 International license.

slight permeability while C60 presented very high lipid permeability in *E. coli* lipid vesicles. Both C30 and C60 presented lysis properties against all the phospholipid membranes, markedly higher in C60, showing a good correlation between the permeability values obtained in our NMR-based assay and the efficacy of these antimicrobials due to their ability to disrupt cell membranes.

In conclusion, we present a high throughput, accessible and low-cost assay to assess the permeation and degree of membrane interaction of small molecules. The assay can be used with any lipid composition, including lipids extracted from natural sources, allowing permeation studies of antimicrobials, and can assess the permeability of any mixture of small molecules with non-overlapping ^{1}H NMR peaks in as little as 20 minutes.

Acknowledgements

J. Hiscock would also like to thank UKRI for the funding of her Future Leaders Fellowship (MR/T020415/1). J. Ortega-Roldan would like to thank Dr Gary Thompson (University of Kent) and Dr Lorena Varela for NMR training, useful discussion, and/or manuscript revision.

References

(1) Velaphi, A. Vongpradith, H. Vu, T. Walsh, S. Waner, T. Wangrangsimakul, T. Wozniak, P. Zheng, B. Sartorius, A. D. Lopez, A. Stergachis, C. Moore, C. Dolecek, M. Naghavi, *The Lancet* 2022, 399, 629--655.
(2) K. L. F. Hilton, C. Manwani, J.E. Boles, L. J. White, S. Ozturk, M. D. Garrett, J. R. Hiscock, *Chem Sci* 2021, *12,* 13273-13282.
(3) D. Benedetto Tiz, D. Kikelj, N. Zidar, *Expert Opin Drug Discov* 2018, *13,* 497-507.
(4) R. J. Ferreira, P. M. Kasson, ACS *Infect Dis* 2019, 5, 2096-2104.
(5) M.A. Cabrera-Perez, M. B. Sanz, V. M. Sanjuan, M. Gonzalez-Alvarez, I. G. Alvarez, in *Concepts and Models for Drug Permeability Studies: Cell and Tissue Based In Vitro Culture Models,* Elsevier Inc., 2016, pp. 3-29.
(6) M. Kansy, F. Senner, K. Gubernator, 1998, *41,* 0-3.
(7) R. B. van Breemen, Y. Li, *Expert Opin Drug Metab Toxicol* 2005, *1,* 175-185.
(8) S. N. Tyuleva, N. Allen, L. J. White, A. Pepes, H.J. Shepherd, P. J. Saines, R. J. Ellaby, D. P. Mulvihill, J. R. Hiscock, *Chemical Communications* 2018, 55, 95-98.
(9) L. J. White, J.E. Boles, N. Allen, L. S. Alesbrook, J.M. Sutton, C. K. Hind, K. L. F. Hilton, L. R. B1ackholly, R. J. Ellaby, G. T. Williams, D. P. Mulvihill, J. R. Hiscock, *J Mater Chem B* 2020, 8, 4694-4700.
(10) N. Allen, L. J. White, J.E. Boles, G. T. Williams, D. F. Chu, R. J. Ellaby, H.J. Shepherd, K. K. L. Ng, L. R. Blackholly, B. Wilson, D. P. Mulvihill, J. R. Hiscock, *ChemMedChem* 2020, *15,* 2193-2205.
(11) N. 0. Dora, E. Blackburn, J.E. Boles, G. T. Williams, L. J. White, S. E.G. Turner, J. D. Hothersall, T. Askwith, J. A. Doolan, D. P. Mulvihill, M. D. Garrett, J. R. Hiscock, RSC *Adv* 2021, *11,* 14213-14217.
(12) J.E. Boles, G. T. Williams, N. Allen, L. J. White, K. L. F Hilton, P. I. A Popoola, D. P. Mulvihill, J. R. Hiscock, J.E. Boles, L. J. White, K. L. F Hilton, P. I. A Popoola, J. R. Hiscock, N. Allen, D. P. Mulvihill, G. T. Williams, *Adv Ther (Weinh)* 2022, *5,* 2200024.
(13) F. A. A. Mulder, L. Tenori, C. Luchinat, *Angewandte Chemie - International Edition* 2019, *58,* 15283-15286.
(14) H. Y. Carr. E. M. Purcell, *Effects of Diffusion on Free Precession in Nuclear Magnetic Resonance Experiments**I,* 1954.
(15) J.E. Boles, C. Bennett, J. Baker, K. L. F. Hilton, H. A. Kotak, E. R. Clark, Y. Long, L. J. White, H. Y. Lai, C. K. Hind, J.M. Sutton, M. D. Garrett, A. Cheasty, J. L. Ortega-Roldan, M. Charles, C. J. E. Haynes, J. R. Hiscock, *Chem Sci* 2022, *13,* 9761-9773.
(16) G. Townshend, G. S. Thompson, L. J. White, J. R. Hiscock, J.-L. J. L. 0. Roldan, *Chem Commun (Camb)* 2020.
(17) H. D. Andersen, C. Wang, L. Arleth, G. H. Peters, P. Westh, *Proc Natl Acad* Sci US *A* 2011, *108,* 1874-1878.

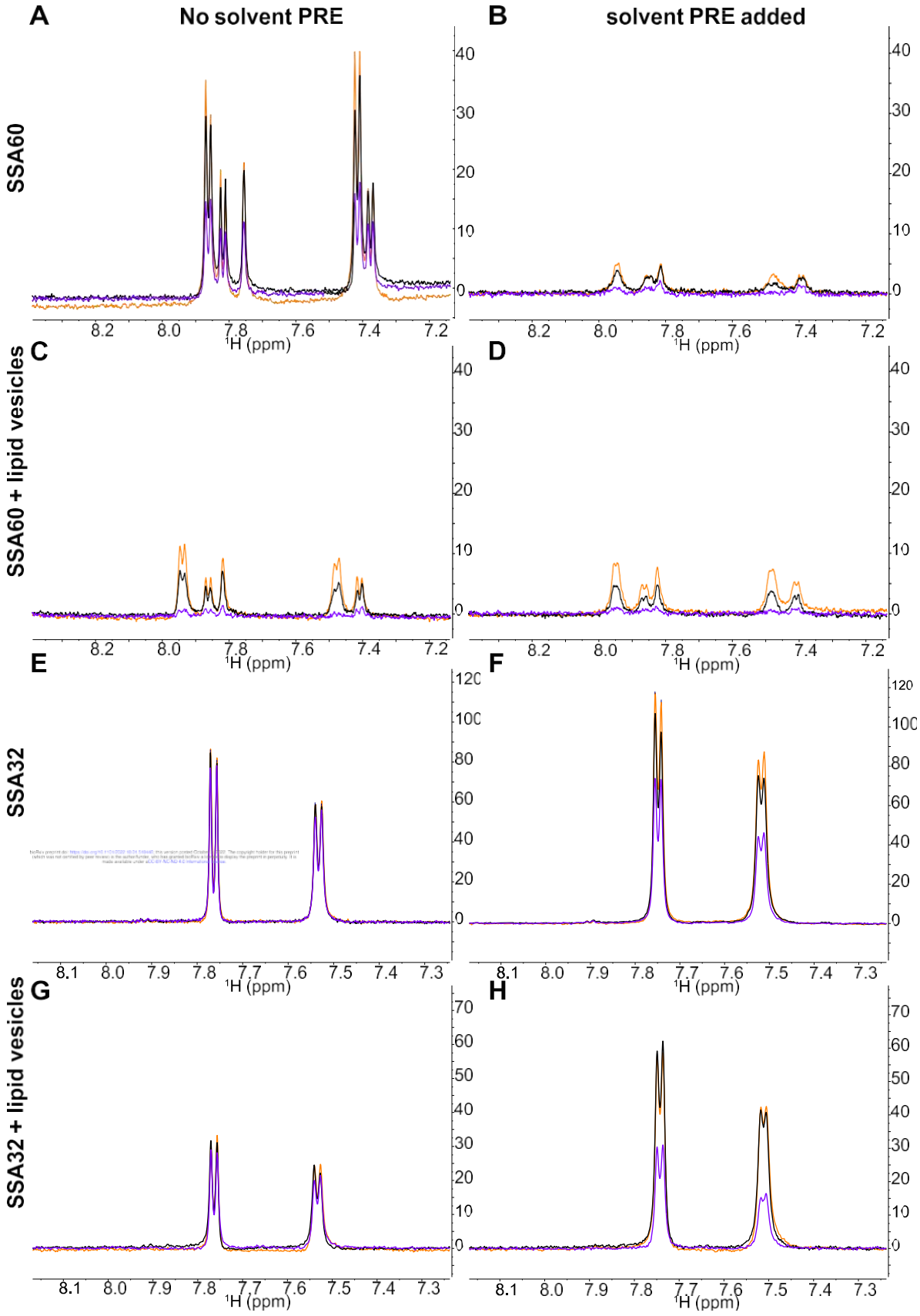
bioRxiv preprint doi: https://doi.org/10.1101/2022.10.01.510446; this version posted October 3, 2022. The copyright holder for this preprint (which was not certified by peer review) is the author/funder, who has granted bioRxiv a license to display the preprint in perpetuity. It is made available under aCC-BY-NC-ND 4.0 International license.

FIGURES

Figure 1: Chemical structures of SSAs C29, C30, C32, C57 and C60. TBA = Tetrabutylammonium.

Figure 2: Proton 1D CPMG NMR spectra collected with a spin-lock time of 20 mS (left column (A, C, E and G) and 150 mS (right column (B, D, F and H) of the reference compounds indole and glucose in the absence and presence of *E. coli* lipid vesicles at increasing concentrtations of Mn^{2}• (0 mM (orange); 0.5 mM (black); 2 mM (blue); 4 mM (magenta)). Samples contained 4mM glucose and 2mM indole ± 1.1 mg/ml vesicles± increasing concentrations of MnCb.

Figure 3: Proton 1D CPMG NMR spectra collected with a spin-lock time of 20, 50 and 150 mS (orange, black and purple, respectively) of SSA60 (A-D) and SSA32 (E-H) in the absence (A-B, E-F) and presence (C-D, G-H) of *E. coli* lipid vesicles without (A, C, E, G) and with (B, D, F, H) the addition of 0.5M Mn^{2}• (left and right column, respectively).Samples contained 200uM of the SSA compounds ± 1.1 mg/ml vesicles± 0.5 mM MnCl2


A
No solvent PRE
B
solvent PRE added
SSA60
C
D
SSA60 + lipid vesicles
E
F
SSA32
G
H
SSA32 + lipid vesicles
¹H (ppm)

Residue	ResidueName	AtomName	Shift(ppm)
1	M	C	173.208
2	A	N	125.424
2	A	H	8.184
2	A	CA	53.702
2	A	CB	20.167
2	A	C	174.876
3	E	N	120.14
3	E	H	8.251
3	E	CA	57.475
3	E	CB	31.296
3	E	C	173.776
4	E	N	122.056
4	E	H	8.343
4	E	CA	57.417
4	E	CB	31.177
4	E	C	173.385
5	Q	N	123.112
5	Q	H	8.272
5	Q	CA	54.334
5	Q	CB	30.797
6	P	CA	63.39
6	P	CB	32.595
6	P	C	172.635
7	Q	N	121.077
7	Q	H	8.286
7	Q	CA	57.121
7	Q	CB	29.664
7	Q	C	172.221
8	V	N	124.409
8	V	H	8.324
8	V	CA	62.544
8	V	CB	34.52
8	V	C	172.343
9	E	N	129.965
9	E	H	9.109
9	E	CA	62.71
9	E	CB	34.151
9	E	C	170.161
10	L	N	128.508
10	L	H	8.711
10	L	CA	54.386
10	L	CB	44.883

10	L	C	170.516
11	F	N	128.161
11	F	H	8.686
11	F	CA	57.303
11	F	CB	40.173
11	F	C	172.53
12	V	N	111.797
12	V	H	8.229
12	V	CA	59.114
12	V	CB	35.412
12	V	C	172.066
13	K	N	121.752
13	K	H	7.738
13	K	CA	58.934
13	K	CB	35.522
13	K	C	174.072
14	A	N	128.179
14	A	H	8.473
14	A	CA	52.376
14	A	C	175.743
15	G	N	107.339
15	G	H	8.732
15	G	CA	45.026
15	G	C	173.898
16	S	N	119.972
16	S	H	10.465
16	S	CA	63.239
16	S	CB	63.927
16	S	C	172.607
17	D	N	120.42
17	D	H	7.408
17	D	CA	53.894
17	D	CB	41.977
17	D	C	174.914
18	G	N	108.837
18	G	H	8.342
18	G	CA	47.048
18	G	C	169.991
19	A	N	123.446
19	A	H	8.515
19	A	CA	54.92
19	A	CB	23.066
19	A	C	175.014

20	K	N	122.582
20	K	H	9.85
20	K	CA	56.977
20	K	CB	33.727
20	K	C	172.986
21	I	N	120.565
21	I	H	8.231
21	I	CA	65.188
21	I	CB	39.06
21	I	C	173.553
22	G	N	113.119
22	G	H	8.063
22	G	CA	44.373
22	G	C	169.771
23	N	N	116.141
23	N	H	8.809
23	N	CA	55.976
23	N	CB	42.221
23	N	C	172.451
24	C	N	129.637
24	C	H	8.714
24	C	CA	61.156
24	C	CB	29.523
37	K	N	117.12
37	K	H	8.279
37	K	CA	57.64
37	K	CB	34.594
37	K	C	174.922
38	G	N	103.79
38	G	H	7.773
38	G	CA	47.36
38	G	C	172.326
39	V	N	116.409
39	V	H	6.705
39	V	CA	61.003
39	V	CB	34.905
39	V	C	171.722
40	T	N	122.968
40	T	H	8.493
40	T	CA	64.578
40	T	CB	69.989
41	F	C	169.155
42	N	N	117.245

42	N	H	7.807
42	N	CA	52.457
42	N	CB	43.119
42	N	C	170.327
43	V	N	122.045
43	V	H	8.118
43	V	CA	61.939
43	V	CB	34.668
43	V	C	172.181
44	T	N	127.675
44	T	H	8.745
44	T	CA	62.077
44	T	CB	71.767
45	T	N	117.294
45	T	H	8.527
45	T	CA	64.428
45	T	CB	70.826
45	T	C	171.941
46	V	N	122.251
46	V	H	8.801
46	V	CA	62.761
46	V	CB	35.405
46	V	C	172.037
47	D	N	130.732
47	D	H	8.862
47	D	CA	53.452
47	D	CB	42.041
48	T	CA	65.803
48	T	CB	67.738
48	T	C	173.32
49	K	N	120.245
49	K	H	8.245
49	K	CA	58.368
49	K	CB	33.35
49	K	C	174.271
50	R	N	122.022
50	R	H	7.671
50	R	CA	56.054
50	R	CB	31.326
50	R	C	172.253
51	R	N	124.586
51	R	H	8.404
51	R	CA	58.316

51	R	CB	31.738
51	R	C	175.12
52	T	N	115.706
52	T	H	8.739
52	T	CA	62.702
52	T	CB	72.139
52	T	C	172.806
54	T	CA	67.712
54	T	CB	70.229
54	T	C	173.183
55	V	N	121.846
55	V	H	7.216
55	V	CA	68.356
55	V	CB	32.428
55	V	C	174.507
56	Q	N	118.671
56	Q	H	8.027
56	Q	CA	60.079
56	Q	CB	29.726
56	Q	C	174.865
57	K	N	116.5
57	K	H	7.484
57	K	CA	59.415
57	K	CB	33.335
57	K	C	175.883
58	L	N	117.745
58	L	H	7.55
58	L	CA	57.827
58	L	CB	44.192
58	L	C	174.103
59	C	N	116.373
59	C	H	7.68
59	C	CA	55.984
59	C	CB	26.664
59	C	C	169.311
61	G	CA	46.809
61	G	C	173.163
62	G	N	106.191
62	G	H	7.414
62	G	CA	46.942
62	G	C	171.353
63	Q	N	122.735
63	Q	H	8.223

63	Q	CA	59.781
63	Q	CB	28.819
63	Q	C	171.913
64	L	N	120.378
64	L	H	7.657
64	L	CA	54.322
64	L	CB	46.725
65	P	CA	64.224
65	P	CB	36.899
65	P	C	172.845
66	F	N	112.183
66	F	H	8.496
66	F	CA	58.634
66	F	CB	41.88
66	F	C	168.489
67	L	N	122.496
67	L	H	8.91
67	L	CA	54.682
67	L	CB	49.345
67	L	C	171.305
68	L	N	130.486
68	L	H	9.585
68	L	CA	55.345
68	L	CB	46.306
68	L	C	171.654
69	Y	N	129.422
69	Y	H	9.216
69	Y	CA	58.275
69	Y	CB	41.376
69	Y	C	173.631
70	G	N	118.15
70	G	H	9.406
70	G	CA	48.823
70	G	C	171.084
71	T	N	117.528
71	T	H	8.53
71	T	CA	62.768
71	T	CB	70.623
71	T	C	171.845
72	E	N	123.734
72	E	H	8.144
72	E	CA	57.064
72	E	CB	33.1

72	E	C	171.965
73	V	N	123.687
73	V	H	8.247
73	V	CA	62.788
73	V	CB	34.091
73	V	C	173.183
74	H	N	128.764
74	H	H	9.477
74	H	CA	56.975
74	H	CB	35.991
74	H	C	172.769
75	T	N	111.55
75	T	H	8.171
75	T	CA	63.079
75	T	CB	72.088
76	D	N	120.264
76	D	H	8.412
76	D	CA	55.986
76	D	CB	43.366
81	E	C	174.491
82	E	N	117.214
82	E	H	7.625
82	E	CA	60.603
82	E	CB	30.91
82	E	C	176.483
83	F	N	121.972
83	F	H	8.098
83	F	CA	62.226
83	F	CB	39.78
83	F	C	173.591
84	L	N	118.419
84	L	H	8.514
84	L	CA	58.664
84	L	CB	42.696
84	L	C	176.33
85	E	N	117.605
85	E	H	7.989
85	E	CA	58.959
85	E	CB	29.944
85	E	C	173.75
86	A	N	119.519
86	A	H	7.339
86	A	CA	55.274

86	A	CB	19.892
86	A	C	177.172
87	V	N	113.555
87	V	H	7.995
87	V	CA	64.865
87	V	CB	32.872
87	V	C	174.225
88	L	N	123.419
88	L	H	7.437
88	L	CA	53.762
88	L	CB	38.5
88	L	C	170.611
89	C	N	119.049
89	C	H	7.659
89	C	CA	55.502
89	C	CB	30.981
91	P	CA	63.364
91	P	CB	32.732
91	P	C	174.681
92	R	N	124.063
92	R	H	8.491
92	R	CA	58.128
92	R	CB	33.973
92	R	C	173.7
93	Y	N	117.671
93	Y	H	6.611
93	Y	CA	55.735
93	Y	CB	42.07
96	L	N	127.536
96	L	H	9.822
96	L	CA	55.22
96	L	CB	45.099
96	L	C	174.8
97	A	N	126.022
97	A	H	7.993
97	A	CA	54.703
97	A	CB	19.874
97	A	C	174.458
98	A	N	123.86
98	A	H	8.942
98	A	CA	53.568
98	A	CB	19.259
98	A	C	175.46

99	L	N	124.942
99	L	H	10.988
99	L	CA	57.338
99	L	CB	43.587
99	L	C	175.741
100	N	N	121.775
100	N	H	9.244
100	N	CA	52.15
100	N	CB	40.336
101	P	CA	66.786
101	P	CB	32.902
101	P	C	176.826
102	E	N	117.534
102	E	H	8.807
102	E	CA	59.957
102	E	CB	29.756
102	E	C	175.763
103	S	N	117.387
103	S	H	8.265
103	S	CA	62.705
103	S	CB	63.758
103	S	C	171.571
104	N	N	112.815
104	N	H	7.302
104	N	CA	55.66
104	N	CB	40.18
104	N	C	173.431
105	T	N	107.431
105	T	H	7.142
105	T	CA	62.73
105	T	CB	70.751
105	T	C	172.879
106	A	N	127.982
106	A	H	7.356
106	A	CA	55.535
106	A	CB	19.54
106	A	C	174.935
107	G	N	105.6
107	G	H	9.027
107	G	CA	46.872
107	G	C	173.213
108	L	N	121.463
108	L	H	7.35

108	L	CA	58.823
108	L	CB	42.839
108	L	C	175.752
109	D	N	115.951
109	D	H	8.717
109	D	CA	56.079
109	D	CB	41.732
109	D	C	174.314
110	I	N	119.455
110	I	H	7.542
110	I	C	174.771
112	A	N	123.413
112	A	H	8.356
112	A	CA	56.525
112	A	CB	19.465
112	A	C	178.537
113	K	N	119.844
113	K	H	8.038
113	K	CA	59.689
113	K	CB	32.328
113	K	C	177.958
114	F	N	123.211
114	F	H	8.886
114	F	CA	50.224
114	F	C	172.374
115	S	N	117.803
115	S	H	8.093
115	S	CA	63.09
115	S	CB	63.841
115	S	C	172.088
116	A	N	120.698
116	A	H	7.285
116	A	CA	55.973
116	A	CB	19.233
116	A	C	176.738
117	Y	N	117.226
117	Y	H	7.326
117	Y	CA	61.143
117	Y	CB	39.926
117	Y	C	174.949
123	P	C	175.656
124	A	N	119.141
124	A	H	7.936

124	A	CA	55.325
124	A	CB	19.179
124	A	C	176.007
125	L	N	115.647
125	L	H	7.337
125	L	CA	55.46
125	L	CB	43.256
125	L	C	174.615
126	N	N	116.848
126	N	H	7.085
126	N	CA	59.566
126	N	CB	41.684
126	N	C	173.162
127	D	N	118.639
127	D	H	8.874
127	D	CA	59.752
127	D	C	175.501
128	N	N	117.522
128	N	H	8.475
128	N	CA	57.817
128	N	CB	39.653
128	N	C	176.23
129	L	N	121.119
129	L	H	7.846
129	L	CA	58.836
129	L	CB	43.239
129	L	C	177.411
130	E	N	125.998
130	E	H	9.226
130	E	CA	61.408
130	E	CB	31.563
130	E	C	175.985
131	K	N	118.74
131	K	H	8.389
131	K	CA	61.249
131	K	CB	32.777
131	K	C	177.272
132	G	N	107.842
132	G	H	7.916
132	G	CA	48.334
132	G	C	173.462
133	L	N	124.946
133	L	H	7.337

133	L	CA	59.358
133	L	CB	41.997
133	L	C	175.217
134	L	N	120.209
134	L	H	8.581
134	L	CA	60.11
134	L	CB	42.869
134	L	C	176.484
135	K	N	119.924
135	K	H	8.487
135	K	CA	60.957
135	K	CB	32.833
135	K	C	175.862
136	A	N	121.56
136	A	H	7.422
136	A	CA	55.939
136	A	CB	19.075
136	A	C	172.406
137	L	N	116.92
137	L	H	7.333
137	L	CA	55.771
137	L	C	170.179
138	K	N	122.963
138	K	H	8.383
138	K	CA	59.352
138	K	CB	32.239
138	K	C	175.168
139	V	N	120.716
139	V	H	7.8
139	V	CA	68.209
139	V	CB	32.449
139	V	C	177.16
140	L	N	121.143
140	L	H	7.009
140	L	CA	59.278
140	L	CB	41.828
140	L	C	174.762
141	D	N	120.47
141	D	H	8.561
141	D	CA	60.95
141	D	CB	44.525
141	D	C	175.856
142	N	N	117.082

142	N	H	8.732
142	N	CA	56.945
142	N	CB	38.984
142	N	C	174.887
143	Y	N	122.045
143	Y	H	7.743
143	Y	CA	62.813
143	Y	CB	39.294
144	L	CA	57.715
144	L	CB	43.775
144	L	C	174.75
145	T	N	110.721
145	T	H	7.905
145	T	CA	64.642
145	T	CB	70.924
145	T	C	172.843
146	S	N	122.802
146	S	H	7.455
146	S	CA	58.356
146	S	CB	64.228
146	S	C	169.56
149	P	CA	67.07
149	P	CB	32.582
149	P	C	175.85
150	E	N	114.406
150	E	H	8.506
150	E	CA	59.083
150	E	CB	29.715
150	E	C	174.22
151	E	N	119.716
151	E	H	7.904
151	E	CA	58.423
151	E	CB	32.108
151	E	C	174.109
152	V	N	120.12
152	V	H	7.523
152	V	CA	64.636
152	V	CB	33.693
152	V	C	173.044
153	D	N	124.153
153	D	H	8.31
153	D	CA	55.482
153	D	CB	42.453

153	D	C	174.056
154	E	N	122.11
154	E	H	8.469
154	E	CA	58.604
154	E	CB	30.79
154	E	C	174.371
155	T	N	113.396
155	T	H	8.179
155	T	CA	63.757
155	T	CB	70.969
155	T	C	172.264
156	S	N	118.144
156	S	H	8.078
156	S	CA	59.582
156	S	CB	65.215
157	A	N	126.399
157	A	H	8.304
157	A	CA	37.215
157	A	CB	19.99
157	A	C	175.454
158	E	N	118.787
158	E	H	8.222
158	E	CA	54.379
158	E	CB	30.959
158	E	C	173.672
159	D	N	120.305
159	D	H	7.983
159	D	CA	55.785
159	D	CB	42.48
159	D	C	173.34
160	E	N	120.656
160	E	H	8.195
160	E	CA	58.276
160	E	CB	30.82
160	E	C	174.361
161	G	N	109.919
161	G	H	8.4
161	G	CA	46.91
161	G	C	170.893
162	V	N	118.029
162	V	H	7.655
162	V	CA	61.989
162	V	CB	34.788

162	V	C	173.252
163	S	N	118.772
163	S	H	8.089
163	S	CA	59.82
163	S	CB	64.682
163	S	C	172.435
164	Q	N	124.353
164	Q	H	8.805
164	Q	CA	55.438
164	Q	CB	30.657
164	Q	C	173.66
165	R	N	123.085
165	R	H	7.62
165	R	CA	56.792
165	R	CB	30.204
165	R	C	173.759
166	K	N	118.793
166	K	H	8.118
166	K	CA	60.312
166	K	CB	47.833
167	F	N	112.725
167	F	H	7.651
167	F	CA	56.124
167	F	CB	42.219
168	L	CA	61.037
168	L	CB	45.187
169	D	N	115.513
169	D	H	9.612
169	D	CA	55.325
169	D	CB	48.122
169	D	C	172.459
170	G	N	102.706
170	G	H	6.93
170	G	CA	47.12
170	G	C	170.048
171	N	N	118.477
171	N	H	8.984
171	N	CA	54.987
171	N	CB	40.222
171	N	C	170.888
172	E	N	118.033
172	E	H	8.149
172	E	CA	55.21

172	E	CB	32.815
172	E	C	173.783
173	L	N	125.321
173	L	H	8.378
173	L	CA	56.982
173	L	CB	44.6
173	L	C	173.992
174	T	N	111.205
174	T	H	9.342
174	T	CA	61.226
174	T	C	175.512
175	L	N	118.832
175	L	H	8.757
175	L	CA	59.335
175	L	CB	41.113
175	L	C	176.872
176	A	N	119.647
176	A	H	6.926
176	A	CA	56.415
176	A	CB	19.101
176	A	C	177.914
177	D	N	117.658
177	D	H	7.275
177	D	CA	58.507
177	D	CB	44.274
177	D	C	174.62
178	C	N	116.844
178	C	H	7.055
184	L	N	117.703
184	L	H	8.042
184	L	CA	57.896
184	L	CB	39.056
184	L	C	174.93
185	H	N	120.751
185	H	H	7.971
185	H	CA	60.006
185	H	CB	32.697
185	H	C	177.667
186	I	N	122.535
186	I	H	9.051
186	I	CA	67.325
186	I	CB	38.444
186	I	C	174.4

187	V	N	120.041
187	V	H	7.955
187	V	CA	67.005
187	V	CB	32
187	V	C	175.561
188	Q	N	116.383
188	Q	H	7.888
188	Q	CA	61.064
188	Q	CB	31.495
188	Q	C	176.371
189	V	N	120.293
189	V	H	7.949
189	V	CA	67.779
189	V	CB	34.125
189	V	C	176.93
190	V	N	119.841
190	V	H	8.833
190	V	CA	68.566
190	V	CB	32.354
190	V	C	176.154
191	C	N	116.484
191	C	H	8.554
191	C	CA	67.397
191	C	CB	28.152
191	C	C	175.712
192	K	N	121.329
192	K	H	7.63
192	K	CA	61.666
192	K	CB	33.186
192	K	C	175.469
193	K	N	117.892
193	K	H	7.17
193	K	CA	59.595
193	K	CB	33.136
193	K	C	175.13
194	Y	N	110.61
194	Y	H	8.149
194	Y	CA	61.463
194	Y	CB	40.219
194	Y	C	174.563
195	R	N	116.299
195	R	H	7.459
195	R	CA	55.113

195	R	CB	34.597
195	R	C	173.611
196	G	N	110.859
196	G	H	7.597
196	G	CA	47.951
196	G	C	170.601
197	F	N	121.751
197	F	H	7.26
197	F	CA	58.524
197	F	CB	42.459
197	F	C	171.609
198	T	N	117.782
198	T	H	7.052
198	T	CA	59.908
198	T	CB	72.342
198	T	C	169.859
199	I	N	123.187
199	I	H	8.873
199	I	CA	61.935
199	I	CB	39.151
199	I	C	172.464
200	P	CA	65.308
200	P	CB	32.73
201	E	N	125.53
201	E	H	8.684
201	E	CA	60.045
201	E	CB	29.85
202	A	N	116.649
202	A	H	7.673
202	A	CA	54.639
202	A	CB	19.429
202	A	C	176.135
203	F	N	121.105
203	F	H	7.606
203	F	CA	54.798
203	F	CB	35.327
203	F	C	173.068
204	R	N	121.253
204	R	H	8.105
204	R	CA	60.156
204	R	CB	31.112
204	R	C	177.574
205	G	N	113.586

205	G	H	9.775
205	G	CA	48.469
205	G	C	172.861
206	V	N	123.129
206	V	H	8.368
206	V	CA	68.438
206	V	CB	32.191
206	V	C	174.874
207	H	N	116.08
207	H	H	8.097
207	H	CA	62.836
207	H	CB	32.166
207	H	C	176.004
208	R	N	123.845
208	R	H	8.122
208	R	CA	61.071
208	R	CB	31.34
208	R	C	174.916
209	Y	N	121.444
209	Y	H	8.026
210	L	N	116.83
210	L	H	8.377
210	L	CA	59.084
210	L	CB	41.886
210	L	C	175.959
211	S	N	114.431
211	S	H	8.27
211	S	CA	63.687
211	S	C	175.277
212	N	N	119.766
212	N	H	8.2
212	N	CA	57.11
212	N	CB	39.712
212	N	C	175.087
213	A	N	124.323
213	A	H	8.638
213	A	CA	57.097
213	A	CB	20.585
213	A	C	175.337
214	Y	N	115.823
214	Y	H	8.936
214	Y	CA	63.451
214	Y	CB	38.235

215	A	N	118.226
215	A	H	6.944
215	A	CA	53.685
215	A	CB	19.804
215	A	C	174.897
216	R	N	120.786
216	R	H	7.964
216	R	CA	53.31
216	R	CB	28.57
216	R	C	173.86
217	E	N	128.08
217	E	H	9.242
217	E	CA	60.358
217	E	CB	30.324
217	E	C	174.231
218	E	N	117.441
218	E	H	10.026
218	E	CA	60.314
218	E	CB	28.758
218	E	C	173.253
219	F	N	111.544
219	F	H	6.689
219	F	CA	58.34
219	F	CB	55.234
219	F	C	173.566
220	A	N	120.886
220	A	H	8.302
220	A	CA	57.123
220	A	CB	19.642
220	A	C	178.336
221	S	N	109.378
221	S	H	8.563
221	S	CA	61.608
221	S	CB	64.533
222	T	N	108.532
222	T	H	6.877
222	T	CA	61.827
222	T	CB	71.127
222	T	C	170.976
223	C	N	119.393
223	C	H	6.326
223	C	CA	59.759
223	C	CB	28.673

224	P	CA	63.13
224	P	CB	32.179
224	P	C	172.712
225	D	N	122.059
225	D	H	9.156
225	D	CA	56.003
225	D	CB	42.072
225	D	C	174.672
226	D	N	123.943
226	D	H	9
226	D	CA	59.468
226	D	C	175.86
227	E	N	117.109
227	E	H	8.949
227	E	CA	61.013
227	E	C	174.084
228	E	N	116.7
228	E	H	7.472
228	E	CB	30.14
228	E	C	177.192
229	I	N	121.706
229	I	H	7.487
229	I	CA	67.009
229	I	C	175.164
230	E	N	117.998
230	E	H	8.676
230	E	CA	61.94
230	E	C	179.08
231	L	N	122.239
231	L	H	8.772
231	L	CA	59.268
231	L	CB	42.864
231	L	C	177.429
232	A	N	121.815
232	A	H	7.76
232	A	CA	55.749
232	A	C	176.594
233	Y	N	115.164
233	Y	H	7.67
233	Y	CA	60.606
233	Y	CB	41.01
233	Y	C	173.164
234	E	N	125.162

234	E	H	7.731
234	E	CA	61.734
234	E	C	174.709
235	Q	C	173.318
236	V	N	118.602
236	V	H	7.186
236	V	CA	64.69
236	V	CB	35.099
236	V	C	173.171
237	A	N	120.239
237	A	H	7.911
237	A	CA	53.097
237	A	CB	19.733
237	A	C	174.236
238	K	N	120.183
238	K	H	7.884
238	K	CA	55.177
238	K	CB	34.543
238	K	C	173.478
239	A	N	124.808
239	A	H	8.142
239	A	CA	53.143
239	A	CB	20.052
239	A	C	174.931
240	L	N	120.976
240	L	H	8.227
240	L	CA	53.146
240	L	CB	42.652
240	L	C	173.86
241	K	N	128.872
241	K	H	8.096
241	K	CA	59.236
241	K	CB	34.991
241	K	C	177.774

Figure 6.2- Backbone assignments of CLIC1 collected for 187 of 241 residues – The spectra were processed using MddNMR and compressed sensing was used. List provided contains H, N, CA and CB assignments.

Residue	R1	R1Err	R2	R2Err
2	0.00138	0.00026	0.0043	0.0013
3	0.000984	0.000045	0.00569	0.0004
4	0.00133	0.000045	0.0107	0.0007
5	0.00121	0.00007	0.0112	0.0006
7	0.000853	0.00002	0.0216	0.0011
8	0.00079	0.000009	0.0211	0.001
9	0.000671	0.000016	0.02359	0.0004
10	0.000792	0.000018	0.0189	0.0009
11	0.000772	0.000016	0.0218	0.0008
12	0.00073	0.000011	0.0238	0.0009
13	0.000641	0.000029	0.0262	0.001
14	0.000757	0.000019	0.0207	0.00044
15	0.00066	0.000014	0.0281	0.0028
16	0.000634	0.000025	0.0228	0.001
17	0.000656	0.000022	0.0237	0.0009
18	0.00074	0.000023	0.0316	0.0032
19	0.000736	0.000023	0.0199	0.0018
20	0.000694	0.000025	0.0255	0.0019
21	0.000749	0.000013	0.0184	0.001
22	0.000651	0.000032	0.0239	0.0018
23	0.000679	0.000023	0.02392	0.0005
24	0.000692	0.000039	0.01891	0.00048
37	0.00076	0.00007	0.0306	0.0013
38	0.000649	0.000013	0.0254	0.0008
39	0.00065	0.000034	0.0236	0.0012
40	0.00071	0.00006	0.0249	0.0017
42	0.0007	0.00006	0.0216	0.0021
43	0.00071	0.000026	0.0268	0.0007
44	0.000742	0.000017	0.021	0.0007
45	0.000598	0.000026	0.02568	0.00049
46	0.00067	0.000011	0.0277	0.0006
47	0.000564	0.000036	0.0266	0.0006
49	0.00108	0.000039	0.00413	0.00044
50	0.000806	0.000022	0.0247	0.0005
51	0.000813	0.000044	0.0197	0.0007
52	0.00081	0.00005	0.0215	0.0006
55	0.00083	0.00005	0.0259	0.0009
56	0.000627	0.000029	0.0249	0.0013
57	0.00076	0.000019	0.02242	0.00044
58	0.000692	0.000032	0.0213	0.0005
59	0.000729	0.000022	0.0227	0.0007

62	0.000759	0.000032	0.02704	0.00049
63	0.000798	0.000025	0.0234	0.002
64	0.00061	0.00007	0.0222	0.001
66	0.000711	0.000016	0.02052	0.00038
67	0.000836	0.00004	0.0287	0.0012
68	0.000659	0.00004	0.0291	0.0009
69	0.000666	0.000022	0.02188	0.00046
70	0.000662	0.00003	0.0219	0.0007
71	0.000699	0.000044	0.0228	0.0009
72	0.000729	0.000017	0.0186	0.0014
73	0.000719	0.000011	0.017	0.0016
74	0.00071	0.000026	0.0194	0.0005
75	0.00068	0.00007	0.0242	0.0017
76	0.00061	0.00008	0.0236	0.0014
82	0.000624	0.00003	0.0271	0.001
83	0.000669	0.000019	0.0278	0.001
84	0.00063	0.00005	0.027	0.001
85	0.000659	0.000024	0.03	0.0012
86	0.000657	0.000033	0.0268	0.0014
87	0.000582	0.000042	0.0254	0.0014
88	0.00076	0.00006	0.0236	0.0016
89	0.000546	0.000022	0.0248	0.0014
92	0.000727	0.000022	0.0215	0.0008
93	0.000585	0.000026	0.02408	0.00044
96	0.000673	0.00004	0.0389	0.004
97	0.0006	0.00005	0.0282	0.0022
98	0.000703	0.000008	0.0192	0.0012
99	0.000698	0.000028	0.0214	0.0005
100	0.000671	0.00002	0.0255	0.0008
102	0.00066	0.00003	0.025	0.0007
103	0.00067	0.000037	0.0258	0.0007
104	0.000746	0.000021	0.0182	0.0013
105	0.000711	0.000029	0.0254	0.0015
106	0.000721	0.00003	0.0229	0.0011
107	0.000661	0.000027	0.0273	0.0006
108	0.000774	0.000034	0.0295	0.0006
109	0.00079	0.00009	0.0243	0.0017
110	0.000643	0.000046	0.0284	0.0005
112	0.000882	0.00003	0.01353	0.00045
113	0.00068	0.00003	0.0267	0.0012
114	0.000687	0.000024	0.0225	0.0005
115	0.000648	0.000045	0.0266	0.0007
116	0.000711	0.000025	0.0273	0.002

117	0.000644	0.000036	0.0246	0.0008
124	0.000697	0.000033	0.0267	0.0008
125	0.000655	0.000041	0.0242	0.0009
126	0.00076	0.00005	0.0243	0.0011
127	0.00069	0.00006	0.0273	0.0007
128	0.000642	0.000033	0.0238	0.001
129	0.000635	0.000027	0.0355	0.0012
130	0.000619	0.000021	0.0211	0.0007
131	0.000618	0.000028	0.0289	0.0018
132	0.000682	0.000012	0.0227	0.0013
133	0.000711	0.000022	0.0262	0.0006
134	0.000651	0.00003	0.0253	0.0008
135	0.000635	0.000021	0.0271	0.0005
136	0.000672	0.000012	0.0321	0.0012
137	0.000693	0.000032	0.02211	0.00047
138	0.000677	0.000012	0.0288	0.0023
139	0.000659	0.000011	0.0253	0.001
140	0.000682	0.000016	0.0327	0.0016
141	0.000621	0.000038	0.0283	0.0033
142	0.000636	0.000019	0.0254	0.001
143	0.000691	0.000019	0.0275	0.0006
145	0.000752	0.000029	0.0193	0.0019
146	0.000664	0.000022	0.0261	0.0017
150	0.000705	0.000024	0.0197	0.0013
151	0.000863	0.00002	0.0199	0.0005
152	0.000953	0.000022	0.01513	0.00044
153	0.00108	0.00001	0.0093	0.0006
154	0.00116	0.000009	0.01129	0.00014
155	0.00114	0.000029	0.00729	0.00037
156	0.00113	0.000037	0.00886	0.00019
157	0.00121	0.00006	0.0073	0.0006
158	0.00119	0.000024	0.00703	0.00011
159	0.00106	0.000023	0.00692	0.00032
160	0.00113	0.000021	0.00616	0.00049
161	0.00123	0.000023	0.0088	0.0006
162	0.000848	0.000028	0.01346	0.00036
163	0.000741	0.000034	0.021	0.0006
164	0.000812	0.000022	0.0202	0.0007
165	0.000832	0.00003	0.0259	0.0014
166	0.000658	0.000028	0.0231	0.0009
167	0.000622	0.000017	0.0265	0.0013
169	0.000711	0.000044	0.0267	0.0009
170	0.000598	0.000049	0.023	0.0006

171	0.00065	0.00007	0.0293	0.0015
172	0.00066	0.00003	0.022	0.0007
173	0.00066	0.00002	0.0236	0.0015
174	0.000734	0.000046	0.0194	0.002
175	0.000611	0.000036	0.0283	0.0005
176	0.000678	0.000019	0.0289	0.001
177	0.000634	0.000036	0.0268	0.001
178	0.0008	0.00015	0.0242	0.0005
184	0.000798	0.000042	0.0241	0.0017
185	0.000608	0.000033	0.0193	0.0012
186	0.00067	0.00005	0.0287	0.0011
187	0.000686	0.000034	0.0104	0.0007
188	0.000655	0.000018	0.02618	0.00039
189	0.00067	0.00002	0.0181	0.0006
190	0.00077	0.00007	0.0339	0.0028
191	0.000641	0.000024	0.0281	0.0007
192	0.000671	0.000012	0.0355	0.0014
193	0.000587	0.000049	0.026	0.0008
194	0.000712	0.00002	0.02	0.001
195	0.000626	0.000027	0.0265	0.001
196	0.000652	0.000049	0.0191	0.0018
197	0.000661	0.000019	0.02761	0.00035
198	0.000618	0.000024	0.0253	0.0006
199	0.000692	0.000014	0.0223	0.0009
201	0.00075	0.00008	0.0266	0.002
202	0.000719	0.000029	0.0268	0.0016
203	0.000631	0.000027	0.0321	0.001
204	0.000623	0.000016	0.0251	0.0013
205	0.000643	0.000022	0.0206	0.0016
206	0.000751	0.000019	0.0196	0.0008
207	0.000645	0.00002	0.0298	0.0009
208	0.000737	0.000013	0.02	0.0014
209	0.00064	0.00006	0.0316	0.0018
210	0.00061	0.00006	0.0231	0.002
211	0.0006	0.000027	0.0259	0.0012
212	0.000674	0.000016	0.0234	0.0021
213	0.000666	0.000021	0.0319	0.0013
214	0.000613	0.00002	0.0284	0.0008
215	0.000617	0.000029	0.0279	0.001
216	0.000564	0.000044	0.0361	0.0037
217	0.000715	0.000019	0.0218	0.0008
218	0.000629	0.000041	0.0257	0.0006
219	0.00076	0.000032	0.0252	0.0019

220	0.00071	0.000024	0.0298	0.0012
221	0.000649	0.00003	0.0235	0.0008
222	0.00055	0.00007	0.0337	0.0047
223	0.000612	0.000027	0.0234	0.0006
225	0.000617	0.000018	0.02824	0.00036
226	0.00073	0.000013	0.0184	0.0012
227	0.00069	0.000028	0.02364	0.00049
228	0.000701	0.000028	0.0247	0.0007
229	0.000694	0.00004	0.0274	0.0006
230	0.000657	0.000032	0.02474	0.00047
231	0.000737	0.000013	0.0287	0.0007
232	0.000754	0.000025	0.026	0.0012
233	0.000661	0.000031	0.0257	0.0006
234	0.000665	0.000016	0.0291	0.0007
236	0.000657	0.00003	0.02018	0.00034
237	0.00073	0.000025	0.0214	0.001
238	0.000787	0.000031	0.01836	0.00019
239	0.00087	0.000016	0.01813	0.00033
240	0.000895	0.000021	0.0182	0.00170000000000
241	0.0012	0.000015	0.00825	0.00022000000000

Figure 6.3- Relaxation data set for apo state CLIC1- Includes R1, R2, R1 errors and R2 errors. Errors were calculated from S/N of spectra.

AtomName	RDC
3HN	4.73404372
4HN	9.61522828
5HN	4.47989136
7HN	0.18605412
8HN	-1.7401532
9HN	31.4540906
10HN	34.1743721
11HN	14.9183787
12HN	19.2292405
13HN	-2.5293632
14HN	8.65698876
15HN	17.0269921
16HN	6.5787764
17HN	16.5186874
18HN	-8.422293
19HN	0.26996088
20HN	4.36436756

21HN	10.1636623
22HN	13.6087036
23HN	-4.0858944
24HN	8.60226696
36HN	8.09639432
37HN	1.945664
38HN	5.3323354
39HN	-0.1544371
40HN	0.88892524
41HN	9.53496964
42HN	33.1115532
43HN	27.270913
44HN	23.4549795
45HN	12.1445915
46HN	-14.324951
47HN	-7.5248555
48HN	8.24E-13
49HN	3.03645188
50HN	-32.890234
51HN	24.988406
52HN	-6.963045
55HN	10.5126658
56HN	4.78754948
57HN	18.1457489
58HN	24.8643699
59HN	3.54232452
62HN	-3.0364519
63HN	-23.78331
64HN	0.70043904
66HN	23.7833103
67HN	15.1810434
68HN	25.1550034
69HN	16.8506663
70HN	21.6856413
71HN	8.24E-13
72HN	5.20100308
73HN	16.0930734
74HN	30.311013
75HN	34.018719
76HN	4.23911544
82HN	3.54232452
83HN	-8.6788775
84HN	1.79122692

85HN	-11.879495
86HN	-3.6979776
87HN	-5.5281178
88HN	12.6492481
89HN	3.22980224
92HN	-2.2581863
93HN	-1.0129613
96HN	5.05994244
97HN	-6.0716877
98HN	9.26379272
99HN	-9.09E-13
100HN	23.316351
102HN	-14.673955
103HN	-17.204534
104HN	7.59052168
105HN	-5.8029429
106HN	1.01174528
107HN	2.49531408
108HN	-4.954147
109HN	-11.754243
110HN	-5.0599424
112HN	-15.181043
113HN	-6.7332135
114HN	-1.2050956
115HN	10.7838427
116HN	38.9765141
117HN	0.85609216
124HN	-7.6488916
125HN	-6.9897979
126HN	-0.3477874
127HN	3.5508368
128HN	11.5645404
129HN	-0.6749022
130HN	9.2479842
131HN	-0.0085123
132HN	-2.1864399
133HN	-2.4904499
134HN	0.27725712
135HN	5.56581508
136HN	-1.9213432
138HN	14.1692981
139HN	-6.6249859
140HN	2.16090308

141HN	-2.068484
142HN	7.08464904
143HN	-8.603483
144HN	-34.458925
145HN	13.9735156
146HN	-7.0445197
150HN	-7.8896675
151HN	11.1328462
152HN	9.80857864
153HN	4.5540698
154HN	-3.0364519
155HN	0.66152576
156HN	-9.09E-13
157HN	-2.27E-13
158HN	1.20631168
159HN	-30.360871
160HN	12.1847208
161HN	12.0302837
162HN	-48.071277
163HN	11.1328462
164HN	1.51761792
165HN	5.411378
166HN	-28.736241
167HN	-1.945664
168HN	15.0983526
169HN	1.01296132
170HN	-2.3554695
171HN	-5.9330592
172HN	1.51883396
173HN	3.03645188
174HN	-3.0352358
175HN	10.6269736
176HN	-5.2727494
177HN	3.18237668
178HN	3.38545536
179HN	-30.477611
180HN	2.0247066
181HN	6.65660296
184HN	2.95740928
185HN	-22.771565
186HN	8.21313416
188HN	-6.8888666
189HN	8.24E-13

190HN	5.76159752
191HN	0.00121604
192HN	-102.88793
193HN	-34.409068
194HN	6.57756036
195HN	9.78182576
196HN	-13.662209
197HN	71.9020131
198HN	6.5787764
199HN	0.50587264
201HN	11.24837
202HN	-2.0234906
203HN	-0.5046566
204HN	-3.0364519
205HN	14.6751707
206HN	16.6986613
207HN	-3.0364519
208HN	-37.261898
209HN	9.14826892
210HN	2.72514564
211HN	-10.626974
212HN	5.54E-13
213HN	6.5787764
214HN	-6.7696947
215HN	8.603483
216HN	-27.831507
217HN	3.54232452
218HN	-1.3619648
219HN	48.5771499
220HN	-10.513882
221HN	-7.5905217
222HN	-54.494401
223HN	8.24E-13
225HN	-13.353335
226HN	18.2162792
227HN	21.2527311
228HN	-9.1300283
229HN	14.0039166
230HN	12.1445915
231HN	15.1798273
232HN	-4.0481972
233HN	11.1328462
234HN	1.01174528

235HN	7.39595528
236HN	19.5393307
237HN	-7.2792154
238HN	8.24E-13
239HN	-8.0963943
240HN	-7.3594741

Figure 6.4- RDC values of apo state CLIC1- RDC values were calculated using standard HSQC-TROSY method and averaged over two sets with different alignment media.